Université de Montréal

Hamiltoniens locaux et information quantique en dimensions réduites

par

Christian Boudreault

Département de physique
Faculté des arts et des sciences

Thèse présentée en vue de l'obtention du grade de
Philosophiæ Doctor (Ph.D.)
en Physique

3 Novembre 2021

Université de Montréal

Faculté des études supérieures et postdoctorales

Cette thèse intitulée

Hamiltoniens locaux et information quantique en dimensions réduites

présentée par

Christian Boudreault

a été évaluée par un jury composé des personnes suivantes :

Luc Vinet, président-rapporteur

Manu Paranjape, directeur de recherche

Richard MacKenzie, codirecteur de recherche

William Witczak-Krempa, codirecteur de recherche

Véronique Hussin, membre du jury

Benjamin Doyon, examinateur externe

Matthias Ernzerhof, représentant du doyen de la FESP

Résumé

Cette thèse exploite les liens profonds entre la physique des systèmes quantiques locaux, les propriétés non locales de leurs états fondamentaux et le contenu en information de ces états. Les deux premiers chapitres sont consacrés à l'application des systèmes quantiques locaux pour les fins d'une tâche informationnelle précise, soit le calcul quantique. Au terme d'un bref survol de la théorie, nous proposons un patron pour le calcul quantique universel et évolutif pouvant être réalisé sur une grande variété de plateformes physiques, et démontrons qu'il est particulièrement résilient face à un bruit anisotrope. Les quatre derniers chapitres sont pour leur part consacrés à l'approche informationnelle des systèmes quantiques à corps multiples. Nous décrivons les principales propriétés des corrélations et de l'intrication dans les états fondamentaux des systèmes de dimensions réduites les plus courants, en distinguant systèmes non critiques et systèmes critiques. Nous montrons que ces propriétés sont fortement modifiées par la présence de frustration géométrique dans les chaînes de spins. Enfin, nous réalisons une analyse exhaustive des corrélations et de l'intrication dans les états fondamentaux de deux théories quantiques de champs non triviales.

Mots-clés : Information quantique, calcul quantique, corrélations et intrication, chaînes de spins frustrées, théories de champs quantiques en dimensions réduites, théories Lifshitz, structure de Rokhsar-Kivelson.

Summary

This thesis exploits the deep connections between the physics of local quantum systems, the nonlocal features in their ground states, and the information content of these states. The first two chapters are dedicated to the application of local quantum systems for the purpose of a definite information-theoretical task, namely quantum computation. After a brief survey of the theory, we propose a scheme for scalable universal quantum computation that, we argue, could be implemented on a wide variety of physical platforms, and show that it is particularly resilient to anisotropic noise. The last four chapters are dedicated to the information-theoretical approach of many-body quantum systems. We describe the main properties of correlations and entanglement in the ground states of the most common low-dimensional many-body systems, distinguishing between noncritical systems and critical ones. We show how these properties can be dramatically modified by the presence of geometric frustration in spin chains. Finally, we perform an intensive study of correlations and entanglement in the ground states of two nontrivial one-dimensional quantum field theories.

Keywords : Quantum information, quantum computation, correlations and entanglement, frustrated spin chains, low-dimensional quantum field theory, Lifshitz theories, Rokhsar-Kivelson structure.

Table des matières

Liste des tableaux

Table des figures

Liste des sigles et des abréviations

AdS/CFT	Dualité anti-de Sitter/théorie de champs conformes
AF	Antiferromagnétique
ANNNI	Modèle d'Ising axial à couplage de seconds voisins, de l'anglais *Axial Next-Nearest Neighbor Ising*,
BCHI	Modèle de Blume-Capel-Haldane-Ising
BPP	Problèmes de décision classiques non déterministes à temps polynomial, de l'anglais *Bounded Probabilistic Polynomial*
BQP	Problèmes de décision quantiques à temps polynomial, de l'anglais *Bounded Quantum Polynomial*
CE	Capacité d'intrication, de l'anglais *Capacity of Entanglement*
CFT	Théorie des champs conformes, de l'anglais *Conformal Field Theory*
CQM	Mécanique quantique conforme, de l'anglais *Conformal Quantum Mechanics*
EE	Entropie d'intrication, de l'anglais *Entanglement Entropy*
EPR	Paire d'Einstein-Podolsky-Rosen
GHZ	État de Greenberger-Horne-Zeilinger
GS	État fondamental, de l'anglais *Ground State*
IR	Infrarouge
LFT	Théorie des champs de Lifshitz, de l'anglais *Lifshitz Field Theory*
LHS	Côté gauche, de l'anglais *Left-hand Side*
MERA	De l'anglais *Multi-scale Entanglement Renormalization Ansatz*
MPS	De l'anglais *Matrix Product State*
n**D**	n-dimensionnel
P	Problèmes de décision classiques déterministes à temps polynomial, de l'anglais *Polynomial*
PEPS	De l'anglais *Projected Entangled Pair State*
QFT	Théorie quantique des champs, de l'anglais *Quantum Field Theory*
RG	Groupe de renormalisation, de l'anglais *Renormalization Group*
RHS	Côté droit, de l'anglais *Right-hand Side*
RK	Structure de Rokhsar-Kivelson
SL	Groupe spécial linéaire
SMF	Forme en matrices stochastiques, de l'anglais *Stochastic Matrix Form*
SU	Groupe spécial unitaire
SUSY	Supersymétrique
U	Groupe unitaire
UV	Ultraviolet
XXZ	Modèle de Heisenberg avec isotropie dans le plan xy

Remerciements

Je remercie chaleureusement mes trois codirecteurs, Richard MacKenzie, Manu Paranjape et William Witczak-Krempa, pour leur grande disponibilité et leur soutien constant. Sous votre gouverne, j'ai pu explorer des sujets en apparence fort différents et qui, à mon étonnement, se sont recoupés maintes fois pour ne plus former qu'un tout. La thèse que voici est un bien modeste rappel des ces rencontres heureuses qui font la science. Je remercie également Clément Berthière, Hichem Eleuch et Michael Hilke, pour leur enthousiasme et leur commentaires pénétrants.

Une mention spéciale pour le Collège militaire royal de Saint-Jean et le Ministère de la défense nationale du Canada, qui m'ont gracieusement offert une année de congé rémunéré pour compléter cette thèse. Il me fait également plaisir de souligner la contribution financière de l'Institut transdisciplinaire d'information quantique (INTRIQ).

Je remercie enfin Anne Plourde et nos trois merveilleuses filles, Saule, Constance et Marion. Pour tout.

Introduction

Les dernières décennies ont été le théâtre d'une rencontre extrêmement fertile entre la théorie quantique des champs, la physique de la matière condensée et la théorie de l'information quantique. Parmi les travaux précurseurs à l'origine de cette convergence, mentionnons l'approche wilsonienne du groupe de renormalisation et l'élucidation de l'universalité des exposants critiques [282, 283, 284], le calcul de l'entropie des trous noirs [34, 141], l'estimation des ressources thermodynamique (prohibitives) nécessaires pour simuler classiquement la plupart des systèmes quantiques [224], la découverte des transitions de phase quantiques [146], les premiers modèles *quantiques* d'ordinateurs (classiques ou quantiques) [36, 101], l'entrée de la complexité computationnelle en physique [27], la divergence logarithmique de l'énergie libre dans les systèmes critiques 2D et sa relation universelle à l'anomalie conforme [61], les premières preuves d'universalité pour le calcul quantique [88, 190] et la simulation quantique [191], le calcul de l'entropie d'intrication dans les théories de champs conformes [255, 149, 55, 53] et la caractérisation du comportement de leur c-fonction sous le flot du groupe de renormalisation [63].

Depuis, une relation d'échange réciproque s'est établie entre la théorie de l'information quantique au sens large, à saveur algorithmique, et la théorie des systèmes physiques à corps multiples [1, 209, 296]. Citons un exemple particulièrement saisissant de cette union. Pour une grande classe apparemment « naturelle » de modèles locaux sur réseau, l'existence d'un gap spectral à la limite thermodynamique est un problème *indécidable* [81] : il n'existe aucun algorithme qui, pour chaque système de cette classe, décide en un temps fini si ce système possède un gap spectral à la limite thermodynamique $N \to \infty$. Il existe donc des systèmes qui effectuent la transition, entre présence et absence de gap, à N arbitrairement grand. Les verres de spin, par exemple, peuvent nécessiter un temps exponentiel (en terme de N) pour atteindre leur état fondamental, qui n'est alors jamais réalisé dans la nature [296]. Les conséquences pratiques et théoriques de ce résultat sont encore un sujet de spéculations [179, 78], mais il paraît vraisemblable que des théorèmes de *décidabilité* contribuent dans les prochaines années à circonscrire la notion de modèle « naturel ».

Dans cet ouvrage, nous nous intéresserons à un fragment de cet imposant programme de recherche. Les Chapitres 1 et 2 seront consacrés à l'usage des systèmes quantiques locaux pour les fins du calcul quantique universel (en circuit), autrement dit, à l'informatique quantique. En contrepartie, les Chapitres 3 à 6 seront dédiés aux applications des outils de l'information quantique pour l'étude des systèmes quantiques à corps multiples, principalement par l'analyse de leurs états fondamentaux et pour des systèmes unidimensionnels, sur réseau ou dans le continuum.

Parmi les nombreux sujets dont nous ne parlerons pas ou très peu, et qui sont également les fruits de cette rencontre heureuse entre théorie quantique de l'information et physique des systèmes à corps multiples, mentionnons la complexité ha-

miltonienne [214], la méthode variationnelle basée sur les deux classes principales, MPS et MERA [280, 273, 100], désormais généralisées aux degrés de libertés continus [271, 128], l'approche holographique fondée sur la recherche de dualités de type AdS/CFT [234], les ordres topologiques et leurs propriétés [278], ainsi que les plateformes de calcul quantique basées sur les états fondamentaux de la matière condensée, telles que les calculateurs adiabatiques [6], unidirectionnels [228], ou topologiques [173].

Chapitre 1

Calcul quantique à l'aide d'hamiltoniens locaux

1.1 Calcul digital quantique

Le support fondamental de l'information digitale classique est la variable booléenne $x \in \mathbb{B} = \{0, 1\}$, ou *bit*. (Notons qu'on nomme aussi «bit» la quantité d'information contenue dans une variable booléenne.) Avec un nombre d'états distincts réduit au minimum, la variable booléenne est en principe le registre le plus incorruptible, le plus facile à initialiser et à lire.

De même, le support fondamental de l'information digitale quantique est le *bit quantique*, ou *qubit*, correspondant en principe à n'importe quel système quantique à deux niveaux, notés $|0\rangle$ et $|1\rangle$. L'état non normalisé du qubit, lorsque représenté dans la *base de calcul* $\{|0\rangle, |1\rangle\}$, est donc

$$\alpha|0\rangle + \beta|1\rangle \quad , \quad \alpha, \beta \in \mathbb{C}. \tag{1.1}$$

L'espace de Hilbert correspondant est isomorphe à $\mathbb{C}^2$. Le qubit présente un aspect analogique par son continuum d'états $\mathbb{C}^2$, et un aspect digital par la propriété qu'une observable sur $\mathbb{C}^2$ n'aura jamais plus de deux valeurs propres distinctes. Une remarque semblable s'applique à un système formé de N qubits, dont l'espace d'états est le produit tensoriel $(\mathbb{C}^2)^{\otimes N} \simeq \mathbb{C}^{2^N}$.

Cette information, pour nous être utile, doit pouvoir être traitée et échangée. C'est au traitement automatisé de l'information quantique, ou *calcul quantique*, que nous nous attarderons maintenant. Le modèle de base du calcul digital quantique, directement inspiré des circuits intégrés de l'électronique classique, est le *modèle en circuit*. Dans le modèle en circuit, le système à N qubits (le registre d'entrée) est d'abord initialisé dans un état déterminé $|\psi_{\text{initial}}\rangle \in \mathbb{C}^{2^N}$, pour évoluer ensuite par l'application d'un opérateur unitaire déterminé $U : \mathbb{C}^{2^N} \to \mathbb{C}^{2^N}$, suivi d'une mesure sur l'état final (le registre de sortie) $|\psi_{\text{final}}\rangle = U|\psi_{\text{initial}}\rangle$, par laquelle est obtenu le résultat du calcul sous la forme d'une séquence de bits classiques. [1] Pour réaliser un algorithme à N qubits, l'opérateur d'évolution requis U correspond donc à une matrice unitaire $2^N \times 2^N$. En pratique, U sera (approximativement) décomposé en une séquence d'opérations élémentaires

$$U \approx V_\ell \cdots V_2 V_1 \tag{1.2}$$

1. i) Dans les faits, l'état initial pourra être un état mixte ρ_{initial}. Pour un ensemble complet d'opérateurs de mesure $\{M_m\}$, une mesure sur l'état final $U\rho_{\text{initial}}U^\dagger$ donnera la valeur m avec la probabilité $\Pr(m) = \text{Tr}(\rho_{\text{initial}}U^\dagger M_m^\dagger M_m U)$. Une série de mesures sur des systèmes semblablement préparés permettra de reconstruire la fonction $\Pr(m)$ avec le degré de certitude recherché. ii) Bien que le circuit puisse comporter des étapes intermédiaires de mesure, le *principe de la mesure différée* assure que toute les mesures peuvent être reportées à la fin du circuit. iii) Enfin, certains circuits ont pour fonction de produire des états quantiques qui ne seront pas mesurés à la sortie, par exemple les circuits d'initialisation ou de téléportation. Dans tous les autres cas, le *principe de la mesure implicite* permet de présumer sans perte de généralité que tous les qubits finaux sont mesurés.

telle que chaque V_i agira de façon non triviale sur un maximum de k qubits (V_i est *k-corps*), pour un $k \leq N$ indépendant de V_i et généralement petit. Ces opérations élémentaires V_i sont appelées *portes logiques*. L'initialisation, la séquence $V_\ell \cdots V_2 V_1$ et la mesure finale constituent ensemble un *circuit quantique*.

D'autres modèles de calcul, échappant à cette description simple, n'en sont pas moins équivalents (en un sens qui sera précisé à la section 1.4) au modèle digital en circuit. Nous en citerons trois. Le *calcul quantique à variables continues* utilise comme support d'information des systèmes dotés d'un spectre continu de valeurs propres, telles que les quadratures de l'espace de phase optique [192]. Dans le *calcul quantique adiabatique*, le système demeure jusqu'à la mesure finale dans son état fondamental non dégénéré et séparé (*gapped*) du premier niveau excité. L'état initial et l'état final sont les états fondamentaux de deux hamiltoniens distincts, H_{initial} et H_{final}. La lente déformation de H_{initial} vers H_{final} permet à l'état $|\psi_{\text{initial}}\rangle$ d'évoluer adiabatiquement vers $|\psi_{\text{final}}\rangle$ [6]. Enfin, pour le *calcul quantique unidirectionnel* (*one-way*), l'évolution de l'état initial vers l'état final consiste en une séquence déterminée de mesures (non unitaires) sur le système [228]. Dans ce qui suit, nous nous concentrerons sur le modèle en circuit du calcul digital quantique.

1.2 Universalité

Pour réaliser les potentialités du calcul quantique à N qubits, un calculateur quantique devra être en mesure d'approcher toute matrice unitaire $2^N \times 2^N$, $U \in \mathbf{U}(2^N)$, par un circuit quantique tel que (1.2). La validité de l'approximation est déterminée par l'erreur acceptable entre U et son approximation $\tilde{U} = V_\ell \ldots V_2 V_1$. Cette erreur entre U et $\tilde{U}$ peut être identifiée à diverses métriques sur $\mathbf{U}(2^N)$, par exemple la *distance d'opérateur*

$$D_{\text{op}}(U, \tilde{U}) = \sup_{\|\psi\|=1} \|(U - \tilde{U})|\psi\rangle\| = \|U - \tilde{U}\|_{\text{op}} \,, \tag{1.3}$$

où $\|\cdot\|_{\text{op}}$ est la norme d'opérateur.[2] La proximité de U et $\tilde{U}$ se manifeste également lors de la mesure des états finaux $U|\psi\rangle$ et $\tilde{U}|\psi\rangle$, obtenus à partir de systèmes identiquement préparés. Les probabilités d'obtenir un même résultat m, notées respectivement $\Pr_U(m)$ et $\Pr_{\tilde{U}}(m)$, satisfont alors [209]

$$|\Pr_U(m) - \Pr_{\tilde{U}}(m)| \leq 2\|U - \tilde{U}\|_{\text{op}}. \tag{1.4}$$

Notons que la distance d'opérateur est sous-additive sous la composition,

$$D_{\text{op}}(U_2 U_1, \tilde{U}_2 \tilde{U}_1) \leq D_{\text{op}}(U_2, \tilde{U}_2) + D_{\text{op}}(U_1, \tilde{U}_1). \tag{1.5}$$

2. Deux autres métriques courantes sont la *distance de trace*, $D_{\text{tr}}(U, V) = \text{Tr}\sqrt{(U-V)^\dagger (U-V)} = \|U - V\|_{\text{tr}}$, où $\|\cdot\|_{\text{tr}}$ est la norme de trace, et la *distance de Hilbert-Schmidt*, $D_{\text{HS}}(U, V) = \sqrt{\text{Tr}(U-V)^\dagger (U-V)} = \|U - V\|_{\text{HS}}$, où $\|\cdot\|_{\text{HS}}$ est la norme de Hilbert-Schmidt ou norme Euclidienne. Puisque $\mathbf{U}(2^N)$ est de dimension finie, il admet une seule topologie naturelle, nommément la *topologie produit* sur $\mathbb{C}^{2^N \times 2^N}$, ou topologie de la convergence ponctuelle. (Elle coincide, entre autres, avec la topologie de la convergence uniforme.) Les trois métriques mentionnées sont équivalentes sur $\mathbf{U}(2^N)$ au sens où elles induisent la même topologie.

Un circuit comportant m opérateurs $U_1, \ldots, U_m$ peut donc être simulé par les opérateurs $\tilde{U}_1, \ldots, \tilde{U}_m$ avec une erreur inférieure à $\epsilon > 0$ sur les statistiques de mesures si les approximations satisfont $D_{\text{op}}(U_i, \tilde{U}_i) < \epsilon/2m$. Un ensemble de portes logiques $\mathbb{V} = \{V_i\}_{i \in I}$ est dit *strictement universel* pour N qubits s'il peut produire une approximation valide pour tout $U \in \mathbf{U}(2^N)$, quelle que soit la précision requise. Formellement,

Définition 1.1 (Universalité stricte)**.** *$\mathbb{V} \subset \mathbf{U}(2^N)$ est strictement universel pour N qubits (N-universel) si pour tout $\epsilon > 0$ et tout $U \in \mathbf{U}(2^N)$, il existe une séquence finie $V_1, V_2, \ldots, V_{\ell(\epsilon)}$ d'éléments de $\mathbb{V}$ (avec de possibles répétitions) telle que*

$$\|U - V_{\ell(\epsilon)} \ldots V_2 V_1\|_{op} < \epsilon. \tag{1.6}$$

Dans l'esprit du calcul digital, l'ensemble universel $\mathbb{V}$ sera de préférence *fini* (donc discret). On le voudra constitué d'un nombre restreint de portes logiques, bien séparées les unes des autres en dépit de leur inévitable étalement dû au bruit en provenance de l'environnement extérieur. De plus, la capacité de construire un ensemble universel à partir d'une collection donnée d'interactions est cruciale pour la réalisation physique de calculateurs quantiques. Puisque la nature semble favoriser les hamiltoniens locaux, on privilégiera un ensemble universel k-corps (avec $k = 2, 3$ en général) : chaque $V_i \in \mathbb{V}$ agira de façon non triviale sur un maximum de k qubits. [3] Un exemple important du point de vue théorique est l'ensemble $\mathbb{V}_W = \{P(W \otimes I^{\otimes N-2})P^\dagger | P \in \mathbf{S}_N\}$, où $\mathbf{S}_N$ est une représentation unitaire du groupe des permutations, $\mathbf{S}_N = \pi(S_N) \subset \mathbf{U}(2^N)$, et où W est une opération *générique* sur les deux premiers qubits : les opérations à deux qubits W pour lesquelles $\mathbb{V}_W$ *n'est pas* N-universel forment un ensemble de mesure nulle dans $\mathbf{U}(4)$ [88, 190]. Les ensembles universels finis et locaux sont donc la norme plutôt que l'exception.

1.3 Théorème de Solovay-Kitaev

L'usage, pour le calcul quantique, d'un ensemble universel constitué d'un nombre fini de portes, agissant chacune sur un nombre restreint de qubits, est une solution utile et durable seulement si, pour tout $U \in \mathbf{SU}(2^N)$, le nombre $\ell(\epsilon)$ d'opérations requises dans l'équation (1.6) croît de manière « raisonnable » lorsque la tolérance ϵ est réduite. [4] Autrement, une solution de rechange doit être envisagée lorsque, fatalement, la tolérance voulue entraîne des exigences intenables en ressources physiques — temps de calcul, espace de mémoire, énergie. De plus, la brièveté du calcul est cruciale, vue la vulnérabilité des superpositions quantiques face à la décohérence. [5]

3. Un hamiltonien sur réseau est k-local lorsqu'il est k-corps et que ces corps doivent être géométriquement voisins pour qu'aie lieu l'interaction. Une théorie de champs est locale lorsque ses régularisations sur réseau sont locales. Bien que les interactions fondamentales soient locales, celles conçues dans les plateformes de calcul pourront être transmises par un intermédiaire entre des qubits distants. On ne conserve donc que la restriction sur le nombre k de corps interagissants.

4. Sans perte de généralité, on peut poser que U est de déterminant 1, la phase globale du système étant inobservable.

5. Le calcul tolérant aux défaillances (*fault-tolerant*) surmonte cette limitation au prix de défis techniques considérables.

Un important théorème, dû indépendamment à Robert M. Solovay (manuscrit de 1995 non publié) et Alexei Kitaev [172], montre que pour N fixe, le nombre $\ell(\epsilon)$ d'opérations universelles requises pour simuler un quelconque $U \in \mathbf{SU}(2^N)$ avec une tolérance ϵ est borné polylogarithmiquement en $1/\epsilon$:

Théorème 1.1 (Solovay-Kitaev)**.** *Si $\mathbb{V}$ est universel pour N qubits, alors pour tout $\epsilon > 0$ il existe un entier $\ell(\epsilon) = O(\log^c(1/\epsilon))$ tel que toute matrice spéciale unitaire $U \in \mathbf{SU}(2^N)$ peut être approchée par une séquence d'éléments de $\mathbb{V}$ de longueur inférieure à $\ell(\epsilon)$, avec une erreur inférieure à ϵ. (La valeur de c dépend de l'algorithme utilisé, avec $c \approx 3.97$ pour la variante standard. L'optimum théorique $c = 1$ est réalisé par certaines variantes avec ou sans qubits auxiliaires [174, 246].)*

Une conséquence immédiate du théorème de Solovay-Kitaev est l'équivalence computationnelle des ensembles universels : la simulation d'un ensemble N-universel $\mathbb{V}$ par un autre ensemble N-universel $\tilde{\mathbb{V}}$ est une tâche de complexité sous-polynomiale, et peut donc être effectuée au prix de ressources supplémentaires (*overhead*) somme toute raisonnables. (Nous y reviendrons à la section 1.4.) L'importance pratique de cette équivalence est la possibilité de simuler l'ensemble universel souhaité, par exemple un ensemble pour lequel existe une construction tolérante aux défaillances (*fault-tolerant*), à l'aide des interactions disponibles dans une implémentation physique donnée, pour peu qu'elles soient elles-mêmes universelles.

Il faut toutefois se garder de conclure qu'il est facile de simuler un opérateur unitaire en général. Le théorème de Solovay-Kitaev affirme que, *pour N fixe*, la taille du circuit satisfait

$$\ell_N(\epsilon) \leq K_N \log^c(1/\epsilon), \tag{1.7}$$

pour une constante positive K_N et ϵ suffisamment petit. Or, K_N diverge rapidement avec N. Un argument de dénombrement permet en effet de montrer qu'un ensemble N-universel à k corps, où $k \ll N$, requerra au moins

$$\text{constante} \times \frac{2^N}{\log N} \log(1/\epsilon) \tag{1.8}$$

opérations pour approcher certaines matrices $U \in \mathbf{SU}(2^N)$ à ϵ près [209]. De tels opérateurs sont intrinsèquement difficiles à simuler : la difficulté ne provient pas de l'ensemble universel choisi puisque, par Solovay-Kitaev, l'utilisation d'un autre ensemble universel à k corps ne permettrait d'épargner que $K_k \log^c(1/\epsilon)$ opérations, tout au plus. La recherche d'opérateurs utiles et faciles à simuler constitue un aspect important de la conception d'algorithmes quantiques, dont nous ne discuterons que très brièvement dans la prochaine section.

1.4 Complexité computationnelle et efficience

La thèse de Church-Turing, que sept décennies de recherche n'ont pas démentie, avance que *tout problème pouvant être résolu par la méthode algorithmique est à la portée d'une machine (classique) de Turing.* Ajoutons à l'appui de cette thèse qu'un problème est résoluble à l'aide d'un calculateur quantique si et seulement s'il est

résoluble par une machine de Turing.[6] Ainsi, à tout problème algorithmiquement résoluble semble correspondre au moins un opérateur unitaire qui le résout sur un calculateur quantique. Pour un problème $\mathcal{P}$ donné, la question se pose alors de savoir si, pour tout $N \in \mathbb{N}$, le problème $\mathcal{P}_N$ à N qubits d'entrée peut être résolu par une matrice unitaire U_N *qui soit facile à simuler* sur un circuit k-corps.

Définition 1.2. *On dira que le problème $\mathcal{P}$ peut être résolu en temps polynomial par un calculateur quantique si, pour tout $N \in \mathbb{N}$,*

1. *il existe un opérateur U_N qui résout $\mathcal{P}_N$ avec une probabilité d'erreur inférieure ou égale à $1/3$,*[7]
2. *U_N peut être simulé avec une erreur inférieure à ϵ par un circuit k-corps de taille*
$$\ell_N(\epsilon) = O(N^g \log^c(1/\epsilon)), \tag{1.9}$$
où $k, g \in \mathbb{N}$ sont fixes, et où c est la constante du théorème de Solovay-Kitaev.[8]

Parce qu'ils exigent des ressources bornées polynomialement en N, les opérateurs U_N sont beaucoup plus faciles à simuler qu'un opérateur unitaire générique, tel qu'expliqué à la section 1.3. Il est convenu de considérer qu'un problème peut être résolu *efficacement* lorsqu'il appartient à l'une des nombreuses classes de complexité computationnelle à temps polynomial, dont voici les plus importantes :

1. **P** est la classe des problèmes de décision solubles en temps polynomial sur une machine classique déterministe.
2. **BPP** est la classe des problèmes de décision solubles en temps polynomial sur une machine classique non déterministe avec probabilité d'erreur $\leq 1/3$.
3. **BQP** est la classe des problèmes de décision solubles en temps polynomial sur une machine quantique avec probabilité d'erreur $\leq 1/3$.

On a vu qu'un ensemble N-universel simule efficacement tout autre ensemble N-universel (Solovay-Kitaev). De même, les différents modèles de calculateurs quantiques universels mentionnés à la section 1.1 se simulent efficacement les uns les autres [32, 228, 6]. Quant aux possibilités de simulations efficaces entre calculateurs classiques et calculateurs quantiques, nous avons le théorème suivant.

Théorème 1.2. *Pour chacune des inclusions suivantes, il n'est pas connu à ce jour s'il s'agit d'une inclusion propre ou d'une égalité :*

$$\mathbf{P} \subseteq \mathbf{BPP} \subseteq \mathbf{BQP}.$$

6. Les circuits classiques, équivalents aux machines de Turing, peuvent être rendus réversibles, leurs opérations devenant de simples permutations qu'on peut identifier aux opérations unitaires d'un circuit quantique. Réciproquement, les amplitudes d'un circuit quantique comportant m opérations k-corps peuvent être calculées classiquement en insérant des relations de complétude entre les opérations et en sommant sur les $O(2^{km})$ parcours résultants.

7. La borne supérieure $q = 1/3$ est conventionnelle et peut être remplacée par n'importe quelle borne $q \in (0, 1/2)$.

8. Techniquement, il convient aussi d'exiger que les circuits $\tilde{U}_N$ qui simuleront les U_N soient *uniformément générés en temps polynomial*, c'est-à-dire qu'une machine de Turing soit en mesure de les identifier en un temps $O(N^\gamma)$, pour $\gamma \in \mathbb{N}$.

Il y a tout lieu de croire, cependant, que **BPP** n'égale pas **BQP**, car cette dernière contient plusieurs problèmes qui résistent depuis longtemps à toute tentative de résolution classique efficace, le plus connu étant le problème de la factorisation première d'un entier M. [9] L'algorithme quantique de Shor [250] donne la solution en $O(N^3)$ étapes, où $N \sim \log M$ est le nombre de bits requis pour représenter M. Pour l'heure, le meilleur algorithme classique requiert en revanche un temps super-polynomial $O(e^{cN^{1/3}})$, où $c \approx 2$. Parmi les problèmes appartenant à **BQP**, mais soupçonnés d'être hors de **BPP**, mentionnons également le calcul des logarithmes discrets [250], l'identification des solutions entières de l'équation de Pell [132], et le problème de l'idéal principal [132]. Ces problèmes de classes cachées (*hidden cosets*) exploitent la capacité de la transformée de Fourier à révéler efficacement des structures de sous-groupes telles que la périodicité et le décalage (*shift*) [268]. D'ailleurs, la transformée de Fourier est peut-être ce qui distingue essentiellement le calcul classique (déterministe) du calcul quantique : il suffit d'augmenter la porte de Toffoli T, universelle pour le calcul classique, par la porte d'Hadamard H (i.e. la transformée de Fourier sur $\mathbb{Z}_2$) pour obtenir l'universalité quantique [247, 7]. [10] Une autre direction de recherche démontre, preuve à l'appui cette fois, la supériorité du traitement quantique de l'information : la théorie de la complexité de communication. [11] Il est démontré que les protocoles quantiques de communication sont exponentiellement plus rapides que les protocoles classiques non-déterministes pour résoudre certains problèmes de communication [229, 112]. On connait également des problèmes pouvant être résolus par des protocoles quantiques bornés spatialement et nécessitant exponentiellement moins d'espace-mémoire que tout algorithme classique borné spatialement [186]. Ces avancées seront capitales pour le traitement quantique de l'information distribuée en réseau.

9. Le problème de décision correspondant consiste à déterminer si l'entier M possède un facteur premier inférieur à $\sqrt{M}$. Puisque la division longue peut être effectuée efficacement (sur une machine classique), le problème de factorisation est polynomial si et seulement le problème de décision correspondant l'est également.

10. Puisque T et H sont des matrices réelles, elles ne peuvent constituer un ensemble *strictement* universel tel que défini à la Définition 1.1. Il est toutefois possible de simuler un circuit quantique à l'aide de matrices réelles en ajoutant un qubit auxiliaire, $|x\rangle \to |x, \xi\rangle$, où $|\xi\rangle$ indique si l'on a affaire à la partie réelle ou imaginaire de l'état du système [37]. Un opérateur complexe U est simulé par l'opérateur réel $\tilde{U}$ défini comme suit :

$$\tilde{U}|x,0\rangle = |(\mathrm{Re}\ U)x, 0\rangle + |(\mathrm{Im}\ U)x, 1\rangle \quad , \quad \tilde{U}|x,1\rangle = -|(\mathrm{Im}\ U)x, 0\rangle + |(\mathrm{Re}\ U)x, 1\rangle.$$

La simulation n'entraîne qu'un coût sous-polynomial (un seul qubit additionnel, ainsi qu'un nombre constant d'opérations additionnelles pour chaque U). L'ensemble $\{\mathsf{T}, \mathsf{H}\}$, sans être strictement universel, possède ainsi une forme efficace d'univeralité appelée *universalité computationelle* [7].

11. Un problème de complexité de communication [290, 165, 75] est la donnée d'un sous-ensemble $\mathcal{R} \subset X \times Y \times Z$, où X, Y, Z sont des ensembles finis et non nuls. Alice se voit attribuée secrètement $x \in X$, tandis que Bob reçoit secrètement $y \in Y$. Le problème consiste pour Alice et Bob à collaborer afin de trouver $z \in Z$ tel que $(x, y, z) \in \mathcal{R}$. La complexité de communication est le nombre de (qu)bits d'information qu'ils doivent échanger, dans le pire des cas, pour mener la tâche à bien, munis d'une puissance de calcul illimitée. Pour certains problèmes, l'espace-mémoire disponible est limité.

Chapitre 2

Premier article.

High-fidelity universal quantum computation with symmetric qubit clusters

par

Christian Boudreault[1,2], Hichem Eleuch[3,4], Michael Hilke[5], Richard MacKenzie[2]

[(1)]Département des sciences de la nature, Collège militaire royal de Saint-Jean, Saint-Jean-sur-Richelieu, QC, Canada, J3B 8R8

[(2)]Département de physique, Université de Montréal, C.P. 6128, succursale Centre-ville, Montréal, QC, Canada, H3C 3J7

[(3)]Department of Applied Physics and Astronomy, University of Sharjah, Sharjah, United Arab Emirates

[(4)]College of Arts and Sciences, Abu Dhabi University, Abu Dhabi 59911, United Arab Emirates

[(5)]Department of Physics, McGill University, Montréal, QC, Canada, H3A 2T8

Cet article a été soumis pour publication dans Physical Review A.

Contribution du candidat et des coauteurs :
Christian Boudreault a contribué à la conceptualisation, a effectué la majorité des calculs et a rédigé l'essentiel de l'article. Hichem Eleuch et Michael Hilke ont contribué à la conceptualisation et à la mise en forme définitive de l'article. Richard MacKenzie a supervisé le projet, contribué à sa conceptualisation et participé à la mise en forme définitive de l'article.

Résumé. L'un des obstacles les plus difficiles à surmonter pour la réalisation d'un ordinateur quantique évolutif est la mise au point d'un système physique assurant un faible taux d'erreur sur chaque opération de traitement d'information. Ces erreurs peuvent avoir pour origine la précision des manipulation quantiques, tel que le *sweeping of a gate voltage* pour les qubits en état solide, ou la durée d'une impulsion laser dans les plateformes optiques. Les erreurs résultent également de la décohérence, souvent considérée plus fondamentale car inhérente au couplage du système quantique avec son environnement. Réunir les qubits en petits groupes au sein d'agrégats possédant une symétrie pourrait servir à protéger de la décohérence une partie des opérations de calcul. Dans ce qui suit, nous utilisons des agrégats à 4 niveaux possédant une généralisation simple de la symétrie sous les rotations discrètes, nommée invariance sous les ω-rotations, afin d'encoder des paires de qubits et des opérations universelles à 2 qubits. Nous considérons les erreurs quantiques comme une source principale de décohérence et montrons que la symétrie rend les opérations particulièrement résilientes aux rotations intempestives anisotropes de qubits. Nous proposons un patron pour le calcul quantique universel et évolutif dans lequel les agrégats tiennent lieu de transistors quantiques, ou *quansistors*. L'initialisation et la mesure sont effectuées en couplant par effet tunnel les quansistors à des chaînes conductrices. Ces chaînes sont considérées explicitement et l'on suppose qu'elles constituent l'autre source principale de décohérence. Parce que les quansistors peuvent être dynamiquement découplés des chaînes en ajustant leurs paramètres internes, ils sont à même de servir d'unités contrôlables de mémoire quantique. Le découplage dynamique protège également les opérations logiques internes aux quansistors du bruit de biais nul dans leurs paramètres. Nous identifions des technologies qui pourraient implémenter l'invariance sous les ω-rotations. Plusieurs résultats peuvent être généralisés à des systèmes à plus de 4 niveaux invariants sous les ω-rotations, ou adaptées à des agrégats possédant d'autres symétries.
Mots-clés : Calcul quantique universel évolutif, haute fidélité, protection par symétrie, implémentation physique, alphabets supérieurs

Abstract. One of the most challenging problems for the realization of a scalable quantum computer is to design a physical device that keeps the error rate for each quantum processing operation low. These errors can originate from the accuracy of quantum manipulation, such as the sweeping of a gate voltage in solid state qubits or the duration of a laser pulse in optical schemes. Errors also result from decoherence, which is often regarded as more crucial in the sense that it is inherent to the quantum system, being fundamentally a consequence of the coupling to the external environment. Grouping small collections of qubits into clusters with symmetries may serve to protect parts of the calculation from decoherence. In this work, we use 4-level cores with a straightforward generalization of discrete rotational symmetry, called ω-rotation invariance, to encode pairs of coupled qubits and universal 2-qubit logical gates. We include quantum errors as a main source of decoherence, and show that symmetry makes logical operations particularly resilient to untimely anisotropic qubit rotations. We propose a scalable scheme for universal quantum computation where cores play the role of quantum-computational transistors, or *quansistors* for short. Initialization and readout are achieved by tunnel-coupling the quansistor to leads. The external leads are explicitly considered and are assumed to be the other main source of decoherence. We show that quansistors can be dynamically decoupled from the leads by tuning their internal parameters,

giving them the versatility required to act as controllable quantum memory units. With this dynamical decoupling, logical operations within quansistors are also symmetry-protected from unbiased noise in their parameters. We identify technologies that could implement ω-rotation invariance. Many of our results can be generalized to higher-level ω-rotation-invariant systems, or adapted to clusters with other symmetries.
Keywords : Scalable universal quantum computation, high fidelity, symmetry protection, physical implementation, higher alphabets

2.1 Introduction

Quantum information theory has become a mature field of research over the last three decades, equipped with its own objectives towards quantum computation and communication [209], as well as quantum simulation [15], while at the same time allowing entirely novel perspectives on other established fields, in particular an algorithmic approach to quantum systems, a structure-of-entanglement characterization of large classes of many-body quantum states (matrix product states, tensor networks) [296], and quantum-enhanced measurements reaching the Heisenberg precision limit (quantum metrology) [118].

Quantum information processing departed from its classical counterpart with the proof that two-qubit gates [230, 93, 30] can simulate arbitrary unitary matrices, followed by the identification of 'simple' quantum universal sets like single-qubit gates with CNOT [31], and *finite* quantum universal sets like Toffoli with Hadamard and $\frac{\pi}{4}$-gate [172], or SWAP with *almost any* two-qubit gate [88, 190]. The deep theorem of Solovay and Kitaev showed that it is possible to translate between strictly universal sets with at most polylogarithmic overhead [172, 209]. Alongside strict universality, encoded universality [24, 168] and computational universality [7] allow even more systems to qualify as universal quantum computers.

Circumstantial evidence suggests that quantum computers might achieve super-polynomial speedups over probabilistic classical ones. Lloyd's universal quantum simulator and Shor's algorithms for integer factorization and for discrete logarithms are prominent examples of efficient quantum solutions for problems suspected to be not computable in polynomial time classically [250, 191]. Quantum communication protocols are provably exponentially faster than classical-probabilistic ones for specific communication complexity problems [229, 112], and there exist problems that space-bounded quantum algorithms can solve using exponentially less work space than any classical algorithm [186]. Nonetheless, large classes of quantum tasks involving highly entangled states are efficiently simulatable classically. Quantum teleportation, superdense coding and computation using only Hadamard, CNOT, and measurements fall into this category according to the Gottesman-Knill theorem [120, 209]. Fermionic linear optics with measurements, and more generally matchgate computation, are also known to be classically simulatable in polynomial time [266, 264, 175]. (This is in contrast to universal bosonic linear optics with measurements [176] and universal fermionic *nonlinear* optics with measurements [50]. The computationally relevant difference between particle-number-preserving fermions and bosons being the easy task of computing a (Slater) determinant versus the hard task (♯P-complete) of com-

puting a permanent [267].)

The physical realization of quantum computers and quantum communication channels is a major endeavor. Most building blocks of quantum computers are based on qubits, which are quantum two-level systems. They form the unit cells that allow us to exploit the potential of quantum information processing, when many of these qubits are coherently coupled and manipulated so as to perform various coherent quantum operations. While many different types of qubits have been developed, such as semiconductor technologies in quantum dots [193], including silicon [301, 277], or GaAs [188], in superconducting technologies [207, 90], in all-optical technologies [211], and in hybrid technologies such as ion traps [44], cold atoms and nitrogen-vacancy centers in diamond [292] that require quantum systems and a laser for control. Topological technologies can also form the basis of qubits [208], though their experimental realization is much harder. These technologies all share the same basic principle of operating as a quantum two level system.

In this work we explore a quantum processing unit based on a four-level system. While there have been some earlier works on such higher-level systems, including multilevel superconducting circuits as single qu$d$its and two-qubit gates [170, 171], here we consider a special four-level system with ω-rotation invariance as discussed below to address one of the biggest challenges in quantum information processing.

Indeed, one of the biggest obstructions for a competitive quantum computation is to keep the error rate low for each quantum operation [121]. These errors can stem from the precision of the quantum manipulation, like the sweeping of a gate voltage in solid state qubits or the duration of a laser pulse in optical schemes [240]. In addition, there are errors due to decoherence [249]. These are often considered more fundamental in the sense that they don't depend on the precision of the instrumentation but are intrinsic to the quantum system considered. They are a reflection of the coupling to the outside environment. Sources of decoherence can be leads, nuclear spins, optical absorption, phonons, and non-linearities. Most of these environments fall into the category of fermionic or bosonic baths [218, 157].

In our basic quantum information unit, based on a four-level system, untimely single-qubit and double-qubit unitaries will correspond to environment-induced logical errors. We will also consider the effect of external leads as the other main source of decoherence. Indeed, in solid-state-based qubits electric leads are often the main source of decoherence, particularly in superconducting qubits and semiconductor quantum dots [197]. While our model is not limited to a particular implementation, we will use the coupled quantum dot geometry as an illustration of our quantum processor unit.

Note that in the present work, we do not aim at a complete benchmarking of our system. Our goal is much more modest as we consider only fidelity of two-qubit gates. In particular, we do not discuss fault tolerance in depth, except for a few opening words in the Discussion.

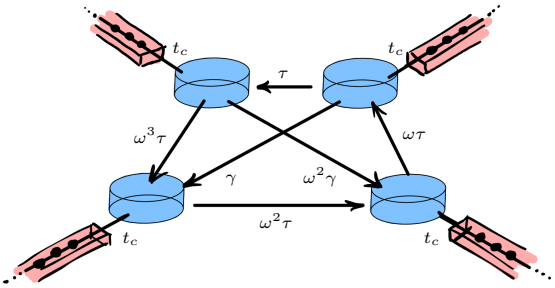

FIGURE 2.1 – (Color online) Depiction of the model, consisting of a 4-site core system (disks and dark arrows) tunnel-coupled to four identical semi-infinite leads (rectangular boxes). The core system is ω-rotation-invariant (see Section 2.3) for any $\omega^4 = 1$. The tunable parameters are $\epsilon, \gamma \in \mathbb{R}$ and $\tau \in \mathbb{C}$. The hopping parameters linking the sites are generally complex. The coupling constants between the core's sites and the leads are equal to t_c. All hopping amplitudes along the leads are set to unity.

2.2 Preliminaries

Let us consider first a physical system formed by a core of four coupled quantum dots with on-site energies ϵ_i. Each quantum dot interacts with all the other dots via complex couplings (we will discuss in section 2.3.6 how it is possible to realize complex couplings physically). The corresponding isolated Hamiltonian is

$$H_{\text{core}} = \frac{1}{2}\sum_{i=1}^{4} \epsilon_i a_i^\dagger a_i + \frac{1}{2}\sum_{i,j=1}^{4} h_{ij} a_i^\dagger a_j + \text{h.c.} \tag{2.1}$$

Each dot is now made to interact with a semi-infinite chain consisting of a semi-infinite hopping Hamiltonian with hopping parameter set to unity (thus setting the scale for all energies). The leads have scattering eigenstates with energies $-2 < E < 2$. Tunnel couplings between dot and chain are initially all identical and are chosen real, positive and small ($0 < t_c \ll 1$). As in the case of double- and triple-dots, the Feshbach projector method shows that the effect of each lead is to modify the self-energies of the dots. In this work, we will study a similar core system formed by 4 sites (though not necessarily quantum dots) tunnel-coupled to semi-infinite leads, but *with a crucial additional core symmetry.*

Specifically, we will consider the single-particle sector of a class of tunable systems possessing a simple geometric symmetry, dubbed ω-*rotation invariance*, to be defined in the next section. A diagram of the model used throughout the paper is displayed in Fig. 2.1. It consists of a completely connected 4-site core system tunnel-coupled to four identical semi-infinite leads (a simple physical example being four quantum

dots tunnel-coupled to semi-infinite leads). The Hamiltonian is

$$\begin{aligned}\mathcal{H} &= \mathcal{H}_{\text{core}} + \mathcal{H}_{\text{int}} + \mathcal{H}_{\text{lead}} \\ &= \frac{1}{2}\sum_{i,j=1}^{4} h_{ij} a_i^\dagger a_j + t_c \sum_{i=1}^{4} a_i^\dagger b_{i,1} + \sum_{i=1}^{4}\sum_{j=1}^{\infty} b_{i,j}^\dagger b_{i,j+1} + \text{ h.c.}\end{aligned} \tag{2.2}$$

restricted to the single-particle sector of Hilbert space. The core couplings h_{ij} are chosen to satisfy relationships ensuring ω-rotation invariance (see Section 2.3). The coupling between site i and lead i is t_c, which can be taken real and positive without loss of generality. The Hamiltonian has been normalized such that the hopping parameter within the semi-infinite chains is unity. The operators a_i and $b_{i,j}$ are annihilation operators, acting respectively on site i of the core system, and on site j of the i-th lead. Since we work in the single-particle sector, these operators could be fermionic or bosonic. (An example of each would be a single electron and a Cooper pair, respectively. Cold atoms can realize either choice.) Our choice of a 4-level core is motivated by our desire to describe two coupled qubits. The four semi-infinite leads simulate individual contact with the environment and enable us to reveal selective protection from decoherence. Most of our results can be generalized to an arbitrary number of sites in the core system with corresponding identical leads. The required modifications will be discussed briefly in the Discussion and in the Appendices.

2.2.1 Outline of the paper

In Section 2.3 we focus on the core system. We define ω-rotation invariance as an obvious generalization of discrete rotation invariance, and show that the tunable parameters of an ω-rotation-invariant system give full control over its eigenenergies while the energy eigenstates remain fixed. Independent control over the energy levels will be used frequently and is the main motivation for implementing ω-rotation invariance. Systems with this symmetry could be realized by applying the technique of synthetic gauge fields on a tight-binding Hamiltonian [14]. Selecting a representative from two distinct ω-classes and following the scheme of Deutsch et al. [88], we show that our 4-level core system is strictly universal for quantum computation. We then consider one possible two-qubit logical basis and discuss single-pulse logical gates as well as symmetry protection against errors, and qubit initialization and readout.

In Section 2.4 we consider the effect of the four identical leads on the core. The effective Hamiltonian of the core will in general be non-Hermitian but will remain ω-rotation-invariant, and as a consequence will still allow independent energy tuning. Our ability to fully control the (potentially complex) eigenenergies will result in the possibility of transmitting an eigenstate through the leads or else of protecting it from decoherence, independently of the other eigenstates. In that sense, the 4-level core may be used as a two-qubit quantum memory unit.

Finally, in Section 2.5 we propose a scalable scheme for universal quantum computation based on 4-level cores as the elementary computational units. The number of cores required scales linearly in the number of qubits. Because cores play a role similar to that of transistors in classical computation, we propose to call them quantum-computational transistors, or more succinctly *quansistors*.

Rotation-invariant (circulant) 4×4 Hamiltonians have recently been advocated [160] as a way to implement the adiabatic Fourier transform on two qubits, with gate fidelities and entanglement benefitting from a symmetry that protects against decoherence. The proposal includes a possible physical implementation of circulant symmetry by tuning spin-spin interactions in ion traps. Although our work also utilizes (generalized) circulant symmetry for protection against decoherence, the aim and scope of the present article are somewhat different. We put forward a blueprint for scalable universal quantum computation based on symmetry-protected qubit clusters, with ω-rotation invariance standing out as the prototype of a symmetry which is provably universal, and realistically implementable physically on a variety of platforms.

2.3 Core system

For a 4×4 matrix, we make a slight generalization of the notion of discrete rotational invariance (which can also be viewed as cyclic permutation of the sites) to ω-*rotation invariance* : M is ω-rotation-invariant if

$$J_\omega^\dagger M J_\omega = M \quad , \quad \omega^4 = 1, \tag{2.3}$$

with a modified shift matrix

$$J_\omega = \begin{pmatrix} 0 & 1 & 0 & 0 \\ 0 & 0 & \omega & 0 \\ 0 & 0 & 0 & \omega^2 \\ \omega^3 & 0 & 0 & 0 \end{pmatrix} \quad , \quad J_\omega^4 = \omega^2 \mathbb{1}. \tag{2.4}$$

Rotational invariance obviously corresponds to $\omega = 1$. The matrices J_1 and $J_{e^{i\pi/2}}$, and their higher dimensional versions, have been discussed in discrete quantum mechanics under the name of Weyl's X and Y matrices, and in quantum information under the name of generalized Pauli X and Y matrices (see Appendix 2.8.1). In the 4×4 case we have

$$\begin{aligned} X &= \begin{pmatrix} 0 & 1 & 0 & 0 \\ 0 & 0 & 1 & 0 \\ 0 & 0 & 0 & 1 \\ 1 & 0 & 0 & 0 \end{pmatrix} = J_1 \quad , \quad Z = \begin{pmatrix} 1 & 0 & 0 & 0 \\ 0 & i & 0 & 0 \\ 0 & 0 & i^2 & 0 \\ 0 & 0 & 0 & i^3 \end{pmatrix} \\ Y &= ZX = J_{e^{i\pi/2}}. \end{aligned} \tag{2.5}$$

(Note that the matrix X is sometimes called $X^\dagger$ in the literature.) Just as rotation-invariant matrices are precisely circulant matrices, ω-rotation-invariant matrices correspond to ω-*circulant* matrices :

$$\omega\mathrm{Circ}(z_0, \ldots, z_3) = \sum_{s=0}^{3} z_s J_\omega^s, \tag{2.6}$$

with $z_s \in \mathbb{C}$. The terms 'ω-rotation-invariant' and 'ω-circulant' will be used interchangeably. For Hermitian ω-circulant 4×4 matrices the number of independent *real*

parameters is reduced to four. Such matrices constitute what we propose to call a *flat class* : mutually commuting matrices $\{H(\mathbf{g}) \mid \mathbf{g} \in \mathbb{R}^4\}$ with common eigenbasis independent of $\mathbf{g}$, and real eigenvalues $\lambda_1(\mathbf{g}), \ldots, \lambda_4(\mathbf{g})$ in one-to-one correspondence with the values of the parameters $\mathbf{g} \in \mathbb{R}^4$. Each fourth root of unity ω corresponds to a flat class. (See Appendix 2.8.1 for details.)

We consider 4-level cores with the ability to take a nonsymmetric form (the *off mode*), and a symmetric form (the *computational mode*). In the off mode, the Hamiltonian is almost diagonal in the single-particle position eigenbasis :

$$H_{\text{off}} = -\sum_{\langle ij \rangle} K_{ij} a_i^\dagger a_j + \sum_i \epsilon_i a_i^\dagger a_i, \tag{2.7}$$

where large energy offsets $|\epsilon_i - \epsilon_j| \gg K_{ij} > 0$ effectively suppress spontaneous transitions. The logical states $\{|00\rangle, |01\rangle, |10\rangle, |11\rangle\}$ are naturally chosen to coincide with the position basis eigenstates $\{|m\rangle\}_{m=1,\ldots,4}$. We will come back to this mode later.

In the computational mode, the core system is ω-rotation-invariant in the position basis for all values of its parameters. The matrix of core couplings $\{h_{ij}\}$ in (2.2) will thus form a class of Hermitian ω-circulant Hamiltonian matrices

$$H^{\text{pos}}(\mathbf{g}, \omega) = \sum_{s=0}^{3} z_s(\mathbf{g}) J_\omega^s, \tag{2.8}$$

with $z_s \in \mathbb{C}$, $\mathbf{g} \in \mathbb{R}^4$, and $\omega^4 = 1$. (Recall that the complex coefficients z_s are constrained by Hermiticity $H^{\text{pos}} = (H^{\text{pos}})^\dagger$, leaving only four real independent parameters $\mathbf{g}$.) For each $q = 0, \ldots, 3$ the class $\omega = e^{iq\pi/2}$ is flat and diagonalized by a modified quantum Fourier transform $\mathcal{F}\mathcal{D}^q$, where $\mathcal{F}$ is the regular quantum Fourier transform

$$\mathcal{F}_{k,m} = \frac{1}{2} e^{-imk(\pi/2)}, \tag{2.9}$$

and

$$\mathcal{D} = \text{diag}(e^{-i\pi/4}, 1, -e^{-i\pi/4}, 1). \tag{2.10}$$

The eigenstates are

$$|\varphi_k^q\rangle = \sum_m (\mathcal{F}\mathcal{D}^q)_{m,k}^\dagger |m\rangle = \frac{1}{2} \sum_m (\mathcal{D}_{m,m}^\dagger)^q e^{imk(\pi/2)} |m\rangle \tag{2.11}$$

for $q, k = 0, \ldots, 3$. Note that the first index of a matrix corresponds to a dual vector component, whereas the second index corresponds to a vector component :

$$\langle m|\varphi_k^q\rangle = (\mathcal{F}\mathcal{D}^q)_{m,k}^\dagger, \quad \langle \varphi_k^q | m\rangle = (\mathcal{F}\mathcal{D}^q)_{k,m}. \tag{2.12}$$

For the purpose of universal quantum computation, two classes of ω-circulant Hamiltonians are necessary and sufficient : for instance, the class X of circulant Hamiltonians ($\omega = 1$), and the class Y of i-circulant Hamiltonians ($\omega = e^{i\pi/2}$). In Section 2.3.3 we will build a universal set comprising only *one* Hamiltonian from each class. We will now consider each of these classes in turn.

2.3.1 Symmetry class X ($\omega = 1$)

Class X is rotation-invariant in the position eigenbasis :

$$H^{\rm pos}(\mathbf{g}, 1) = \sum_{s=0}^{3} z_s(\mathbf{g}) X^s \quad (z_s \in \mathbb{C}, \mathbf{g} \in \mathbb{R}^4). \tag{2.13}$$

The most general form of the Hamiltonian matrix is

$$H^{\rm pos}(\mathbf{g}, 1) = \begin{bmatrix} \epsilon & \tau & \gamma & \tau^\dagger \\ \tau^\dagger & \epsilon & \tau & \gamma \\ \gamma & \tau^\dagger & \epsilon & \tau \\ \tau & \gamma & \tau^\dagger & \epsilon \end{bmatrix} \tag{2.14}$$

with $\epsilon, \gamma \in \mathbb{R}$ and $\tau = |\tau| e^{i\theta} = \alpha + i\beta$ giving the four real parameters embodied in $\mathbf{g}$. For any value of $\mathbf{g}$ the normalized eigenstates of $H^{\rm pos}(\mathbf{g}, 1)$ are

$$|\phi_k\rangle = \sum_m \mathcal{F}^\dagger_{m,k} |m\rangle = \frac{1}{2} \sum_m e^{imk(\pi/2)} |m\rangle \tag{2.15}$$

for $k = 1, \ldots, 4$, with eigenenergies

$$\lambda_k = \epsilon + 2|\tau| \cos(\theta + \tfrac{k\pi}{2}) + (-1)^k \gamma \tag{2.16}$$

or

$$\begin{array}{rclccccccl} \lambda_1 &=& \epsilon & & & - & 2\beta & - & \gamma, \\ \lambda_2 &=& \epsilon & - & 2\alpha & & & + & \gamma, \\ \lambda_3 &=& \epsilon & & & + & 2\beta & - & \gamma, \\ \lambda_4 &=& \epsilon & + & 2\alpha & & & + & \gamma. \end{array} \tag{2.17}$$

These can be inverted, giving

$$\begin{array}{rclccccccl} \epsilon &=& \frac{\lambda_1}{4} & + & \frac{\lambda_2}{4} & + & \frac{\lambda_3}{4} & + & \frac{\lambda_4}{4}, \\ \alpha &=& & - & \frac{\lambda_2}{4} & & & + & \frac{\lambda_4}{4}, \\ \beta &=& -\frac{\lambda_1}{4} & & & + & \frac{\lambda_3}{4} & & , \\ \gamma &=& -\frac{\lambda_1}{4} & + & \frac{\lambda_2}{4} & - & \frac{\lambda_3}{4} & + & \frac{\lambda_4}{4}. \end{array} \tag{2.18}$$

Any path in energy space $(\lambda_1, \lambda_2, \lambda_3, \lambda_4)$ corresponds to a unique path in parameter space $(\epsilon, \alpha, \beta, \gamma)$, giving full control over the energy levels of the class.

2.3.2 Symmetry class Y ($\omega = e^{i\pi/2}$)

Class Y is $e^{i\pi/2}$-rotation-invariant in the position eigenbasis :

$$H^{\rm pos}(\mathbf{g}, e^{i\pi/2}) = \sum_{s=0}^{3} z_s(\mathbf{g}) Y^s \quad (z_s \in \mathbb{C}, \mathbf{g} \in \mathbb{R}^4). \tag{2.19}$$

The most general form of the Hamiltonian is

$$H^{\rm pos}(\mathbf{g}, e^{i\pi/2}) = \begin{bmatrix} \epsilon & \tau & -\gamma & i\tau^\dagger \\ \tau^\dagger & \epsilon & i\tau & \gamma \\ -\gamma & -i\tau^\dagger & \epsilon & -\tau \\ -i\tau & \gamma & -\tau^\dagger & \epsilon \end{bmatrix} \tag{2.20}$$

where the parameters $\epsilon, \gamma \in \mathbb{R}$ and $\tau \in \mathbb{C}$ are chosen to have exactly the same form as those of (2.14). The entries in class X and Y are seen to differ by at most a prefactor. For any value of $\mathbf{g}$ the normalized eigenstates of $H^{\rm pos}(\mathbf{g}, e^{i\pi/2})$ are

$$|\chi_k\rangle = \sum_m (\mathcal{F}\mathcal{D})^\dagger_{m,k} |m\rangle = \frac{1}{2} \sum_m \mathcal{D}^\dagger_{m,m} e^{imk(\pi/2)} |m\rangle \tag{2.21}$$

for $k = 1, \ldots, 4$, where the coefficients $\mathcal{D}^\dagger_{m,m}$ are given in Eq. (2.10). The eigenenergies are

$$\begin{array}{rclccccl} \lambda'_1 &=& \epsilon &+& \sqrt{2}\alpha &-& \sqrt{2}\beta &-\ \gamma, \\ \lambda'_2 &=& \epsilon &-& \sqrt{2}\alpha &-& \sqrt{2}\beta &+\ \gamma, \\ \lambda'_3 &=& \epsilon &-& \sqrt{2}\alpha &+& \sqrt{2}\beta &-\ \gamma, \\ \lambda'_4 &=& \epsilon &+& \sqrt{2}\alpha &+& \sqrt{2}\beta &+\ \gamma, \end{array} \tag{2.22}$$

which can be inverted, giving

$$\begin{array}{rclccccl} \epsilon &=& \frac{\lambda'_1}{4} &+& \frac{\lambda'_2}{4} &+& \frac{\lambda'_3}{4} &+\ \frac{\lambda'_4}{4}, \\ \alpha &=& \frac{\lambda'_1}{4\sqrt{2}} &-& \frac{\lambda'_2}{4\sqrt{2}} &-& \frac{\lambda'_3}{4\sqrt{2}} &+\ \frac{\lambda'_4}{4\sqrt{2}}, \\ \beta &=& -\frac{\lambda'_1}{4\sqrt{2}} &-& \frac{\lambda'_2}{4\sqrt{2}} &+& \frac{\lambda'_3}{4\sqrt{2}} &+\ \frac{\lambda'_4}{4\sqrt{2}}, \\ \gamma &=& -\frac{\lambda'_1}{4} &+& \frac{\lambda'_2}{4} &-& \frac{\lambda'_3}{4} &+\ \frac{\lambda'_4}{4}. \end{array} \tag{2.23}$$

Again, any path in energy space $(\lambda'_1, \lambda'_2, \lambda'_3, \lambda'_4)$ corresponds to a unique path in parameter space $(\epsilon, \alpha, \beta, \gamma)$, giving full control over the energy levels of the class.

Independent control over the energy levels will be used later and is a prime motivation for using ω-rotation invariance, but we stress that this choice of symmetry is not unique. (See Section 2.8.1 for details.) We can now distinguish four 'natural' bases for the system, namely the position basis $\{|m\rangle\}$, the energy bases $\{|\phi_k\rangle\}$ and $\{|\chi_k\rangle\}$, and the logical (or computational) basis $\{|00\rangle, |01\rangle, |10\rangle, |11\rangle\}$, defined by identification with the position eigenstates $|m\rangle$:

$$|\ell\rangle = \sum_{m=1}^{4} \mathbb{1}_{m,\ell} |m\rangle, \tag{2.24}$$

where the index ℓ of the identity matrix $\mathbb{1}$ runs over the *ordered* set $(00, 01, 10, 11)$. Our choice is motivated by simplicity, and by the proposal for quansistor interaction, to be discussed later. The universality result discussed in the next section is independent of this choice. Moreover, the Solovay-Kitaev theorem teaches us that simulating one universal set with another can be done in a fault-tolerant manner with polylogarithmic overhead, usually a quite acceptable cost. The four working bases $\{|m\rangle\}, \{|\phi_k\rangle\}, \{|\chi_k\rangle\}, \{|\ell\rangle\}$, and their relationships (2.15),(2.21),(2.24) are summarized in the commutative diagram of Fig. 2.2.

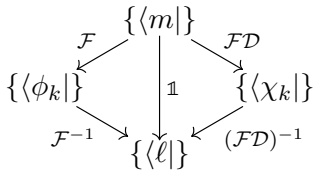

FIGURE 2.2 – (Color online) Commutative diagram of the four working dual bases and their relationships. **Top :** Position basis $\{\langle m|\}$. **Middle left :** Class X energy basis $\{\langle\phi_k|\}$. **Middle right :** Class Y energy basis $\{\langle\chi_k|\}$. **Bottom :** Logical basis $\{\langle\ell|\}$.

2.3.3 Strict universality on two qubits

The system $H^{\rm pos}(\mathbf{g},\omega)$ of (2.8), with ω equal to either 1 or $e^{i\pi/2}$, generates a strictly universal set of 2-qubit gates. In fact we prove the stronger result that the finite set $\{\mathsf{V},\mathsf{W}\}\subset\mathbf{U}(4)$ is strictly universal, where the unitaries V and W, defined below, belong to classes X and Y, respectively. (A word about notation : Sans-serif symbols, like V and W, will always denote logical gates, other more common examples being the π-phase shift Z, the qubit flip X or NOT, the Hadamard gate H, the swapping gate SWAP, and the controlled-not CNOT.) We use the scheme of Ref. [88] to prove our claim. We construct sixteen Hermitian 4×4 matrices $H_1,\ldots,H_{16}$ whose evolution unitaries are all within our *repertoire*, meaning that those unitaries can be approximated with arbitrary accuracy by repeatedly applying the gates V and W. The set $\{H_1,\ldots,H_{16}\}$ is linearly independent over $\mathbb{R}$ so it spans the 16-dimensional $\mathbb{R}$-space of Hermitian 4×4 matrices, which are evolved to generate all 4×4 unitaries. Our repertoire therefore coincides with $\mathbf{U}(4)$, or in other words, is strictly universal on two qubits.

We first define

$$\begin{aligned} H_1 &= \tfrac{1}{2}\mathbb{1} + (\pi+i)X + X^2 + \text{h.c.} \\ &= \begin{pmatrix} 1 & \pi+i & 2 & \pi-i \\ \pi-i & 1 & \pi+i & 2 \\ 2 & \pi-i & 1 & \pi+i \\ \pi+i & 2 & \pi-i & 1 \end{pmatrix}, \end{aligned} \tag{2.25}$$

and the unitary $\mathsf{V}=e^{-iH_1}$, both of class X. We also define

$$\tilde{H} = \tfrac{1}{2}\mathbb{1} + \pi(1+\tfrac{i}{4})Y + \text{h.c.} \tag{2.26}$$

and the unitary $\mathsf{W}=e^{-i\tilde{H}/\sqrt{2}}$, both of class Y. All unitaries of the form $\mathsf{V}^s=e^{-isH_1}$ for $s\in[0,2\pi)$ are in our repertoire, because integers mod 2π can be found arbitrarily close to s. The repertoire also comprises $\mathsf{WVW}^\dagger$, and more generally $\mathsf{WV}^s\mathsf{W}^\dagger$ for $s\in[0,2\pi)$, which are generated by the Hamiltonian

$$H_2 = \mathsf{W}H_1\mathsf{W}^\dagger. \tag{2.27}$$

(Note that whether or not H_2 can be obtained from the system's Hamiltonian is irrelevant. It is sufficient that the unitary $\mathsf{WV}^s\mathsf{W}^\dagger$ be in the repertoire for any s.)

We finally define

$$\begin{aligned} H_j &= i[H_1, H_{j-1}] \quad , \quad j = 3, \ldots, 14 \\ H_{15} &= i[H_2, H_3] \\ H_{16} &= i[H_2, H_5]. \end{aligned} \tag{2.28}$$

Any unitary generated by H_j, for $j \in \{1, \ldots, 16\}$, is in the repertoire because of the identity

$$e^{[P,Q]} = \lim_{n\to\infty} \left(e^{-iP/\sqrt{n}} e^{iQ/\sqrt{n}} e^{iP/\sqrt{n}} e^{-iQ/\sqrt{n}} \right)^n, \tag{2.29}$$

which ultimately boils down to a sequence of V's and W's. Unitaries generated by real linear combinations of the H_j's are in the repertoire as well because of the identity

$$e^{i(xP+yQ)} = \lim_{n\to\infty} \left(e^{ixP/n} e^{iyQ/n} \right)^n. \tag{2.30}$$

To show that $\{H_1, \ldots, H_{16}\}$ is linearly independent over $\mathbb{R}$ we consider the 4×4 matrices H_j as 16-component vectors (obtained by stacking the columns of the matrix one on top of the next from left to right), and compute the determinant of the 16×16 matrix $[H_1|\cdots|H_{16}]$ whose columns are made of these 16-component vectors. We find $\det[H_1|\cdots|H_{16}] = P(\pi)$, where P is a polynomial of high order with nontranscendental coefficients (specifically, coefficients in $\mathbb{Q}[\sqrt{2}, i]$). Since π is transcendental we conclude that $P(\pi) \neq 0$ — actually $|P(\pi)| \sim 10^{73}$ — so $\{H_1, \ldots, H_{16}\}$ spans the space of 4×4 Hermitian matrices, as required. We have thus proved that the repertoire of $\{\mathsf{V}, \mathsf{W}\}$ is all of $\mathbf{U}(4)$.

We conclude with a word about the Hamiltonians $H_1, \tilde{H}$ chosen to generate the gates V, W in the above construction. Firstly, these Hamiltonians were chosen to produce a sequence of matrices $H_1, \ldots, H_{16}$ with coefficients in $\mathbb{Q}[\sqrt{2}, \pi, i]$, a property used in the proof of linear independence of the H_j's. This condition is by no means *necessary* for linear independence, and many sets of gates other than $\{\mathsf{V}, \mathsf{W}\}$ would qualify as universal. Secondly, the Hamiltonians $H_1, \tilde{H}$ were also chosen to be nondegenerate, with spectra $\{3 \pm 2\pi, -3, 1\}$ and $\{1 \pm \frac{5}{2\sqrt{2}}\pi, 1 \pm \frac{3}{2\sqrt{2}}\pi\}$, respectively, a property also shared with the off mode, Eq. (2.7). Nondegeneracy plays no role in the above argument, but is desirable in any physical implementation in order to avoid spurious transitions due to coupling with external degrees of freedom.

2.3.4 Symmetry-protected logical operations

Now let us consider how robust our proposal is against errors. We first mention a somewhat obvious fact about *parameter* noise. When a quansistor is in its symmetric form, performing a logical operation in either ω-class, its eigenstates are independent of the (real) parameters $\mathbf{g} = (\epsilon, \alpha, \beta, \gamma)$ in the Hamiltonian. As a consequence, when these parameters evolve,

$$(\epsilon, \alpha, \beta, \gamma) \to (\epsilon(t), \alpha(t), \beta(t), \gamma(t)), \qquad t \in [0, T], \tag{2.31}$$

the corresponding logical gate unitary $U(T)$ is a function of the parameters' time averages only

$$U(T) = U(\langle\epsilon\rangle, \langle\alpha\rangle, \langle\beta\rangle, \langle\gamma\rangle), \tag{2.32}$$

with $\langle\cdot\rangle = \frac{1}{T}\int_0^T dt(\cdot)$. This is easily seen by recognizing that $H(\epsilon,\alpha,\beta,\gamma)$ is diagonalized by a common unitary V for all values of the parameters :

$$V^\dagger H(\mathbf{g})V = \mathrm{diag}(\lambda_1(\mathbf{g}),\ldots,\lambda_4(\mathbf{g})). \tag{2.33}$$

Thus

$$\begin{aligned} U(T) &= V\exp\left(-i\int dt\, V^\dagger H(\mathbf{g})V\right)V^\dagger \\ &= V\mathrm{diag}\left(e^{-iT\langle\lambda_1\rangle},\ldots,e^{-iT\langle\lambda_4\rangle}\right)V^\dagger. \end{aligned} \tag{2.34}$$

From (2.17) and (2.22) we get immediately that $U(T) = U(\langle\epsilon\rangle,\langle\alpha\rangle,\langle\beta\rangle,\langle\gamma\rangle)$. Accordingly, any parameter noise $\mathbf{h}(t)$ without bias, $\langle\mathbf{h}\rangle = 0$, will leave the unitary evolution operator $U(t)$ unaffected :

$$U(\mathbf{g}(t)+\mathbf{h}(t)) = U(\langle\mathbf{g}+\mathbf{h}\rangle) = U(\langle\mathbf{g}\rangle). \tag{2.35}$$

If the quansistor interacts with the environment in such a way that the dominant effect of the latter on the quansistor is unbiased noise in the parameters, then logical operations internal to the quansistor are protected from those influences by symmetry. And if the bias has a nonzero but known value, it is easily compensated for. The argument is valid for any flat class (see Appendix 2.8.1), i.e., generalizing from four states to N, any class of Hamiltonians of the form $V\mathrm{diag}(\lambda_1(\mathbf{g}),\ldots,\lambda_N(\mathbf{g}))V^\dagger$ for some unitary V, and functions $\lambda_r(\mathbf{g}) = \sum_s g_s\lambda_{sr}$ with $\det[\lambda_{sr}] \neq 0$. Of course, the symmetry itself, being the key ingredient here, must be enforced.

On a more interesting level, we now consider the robustness of our logical gates against genuine *quantum* errors. We empirically find that the universal set $\{\mathsf{V},\mathsf{W}\}$, defined in the previous section, is particularly resilient to small single-qubit x- and z-rotations, i.e. errors of the form

$$\mathcal{E}_x^{(1)}(\tau) = e^{-i\tau(\sigma_x\otimes\mathbb{1})} \quad , \quad \mathcal{E}_x^{(2)}(\tau) = e^{-i\tau(\mathbb{1}\otimes\sigma_x)}, \tag{2.36}$$

and

$$\mathcal{E}_z^{(1)}(\tau) = e^{-i\tau(\sigma_z\otimes\mathbb{1})} \quad , \quad \mathcal{E}_z^{(2)}(\tau) = e^{-i\tau(\mathbb{1}\otimes\sigma_z)}, \tag{2.37}$$

for small τ. For particular values $\tau_k = \frac{\pi}{2} + k\pi$, $k \in \mathbb{N}$, the unitaries $\mathcal{E}_x^{(1,2)}$ produce single-qubit flips, while $\mathcal{E}_z^{(1,2)}$ generate phase shifts,

$$\begin{aligned} &\mathcal{E}_x^{(1)}(\tau_k) \propto \mathsf{X}\otimes\mathbb{1}, \qquad &&\mathcal{E}_x^{(2)}(\tau_k) \propto \mathbb{1}\otimes\mathsf{X}, \\ &\mathcal{E}_z^{(1)}(\tau_k) \propto \mathsf{Z}\otimes\mathbb{1}, \qquad &&\mathcal{E}_z^{(2)}(\tau_k) \propto \mathbb{1}\otimes\mathsf{Z}. \end{aligned} \tag{2.38}$$

As a first figure of merit, we have numerically evaluated the average fidelity of computational sequences belonging to the set $\{\mathsf{V},\mathsf{W}\}$, when affected at each computational step by an error randomly chosen among $\{\mathcal{E}_x^{(1,2)}(\tau),\mathcal{E}_z^{(1,2)}(\tau)\}$, for a small *fixed* value of τ. (In certain situations, static imperfections are known to dominate random fluctuation errors [106], to be considered next.) For comparison, we have repeated the same steps with two other computational sequences belonging respectively to two other strictly universal sets, namely the Kitaev set $\{\mathsf{H}\otimes\mathbb{1},\mathsf{CP}(i),\mathsf{SWAP}\}$ [172], and

the set $\{\mathsf{A}, \mathsf{SWAP}\}$. Here, $\mathsf{H} \otimes \mathbb{1}$ is the first-qubit Hadamard gate, and $\mathsf{CP}(i)$ is the controlled i-phase gate

$$\mathsf{H} \otimes \mathbb{1} = \frac{1}{\sqrt{2}} \begin{pmatrix} 1 & 1 \\ 1 & -1 \end{pmatrix} \otimes \mathbb{1} \quad , \quad \mathsf{CP}(i) = \mathrm{diag}(1, 1, 1, i). \tag{2.39}$$

The A gate is a variant upon CNOT, and is part of a class of unitaries $A(\phi, \alpha, \theta)$ known to be strictly universal individually (in combination with the SWAP gate) for many values of the parameters [252, 30, 88]. Specifically, the A gate is

$$\mathsf{A} = \begin{pmatrix} 1 & 0 & 0 & 0 \\ 0 & 1 & 0 & 0 \\ 0 & 0 & i\cos(1) & -\sin(1) \\ 0 & 0 & -\sin(1) & i\cos(1) \end{pmatrix}. \tag{2.40}$$

Let us describe the method more precisely. For each universal set S considered, and for integers $m \in [1, 400]$, $r \in [1, 100]$, we generate the sequence $G^S_{1,r}, \ldots, G^S_{m,r}$ of gates picked randomly from S (with equal probabilities). We call m the *computational length*. We also generate sequences $E_{1,r}, \ldots, E_{m-1,r}$ of errors picked randomly (with equal probabilities) from $\{\mathcal{E}^{(1,2)}_x(\tau), \mathcal{E}^{(1,2)}_z(\tau)\}$, with $\tau = 5 \times 10^{-4}$. The ideal computations are then

$$\mathcal{G}^S_{m,r} = \bigcirc_{i=1}^{m} G^S_{i,r}, \tag{2.41}$$

while the faulty computations are

$$\widetilde{\mathcal{G}}^S_{m,r} = G^S_{m,r} \bigcirc_{i=1}^{m-1} (E_{i,r} G^S_{i,r}). \tag{2.42}$$

(The symbol "$\bigcirc$" indicates composition from right to left.) The average fidelity of the rth computation $\widetilde{\mathcal{G}}^S_{m,r}$ being

$$\tilde{F}^{xz}_{\mathrm{avg}}(S, m, r) = \left| \frac{1}{4} \mathrm{Tr}(\mathcal{G}^{S,\dagger}_{m,r} \widetilde{\mathcal{G}}^S_{m,r}) \right|^2, \tag{2.43}$$

we finally average over all computations

$$F^{xz}_{\mathrm{avg}}(S, m) = \frac{1}{100} \sum_{r=1}^{100} \tilde{F}^{xz}_{\mathrm{avg}}(S, m, r). \tag{2.44}$$

A plot of $F^{xz}_{\mathrm{avg}}(S, m)$ as a function of computational length m is given in Fig. 2.3 for each universal set considered, $\{\mathsf{V}, \mathsf{W}\}$, $\{\mathsf{A}, \mathsf{SWAP}\}$, and $\{\mathsf{H} \otimes \mathbb{1}, \mathsf{CP}(i), \mathsf{SWAP}\}$. The region shown lies within the stage of polynomial decay, and does not show the decaying exponential behavior of the saturation stage, less relevant from the point of view of quantum-coherent computation. The power-law best fit $F^{xz}_{\mathrm{avg}}(S, m) = 1 - \alpha m^\beta$ gives

$$F^{xz}_{\mathrm{avg}} \approx \begin{cases} 1 - 3.0 \times 10^{-7} m^{1.10} & \text{for } \{\mathsf{V}, \mathsf{W}\} \\ 1 - 3.0 \times 10^{-8} m^{1.95} & \text{for } \{\mathsf{A}, \mathsf{SWAP}\} \\ 1 - 5.7 \times 10^{-7} m^{1.37} & \text{for } \{\mathsf{H} \otimes \mathbb{1}, \mathsf{CP}, \mathsf{SWAP}\}. \end{cases} \tag{2.45}$$

Manifestly, the set $\{\mathsf{V},\mathsf{W}\}$ fares much better than the other two against this type of error, with an *almost-linear* decay of fidelity (depending on the degree of error anisotropy). When equiprobable x-, y-, and z-rotation errors are considered, the three universal sets show comparable performances. This hard-y-axis, easy-xz-axes anisotropy is a non-trivial property of the set $\{\mathsf{V},\mathsf{W}\}$. (Additional numerical results point to the special role of the W gate.) It is worth emphasizing that, while being more sensitive to y-rotations, the set $\{\mathsf{V},\mathsf{W}\}$ outperforms the other two universal sets with respect to both x- and z-rotations.

As a second figure of merit, let us consider fidelity against a fluctuating noise corresponding to the larger error set

$$\begin{aligned}\mathcal{E}_a^{(1)} &= e^{-i\tau_a(\sigma_a\otimes\mathbb{1})}\\ \mathcal{E}_b^{(2)} &= e^{-i\tau_b(\mathbb{1}\otimes\sigma_b)}\\ \mathcal{E}_{ab} &= e^{-i\tau_a\tau_b(\sigma_a\otimes\sigma_b)},\end{aligned} \tag{2.46}$$

for $a,b\in\{x,y,z\}$, and normally distributed couplings τ_a,τ_b. The 15 corresponding generators constitute, along with the identity, a basis for all 4×4 Hamiltonians. For now, these 15 errors are picked with equal probability $1/15$ to generate the faulty computations of Eq. (2.42), and the average fidelity

$$F_{\text{avg}}^{xyz}(S,m)=\frac{1}{900}\sum_{r=1}^{900}\tilde{F}_{\text{avg}}^{xyz}(S,m,r) \tag{2.47}$$

is evaluated as a function of computational length m. Here, r enumerates 30 random generations of τ_x,τ_y,τ_z times 30 random faulty sequences for each generation. For identically distributed couplings τ_a the three universal sets again show comparable performance (the Kitaev set showing a slight advantage). However, if the interactions with the environment are such as to produce a stronger bias on x- and z-rotations, then the set $\{\mathsf{V},\mathsf{W}\}$ is at an advantage. This is seen in Fig. 2.4 where τ_x and τ_z have average $\langle\tau_x\rangle=\langle\tau_z\rangle=10^{-3}$, while τ_y has average one order smaller, $\langle\tau_y\rangle=10^{-4}$. All standard deviations are equal to 10^{-4}. The power-law best fit $F_{\text{avg}}^{xyz}(S,m)=1-\alpha m^{\beta}$ gives

$$F_{\text{avg}}^{xyz}\approx\begin{cases}1-2.1\times10^{-7}m^{1.10} & \text{for } \{\mathsf{V},\mathsf{W}\}\\ 1-2.0\times10^{-8}m^{1.81} & \text{for } \{\mathsf{A},\mathsf{SWAP}\}\\ 1-2.7\times10^{-7}m^{1.31} & \text{for } \{\mathsf{H}\otimes\mathbb{1},\mathsf{CP},\mathsf{SWAP}\}.\end{cases} \tag{2.48}$$

For this degree of error anisotropy, the set $\{\mathsf{V},\mathsf{W}\}$ presents an almost-linear decay of fidelity.

As our third and last figure of merit, we once more consider fidelity against a fluctuating noise corresponding to the error set (2.46), but we now assume that interactions with the environment are such as to make the system more prone to x- and z-rotations. For definiteness, the 8 errors $\mathcal{E}_a^{(1)},\mathcal{E}_a^{(1)},\mathcal{E}_{ab}$, for $a,b\in\{x,z\}$, are picked randomly with probability $3/31$, while the 7 remaining errors, each containing at least one y-rotation, are picked with probability $1/31$. The couplings τ_a are now

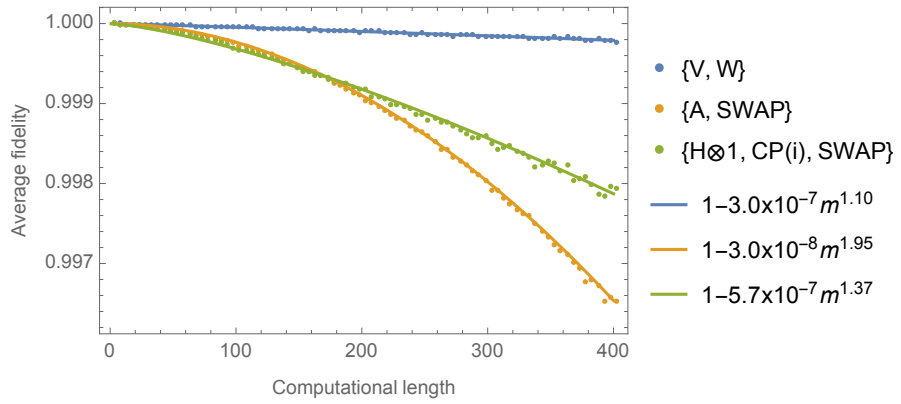

FIGURE 2.3 – (Color online) Average fidelity $F_{\text{avg}}^{xz}(S,m)$, Eq. (2.44), against single-qubit x- and z-rotations, Eqs. (2.36), (2.37), as a function of computational length m, for three strictly universal sets : $\{\mathsf{V},\mathsf{W}\}$, $\{\mathsf{A},\mathsf{SWAP}\}$, and $\{\mathsf{H}\otimes\mathbb{1},\mathsf{CP}(i),\mathsf{SWAP}\}$. The coupling τ is set to 5×10^{-4}. We find power-law best fits $1-F_{\text{avg}}^{xz}(S,m)=1-\alpha m^{\beta}$ with respective powers $\beta_1=1.10$, $\beta_2=1.95$, $\beta_3=1.37$.

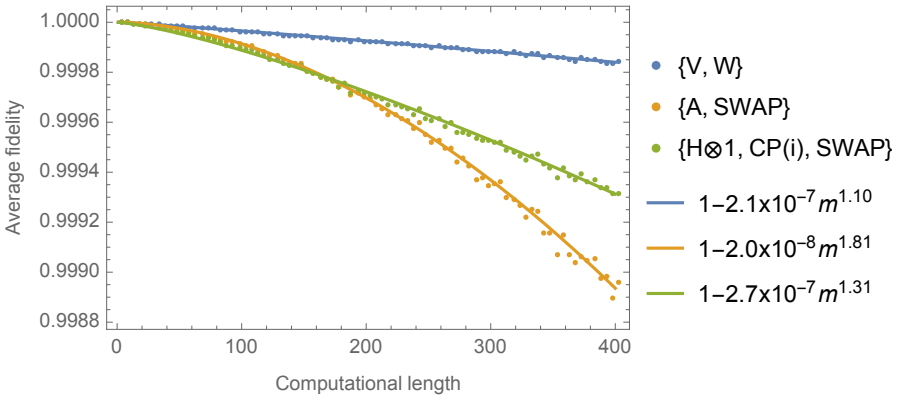

FIGURE 2.4 – (Color online) Average fidelity $F_{\text{avg}}^{xyz}(S,m)$, Eq. (2.47), against the equiprobable Pauli error-set (2.46), as a function of computational length m, for three strictly universal sets : $\{\mathsf{V},\mathsf{W}\}$, $\{\mathsf{A},\mathsf{SWAP}\}$, and $\{\mathsf{H}\otimes\mathbb{1},\mathsf{CP}(i),\mathsf{SWAP}\}$. The couplings τ_a are normally distributed with standard deviation 10^{-4}. The means are $\langle\tau_x\rangle=\langle\tau_z\rangle=10^{-3}$, and $\langle\tau_y\rangle=10^{-4}$. We find power-law best fits $1-F_{\text{avg}}^{xyz}(S,m)=1-\alpha m^{\beta}$ with respective powers $\beta_1=1.10$, $\beta_2=1.81$, $\beta_3=1.31$.

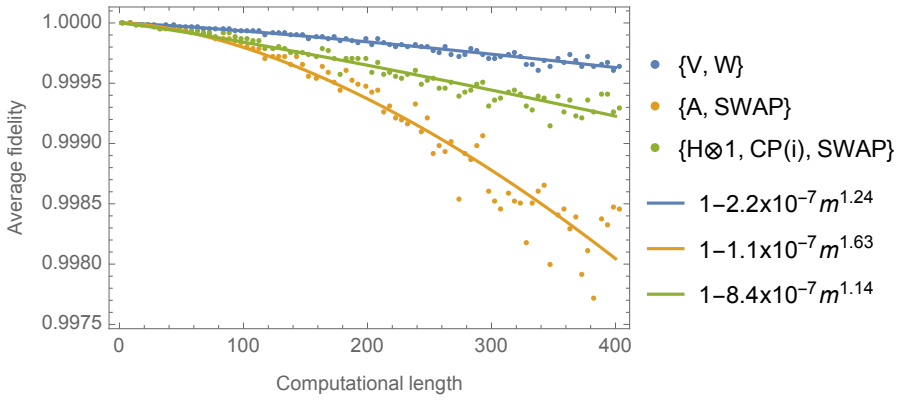

FIGURE 2.5 – (Color online) Average fidelity $F_{\text{avg}}^{xyz}(S,m)$, Eq. (2.49), against the Pauli error-set (2.46), as a function of computational length m, for three strictly universal sets : $\{\mathsf{V},\mathsf{W}\}$, $\{\mathsf{A},\mathsf{SWAP}\}$, and $\{\mathsf{H}\otimes\mathbb{1},\mathsf{CP}(i),\mathsf{SWAP}\}$. Errors without a y-rotation have probability $3/31$; other errors have probability $1/31$. The couplings τ_a are normally distributed without bias, and with standard deviation 10^{-3}.

identically distributed without bias, $\langle\tau_a\rangle = 0$, and with standard deviation 10^{-3}. The average fidelity

$$F_{\text{avg}}^{xyz}(S,m) = \frac{1}{2500}\sum_{r=1}^{2500}\tilde{F}_{\text{avg}}^{xyz}(S,m,r) \tag{2.49}$$

is plotted in Fig. 2.5. Here, r enumerates 50 random generations of τ_x,τ_y,τ_z times 50 random faulty sequences for each generation. The power-law best fit $F_{\text{avg}}^{xyz}(S,m) = 1-\alpha m^{\beta}$ gives

$$F_{\text{avg}}^{xyz} \approx \begin{cases} 1-2.2\times10^{-7}m^{1.24} & \text{for } \{\mathsf{V},\mathsf{W}\} \\ 1-1.1\times10^{-7}m^{1.63} & \text{for } \{\mathsf{A},\mathsf{SWAP}\} \\ 1-8.4\times10^{-7}m^{1.14} & \text{for } \{\mathsf{H}\otimes\mathbb{1},\mathsf{CP},\mathsf{SWAP}\}. \end{cases} \tag{2.50}$$

In spite of the fact that the Kitaev has a smaller β exponent than $\{\mathsf{V},\mathsf{W}\}$, the corresponding curves never cross at a positive fidelity value, all the less when m is restricted to the moderate values for which these polynomial best fits are indicated. We conclude that $\{\mathsf{V},\mathsf{W}\}$ is at an advantage in the presence of a hard-y-axis anisotropy. Evaluating the performance of $\{\mathsf{V},\mathsf{W}\}$ on a larger error-set, generated by linear combinations of Pauli tensors, is the object of a future work.

Although we have been concerned with the short-m stage of polynomial decay, it should be mentioned that for larger m, some of the curves plotted in Figs. 2.3, 2.4, 2.5 present fidelity revivals ("echoes" in the Loschmidt echo [220, 82, 125], not shown) before reaching the large-m saturation stage.

2.3.5 Gauge potentials for ω-classes

We now provide a "lattice gauge field" description of ω-rotation invariance. In Fig. 2.6 the core is displayed so that it can be visualized as either planar (as shown)

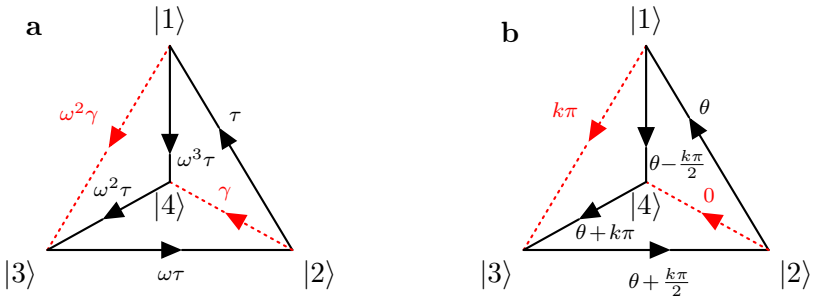

FIGURE 2.6 – (Color online) Core displayed as either planar or tetrahedral. The parameters are as in Fig. 2.1, with $\tau = |\tau|e^{i\theta}$, $\gamma \in \mathbb{R}$, and $\omega = e^{ik\pi/2}$. **a** Transition amplitudes. The part of the Hamiltonian in $\mathrm{span}(J_\omega, J_\omega^3)$ is proportional to τ (solid black). The part of the Hamiltonian in $\mathrm{span}(J_\omega^2)$ is proportional to γ (dotted red). **b** Gauge phases on links for $\gamma > 0$. If $\gamma \in \mathbb{R}^{<0}$, there is an additional phase of π on θ_{13} and θ_{24} (dotted red). If $\gamma = 0$, then both θ_{13} and θ_{24} vanish.

or tetrahedral (by raising the central point $|4\rangle$). The complex hopping parameters linking the sites (the *link variables*) have the form $h_{jk} = |h_{jk}|e^{i\theta_{jk}}$. In the lattice picture, vertices $|j\rangle$ stand for the matter field, and the phases on the links $|j\rangle \xrightarrow{\theta_{jk}} |k\rangle$ correspond to a $\mathbf{U}(1)$ gauge potential $\theta_{jk} = \int_j^k \mathbf{A} \cdot d\mathbf{r}$. Paths around elementary triangular plaquettes yield gauge-invariant plaquette fluxes,

$$\Phi_j = \oint_{\triangle_j} \mathbf{A} \cdot d\mathbf{r}, \tag{2.51}$$

which may be written $\oint_{\triangle_j} \mathbf{A} \cdot d\mathbf{r} = \iint_{\triangle_j} (\nabla \times \mathbf{A}) \cdot d\mathbf{s}$. A Hermitian Hamiltonian has $\theta_{jk} = -\theta_{kj}$, and it is straightforward to check directly that the field $\mathbf{B} = \nabla \times \mathbf{A}$ is divergence-free in the tetrahedron,

$$\sum_j \Phi_j = 0. \tag{2.52}$$

As a consequence, only three plaquette fluxes are linearly independent, and the planar and tetrahedral models are completely equivalent. (The 4-level quansistor is essentially 2-dimensional. This is in contrast to higher-level quansistors, which are intrinsically higher-dimensional, as explained in the Discussion.) Of the six gauge phases θ_{jk}, $j < k$, three are independent and generate a manifold of Hamiltonians for each given flux structure. It is convenient to distinguish ω-circulant Hamiltonians by their flux structure or "magnetic" field, whether fundamental or synthetic. Hamiltonians with different flux structures belong to gauge-inequivalent classes, and are measurably different. Fig. 2.6 displays (a) transition amplitudes, and (b) gauge phases. As before, the parameters are $\tau = |\tau|e^{i\theta}$, $\gamma \in \mathbb{R}$, and $\omega = e^{ik\pi/2}$. The corresponding flux structures (modulo 2π) are represented in Figs. 2.7 and 2.8. For any Hamiltonian of class X, the flux structure is as in the left diagram of Fig. 2.7. Therefore, the topological flux structure $\Phi_j \equiv -\frac{\pi}{2}$ observed in the right diagram of

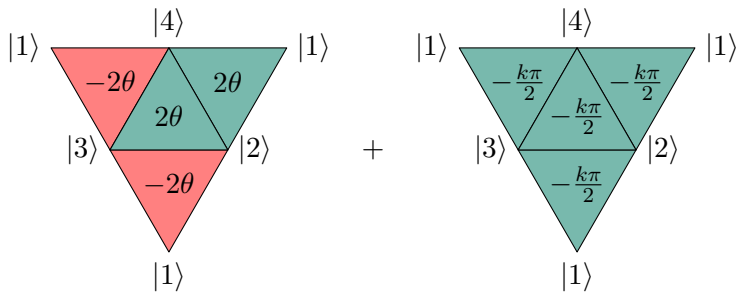

FIGURE 2.7 – (Color online) Flux structure modulo 2π for $H \in \mathrm{span}(J_\omega, J_\omega^3)$. The parameters are $\tau = |\tau|e^{i\theta}$, and $\omega = e^{ik\pi/2}$. The first structure depends on the coupling τ. The second structure is topological, and depends only on the class ω.

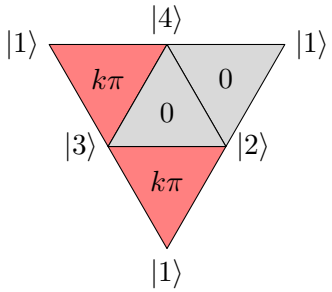

FIGURE 2.8 – (Color online) Flux structure modulo 2π for $H \in \mathrm{span}(J_\omega^2)$. The parameters are $\gamma \in \mathbb{R}^{>0}$, and $\omega = e^{ik\pi/2}$. If $\gamma < 0$, there is an additional flux π in each plaquette. If $\gamma = 0$, all fluxes vanish.

Fig. 2.7, characteristic of Hamiltonians $H \in \mathrm{span}(Y, Y^3)$, cannot be realized by any Hamiltonian of class X. Symbolically, $\mathrm{span}(X, X^2, X^3) \ncong \mathrm{span}(Y, Y^3)$. Similarly, the topological flux structure observed in Fig. 2.8 cannot be realized by Hamiltonians of class X, hence $\mathrm{span}(X, X^2, X^3) \ncong \mathrm{span}(Y^2)$. On the other hand, by combining the diagrams of Figs. 2.7 and 2.8 we see that $\mathrm{span}(X, X^2, X^3) \cong \mathrm{span}(Y, Y^2, Y^3)$. Indeed, a matrix of class X with X^1 coefficient $\tau = |\tau|e^{i\theta}$ is gauge-equivalent to a matrix of class Y with Y^1 coefficient $\tau' = |\tau'|e^{i\theta'}$ if and only if $\theta \equiv \theta' - \pi/4 \mod 2\pi$. In particular, the Hamiltonians H_1 and $\tilde{H}$ from the universality proof, Eqs. 2.25 and 2.26, belong to inequivalent flux structures (although it does not have to be the case in principle, as discussed in Appendix 2.8.1.)

2.3.6 Physical implementation

In the previous section, we have argued that Hamiltonians from different ω-classes may have different flux structures, with three linearly independent plaquette fluxes. They could therefore be realized by applying magnetic fields onto 2-dimensional or 3-dimensional charged systems with initial Hamiltonians in the form of the off mode Hamiltonian, Eq. (2.7). The topological (rightmost) flux structure from Fig. 2.7,

for instance, could be produced from a very long and thin solenoid penetrating a tetrahedron through one face, and isotropically releasing a flux of 2π at the center of the tetrahedron. This flux structure properly belongs to class Y, and cannot be realized in class X.

In this section we sketch how the classes X and Y could be implemented in a wide range of physical systems, comprised of either charged or neutral levels, using the techniques of synthetic gauge fields. The appearance of gauge structures in systems with parameter-dependent Hamiltonians [40, 251] or time-periodic Hamiltonians [254] is well known. In the former case, and when the adiabatic approximation holds, the dynamics of an adiabatically evolving particle can be projected onto the subspace spanned by the mth eigenstate $\psi_m(\mathbf{R}(t))$. The resulting effective Schrödinger equation for $\psi_m(\mathbf{R}(t))$ involves a *Berry connection* $\mathbf{A}(\mathbf{R})$ playing the role of a gauge potential, through the substitution $\mathbf{p} \to \mathbf{p} - \mathbf{A}$ in the effective Hamiltonian, or equivalently, as a geometric phase $\exp i \int d\mathbf{R} \cdot \mathbf{A}$ acquired by $\psi_m(\mathbf{R}(t))$ over the displacement. This has been shown to occur in mechanical systems [281], molecular systems [200], and condensed matter systems [288]. Similarly, for systems driven by fast time-periodic modulations (Floquet engineering), one may consider the evolution at stroboscopic times $t_N = NT$, where T is the driving period [126, 14]. Here again, the resulting effective dynamics has been shown to yield non-trivial gauge structures in different platforms such as condensed matter systems [94, 71], photonics [129, 217], ultracold atoms in optical lattices [16, 262, 140, 13, 111, 110], and ions in micro-fabricated traps [38, 39]. In a lattice with coordination number d, nearest-neighbor hopping terms $K_{\mathbf{m},\mathbf{m}+\mathbf{u}}|\mathbf{m}\rangle\langle\mathbf{m}+\mathbf{u}|$ act on wavefunctions as

$$\psi(\mathbf{m}) \to K_{\mathbf{m},\mathbf{m}+\mathbf{u}}\psi(\mathbf{m}+\mathbf{u}) = K_{\mathbf{m},\mathbf{m}+\mathbf{u}}e^{-i\mathbf{u}\cdot\mathbf{p}}\psi(\mathbf{m}), \tag{2.53}$$

where naturally $\mathbf{p}$ is the momentum operator and $\mathbf{u}$ is a vector of unit norm in $\mathbb{Z}^d$. In the presence of an effective gauge potential $\mathbf{A}(\mathbf{m})$, the *Peierls substitution* $\mathbf{p} \to \mathbf{p} - \mathbf{A}(\mathbf{m})$ amounts to the complexification of real hopping parameters

$$K_{\mathbf{m},\mathbf{m}+\mathbf{u}} \to K_{\mathbf{m},\mathbf{m}+\mathbf{u}}e^{i\mathbf{u}\cdot\mathbf{A}(\mathbf{m})} = K_{\mathbf{m},\mathbf{m}+\mathbf{u}}e^{i\theta_{\mathbf{m},\mathbf{m}+\mathbf{u}}}. \tag{2.54}$$

The Peierls phases $\theta_{\mathbf{m},\mathbf{m}+\mathbf{u}}$ may also depend on internal degrees of freedom (pseudospin) and can then be thought of as resulting from an artificial or synthetic non-abelian gauge field [14]. For the implementation of the classes X and Y, we need to realize the gauge-invariant flux structures described in Section 2.3.5, whether fundamental or artificial. One possibility is to Floquet engineer Peierls phases as in the Hamiltonians (2.14) and (2.20). In the former, we have Peierls phases $\theta_{j,j+1} \equiv \theta$, and all others zero. In the latter, we have instead $\theta_{j,j+1} = \theta + (\pi/2)^{j-1}$ and $\theta_{13} = \pi$, and all others zero.

In [140], for instance, lattice shaking is used to prompt a fast periodic modulation of the on-site energies of a tight-binding Hamiltonian analogous to our off-mode Hamiltonian, Eq. (2.7) :

$$H(t) = -\sum_{\langle ij\rangle} K_{ij}a_i^\dagger a_j + \sum_i (\epsilon_i + v_i(t))a_i^\dagger a_i \tag{2.55}$$

where $K_{ij} > 0$, $v_i(t) = v_i(t+T)$, and $\langle v_i \rangle_T = \frac{1}{T}\int_0^T dt\ v_i(t) = 0$. Using Floquet analysis, the resulting effective time-independent Hamiltonian proves to be of the form

$$H_{\text{eff}} = -\sum_{\langle ij \rangle} |K_{ij}^{\text{eff}}| e^{i\theta_{ij}} a_i^\dagger a_j + \epsilon^{\text{eff}} \sum_i a_i^\dagger a_i, \tag{2.56}$$

with complex tunneling amplitudes

$$|K_{ij}^{\text{eff}}| e^{i\theta_{ij}} = K_{ij} \langle e^{i(w_j - w_i)/\hbar} \rangle_T, \tag{2.57}$$

where $w_i(t) = -\int_{t_0}^t dt' v_i(t') + \langle \int_{t_0}^t dt' v_i(t') \rangle_T$. As long as the driving functions break certain symmetries, the Peierls phases can be varied smoothly to any value between 0 and 2π. Producing non-trivial Peierls phases that cannot be gauged away may require additional static structure, like large energy offsets $|\epsilon_j - \epsilon_i| \gg K_{ij}$ [140]. In our setup, these large energy offsets are already present in the off-mode Hamiltonian to effectively suppress spontaneous transitions between logical states (position eigenstates).

2.4 Coupling to leads

We now consider the effect of the semi-infinite leads on the core system. As indicated in the Hamiltonian (2.2) and in Fig. 2.1, each site (for example, a quantum dot) is tunnel-coupled to its own lead (which could be, for example, a semi-infinite spin chain) but the parameters and coupling constants of the four leads are chosen to be identical. The transition amplitudes in the leads are set to unity, and the lead-to-site coupling t_c can be chosen real and positive with no loss of generality. Coupling the core to the leads may serve to model the core's immersion in its immediate environment, and that is the point of view adopted in Section 2.4.1. Alternatively, the leads may represent designed transmission wires between the core and distant devices. This perspective is explored in Section 2.4.2.

It is shown in Appendix 2.8.2 that the effect of the leads on the core Hamiltonian (2.8) can be summarized in an effective, energy-dependent diagonal offset :

$$H_\infty(E) = H^{\text{pos}}(\mathbf{g}, \omega) + t_c^2 \Sigma(E) \mathbb{1}, \tag{2.58}$$

where $\Sigma(E)$ is the surface Green's function of a semi-infinite lead :

$$\Sigma(E) = \frac{E}{2} - \frac{\sqrt{(E + i0^+)^2 - 4}}{2}\ . \tag{2.59}$$

It follows that ω-circulation is preserved. For instance, when $\omega = 1$ (class X) we have the circulant effective Hamiltonian

$$H_\infty(E) = \begin{bmatrix} \epsilon_\infty(E) & \tau & \gamma & \tau^\dagger \\ \tau^\dagger & \epsilon_\infty(E) & \tau & \gamma \\ \gamma & \tau^\dagger & \epsilon_\infty(E) & \tau \\ \tau & \gamma & \tau^\dagger & \epsilon_\infty(E) \end{bmatrix} \tag{2.60}$$

with effective self-energies

$$\begin{aligned}\epsilon_\infty(E) &= \epsilon + t_c^2\Sigma(E) \\ &= \epsilon + t_c^2\left(\frac{E}{2} - \frac{\sqrt{(E+i0^+)^2-4}}{2}\right).\end{aligned} \tag{2.61}$$

Because ω-rotation invariance is preserved, the eigenstates are *energy-independent*, and still given by (2.15). The corresponding effective eigenvalues are obtained from the isolated levels λ_k, (2.16), by the replacement $\epsilon \to \epsilon_\infty(E)$:

$$\begin{aligned}\lambda_{k,\infty}(E) &= \epsilon_\infty(E) + 2|\tau|\cos(\theta + \tfrac{k\pi}{2}) + (-1)^k\gamma \\ &= t_c^2\Sigma(E) + \lambda_k\end{aligned} \tag{2.62}$$

for $k = 1, \ldots, 4$. But these are not effective eigenenergies as can be seen from the Green's function :

$$G_{\rm core}(E) = (E - H_\infty(E))^{-1} = \sum_k \frac{|\phi_k\rangle\langle\phi_k|}{E - \lambda_{k,\infty}(E)}, \tag{2.63}$$

the effective energy levels of the core-with-leads are fixed points $E_k^\star = \lambda_{k,\infty}(E_k^\star)$. (From now on the symbol "$\star$" will always indicate an effective energy due to the presence of the leads.) From (2.61), and the convention used for the definition of the complex square root,

$$\begin{aligned}E_k^\star &= \frac{1}{1-t_c^2}\left[\left(1-\tfrac{t_c^2}{2}\right)\lambda_k - \tfrac{t_c^2}{2}\sqrt{\lambda_k^2 - 4(1-t_c^2)}\right] \\ &= \frac{1}{1-t_c^2}\left[\left(1-\tfrac{t_c^2}{2}\right)\lambda_k - i\tfrac{t_c^2}{2}\sqrt{4(1-t_c^2) - \lambda_k^2}\right].\end{aligned} \tag{2.64}$$

Since each k-mode is decoupled from the others, we have chosen $\lambda_k \geq 0$ with no loss of generality. Eq. (2.64) and the corresponding expression for negative λ_k is obtained in Appendix 2.8.3 by analytically solving the core-with-leads Schrödinger equation. Because the effective eigenstates do not depend on the scattering energy, it is easy to define a first-order effective core Hamiltonian which is energy-independent

$$G_{\rm core}(E) \approx (E - H_{\rm eff})^{-1} = \sum_k \frac{|\phi_k\rangle\langle\phi_k|}{E - E_k^\star}. \tag{2.65}$$

In the ordered eigenbasis $\{|\phi_1\rangle, |\phi_2\rangle, |\phi_3\rangle, |\phi_4\rangle\}$ we have $\langle\phi_j|H_{\rm eff}|\phi_k\rangle = E_j^\star\delta_{jk}$. All the results from Section 2.3 can now be modified by the replacement $\lambda_k \to E_k^\star$. Note that $E_k^\star$ is real if and only if $|\lambda_k| \geq 2\sqrt{1-t_c^2} + O(t_c^4)$. (More precisely, $|\lambda_k| \geq 2 - t_c^2$, as shown in the Appendix. See (2.134),(2.135).) Since any path in $(\lambda_1, \lambda_2, \lambda_3, \lambda_4)$-space corresponds to a unique path in parameter space $(\epsilon, \alpha, \beta, \gamma)$, each $E_k^\star$ can be made real or complex independently of the other three. Thus, each eigenstate can be made to evolve unitarily or not by adjusting the internal parameters of the core, permitting exquisite control over (partial) decoherence [12].

For class Y (i.e. $\omega = e^{i\pi/2}$), expressions identical to (2.64),(2.65) hold with the replacements $\phi_k \to \chi_k$ (2.21) and $\lambda_k \to \lambda'_k$ (2.22). Again, full control over the core energies allows to make each $E_k^\star$ real or complex independently of the other three.

The same is true, with a caveat, when the core is in the nonsymmetric off mode,

$$H_{\text{off}} = -\sum_{\langle ij \rangle} K_{ij} a_i^\dagger a_j + \sum_i \epsilon_i a_i^\dagger a_i, \tag{2.66}$$

where large energy offsets $|\epsilon_i - \epsilon_j| \gg K_{ij} > 0$ effectively suppress spontaneous transitions, so that position i is almost a good quantum number. Then again $G_{\text{core}}(E) \approx (E - H_{\text{eff}})^{-1} = \sum_m \frac{|m\rangle\langle m|}{E-\epsilon_m^\star}$ with $\epsilon_m^\star = \frac{1}{1-t_c^2}\left[\left(1 - \frac{t_c^2}{2}\right)\epsilon_m - \frac{t_c^2}{2}\sqrt{\epsilon_m^2 - 4(1-t_c^2)}\right]$. This time care must be taken to maintain the large-offset condition when lowering the ϵ_m's below the escape threshold, in order to prevent spurious logical transitions.

2.4.1 Leakage-free logical operations

In this section we show that, even in the presence of leads, all logical gates can be realized without leakage, and are still symmetry-protected from unbiased parameter noise. It is sufficient to consider single-pulse, ω-circulant gates, since they are universal for quantum computation. We could use only the gates $\{\mathsf{V}, \mathsf{W}\}$ from Section 2.3.3, for instance, which are especially resilient against x- and z-rotation errors. Let a single pulse producing the gate U be given in the time interval $t \in [0, T]$ by the path $(\lambda_1(t), \ldots, \lambda_4(t))$ in the energy space of the bare core. With a lead coupled to each site, eigenenergies λ_k are modified to possibly complex effective eigenenergies $E_k^\star$. We must make sure that $|\lambda_k| \geq 2 - t_c^2$ at all times to keep $E_k^\star$ real and prevent escape through the leads. If not, rescaling the energies by n and the time by $1/n$ leaves unchanged the unitary $U = \exp\left(-i\int_0^T dt\, H_{\text{core}}(t)\right)$. Avoiding the energy band of the leads is therefore not an issue. Moreover, for these values of λ_k, the function $E_k^\star(\lambda_k)$ increases monotonically, and hence is one-to-one. As an immediate consequence, there is a (unique) path $(p_1(t), \ldots, p_4(t))$ lying entirely outside the band of the leads such that

$$E_k^\star(p_k(t)) = \lambda_k(t) \qquad k \in \{1, \ldots, 4\},\ t \in [0, T]. \tag{2.67}$$

We thus obtain

$$U_{\text{eff}} = \exp\left(-i\int_0^T dt\, H_{\text{eff}}(t)\right) = U. \tag{2.68}$$

Having reproduced the ideal gate U in the presence of the leads, and recalling that identical leads preserve ω-rotation invariance, we conclude that the effective gate U_{eff} is symmetry-protected from unbiased noise in the *effective* parameters $E_k^\star$. And since the functions $E_k^\star(\lambda_k)$ are very nearly linear outside the band, unbiased noise in $E_k^\star$ is equivalent to unbiased noise in the bare parameters. This completes our claim that, even in the presence of leads, logical gates can be realized without leakage and are still protected against unbiased noise in the parameters (whether bare or effective).

2.4.2 Core as quantum memory

Within each ω-class the effective eigenenergies can be chosen real or complex independently of one another, and as a consequence each energy eigenstate can independently be made to dissipate in the leads or remain stationary. (The off mode offers comparatively less flexibility because of the condition $|\epsilon_i - \epsilon_j| \gg K_{ij} > 0$, although crossing levels is ill-advised in any mode.) The dissipation of the k-th eigenstate is characterized by the *tunable* dynamical rate

$$\tau^{-1}(\lambda_k) = |\mathrm{Im}(E_k^\star)|, \tag{2.69}$$

which is found from (2.64) to be a continuous function of the (fully controllable) energy λ_k, with values in the interval $[0, 2/3\sqrt{3}] \approx [0, 0.385]$. The ability to prevent the eigenstates from escaping to the leads allows us to consider the core as a versatile quantum memory unit that can protect a state $\sum_k a_k|\phi_k\rangle$ for a long time, and then release it entirely or partially at a later time. (In what follows $|\phi_k\rangle$ will stand for an eigenstate of either class X or Y, unless specified otherwise.) This is the perspective that we adopt in this section, and to do so it is convenient to go beyond the first-order Green's function analysis that we have employed so far, which loses track of effective core eigenstates as they escape, with no possibility of ever coming back. We emphasize that our proposal assumes nothing other than the existence of a flat symmetry class in the physical support of information, an aspect which to the best of our knowledge has not been exploited in quantum memory technologies [210, 5, 147, 239, 178].

We consider the following *finite* system : it consists of two ω-circulant 4-level cores standing face to face, and connected by four identical leads, each comprised of L sites. One may think of it as a square prism of height L, with the cores as top and bottom faces. The cores act as memory storage units. We will identify when and why a state localized on one core will scatter within characteristic time τ_s, eventually reaching the other core. Alternatively, we discuss how the localized state can be protected from scattering over a timescale $\tau_b \gg \tau_s$. The index b stands for *bound states*, whose presence or absence determines the dissipation regime.

In Appendix 2.8.3 we show that the ω-circulant system decouples into four identical modes, each in the form of two sites of self-energies λ, μ connected by a finite lead of L sites. The single-particle Hamiltonian of one mode is

$$H_{1P} = \left[\begin{array}{c|ccc|c} \lambda & t_{c,1} & & & \\ \hline t_{c,1}^* & 0 & 1 & & \\ & 1 & 0 & \ddots & \\ & & \ddots & \ddots & t_{c,2} \\ \hline & & & t_{c,2}^* & \mu \end{array}\right]. \tag{2.70}$$

(The argument generalizes in a straightforward manner if the 4-level cores are replaced by N-level cores.) The corresponding Schrödinger equation is easily solved, yielding eigenenergies E in implicit form

$$\frac{\Delta\tilde{\Delta}E - \Delta - \tilde{\Delta}}{\Delta\tilde{\Delta} - 1} = \frac{U_{L-2}(E/2)}{U_{L-1}(E/2)}, \tag{2.71}$$

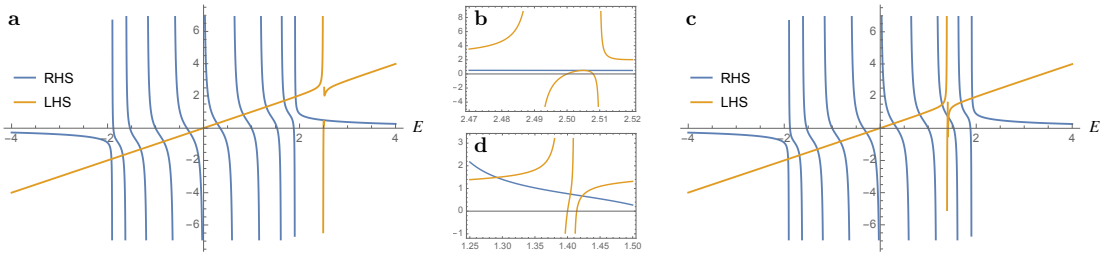

FIGURE 2.9 – (Color online) Left-hand (LHS) and right-hand (RHS) sides of the energy constraint equation (2.71) as a function of E for $(L, t_{c,1}, t_{c,2}) = (10, 0.1, 0.1)$. The LHS curve crosses the RHS curve $L+2$ times. **a** For $\lambda = \mu = 2.5$, the crossings correspond to L continuum states in the band, plus two bound states near λ. **b** Zoom-in of the neighborhood of λ for $\lambda = \mu = 2.5$. The nearly degenerate bound state energies $E = 2.5049765$ and $E = 2.5049904$ are not yet resolved, but we plot these states in Fig. 2.10. **c** For $\lambda = \mu = 1.4$ the LHS curve crosses the RHS curve $L+2$ times within the band. **d** Zoom-in of the neighborhood of λ for $\lambda = \mu = 1.4$, showing one continuous scattering mode (leftmost) and two hybridized scattering modes with energy separation $\sim 10^{-2}$.

where

$$\Delta = \frac{E-\lambda}{|t_{c,1}|^2}, \qquad \tilde{\Delta} = \frac{E-\mu}{|t_{c,2}|^2}, \tag{2.72}$$

and $U_n(x)$ is a Chebyshev polynomial of the second kind. The $L+2$ solutions of (2.71) are the system's eigenenergies. Unsurprisingly, this equation cannot be solved analytically ; a graphical solution is displayed in Fig. 2.9. Note that the RHS (blue curves) is independent of the couplings to the cores and pertains to the spectrum of the leads whereas the LHS (yellow curves) is independent of the lead parameters and pertains to the coupling. L solutions always belong to the energy band $[-2, 2]$, and form the (perturbed) continuous spectrum of the leads. The two remaining solutions may lie outside the band (bound states) or within the band (hybridized scattering states). We now discuss these cases in turn.

Let us write single-particle states as

$$|E\rangle = \frac{\beta_0}{t_{c,1}^*}|0\rangle + \sum_{j=1}^{L} \beta_j |j\rangle + \frac{\beta_{L+1}}{t_{c,2}}|L+1\rangle, \tag{2.73}$$

where $|j\rangle$ is the state with one particle on site j. The coefficients of bound states, with energies $|E| > 2$, are given by

$$\beta_j = (\pm 1)^j \mathcal{N} \left[\tfrac{|E| \pm \lambda}{|t_{c,1}|^2} \sinh j\xi - \sinh(j-1)\xi \right], \tag{2.74}$$

for $0 \leq j \leq L+1$. Here $\pm = \mathrm{sgn}(E)$, $\xi = \cosh^{-1}(|E|/2)$ and $\mathcal{N}$ is a normalization factor. These states are localized around both endpoints, decaying exponentially over the characteristic length scale ξ^{-1} from the endpoints.

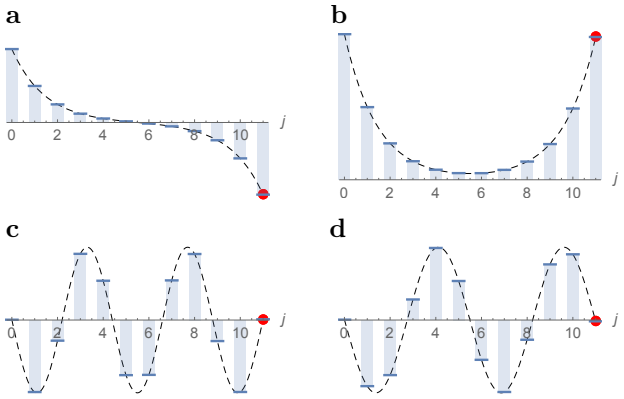

FIGURE 2.10 – (Color online) The two bound states (**a,b**) and two states from the continuum (**c,d**) for $(L, t_{c,1}, t_{c,2}) = (10, 0.1, 0.1)$ and $\lambda = \mu = 2.5$. **a** Antisymmetric bound state, $E = 2.5049765$. **b** Symmetric bound state, $E = 2.5049904$. The energy separation is $\sim 10^{-5}$. A generic feature of bound states is their large amplitude at the endpoints (sites 0 and $L+1$). **c** A symmetric continuum state, $E = 0.282$. **d** An antisymmetric continuum state, $E = 0.827$. A generic feature of continuum states is their small amplitude at the endpoints. In each graph, the red dot represents a consistency condition on β_{L+1}. See Appendix 2.8.3, Eq. (2.118) for details.

Throughout this section, all calculations will be done using $L = 10$ and $t_{c,1} = t_{c,2} \equiv t_c = 0.1$. The bound states for $\lambda = \mu = 2.5$ are displayed in Fig. 2.10 **a,b**. We see that there is a symmetric state $|b_S\rangle$ and an antisymmetric state $|b_A\rangle$, a consequence of the Schrödinger equation symmetry $j \leftrightarrow L + 1 - j$ resulting from $\Delta = \tilde{\Delta}$ (see Appendix 2.8.3). When $L \to \infty$, the limiting expression for β_j describes a bound state localized at the left endpoint and decaying exponentially with distance. Similarly, the limiting expression for β_{L+1-j} describes a state localized at the right endpoint. In that limit, the eigenvalue equation (2.71) is equivalent to the fixed-point relations $E = \lambda \pm |t_{c,1}|^2 \Sigma(E)$ and $E = \mu \pm |t_{c,2}|^2 \Sigma(E)$ for the states localized on the left and right, respectively. In the Green's function treatment of the core with semi-infinite leads (see Appendix 2.8.2), the same fixed-point relation appears as the effective self-energy of the core once the leads are traced out. In the finite-L case, states localized around a single end of the lead will only be approximately stationary. If the system evolves for a long time, the state localized on one end will eventually tunnel through the lead.

All other single-particle solutions, Eq. (2.73), fall within the band of the leads, $E \in [-2, 2]$, with coefficients given by

$$\beta_j = \mathcal{N}\Big[\tfrac{E-\lambda}{|t_{c,1}|^2} \sin j\theta - \sin(j-1)\theta\Big], \tag{2.75}$$

where $\theta = \cos^{-1}(E/2)$. For any finite L, there are L scattering states from the (perturbed) continuous spectrum of the leads. A generic feature of these L states is their small amplitude at the endpoints. Two continuum states for $\lambda = \mu = 2.5$ are displayed in Fig. 2.10 **c,d**.

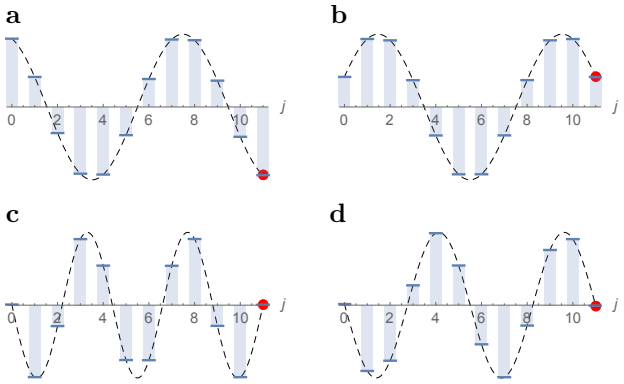

FIGURE 2.11 – (Color online) The two hybridized scattering states (**a,b**) and two states from the continuum (**c,d**) for $(L, t_{c,1}, t_{c,2}) = (10, 0.1, 0.1)$ and $\lambda = \mu = 1.4$. **a** Antisymmetric hybridized state, $E = 1.4044$. **b** Symmetric hybridized state, $E = 1.4226$. The energy separation is $\sim 10^{-2}$. A generic feature of hybridized states is their relatively large amplitude at the endpoints (sites 0 and $L+1$). **c** A symmetric continuum state, $E = 0.282$. **d** An antisymmetric continuum state, $E = 0.827$. Continuum states are visually indistinguishable from those of Fig. 2.10.

When bound states are not present, in addition to the continuum states there will be two hybridized scattering states : one symmetric $|h_S\rangle$ and one antisymmetric $|h_A\rangle$. A generic feature of these states is their relatively large amplitude at the endpoints. Such states are displayed in Fig. 2.11 **a,b** for $\lambda = \mu = 1.4$; for this same case example scattering states with $E \in [-2, 2]$ are displayed in Fig. 2.11 **c,d**.

Decay rates in the presence of bound states $|b_S\rangle$ and $|b_A\rangle$ are compared with decay rates in the presence of hybridized states $|h_S\rangle$ and $|h_A\rangle$. Let the state be

$$|\psi\rangle = \sum_{1}^{L} a_n|n\rangle + c_S|\varphi_S\rangle + c_A|\varphi_A\rangle, \tag{2.76}$$

where $|n\rangle$ is a state from the continuous spectrum, and $|\varphi_{S,A}\rangle$ is bound or hybridized. Then

$$\langle\psi|e^{-itH}|\psi\rangle = \sum_{n=1}^{L} |a_n|^2 e^{-itE_n} + |c_S|^2 e^{-itE_S} + |c_A|^2 e^{-itE_A}. \tag{2.77}$$

Let $f(E_m) = |a_m|^2$ and assume $E_m - E_n \approx (m-n)\epsilon$ where $\epsilon = 4/(L-1)$. In the continuous limit,

$$\langle\psi|e^{-itH}|\psi\rangle \sim \tilde{f}(t) + |c_S|^2 e^{-itE_S} + |c_A|^2 e^{-itE_A}, \tag{2.78}$$

where $\tilde{f}$ is the inverse Fourier transform of f, and

$$\begin{aligned} &|\langle\psi|e^{-itH}|\psi\rangle|^2 \sim \\ &\quad |\tilde{f}(t)|^2 + 2\tilde{f}(t)\big(|c_S|^2 \sin E_S t + |c_A|^2 \sin E_A t\big) \\ &\quad + |c_S|^4 + |c_A|^4 + 2|c_S|^2|c_A|^2 \cos(E_S - E_S)t. \end{aligned} \tag{2.79}$$

If $f(E)$ has support of width ΔE (in $[-2,2]$), its inverse Fourier transform $\tilde{f}(t)$ will decay within time $\Delta t \sim O(1/\Delta E)$. A small decay rate implies that $|\psi\rangle$ has overlap almost zero with most states of the continuous spectrum. This is possible for a *localized* $|\psi\rangle$ only if bound states $|b_S\rangle$ and $|b_A\rangle$ are available, e.g., if $\lambda = \mu \notin [-2,2]$. An example is $|\psi\rangle = (|b_S\rangle + |b_A\rangle)/\sqrt{2}$, which is well localized around the left-hand dot. Then

$$|\langle\psi|e^{-itH}|\psi\rangle|^2 = \frac{1}{2}\big(1+\cos(E_S^b - E_A^b)t\big). \tag{2.80}$$

With the canonical parameter values $(L, t_c) = (10, 0.1)$, this goes slowly to zero with rate $\tau_b^{-1} = E_S^b - E_A^b \sim 10^{-5}$ (and oscillates back and forth unless L is infinite).

If bound states are not available (e.g., if $\lambda = \mu \in [-2,2]$), then a localized state necessarily has an $f(E)$ with large support ΔE, and $|\langle\psi|e^{-itH}|\psi\rangle|^2$ will decay within time $\Delta t \sim O(1/\Delta E)$ to the oscillating steady-state

$$|\langle\psi|e^{-itH}|\psi\rangle|^2 \sim |c_S|^4 + |c_A|^4 + 2|c_S|^2|c_A|^2\cos(E_S^h - E_A^h)t. \tag{2.81}$$

With the same canonical parameter values, this oscillates with rate $\tau_s^{-1} = E_S^h - E_A^h \sim 10^{-2}$. With these values, the characteristic escape time of localized states is reduced by a factor of 10^3 when effective eigenenergies become complex and bound states are no longer available. The overall rate of decay, $\max(\Delta E, E_S^h - E_A^h) \leq 4$, can be as large as $O(1)$. The above analysis shows that the core in either ω-class has the ability to receive and release states over the timescale τ_s or shorter, and to store a state over the much larger timescale τ_b. Switching between these two coupling regimes is performed by tuning the internal parameters of the core. The same procedure is also possible in the nonsymmetric off mode, with somewhat less flexibility due to the large-offset condition.

2.4.3 Qubit initialization and readout

Initializations and measurements are naturally performed through position measurements or energy measurements of either ω-class. Position eigenstates correspond to logical states :

$$|m\rangle = \sum_\ell \mathbb{1}_{\ell,m}|\ell\rangle, \tag{2.82}$$

whereas energy eigenstates of classes X and Y correspond to columns of $\mathcal{F}^\dagger$ and $(\mathcal{F}\mathcal{D})^\dagger$, respectively :

$$|\phi_k\rangle = \sum_\ell \mathcal{F}^\dagger_{\ell,k}|\ell\rangle, \quad |\chi_k\rangle = \sum_\ell (\mathcal{F}\mathcal{D})^\dagger_{\ell,k}|\ell\rangle. \tag{2.83}$$

Define, for instance, the POVM $\{E_0, E_1\}$ with elements the joint-position projectors

$$\begin{aligned} E_0 &= |1\rangle\langle 1| + |2\rangle\langle 2| \\ E_1 &= |3\rangle\langle 3| + |4\rangle\langle 4|. \end{aligned} \tag{2.84}$$

These operators correspond to the measurement/initialization of the *first* qubit only :

$$\begin{aligned} E_0 &= |00\rangle\langle 00| + |01\rangle\langle 01| = |0\rangle\langle 0| \otimes \mathbb{1} \\ E_1 &= |10\rangle\langle 10| + |11\rangle\langle 11| = |1\rangle\langle 1| \otimes \mathbb{1}. \end{aligned} \tag{2.85}$$

Similarly, the POVM $\{E^0, E^1\}$ with elements

$$\begin{aligned} E^0 &= |1\rangle\langle 1| + |3\rangle\langle 3| \\ E^1 &= |2\rangle\langle 2| + |4\rangle\langle 4| \end{aligned} \tag{2.86}$$

corresponds to the measurement/initialization of the *second* qubit :

$$\begin{aligned} E^0 &= |00\rangle\langle 00| + |10\rangle\langle 10| = \mathbb{1} \otimes |0\rangle\langle 0| \\ E^1 &= |01\rangle\langle 01| + |11\rangle\langle 11| = \mathbb{1} \otimes |1\rangle\langle 1|. \end{aligned} \tag{2.87}$$

2.5 Scalability

We now propose a scalable technology for universal quantum computation. The idea is strongly reminiscent of classical computer architecture, in which operations are decomposed into elementary two-bit steps to be performed on large arrays of transistors. Here we use the fact that any unitary U on d qubits can be approximated to arbitrary accuracy by finite products of elementary two-qubit unitaries, i.e., operations of the form $S(m, K) = \mathbb{1}^{\otimes m} \otimes K \otimes \mathbb{1}^{\otimes d-m-2}$, where K is a 4×4 unitary [93]. For any $\epsilon > 0$ there exists a finite sequence of such two-qubit unitaries $S_1, \ldots, S_k$ achieving

$$\max_{|\psi\rangle} \|(U_d - S_1 S_2 \cdots S_k)|\psi\rangle\| < \epsilon, \tag{2.88}$$

where $|\psi\rangle$ is any normalized d-qubit state. We thus consider the possibility of realizing quantum computation on scalable grids of 4-level cores. By analogy with the role played by transistors in classical computation, we may consider the cores to be quantum-computational transistors, or more succinctly, *quansistors*.

2.5.1 Quansistors

The core, or quansistor, is a four-level tight-binding system with the ability to become ω-rotation-invariant for $\omega = 1, e^{i\pi/2}$ (classes X, Y). Until now we have mostly considered the quansistor in its symmetric form, performing computation on its double qubit. From the universality proof of Section 2.3.3, we know that the set of gates $\{\mathsf{V}, \mathsf{W}\}$, constructed from the Hamiltonians (2.25),(2.26), is universal on two qubits. This set contains one representative from each class, X and Y, and these representatives realize inequivalent flux structures. The next step is to allow interactions between quansistors. We choose the most basic two-quansistor interaction, involving one qubit from each quansistor. To that end, we need to materialize the tensor product structure inherent to the quansistor logical basis $\{|00\rangle, |01\rangle, |10\rangle, |11\rangle\}$. Thus far, these qubit states merely label the states of the quansistor, and need to be factored into pairs of *spatially separable* qubits before they can be shared with distinct target quansistors. Let us devote some attention to the nonsymmetric form of the quansistor, which is also the off mode for computation. Note that the off-mode Hamiltonian cannot be the ω-circulant matrix $\epsilon\mathbb{1}$, because the degenerate eigenstates of the latter are unstable to perturbations.

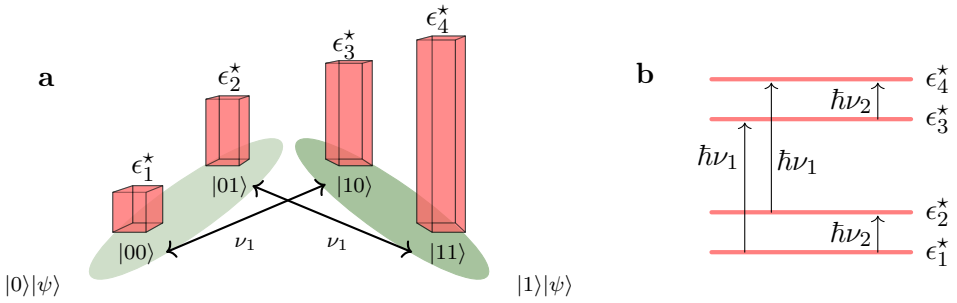

FIGURE 2.12 – (Color online) Quansistor's off mode. **a** Real effective on-site energies $\epsilon_i^\star$ and negligible transition amplitudes $0 < K_{ij} \ll |\epsilon_i^\star - \epsilon_j^\star|$ (not shown). Position is almost a good quantum number, and logical states (position eigenstates) are almost stationary. Resonance at the qubit-splitting frequency ν_1 corresponds to 1st qubit oscillation. The quansistor is then effectively a single qubit with basis states $|0\rangle|\psi\rangle$ and $|1\rangle|\psi\rangle$ (light green and dark green, respectively). **b** Energy diagram satisfying the qubit-splitting conditions (2.92), (2.93).

In the off mode, the Hamiltonian is simply

$$H_{\text{off}} = -\sum_{\langle ij \rangle} K_{ij} a_i^\dagger a_j + \sum_i \epsilon_i^\star a_i^\dagger a_i, \tag{2.89}$$

where $K_{ij} > 0$, and large energy offsets $|\epsilon_i^\star - \epsilon_j^\star| \gg K_{ij}$ effectively suppress spontaneous transitions, so that position i is almost a good quantum number in the off mode. (As before, the symbol "$\star$" indicates an effective energy due to the presence of the leads.) Logical states $\{|00\rangle, |01\rangle, |10\rangle, |11\rangle\}$ coincide with position eigenstates $\{|1\rangle, |2\rangle, |3\rangle, |4\rangle\}$, respectively. Section 2.3.6 illustrates how the system can be switched from (2.89) to ω-circulant Hamiltonians of class X or Y and back using electrically charged levels and magnetic fields on the one hand, and neutral levels and synthetic gauge fields on the other. Notice that

$$\begin{aligned} \text{span}\{|1\rangle, |2\rangle\} &= \{|0\rangle|\psi\rangle \,|\, \psi \text{ any 2nd qubit state } \} \\ \text{span}\{|3\rangle, |4\rangle\} &= \{|1\rangle|\psi\rangle \,|\, \psi \text{ any 2nd qubit state } \} \end{aligned} \tag{2.90}$$

(see Fig. 2.12). Similarly,

$$\begin{aligned} \text{span}\{|1\rangle, |3\rangle\} &= \{|\psi\rangle|0\rangle \,|\, \psi \text{ any 1st qubit state } \} \\ \text{span}\{|2\rangle, |4\rangle\} &= \{|\psi\rangle|1\rangle \,|\, \psi \text{ any 1st qubit state } \} \end{aligned} \tag{2.91}$$

(see Fig. 2.13). We now demand that the off-mode on-site energies satisfy

$$\epsilon_3^\star - \epsilon_1^\star = \hbar\nu_1 = \epsilon_4^\star - \epsilon_2^\star, \tag{2.92}$$

$$\epsilon_2^\star - \epsilon_1^\star = \hbar\nu_2 = \epsilon_4^\star - \epsilon_3^\star \tag{2.93}$$

Eqs. (2.90) and (2.92) imply that setting the quansistor into resonance at frequency ν_1 prompts the onset of 1st-qubit oscillations $|0\rangle|\psi\rangle \leftrightarrow |1\rangle|\psi\rangle$ with frequency ν_1. By

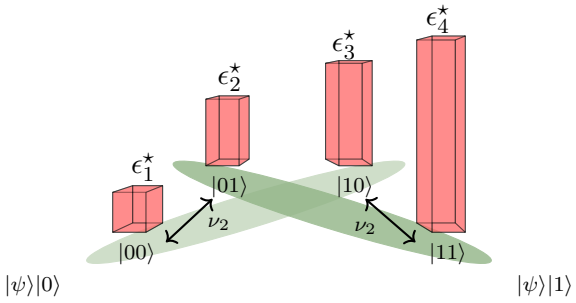

FIGURE 2.13 – (Color online) Quansistor's off mode. Resonance at the qubit-splitting frequency ν_2 corresponds to 2nd qubit oscillation. The quansistor is then effectively a single qubit with basis states $|\psi\rangle|0\rangle$ and $|\psi\rangle|1\rangle$ (light green and dark green, respectively).

the same token, Eqs. (2.91) and (2.93) imply that quansistor resonance at frequency ν_2 corresponds to 2nd-qubit oscillations $|\psi\rangle|0\rangle \leftrightarrow |\psi\rangle|1\rangle$ at frequency ν_2. For this reason, the frequencies ν_1 and ν_2 may be called *qubit splitting*, and will be used to exchange single qubits between distant quansistors. When coupled to a single-mode resonator, the quansistor resonating at one of these frequencies ν_q will effectively look like a single qubit coupled to the oscillator as described by the Jaynes-Cummings Hamiltonian

$$H_{\rm JC} = \hbar\nu_r a^\dagger a + \frac{\hbar\nu_q}{2}\sigma_z + \hbar g(a^\dagger\sigma^+ + a\sigma^-), \tag{2.94}$$

where $\sigma_z = |1\rangle\langle 1| - |0\rangle\langle 0|$. The frequencies $\nu_1 \pm \nu_2$, on the other hand, are not qubit splitting, and correspond to the oscillations $|00\rangle \leftrightarrow |11\rangle$ and $|01\rangle \leftrightarrow |10\rangle$, respectively.

2.5.2 Scalable architecture

Interactions between quansistors are to be performed by bringning their qubit-splitting frequencies into resonance. It seems desirable to mediate the coupling with single-mode resonators, allowing distributed circuit elements, and to work in the dispersive regime where two quansistors A, B are mutually resonant, but far-detuned from the resonator :

$$\nu_A = \nu_B \neq \nu_r. \tag{2.95}$$

The interaction then proceeds through virtual photon exchange, as opposed to real photons in the resonant regime, alleviating the major drawback of the latter, namely the resonator-induced decay due to energy exchange with the resonator (Purcell effect) [43]. In the rotating wave approximation, the Hamiltonian in the absence of direct coupling between the quansistors is

$$H = \hbar\nu_r a^\dagger a + \sum_{j=A,B}\frac{\hbar\nu_q}{2}\sigma_{z,j} + \sum_{j=A,B}\hbar g_j(a^\dagger\sigma_j^- + a\sigma_j^+), \tag{2.96}$$

where ν_q is the common frequency of A and B. We use the Baker-Campbell-Hausdorff formula $e^S H e^{-S} = H + [S,H] + \frac{1}{2!}[S,[S,H]] + \dots$ to perform the unitary transfor-

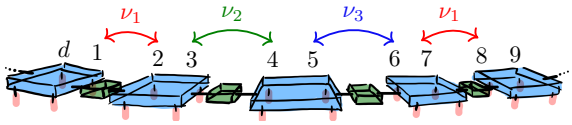

FIGURE 2.14 – (Color online) A d-quansistor linear array for universal computation on $2d$ qubits. The numbers schematically represent the qubits. Quansistors (larger, blue) perform two-qubit universal operations on qubit pairs $(2j, 2j+1)$, $j = 0, \ldots, d-1 \,(\mathrm{mod}\, d)$. Couplers (smaller, green) perform entangling $\sqrt{i\mathsf{SWAP}}$ gates on qubit pairs $(2j-1, 2j)$, $j = 0, \ldots, d-1 \,(\mathrm{mod}\, d)$. Leads are attached to the lower faces of the quansistors. With only three qubit-splitting frequencies in the system, ν_1, ν_2, ν_3, untimely second-nearest-quansistor interactions occur at higher orders. (For instance, pairs (2,3) and (6,7) both respond to ν_1.) More frequencies may be added to suppress these unwanted exchanges. The required physical resources scale linearly in the number of qubits.

mation $U = \exp \sum_j \frac{g_j}{\Delta}(a^\dagger \sigma_j^- - a\sigma_j^+)$, with detuning $\Delta = |\nu_r - \nu_q|$. To first order in g_j/Δ we get

$$H = \hbar\nu_r a^\dagger a + \sum_{j=A,B} \frac{\hbar\nu_q}{2}\sigma_{z,j} + \hbar K(\sigma_A^+\sigma_B^- + \sigma_A^-\sigma_B^+), \tag{2.97}$$

where $K = 2\hbar g_A g_B/\Delta$. The qubit-cavity interaction terms cancel out exactly, leaving only an effective qubit-qubit interaction with coupling K. This term, when evolved for a time $\pi/4K$, generates the $\sqrt{i\mathsf{SWAP}}$ gate, which is entangling and equivalent to the CNOT gate [193, 43], up to single-qubit operations already available within the quansistors. The dispersive regime thus allows for the possibility of long-distance entangling interactions between quansistors.

One possible architecture for universal computation on $2d$ qubits consists in a closed linear array of d quansistors coupled through resonators. Each quansistor represents a pair of qubits, and every qubit is represented exactly once (see Fig. 2.14). Additional qubit-splitting frequencies may be added to prevent untimely higher-order, mth-nearest-neighbor couplings. To cut down space and running time costs, a physical implementation of the array would likely be folded, and a resonator would couple every adjacent pair of quansistors, thus reducing considerably the need for qubit-shuffling operations. Fig. 2.15 schematically depicts a planar-grid computer. Each quansistor would be coupled to four identical leads (not shown in the figure) for initialization and readout.

2.6 Discussion

In this work, we have not discussed encoded logic and fault tolerance. Error-correcting codes are a promising avenue to make quantum computation fault-tolerant. In our technology, quansistors are the support of the *physical* qubits, whose states and interactions are symmetry-protected, to some extent, against external influences.

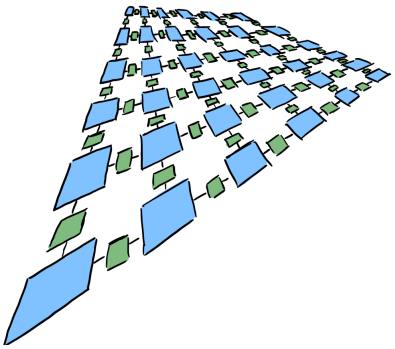

FIGURE 2.15 – (Color online) A 36-quansistor grid for universal computation on 72 qubits. Quansistors (large blue squares) perform universal two-qubit operations. Couplers (smaller green squares) perform entangling $\sqrt{i\mathsf{SWAP}}$ between qubits of adjacent quansistors. Each quansistor is coupled to four identical leads (not shown) for initialization and readout. The required physical resources scale linearly in the number of qubits.

Once we identify the dominant errors affecting them, we can find k-qubit states (typically $k = 5, 7, 9$) that are invariant under those errors. These are the encoded *logical* qubits. (In the standard Hamming notation, we get a code of type $[kn, n]$ using kn physical qubits, and having 2^n logical codewords [256].) Having *physical* universality at hand gives the freedom to encode qubits and operations yielding *encoded* universality. Because our technology is scalable (Q quansistors making $2Q$ qubits), the value of k is not an issue : the encoding merely uses k identical 'processors' instead of one. Crucially, we must determine whether the dominant errors are constrained by the symmetry of the quansistors. We have already observed a significant robustness of the universal set $\{\mathsf{V}, \mathsf{W}\}$ against single-qubit and double-qubit x- and z-rotation errors. As a second source of decoherence we considered the coupling to semi-infinite leads, and have omitted other factors such as the effect of a heat bath on the system, the types of errors that it would produce, and the extent to which it would destroy symmetry.

Throughout, we have used ω-rotation invariance as the prototype of a symmetry of flat classes, universal for quantum computation, and realistically implementable physically. Other flat classes would perform equally well at protecting information and operations, as long as leads (or any other immediate environment of the clusters) do not break the corresponding symmetry. Universal sets of gates originating from nondegenerate Hamiltonians are symmetry-specific, but should not be too difficult to find given the relative scarcity of non-universal sets and the completeness of flat classes. The possibilities of physical implementation, on the other hand, will strongly depend on the chosen symmetry and would have to be found on a case-by-case basis.

There might be additional value to using larger qubit clusters, i.e. k-qubit quansistors realized as 2^k sites with symmetries, for $k = 3, 4, 5$. All observations from the previous point regarding protection, universality, and implementation, apply here as well. Larger clusters and symmetry classes would offer protection to k-qubit ope-

rations. It could also allow the encoding of a logical qubit within a *single* k-qubit quansistor. Encodings with $k = 3$ (8 sites) can already correct some single-qubit errors, while some encodings with $k = 5$ (32 sites) can correct *any* single-qubit error [209].

There is provable surplus value to using higher alphabets (ququarts, specifically), instead of qubit pairs, in encrypted communications [33]. Since ω-circulant 4-level quansistors are universal in $\mathbf{U}(4)$, i.e. universal for single-*ququart* operations, and have the ability to dynamically decouple from the leads, a quansistor-with-leads could be a versatile memory unit for ququarts, and become an essential component of quantum-secure communications. Generalizations to d-level quansistors (qudits), with $d > 4$, is also conceivable, as argued in the previous point. Error-correcting codes, notably, have been developed for qudits, that use $d \times d$ Weyl matrices (or equivalently the $d \times d$ version of our matrices X and Y) [122, 124]. Note, however, that the diagram of transition amplitudes of the general qudit (K_d in graph theory terminology) is non-planar for $d \geq 5$ [233], in contrast to the essentially planar diagram K_4 of the 4-level system, Fig. 2.6. A gauge potential implementation of ω-rotation invariant qudits, in the spirit of Sections 2.3.5 and 2.3.6, might then be essentially three-dimensional.

For the purpose of reconstructing the final state of an N-qubit system, a symmetry based on Pauli tensors of dimension $d = 2^N$ is better suited than ω-rotation invariance (based on Weyl matrices) as it allows for the maximal number $(2^N + 1)$ of mutually unbiased bases, and complete state characterization via state tomography [26, 185]. By contrast, the 4-level quansistor ($N = 2$) based on ω-rotation invariance has only *three* unbiased bases : $\{|m\rangle\}$, $\{|\phi_k\rangle\}$, $\{|\chi_k\rangle\}$, the respective eigenbases of Z, X, Y. As for reconstructing the final state of an N-qu$p$it system (where p is an odd prime), the Weyl-based scheme of dimension $d = p^N$ allows for the maximal number $(p^N + 1)$ of mutually unbiased bases, and complete state characterization via quantum tomography [26, 95]. This could be of value for encrypted communication using a higher (prime) alphabet (see previous point), and could be based on p-site quansistors with ω-rotation invariance.

To perform inter-quansistor interactions, we have used the simplest possible scenario involving a single qubit from each quansistor. It would be worth investigating whether a combined use of resonators and symmetry could make possible the implementation of robust 3- and 4-qubit gates, or even interactions soliciting three quansistors or more. However, this is beyond the scope of this work.

2.7 Conclusion

In this work, we have put forward a blueprint for scalable universal quantum computation based on 2-qubit clusters (quansistors) protected by symmetry (ω-rotation invariance). We find a significant robustness of the proposed universal set against single-qubit and double-qubit x- and z-rotation errors. Embedding in the environment, initialization and readout are achieved by tunnel-coupling each quansistor to four identical semi-infinite leads. We show that quansistors can be dynamically decoupled from the leads by tuning their internal parameters, giving them

the versatility required to act as controllable quantum memory units. With this dynamical decoupling, universal 2-qubit logical operations within quansistors are also symmetry-protected against unbiased noise in their parameters. Two-quansistor entangling operations are achieved by resonator-coupling their qubit-splitting frequencies to effectively carry out the $\sqrt{i\mathsf{SWAP}}$ gate, with one qubit coming from each quansistor. We have also identified platforms that could implement ω-rotation invariance.

2.8 Appendices

2.8.1 Mathematical framework

This section describes some mathematical aspects of ω-rotation invariance. Although this paper has focused on a four-level system, many of the results are easily generalized. Here we consider the more general case of an N-level system. For multiple reasons it may be desirable to have full control over the N eigenenergies of the system. In what follows we consider what we propose to call *flat classes* of Hamiltonians : classes of Hermitian matrices $\{H(\mathbf{g}) \mid \mathbf{g} \in \mathbb{R}^N\}$ with a common eigenbasis, and real eigenenergies $\lambda_1(\mathbf{g}), \ldots, \lambda_N(\mathbf{g})$ in one-to-one linear correspondence with the values of the parameters, that is $\lambda_r(\mathbf{g}) = \sum_s g_s \lambda_{sr}$ with $\det[\lambda_{sr}] \neq 0$. (The term *flat* refers to vanishing Berry curvature in $\mathbf{g}$-space.) A class of Hamiltonians is flat in this sense if and only if it can be represented as a sum of $N \times N$ Hermitian matrices,

$$H(g_1, \ldots, g_N) = \sum_{s=1}^{N} g_s H_s \quad , \quad [H_s, H_r] = 0 \quad (\forall s, r) \tag{2.98}$$

and the $N \times N$ matrix $[\lambda_{sr}]$ of all eigenvalues of the H_s's is nonsingular, $\det[\lambda_{sr}] \neq 0$. (The key observation is the action of the diagonalizing unitary : $\mathcal{U}^{-1}(\sum_s g_s H_s)\mathcal{U} = \sum_s g_s \mathrm{diag}(\lambda_{s1}, \ldots, \lambda_{sN}) = \mathrm{diag}(\lambda_1(\mathbf{g}), \ldots, \lambda_N(\mathbf{g}))$.) Flat classes therefore coincide with N-dimensional commutative algebras of $N \times N$ Hermitian matrices, the nonsingularity of $[\lambda_{sr}]$ being equivalent to the linear independence of the H_s's. Because each flat class is diagonalized by a common unitary $\mathcal{U}$ (unique up to permutations), the set of all flat classes that correspond to the same $[\lambda_{sr}]$ is in one-to-one correspondence with unitaries modulo permutations. (In this paper, we do not consider non-unitarily diagonalizable matrices, like non-Hermitian $\mathcal{PT}$-symmetric Hamiltonians, for instance.) The exponentials of a flat class also share the common eigenbasis of the class, and their eigenenergies are in (nonlinear) one-to-one correspondance with the values of the parameters $\mathbf{g}$. There seems to be an interesting connection between flat classes, on the one hand, and commuting bases of unitary matrices [26] and stabilizers of quantum error-correcting codes [122], on the other.

For the purpose of quantum computation a single flat class is clearly not enough because it is commutative. The ω-circulant matrices defined in (2.6) are of the form (2.98), and constitute a flat class for each ω. Independent control over the energy levels is a prime motivation for using ω-rotation invariance, but we stress again that this choice of symmetry is far from unique. Starting from any nonsingular matrix

$[\lambda_{sr}]$, defining the functions $\lambda_r(\mathbf{g}) = \sum_s g_s \lambda_{sr}$, and applying any unitary $\mathcal{U}$ to the matrix class $\{\mathrm{diag}(\lambda_1(\mathbf{g}), \ldots, \lambda_N(\mathbf{g})) \mid \mathbf{g} \in \mathbb{R}^N\}$ will produce a commutative family of (Hermitian) Hamiltonian matrices $\mathcal{H}(\mathbf{g})$ with eigenstates independent of $\mathbf{g}$, and linearly controlled eigenenergies $\lambda_r(\mathbf{g})$, i.e. a flat class. If symmetries other than ω-rotation invariance were preferred for practical reasons, one would replace the diagonalizing unitaries $\mathcal{F}$ and $\mathcal{FD}$, defined in Eqs. (2.9),(2.10), with the appropriate operations.

Although the particular universal set $\{\mathsf{V}, \mathsf{W}\}$ mentioned in the text is generated by representatives of two gauge-inequivalent flat classes, we should mention that this is not necessary in principle. The simplest two-qubit counterexample would involve, on the one hand, the flat class spanned by $\{\sigma_x \otimes \mathbb{1}, \mathbb{1} \otimes \sigma_x, \sigma_x \otimes \sigma_x\}$, and on the other hand the flat class spanned by $\{\sigma_y \otimes \mathbb{1}, \mathbb{1} \otimes \sigma_y, \sigma_y \otimes \sigma_y\}$. These classes are gauge-equivalent under the diagonal unitary

$$\mathcal{U} = \begin{pmatrix} 1 & 0 \\ 0 & i \end{pmatrix}^{\otimes 2}, \tag{2.99}$$

and yet together they are universal on two qubits. [1]

It is instructive to recast ω-rotations in terms of Sylvester's clock-and-shift matrices (also called Weyl's matrices or generalized Pauli matrices)

$$Z_4 = \begin{pmatrix} 1 & & & \\ & \omega & & \\ & & \omega^2 & \\ & & & \omega^3 \end{pmatrix}, \quad X_4 = \begin{pmatrix} 0 & 1 & 0 & 0 \\ 0 & 0 & 1 & 0 \\ 0 & 0 & 0 & 1 \\ 1 & 0 & 0 & 0 \end{pmatrix}, \tag{2.100}$$

with $\omega = e^{i\pi/2}$. For $k = 0, \ldots, 3$ we have the identity $Z_4^k X_4 = J_{e^{ik\pi/2}}$. The matrices $\{Z_4^k X_4^j\}_{k,j=0,\ldots,3}$ constitute a non-Hermitian trace-orthogonal basis for $\mathfrak{gl}(4, \mathbb{C})$, and in fact the same is true of their obvious N-dimensional generalization, with $\omega = e^{i2\pi/N}$, which span $\mathfrak{gl}(N, \mathbb{C})$ and are orthogonal under the Hilbert-Schmidt inner product. If $N = 2$, they reduce (up to a factor) to the Pauli matrices. The matrices X_N and Z_N are central to Weyl's formulation of periodic finite-dimensional quantum mechanics where they respectively correspond to finite position and momentum shifts :

$$\begin{aligned} X_N &= e^{i(2\pi/N)\hat{p}}, \quad X_N|x\rangle = |x - 1 \bmod N\rangle \\ Z_N &= e^{i(2\pi/N)\hat{x}}, \quad Z_N|p\rangle = |p + 1 \bmod N\rangle \end{aligned} \tag{2.101}$$

where of course $|x\rangle$ and $|p\rangle$ are position and momentum eigenstates, respectively. Thus ω-rotation invariance is a symmetry in quantum (or optical) phase space, and is not found in other, internal-space generalizations of Pauli matrices like Pauli tensor products or Gell-Mann matrices.

In any dimension larger than 2, the eigenbases of Z_N, X_N, and $Z_N X_N$ are *mutually unbiased* : a measurement in one (orthonormal) basis $\{|\psi_r\rangle\}$ provides no information about measurements in another (orthonormal) basis $\{|\eta_s\rangle\}$ because $|\langle\psi_r|\eta_s\rangle| = \frac{1}{\sqrt{N}}$ for any r, s. In particular when $N = 4$, the flat classes of Z_4, X_4 (the

1. We thank one of the Referees for this observation.

matrix X in the main text), and Y_4 (the matrix Y in the main text) have mutually unbiased eigenbases $\{|m\rangle\}, \{|\phi_k\rangle\}$, and $\{|\chi_k\rangle\}$ respectively. (See (2.15) and (2.21).)

2.8.2 Effective core Hamiltonian

Consider an N-level core tunnel-coupled to N identical semi-infinite leads :

$$\begin{aligned}\mathcal{H} &= \mathcal{H}_{\text{core}} + \mathcal{H}_{\text{int}} + \mathcal{H}_{\text{lead}} \\ &= \frac{1}{2}\sum_{i,j=1}^{4} h_{ij} a_i^\dagger a_j + \sum_{i=1}^{4} t_{c,i} a_i^\dagger b_{i,1} + \sum_{i=1}^{4}\sum_{j=1}^{\infty} b_{i,j}^\dagger b_{i,j+1} + \text{ h.c.}\end{aligned} \tag{2.102}$$

For the time being, the matrix h is not required to be Hermitian, and the couplings $t_{c,i}$ need not be equal, but could be chosen real positive with no loss of generality since the Hamiltonian is invariant under $t_{c,i} \to t_{c,i}e^{i\theta_i}$, $b_{i,j} \to b_{i,j}e^{-i\theta_i}$. We let them be complex anyways. Let us restrict the system's dynamics to the single-particle sector of Hilbert space. For illustration purposes, our examples below will use a core with $N = 3$ levels, but all the results go over to general N. The one-particle Hamiltonian matrix H with $N = 3$ is

$$\left[\begin{array}{ccc|ccc|ccc} h_{11} & h_{12} & h_{13} & t_{c,1} & & & & & & & & \\ h_{21} & h_{22} & h_{23} & & & & t_{c,2} & & & & & \\ h_{31} & h_{32} & h_{33} & & & & & & & t_{c,3} & & \\ \hline t_{c,1}^* & & & 0 & 1 & & & & & & & \\ & & & 1 & 0 & \ddots & & & & & & \\ & & & & \ddots & \ddots & & & & & & \\ \hline & t_{c,2}^* & & & & & 0 & 1 & & & & \\ & & & & & & 1 & 0 & \ddots & & & \\ & & & & & & & \ddots & \ddots & & & \\ \hline & & t_{c,3}^* & & & & & & & 0 & 1 & \\ & & & & & & & & & 1 & 0 & \ddots \\ & & & & & & & & & & \ddots & \ddots \end{array}\right] \tag{2.103}$$

which we write as

$$H = \left[\begin{array}{c|c} h & V \\ \hline V^\dagger & \mathbb{1}_3 \otimes h_{\text{lead}} \end{array}\right] \tag{2.104}$$

in obvious notation. The corresponding Green's function is

$$\begin{aligned} G(E) &= (E\mathbb{1} - H)^{-1} \\ &= \left[\begin{array}{c|c} E\mathbb{1}_3 - h & -V \\ \hline -V^\dagger & \mathbb{1}_3 \otimes (E\mathbb{1}_{\text{lead}} - h_{\text{lead}}) \end{array}\right]^{-1}, \end{aligned} \tag{2.105}$$

where $\mathbb{1}_{\text{lead}}$ is the identity on the single-lead space. The top-left 3×3 block of the Green's function, $G_{\text{core}}(E)$, can be obtained using the blockwise inversion formula

$$\left[\begin{array}{c|c} A & B \\ \hline C & D \end{array}\right]^{-1} = \left[\begin{array}{c|c} \left(A - BD^{-1}C\right)^{-1} & \cdots \\ \hline \cdots & \cdots \end{array}\right]. \tag{2.106}$$

We obtain

$$\begin{aligned} G_{\text{core}}(E) &= \left(E\mathbb{1}_3 - h - V\left[\mathbb{1}_3 \otimes (E\mathbb{1}_{\text{lead}} - h_{\text{lead}})\right]^{-1} V^\dagger\right)^{-1} \\ &= \left(E\mathbb{1}_3 - h_\infty(E)\right)^{-1}. \end{aligned} \tag{2.107}$$

Noticing that

$$\left(\mathbb{1}_3 \otimes (E\mathbb{1}_{\text{lead}} - h_{\text{lead}})\right)^{-1} = \mathbb{1}_3 \otimes G_{\text{lead}}(E), \tag{2.108}$$

$G_{\text{lead}}(E)$ being the Green function of a single lead, we obtain from (2.107)

$$h_\infty(E) = h + V\left(\mathbb{1}_3 \otimes G_{\text{lead}}(E)\right) V^\dagger. \tag{2.109}$$

A straightforward calculation yields

$$h_\infty(E) = h + \begin{bmatrix} |t_{c,1}|^2 & & \\ & |t_{c,2}|^2 & \\ & & |t_{c,3}|^2 \end{bmatrix} \Sigma(E), \tag{2.110}$$

where $\Sigma(E)$ is the surface Green's function of a single lead :

$$\Sigma(E) = (G_{\text{lead}})_{00}(E) = \frac{E}{2} - \frac{\sqrt{(E+i0^+)^2 - 4}}{2}. \tag{2.111}$$

The analogous version of (2.110) for general N is now obvious. Remarkably, if h is ω-circulant and $|t_{c,i}| = t_c$ for all i, the effective Hamiltonian $h_\infty(E)$ is also ω-circulant :

$$h = \sum_{s=0}^{3} z_s J_\omega^s \;\longrightarrow\; h_\infty(E) = \left(z_0 + t_c^2 \Sigma(E)\right)\mathbb{1} + \sum_{s=1}^{3} z_s J_\omega^s. \tag{2.112}$$

In particular, when h is 4×4 Hermitian we obtain expression (2.58) in the main text. Again, the fact that $h_\infty(E)$ is unaffected by the presence of phase factors, dynamical or stochastic, in the core-to-lead couplings $t_{c,i}$ is a consequence of (2.102) being invariant under $t_{c,i} \to t_{c,i} e^{i\theta_i}$, $b_{i,j} \to b_{i,j} e^{-i\theta_i}$.

2.8.3 Analytical solution : Two cores connected by finite leads

We analytically solve the Schrödinger equation of two ω-circulant N-level cores (with the same ω, but possibly different core Hamiltonians h_1 and h_2) connected face-to-face by N identical leads of L sites. The Hamiltonian is

$$\begin{aligned} H =& \frac{1}{2}\sum_{s=1}^{2} \mathbf{a}_s^\dagger \cdot h_s \cdot \mathbf{a}_s + t_{c,1}\, \mathbf{a}_1^\dagger \cdot \mathbf{b}_1 + t_{c,2}\, \mathbf{a}_2^\dagger \cdot \mathbf{b}_L \\ &+ \sum_{j=1}^{L-1} \mathbf{b}_j^\dagger \cdot \mathbf{b}_{j+1} + \text{h.c.}\,, \end{aligned} \tag{2.113}$$

where $\mathbf{a}_s = (a_{s,1}, \ldots, a_{s,N})$ and $\mathbf{b}_j = (b_{1,j}, \ldots, b_{N,j})$. Leads have hopping energies all equal, and set to unity (thus setting the scale for all energies). Eigenvalues of the

unitary symmetry (ω-rotation) correspond to superselection sectors. Without loss of generality, energy eigenstates may be chosen to have support in exactly one sector k. If h_1, h_2 are ω-circulant with $\omega = e^{iq\pi/2}$ and $q = 0, \ldots, 3$, the change of basis Eqs. (2.9),(2.10)

$$\mathbf{a}_s \to \tilde{\mathbf{a}}_s = \mathcal{F}\mathcal{D}^q \mathbf{a}_s \quad , \quad \mathbf{b}_j \to \tilde{\mathbf{b}}_j = \mathcal{F}\mathcal{D}^q \mathbf{b}_j, \tag{2.114}$$

decouples the system into N identical modes, each in the form of two dots of self-energies λ_k, μ_k connected by a finite lead of L sites. The single-particle Hamiltonian for one of these modes is

$$H_{1P} = \left[\begin{array}{c|cccc} \lambda_k & t_{c,1} & & & \\ \hline t_{c,1}^* & 0 & 1 & & \\ & 1 & 0 & \ddots & \\ & & \ddots & \ddots & t_{c,2} \\ \hline & & & t_{c,2}^* & \mu_k \end{array}\right]. \tag{2.115}$$

Let $|\psi\rangle = \alpha|0\rangle + \sum_{j=1}^{L} \beta_j |j\rangle + \gamma|L+1\rangle$ be a single-particle eigenstate in sector k, where $|j\rangle$ is the state with a single particle in the jth site. The Schrödinger equation $E|\psi\rangle = H_{1P}|\psi\rangle$ yields the relations

$$\beta_1 = \Delta\beta_0 \tag{2.116}$$

$$\beta_j + \beta_{j+2} = E\beta_{j+1} \qquad (0 \le j \le L-1) \tag{2.117}$$

$$\beta_L = \tilde{\Delta}\beta_{L+1} \tag{2.118}$$

$$\Delta = \frac{E-\lambda}{|t_{c,1}|^2} \tag{2.119}$$

$$\tilde{\Delta} = \frac{E-\mu}{|t_{c,2}|^2}. \tag{2.120}$$

where we have assumed that $t_{c,i} \neq 0$, and defined $\beta_0 = t_{c,1}^* \alpha$ and $\beta_{L+1} = t_{c,2}\gamma$. The bulk equation (2.117) is translation-invariant with general solution

$$\beta_j = Ae^{ij\theta} + Be^{-ij\theta} \quad , \quad \theta = \cos^{-1}\frac{E}{2}. \tag{2.121}$$

The boundary conditions (2.116),(2.118) give the ratio

$$\frac{A}{B} = \frac{\Delta - e^{-i\theta}}{e^{i\theta} - \Delta} = e^{-2i\theta(L+1)} \left(\frac{\tilde{\Delta} - e^{i\theta}}{e^{-i\theta} - \tilde{\Delta}}\right), \tag{2.122}$$

and the eigenenergies, $E = 2\cos\theta$, in implicit form

$$(\Delta + \tilde{\Delta})\sin\theta L - \Delta\tilde{\Delta}\sin\theta(L+1) - \sin\theta(L-1) = 0. \tag{2.123}$$

In terms of Chebyshev polynomials of the second kind

$$U_n(\cos\theta) = \frac{\sin(n+1)\theta}{\sin\theta}, \tag{2.124}$$

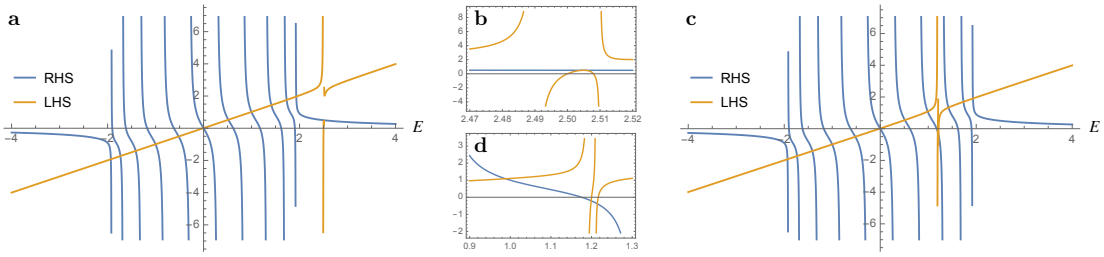

FIGURE 2.16 – (Color online) Left-hand (LHS) and right-hand (RHS) sides of (2.127) for $L = 11$, and $|t_{c,1}| = |t_{c,2}| = 0.1$. The LHS curve crosses the RHS curve $L+2$ times. One solution has energy $\sim O(\lambda|t_{c,1}|^2)$, a consequence of weakly broken spectrum symmetry $E \leftrightarrow -E$ due to simultaneous nonzero $t_{c,1}$ and nonzero λ. **a** For $\lambda = \mu = 2.5$, the crossings correspond to L continuum states in the band, plus two bound states near λ. **b** Zoom-in of λ's neighborhood for $\lambda = \mu = 2.5$. The nearly degenerate bound state energies $E = 2.504980$ and $E = 2.504987$ are not resolved yet, but we plot these states in Fig. 2.17. **c** For $\lambda = \mu = 1.2$ the LHS curve crosses the RHS curve $L+2$ times within the band. **d** Zoom-in of the neighborhood of λ for $\lambda = \mu = 1.2$, showing one continuous scattering mode (leftmost) and two hybridized scattering modes with energy separation $\sim 10^{-2}$.

and recalling the recursion relation

$$U_n(x) = 2xU_{n-1}(x) - U_{n-2}(x), \tag{2.125}$$

we find

$$\boxed{\frac{\Delta\tilde{\Delta}E - \Delta - \tilde{\Delta}}{\Delta\tilde{\Delta} - 1} = \frac{U_{L-2}(E/2)}{U_{L-1}(E/2)}} \tag{2.126}$$

as in Eq.(2.71) of the main text. In the simplest case where $\lambda = \mu$ and $|t_{c,1}|^2 = |t_{c,2}|^2$ (identical dots, identical couplings), we have

$$\frac{(E-\lambda)\left(E(E-\lambda) - 2|t_{c,1}|^2\right)}{(E-\lambda+|t_{c,1}|^2)(E-\lambda-|t_{c,1}|^2)} = \frac{U_{L-2}(E/2)}{U_{L-1}(E/2)}. \tag{2.127}$$

The system's $L+2$ eigenvalues coincide with the solutions of the above equation. Notice that for small $|t_{c,1}|$ the LHS is $\sim E + O(|t_{c,1}|^2)$ when E is not in the vicinity of the singularities $\lambda \pm |t_{c,1}|^2$. This is illustrated in Fig. 2.9 of the main text for L even ($L = 10$), and in Fig. 2.16 for L odd ($L = 11$). In this symmetric case for which $\Delta = \tilde{\Delta}$, all eigenstates are either symmetric or antisymmetric. This is seen from (2.122), which becomes $A/B = e^{-2i\theta(L+1)}(A/B)^{-1}$, implying

$$\left(\frac{A}{B}\right) = 1 \quad \text{and} \quad e^{-i\theta(L+1)} = \pm\frac{A}{B}. \tag{2.128}$$

Substituting in (2.121) gives $\beta_{L+1-j} = \pm\beta_j$.We must consider two cases : when E is outside the energy band of the leads, and when it is within this energy band.

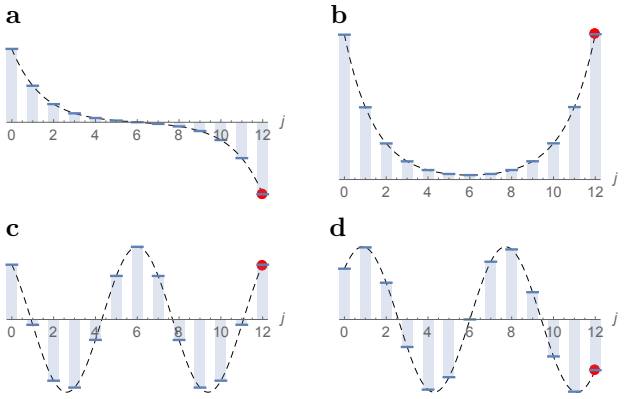

FIGURE 2.17 – (Color online) States from the case $L = 11$, and $|t_{c,1}| = |t_{c,2}| = 0.1$. **a,b** The two bound states for $\lambda = \mu = 2.5$ **a** Antisymmetric bound state, $E = 2.504980$. **b** Symmetric bound state, $E = 2.504987$. The energy separation is $\sim 10^{-5}$. **c,d** The two hybridized states for $\lambda = \mu = 1.2$. **c** Symmetric hybridized state, $E = 1.1990$. **d** Antisymmetric hybridized state, $E = 1.2142$. The energy separation is $\sim 10^{-2}$. In each graph, the red dot represents the value of β_{L+1} from the consistency condition (2.118).

2.8.3.1 Bound states (E outside the band)

When E is outside the energy band of the leads, we have $\theta = i\xi$ if $E > 2$, and $\theta = \pi + i\xi$ if $E < -2$, where $\xi = \cosh^{-1}(|E|/2)$ is a real parameter. Then

$$\beta_j = (\pm 1)^j \mathcal{N} \left[\tfrac{|E| \pm \lambda}{|t_{c,1}|^2} \sinh j\xi - \sinh(j-1)\xi \right] \tag{2.129}$$

with $\pm = \mathrm{sgn}(E)$, where $\mathcal{N}$ is a normalization factor, and where the eigenenergies satisfy the constraint

$$\Delta\tilde{\Delta} \sinh(L+1)\xi \mp (\Delta + \tilde{\Delta}) \sinh L\xi + \sinh(L-1)\xi = 0. \tag{2.130}$$

Alternatively, we can write the solution as

$$\beta_{L+1-j} = (\pm 1)^j \mathcal{N}' \left[\tfrac{|E| \pm \mu}{|t_{c,2}|^2} \sinh j\xi - \sinh(j-1)\xi \right]. \tag{2.131}$$

A generic feature of these bound states is their large amplitude at the dots. Because there are at least L states from the continuous spectrum (see next section), there are at most two bound states. The bound states for $L = 10$ and $\lambda = \mu = 2.5$ are displayed in Fig.2.10 **a,b** of the main text. The bound states for $L = 11$ are plotted in Fig. 2.17 **a,b**.

In the limit $L \to \infty$, the constraint is equivalent to

$$e^{2\xi} \mp \left(\frac{1}{\Delta} + \frac{1}{\tilde{\Delta}} \right) e^{\xi} + \frac{1}{\Delta\tilde{\Delta}} = \left(e^{\xi} \mp \frac{1}{\Delta} \right) \left(e^{\xi} \mp \frac{1}{\tilde{\Delta}} \right) = 0, \tag{2.132}$$

yielding $e^{-\xi} = \pm\Delta$ or $e^{-\xi} = \pm\tilde{\Delta}$. The resulting expressions for β_j and β_{L+1-j} describe bound states localized at either dot and decaying exponentially with distance

over the characteristic length ξ^{-1}. Moreover, the constraint equations for $e^{-\xi}$ are equivalent to the fixed-point relations $E = \lambda \pm |t_{c,1}|^2\Sigma(E)$ and $E = \mu \pm |t_{c,2}|^2\Sigma(E)$, respectively. These relations can be obtained as normalizability conditions on the eigenstates of a dot connected to a *semi-infinite* lead, by solving the corresponding Schrödinger equation. Alternatively, the Green's function treatment of the core with semi-infinite leads, Appendix 2.8.2, gives the same fixed-point relations as effective self-energies of the core once the leads are traced out. The bound state condition on Δ for $E \geq 2$ amounts to

$$\lambda_k = \left(1 - \frac{|t_c|^2}{2}\right) E + |t_c|^2 \sqrt{\left(\frac{E}{2}\right)^2 - 1}\,, \tag{2.133}$$

or equivalently

$$E = \frac{1}{1-|t_c|^2}\left[\left(1 - \frac{|t_c|^2}{2}\right)\lambda_k - \frac{|t_c|^2}{2}\sqrt{\lambda_k^2 - 4(1-|t_c|^2)}\right], \tag{2.134}$$

with $\lambda_k \geq 2 - |t_c|^2$, in agreement with (2.64) from the main text. For $E \leq -2$, the condition on Δ gives instead

$$E = \frac{1}{1+|t_c|^2}\left[\left(1 + \frac{|t_c|^2}{2}\right)\lambda_k + \frac{|t_c|^2}{2}\sqrt{\lambda_k^2 - 4(1+|t_c|^2)}\right], \tag{2.135}$$

with $\lambda_k \leq -2 + |t_c|^2$. Similar relations hold for the bound state condition on $\tilde{\Delta}$.

2.8.3.2 Scattering states (E within the band)

When $E \in [-2, 2]$, θ is real and we find

$$\beta_j = \mathcal{N}\Big[\tfrac{E-\lambda}{|t_{c,1}|^2}\sin j\theta - \sin(j-1)\theta\Big], \tag{2.136}$$

where $\mathcal{N}$ is a normalization factor. For any finite L, there are L scattering states from the (perturbed) continuous spectrum of the lead. A generic feature of these L states is their small amplitude at the quantum dots. Additionally, there can be two scattering hybridized states. A generic feature of these states is their relatively large amplitude on the dots. The hybridized states for $L = 10$ and $\lambda = \mu = 1.4$ are displayed in Fig. 2.11 **a,b**. States from the (perturbed) continuous spectrum are displayed in Figs. 2.10 **c,d**, and 2.11 **c,d**. The hybridized states for $L = 11$ and $\lambda = \mu = 1.2$ are displayed in Fig. 2.17 **c,d**.

Chapitre 3

Information dans les états fondamentaux d'hamiltoniens locaux non critiques

3.1 Intrication et corrélations

Puisque nous étudierons le contenu en information d'états de systèmes composites, nous débutons par un rappel sur les états quantiques composites et sur la nature des corrélations qu'ils présentent. Pour un système quantique défini sur $\mathscr{H}$, on appelle *état pur* un élément (normalisé) de $\mathscr{H}$,

$$|\psi\rangle \in \mathscr{H} \qquad , \qquad \|\psi\|^2 = 1, \tag{3.1}$$

ou, indifféremment, le projecteur $\rho = |\psi\rangle\langle\psi|$. On appelle *opérateur de densité* un mélange statistique d'états purs

$$\rho = \sum_i p_i |\psi_i\rangle\langle\psi_i| \qquad , \qquad p_i \geq 0 \qquad , \qquad \|\rho\|_{\rm tr} = 1, \tag{3.2}$$

ou, de façon équivalente, un opérateur hermitien ($\rho^\dagger = \rho$), semi-défini positif ($\rho \geq 0$) et de trace unité (${\rm Tr}\rho = 1$). La norme de Hilbert-Schmidt de ρ est bornée, $\|\rho\|_{\rm HS} = \sqrt{{\rm Tr}(\rho^\dagger\rho)} \leq 1$, et égale à l'unité si et seulement si ρ est un état pur. Autrement, ρ est qualifié d'*état mixte*.

Il est commode de munir l'ensemble des opérateurs sur $\mathscr{H}$ [1] du produit scalaire de Hilbert-Schmidt $\langle\chi,\eta\rangle_{\rm HS} = {\rm Tr}(\chi^\dagger\eta)$. L'espace hilbertien qui en résulte est une extension de l'espace des états purs et permet un traitement unifié des états, qu'ils soient purs ou mixtes [187]. Pour des états purs $\rho_1 = |\psi_1\rangle\langle\psi_1|$ et $\rho_2 = |\psi_2\rangle\langle\psi_2|$, on a $\langle\rho_1,\rho_2\rangle_{\rm HS} = |\langle\psi_1|\psi_2\rangle|^2$. Pour une densité ρ et une observable $\mathcal{O}$, on a $\langle\rho,\mathcal{O}\rangle_{\rm HS} = {\rm Tr}(\rho\mathcal{O}) = \langle\mathcal{O}\rangle_\rho$.

3.1.1 États purs composites

L'évolution unitaire de deux systèmes quantiques interagissants, A et B, dont les états initialement purs sont définis sur les espaces de Hilbert $\mathscr{H}_A$ et $\mathscr{H}_B$, résulte en un état pur composite défini sur $\mathscr{H}_A \otimes \mathscr{H}_B$, dont une base est $\{|\alpha_i\rangle \otimes |\beta_j\rangle\}_{I\times J}$,

1. Plus précisément, l'ensemble des opérateurs bornés (dans la norme d'opérateur) et dont la norme de Hilbert-Schmidt est finie. Cet ensemble comprend entre autres les opérateurs de rang fini, ainsi que les opérateurs de classe trace, dont les opérateurs de densité. Si l'on réintroduit les observables bornées $\|\mathcal{O}\|_{\rm op} < \infty$, mais non Hilbert-Schmidt, l'inégalité de trace de von Neumann entraîne $|\langle\mathcal{O}\rangle_\rho| = |{\rm Tr}\rho\mathcal{O}| \leq \|\rho\|_{\rm tr}\|\mathcal{O}\|_{\rm op} < \infty$. De telles observables conservent donc une signification physique claire, bien que le produit $\langle\cdot,\cdot\rangle_{\rm HS}$ ne soient plus alors définis sur toutes les paires d'opérateurs. Montionons également la construction de Gelfand-Naimark-Segal [245] qui, pour un état ρ sur $\mathscr{H}$, associe un espace d'Hilbert $\mathscr{H}_\rho$ et un vecteur $x_\rho \in \mathscr{H}_\rho$, et à tout opérateur borné $\mathcal{O}$ de $\mathscr{H}$, un opérateur borné $\pi(\mathcal{O})$ de $\mathscr{H}_\rho$ tel que ${\rm Tr}\rho\mathcal{O} = \langle x_\rho, \pi(\mathcal{O})x_\rho\rangle_{\mathscr{H}_\rho}$. Par la construction de $\mathscr{H}_\rho$, on aura la norme $\|\mathcal{O}\|^2_{\mathscr{H}_\rho} = {\rm Tr}\rho\mathcal{O}^\dagger\mathcal{O}$, dont la finitude est *relative à l'état* ρ.

pour $\{|\alpha_i\rangle\}_{i\in I}$ et $\{|\beta_j\rangle\}_{j\in J}$ des bases orthonormales de A et B, respectivement. Un élément normalisé de $\mathscr{H}_A \otimes \mathscr{H}_B$ (un état pur composite) est de la forme

$$|\psi_{AB}\rangle = \sum_{ij} c_{ij}|\alpha_i\rangle \otimes |\beta_j\rangle \qquad , \qquad \sum_{ij} |c_{ij}|^2 = 1, \tag{3.3}$$

où les sommes n'impliquent au plus qu'une infinité dénombrable de termes non nuls. [2] On appelle *état produit* un élément de $\mathscr{H}_A \otimes \mathscr{H}_B$ de la forme $|\psi_A\rangle \otimes |\psi_B\rangle$, où $|\psi_A\rangle \in \mathscr{H}_A$ et $|\psi_B\rangle \in \mathscr{H}_B$. L'état pur (3.3) sera de la forme produit si et seulement si $c_{ij} = a_i b_j$ pour $a_i, b_j \in \mathbb{C}$, i.e. $\{c_{ij}\}_{I\times J}$ est un opérateur de rang 1. Dans le cas contraire, l'état $|\psi_{AB}\rangle$ sera dit *intriqué* par rapport à la partition $\{A, B\}$.

Une représentation importante d'un état pur bipartite normalisé est la *décomposition de Schmidt*,

$$|\psi_{AB}\rangle = \sum_{i=1}^{R} \sqrt{\lambda_i}|u_i\rangle \otimes |v_i\rangle, \tag{3.4}$$

où la somme est dénombrable, et où le rang de Schmidt R est fini ou infini, mais satisfait $R \leq \min(\dim\mathcal{H}_A, \dim\mathcal{H}_B)$. Les coefficients λ_i sont strictement positifs, satisfont $\sum_{i=1}^{R} \lambda_i = 1$, et convergent vers zéro si R est infini. Enfin $\{|u_i\rangle\}$ et $\{|v_i\rangle\}$ sont des ensembles orthonormaux de vecteurs de $\mathscr{H}_A$ et de $\mathscr{H}_B$, respectivement. La décomposition de Schmidt de l'état (3.3) est toujours possible, que $\mathscr{H}_A$ et $\mathscr{H}_B$ soient séparables ou non :

Théorème 3.1 (Schmidt)**.** *Tout état pur bipartite normalisé, éq.* (3.3)*, peut être ramené à la forme en décomposition de Schmidt, éq.* (5.17)*.*

Démonstration. La transformation réversible

$$|\alpha_i\rangle \otimes |\beta_j\rangle \overset{T}{\mapsto} |\alpha_i\rangle\langle\beta_j| \qquad , \qquad \forall (i,j) \in I \times J \tag{3.5}$$

constitue une isométrie entre $\mathscr{H}_A \otimes \mathscr{H}_B$ et l'espace des opérateurs de Hilbert-Schmidt de $\mathscr{H}_B$ vers $\mathscr{H}_A$:

$$\begin{aligned} &|\psi\rangle = \sum_{ij} c_{ij}|\alpha_i\rangle \otimes |\beta_j\rangle \leftrightarrow T_\psi = \sum_{ij} c_{ij}|\alpha_i\rangle\langle\beta_j|, \\ &\|T_\psi\|_{\mathrm{HS}}^2 = \operatorname{Tr} T_\psi^\dagger T_\psi = \sum_{ij} |c_{ij}|^2 = \|\psi\|_{\mathscr{H}_A\otimes\mathscr{H}_B}^2. \end{aligned} \tag{3.6}$$

Par la propriété d'approximation des espaces de Hilbert [242], tout opérateur de Hilbert-Schmidt peut être approché par une séquence d'opérateurs de rang fini, et consiste donc en une somme convergente (dans la norme $\|\cdot\|_{\mathrm{HS}}$) d'opérateurs de rang 1 (appelée *décomposition en valeurs singulières*),

$$T_\psi = \sum_{i=1}^{R} \sigma_i |u_i\rangle\langle v_i|, \tag{3.7}$$

2. Pour des espaces $\mathscr{H}_A$ et $\mathscr{H}_B$ non séparables, les bases orthonormales $\{|\alpha_i\rangle\}_{i\in I}$ et $\{|\beta_j\rangle\}_{j\in J}$ seront non dénombrables, mais chaque vecteur (normalisable) ne fera intervenir qu'un nombre fini ou une infinité dénombrable de vecteurs de base. La notion de *séparabilité d'espace* réfère ici à l'existence d'une base de Hilbert dénombrable, indexée par exemple à l'aide de fonctions orthogonales. Elle ne doit pas être confondue avec la *séparabilité d'état*, définie plus loin.

où $\{|u_i\rangle\}$ et $\{|v_i\rangle\}$ sont des ensembles orthonormaux dans $\mathscr{H}_A$ et $\mathscr{H}_B$, respectivement, et par conséquent $R \leq \min(\dim\mathcal{H}_A, \dim\mathcal{H}_B)$. Sans perte de généralité, chaque coefficient σ_i peut être choisi strictement positif en absorbant un facteur de phase dans $|u_i\rangle$. En définissant $\lambda_i = \sigma_i^2$, on trouve

$$|\psi\rangle = T^{-1}T_\psi = \sum_{i=1}^{R} \sqrt{\lambda_i}|u_i\rangle \otimes |v_i\rangle. \tag{3.8}$$

La normalisation de $|\psi\rangle$ donne $\sum_{i=1}^{R} \lambda_i = 1$. □

La décomposition de Schmidt permet de mesurer l'intrication d'un état bipartite en lui associant l'entropie de Rényi d'ordre $n \geq 0$ des coefficients λ_i :

$$S_n(\{\lambda_i\}) = \frac{1}{1-n} \log \sum_{i=1}^{R} \lambda_i^n, \tag{3.9}$$

dite *entropie d'intrication de Rényi.*[3] Notons que les λ_i sont les valeurs propres des réductions[4] de l'opérateur densité $\rho_{AB} = |\psi_{AB}\rangle\langle\psi_{AB}|$,

$$\rho_A = \mathrm{Tr}_B \rho_{AB} = \sum_i \lambda_i |u_i\rangle\langle u_i| \qquad , \qquad \rho_B = \mathrm{Tr}_A \rho_{AB} = \sum_i \lambda_i |v_i\rangle\langle v_i|. \tag{3.10}$$

On a donc pour $S_n(\{\lambda_i\})$ les expressions équivalentes

$$S_n(A) \stackrel{\text{def}}{=} \frac{1}{1-n} \log \mathrm{Tr}_A \rho_A^n \qquad , \qquad S_n(B) \stackrel{\text{def}}{=} \frac{1}{1-n} \log \mathrm{Tr}_B \rho_B^n. \tag{3.11}$$

L'entropie de Rényi d'ordre 1 (notée simplement S) coincide avec l'entropie d'intrication de von Neumann, $S(A) = -\mathrm{Tr}_A(\rho_A \log \rho_A)$, et mesure l'incertitude sur la valeur de l'indice $i \in \{1, \ldots, R\}$ considéré comme une variable aléatoire munie de la fonction de probabilité $\mathrm{Prob}(i) = \lambda_i$. En particulier [226],

1. Un état produit (un seul λ_i non nul, ρ_A et ρ_B des états purs, et $\rho_{AB} = \rho_A \otimes \rho_B$) implique $S(A) = 0$.
2. Un état intriqué (plusieurs λ_i non nuls, ρ_A et ρ_B des états mixtes, et $\rho_{AB} \neq \rho_A \otimes \rho_B$) implique $S(A) > 0$.
3. Si le rang de Schmidt R est fini, l'état est maximalement intriqué quand tous les λ_i sont non nuls et égaux.

Pour des observables locales $\mathcal{O}_A$ et $\mathcal{O}_B$, respectivement définie sur $\mathscr{H}_A$ et $\mathscr{H}_B$, on définit leur corrélateur connexe sur $|\psi_{AB}\rangle$,

$$C(\mathcal{O}_A, \mathcal{O}_B) = \langle \mathcal{O}_A \otimes \mathcal{O}_B \rangle - \langle \mathcal{O}_A \otimes 1_B \rangle \langle 1_A \otimes \mathcal{O}_B \rangle, \tag{3.12}$$

où $\langle\cdot\rangle = \langle\psi_{AB}|\cdot|\psi_{AB}\rangle$. À l'aide de la décomposition de Schmidt, on montre aisément le résultat suivant [296]. Il s'agit d'un cas particulier du Théorème 3.3.

3. Une autre mesure de l'intrication bipartite d'un état pur, non équivalente à l'entropie d'intrication, est la fonction E_χ [273] définie à l'Éq. (3.39). L'entropie d'intrication et la fonction E_χ sont (i) nulles sur les états produits, (ii) additives sous le produit tensoriel et (iii) monotones décroissantes sous les opérations locales et communications classiques (LOCC).

4. En terme des opérateurs $T_\psi : \mathscr{H}_B \to \mathscr{H}_A$ du Théorème 3.1, les densités réduites sont simplement $\rho_A = T_\psi T_\psi^\dagger$ et $\rho_B = T_\psi^\dagger T_\psi$.

Théorème 3.2. *L'état pur $|\psi_{AB}\rangle \in \mathscr{H}_A \otimes \mathscr{H}_B$ est un état produit par rapport à la partition $\{A, B\}$,*

$$|\psi_{AB}\rangle = |\psi_A\rangle \otimes |\psi_B\rangle \qquad ou \qquad \rho_{AB} = \rho_A \otimes \rho_B, \tag{3.13}$$

si et seulement s'il est sans corrélations par rapport à la partition $\{A, B\}$,

$$C(\mathcal{O}_A, \mathcal{O}_B) = 0 \qquad , \qquad \forall \mathcal{O}_A, \mathcal{O}_B. \tag{3.14}$$

Une conséquence immédiate du théorème ci-dessus est que l'intrication d'un état pur bipartite entraîne des corrélations entre les parties, qualifiées de *corrélations quantiques* parce qu'étrangères aux états classiques. Il faut toutefois se garder d'identifier intrication et corrélations. Des états existent qui sont fortement corrélés, mais sans intrication (voir les états mixtes de la section suivante). Fait plus surprenant, certains états sont connus pour être hautement intriqués, mais faiblement corrélés (par exemple, les *expander graph states* possèdent une entropie d'intrication qui croît exponentiellement avec la longueur de corrélation [139]). De tels états sont appelés à jouer un rôle proéminent dans les technologies de dissimulation de données (*data hiding*) et de communications quantiques sécurisées [142].

3.1.2 États mixtes composites

Les états purs de la section précédente correspondent aux opérateurs de densité $\rho_{AB} = |\psi_{AB}\rangle\langle\psi_{AB}|$. Plus généralement, un système bipartite $\{A, B\}$ se trouvera dans un état mixte composite, c'est à dire un mélange statistique d'états purs composites :

$$\rho_{AB} = \sum_\ell p_\ell |\psi^\ell_{AB}\rangle\langle\psi^\ell_{AB}| \qquad , \qquad p_\ell \geq 0 \qquad , \qquad \mathrm{Tr}\rho_{AB} = 1. \tag{3.15}$$

Les opérateurs $J_{A,im} \otimes J_{B,jn} = |\alpha_i\rangle\langle\alpha_m| \otimes |\beta_j\rangle\langle\beta_n|$ forment une base orthonormale pour les opérateurs sur $\mathscr{H}_A \otimes \mathscr{H}_B$ munis du produit Hilbert-Schmidt $\langle\chi, \eta\rangle_{\mathrm{HS}} = \mathrm{Tr}(\chi^\dagger\eta)$. Ainsi, tout état bipartite se ramène à la forme

$$\rho_{AB} = \sum_{a,b} \zeta_{ab} J_{A,a} \otimes J_{B,b} \tag{3.16}$$

où l'on a défini les multi-indices $a = (i, m)$ et $b = (j, n)$. Si $\mathrm{Tr}\rho^2_{AB} = \sum_{ab} |\zeta_{ab}|^2 = 1$, l'état est pur et se ramène à la forme de Schmidt $\rho_{AB} = \sum_{ij} \sqrt{\lambda_i\lambda_j}|u_i\rangle\langle u_j| \otimes |v_i\rangle\langle v_j|$. [5]

5. Par ailleurs, les opérateurs sur $\mathscr{H}_A$ et les opérateurs sur $\mathscr{H}_B$ forment des espaces hilbertiens. Le théorème 3.1 s'applique donc à l'expression (3.16) et donne la décomposition de Schmidt

$$\rho_{AB} = \sum_a^Q \tilde{\zeta}_a \tilde{J}_{A,a} \otimes \tilde{J}_{B,a} \qquad , \qquad Q \leq \min(\dim\mathcal{H}^2_A, \dim\mathcal{H}^2_B). \tag{3.17}$$

Les $\tilde{J}_{A,a}$ et les $\tilde{J}_{B,a}$ peuvent être choisis hermitiens, et leur orthonormalité signifie que $\mathrm{Tr}\tilde{J}_{A,a}\tilde{J}_{A,b} = \delta_{ab} = \mathrm{Tr}\tilde{J}_{B,a}\tilde{J}_{B,b}$. Toutefois, ces opérateurs ne sont pas des densités en général. Lorsqu'ils le sont (i.e. $\mathrm{Tr}\tilde{J}_{A,a} = 1 = \mathrm{Tr}\tilde{J}_{B,b}$, $\tilde{J}_{A,a} \geq 0$ et $\tilde{J}_{B,b} \geq 0$), l'état est dit *séparable*. Voir l'équation (3.21).

Théorème 3.3. *L'état bipartite ρ_{AB} est sans corrélations par rapport à la partition $\{A, B\}$,*

$$C(\mathcal{O}_A, \mathcal{O}_B) = 0 \qquad , \qquad \forall \mathcal{O}_A, \mathcal{O}_B. \tag{3.18}$$

si et seulement si

$$\rho_{AB} = \rho_A \otimes \rho_B. \tag{3.19}$$

Démonstration. Il suffit de développer

$$\begin{aligned} C(J_{A,im}, J_{B,jn}) &= \mathrm{Tr}(J_{A,im} \otimes J_{B,jn}(\rho_{AB} - \rho_A \otimes \rho_B)) \\ &= \langle J_{A,im} \otimes J_{B,jn} | \rho_{AB} - \rho_A \otimes \rho_B \rangle_{\mathrm{HS}} \end{aligned} \tag{3.20}$$

pour conclure que $C(J_{A,im}, J_{B,jn}) = 0$ pour tout i, j, m, n si et seulement si $\rho_{AB} = \rho_A \otimes \rho_B$. □

Tel que discuté à la section précédente, il est possible d'introduire des corrélations (quantiques) en ajoutant de l'intrication dans l'état. Une alternative consiste à produire un mélange statistique d'états non intriqués

$$\rho_{AB} = \sum_a p_a \rho_{A,a} \otimes \rho_{B,a}\,, \tag{3.21}$$

où $\rho_{A,a}$ et $\rho_{B,a}$ sont des densités supportées respectivement dans $\mathscr{H}_A$ et $\mathscr{H}_B$, et où la normalisation, $\mathrm{Tr}\rho_{AB} = 1$, donne $\sum_a p_a = 1$. On appelle *état séparable* un état de la forme (3.21). Parce qu'un état séparable est un mélange statistique d'états produits $\rho_{A,a} \otimes \rho_{B,a}$, il est exempt d'intrication. Ses corrélations résultent uniquement de la mixité de l'éq.(3.21) et sont appelées *corrélations classiques.*[6] Un état sans corrélations, de la forme (3.19), est dit *simplement séparable.*[7]

Une mesure importante de la quantité de corrélations dans un état quantique, pur ou mixte, est l'*information mutuelle*, définie comme suit[8]. Pour des sous-systèmes A et B, l'information mutuelle (d'ordre n) entre ces sous-systèmes est

$$I_n(A : B) = S_n(A) + S_n(B) - S_n(A \cup B), \tag{3.23}$$

où S_n est l'entropie de Rényi d'ordre n, définie à la section précédente. L'information mutuelle d'ordre 1 (simplement appelée *information mutuelle*) est notée $I(A : B)$. On montre aisément les propriétés suivantes :

6. Ce portrait simple n'est pas tout à fait exhaustif. Il existe des états séparables, donc exempts d'intrication, qui présentent néanmoins des corrélations ayant pour origine la non-commutativité de certains opérateurs [213, 117], un phénomène proprement quantique. La *discorde quantique* permet de mesurer l'ampleur de ces corrélations non-classiques ne résultant pas de l'intrication. Mentionnons également que la discorde quantique peut révéler des transitions de phase quantiques à température finie [279], qu'elle semble plus robuste que l'intrication face aux environnements dissipatifs [279], et qu'elle peut servir de ressource pour le calcul quantique et la cryptographie quantique [127, 221].

7. En ce qui concerne les états purs, on a

$$\{\text{purs}\} \cap \{\text{séparables}\} = \{\text{purs}\} \cap \{\text{simplement séparables}\} = \{\text{produits}\}. \tag{3.22}$$

8. Une autre mesure importante des corrélations d'un état mixte est la négativité logarithmique E_N [275, 222] dont nous ne discuterons pas ici.

1. $I(A:B) \geq 0$ pour tout sous-systèmes A, B.
2. Pour un état simplement séparable $\rho_{AB} = \rho_A \otimes \rho_B$ (donc sans corrélations entre A et B), on a $I(A:B) = 0$.
3. Pour un état pur $\rho_{AB} = |\psi_{AB}\rangle\langle\psi_{AB}| = \sum_{ij} \sqrt{\lambda_i \lambda_j} |u_i\rangle\langle u_j| \otimes |v_i\rangle\langle v_j|$ (corrélations entièrement quantiques entre A et B), on a

$$I(A:B) = 2S(\{p_i\}). \tag{3.24}$$

4. Pour un état séparable $\rho_{AB} = \sum_a p_a \rho_{A,a} \otimes \rho_{B,a}$ (corrélations entièrement classiques [9] entre A et B), on a

$$I(A:B) = S(\{p_a\}), \tag{3.25}$$

où l'on a présumé que $\langle \rho_{A,a}, \rho_{A,a'} \rangle_{\text{HS}} = \delta_{aa'} = \langle \rho_{B,a}, \rho_{B,a'} \rangle_{\text{HS}}$.

L'importance de l'information mutuelle peut être appréciée par le théorème suivant, révélant qu'elle est une borne supérieure pour la quantité de corrélations dans un état [287].

Théorème 3.4. *Pour des observables bornées $\mathcal{O}_A, \mathcal{O}_B$ supportées par A et B, respectivement,*

$$I(A:B) \geq \frac{C\left(\mathcal{O}_A, \mathcal{O}_B\right)^2}{2\|\mathcal{O}_A\|_{\text{op}}^2 \|\mathcal{O}_B\|_{\text{op}}^2}, \tag{3.26}$$

où $C\left(\mathcal{O}_A, \mathcal{O}_B\right)$ est le corrélateur connexe (3.12).

Les états mixtes qui nous intéresseront résultent toujours de l'application d'une trace partielle à un état pur $|\psi_{ABC}\rangle$ d'un espace $\mathscr{H}_A \otimes \mathscr{H}_B \otimes \mathscr{H}_C$ strictement plus grand que $\mathscr{H}_A \otimes \mathscr{H}_B \otimes \{0\}$. [10] Les corrélations de ρ_{AB} que nous qualifions de 'classiques' sont, elles aussi, proprement quantiques dans l'état pur $|\psi_{ABC}\rangle$.

3.2 Corrélations hors criticalité

Les concepts de corrélations et d'intrication dans les états fondamentaux de systèmes à N degrés de libertés permettent de caractériser les propriétés macroscopiques qui émergent dans ces systèmes à la limite thermodynamique $N \to \infty$. Certaines caractéristiques d'un système contraignent la forme des corrélations et de l'intrication dans l'état fondamental, dont la présence ou l'absence d'un gap spectral (ou bande interdite) au-dessus du niveau fondamental, sa dégénérescence, ainsi que la présence ou l'absence de frustration. Dans cette section, nous nous pencherons sur les corrélations de l'état fondamental pourvu d'un gap spectral.

Définition 3.1 (Gap spectral)**.** *Soit une séquence $\{H_N, \sigma_N\}$, où l'hamiltonien H_N comporte N degrés de liberté, $\sigma_N \subset \mathbb{R}$ est le spectre de H_N et $\lim_{N\to\infty} \sigma_N$ est bien définie. On dit que la séquence $\{H_N, \sigma_N\}$ possède un gap spectral lorsqu'il existe des constantes N_0, Δ, g strictement positives et indépendantes de N telles que [296]*

9. Voir note 6.
10. Il s'agit en fait du phénomène général de *purification* [209].

1. *Pour tout $N \geq N_0$, le spectre σ_N comporte une bande interdite de largeur $\Delta_N \geq \Delta$* [11] ;
2. *Pour tout $N \geq N_0$, il y a $g_N \leq g$ niveaux sous la bande interdite de σ_N, et ces niveaux ont une limite commune* [12] ;
3. *Pour tout $N \geq N_0$, il existe au moins un niveau au-dessus de la bande interdite.*

Le suprémum des valeurs possibles de Δ est le *gap spectral*. Les états sous le gap constituent l'espace fondamental, de dégénérescence (finie ou infinie) égale au suprémum des valeurs possibles de g, tandis que les états au-dessus du gap sont les états excités.

Un hamiltonien k-local est de la forme $H = \sum_i H_i$, où chaque H_i agit de façon non triviale sur au plus sur k degrés de libertés voisins les uns des autres. On dit que l'hamiltonien local H est *sans frustration* si ses états fondamentaux sont également des états propres fondamentaux de chacun des H_i. Autrement, H et ses états fondamentaux sont dits *frustrés*.

Théorème 3.5 (Gap et corrélations exponentielles, [138])**.** *Pour des entiers D, d, soit L un réseau de dimension spatiale D, et $H = \sum_i H_i$ un hamiltonien local sur $\otimes_{\ell \in L} \mathbb{C}^d$, tel que $\|H_i\| \leq J < \infty$ et sans frustration, et possédant un état fondamental unique $|\psi_0\rangle$ et un gap spectral $\Delta > 0$. Pour des sous-systèmes A, B séparés par une distance $r > 0$ et supportant des observables bosoniques, locales et bornées $\mathcal{O}_A, \mathcal{O}_B$, il existe $\xi > 0$ tel que*

$$|C(\mathcal{O}_A, \mathcal{O}_B)| = |\langle \mathcal{O}_A \otimes \mathcal{O}_B \rangle - \langle \mathcal{O}_A \otimes 1_B \rangle \langle 1_A \otimes \mathcal{O}_B \rangle| \leq \|\mathcal{O}_A\| \, \|\mathcal{O}_B\| \, e^{-r/\xi}, \quad (3.27)$$

où $\langle \cdot \rangle = \langle \psi_0 | \cdot | \psi_0 \rangle$. La longueur de corrélation ξ est telle que $\lim_{\Delta \to 0} \xi = \infty$.

Le théorème 3.5 est une version non relativiste du théorème de Fredenhagen (*Cluster Decomposition Theorem*) pour les QFT relativistes [107, 137]. Des versions du théorème 3.5 s'appliquent à des hamiltoniens locaux définis sur des réseaux plus généraux dont la dimension peut être fractale [13], pour des observables bosoniques ou fermioniques [137]. Pour une large classe de modèles, la présence d'un gap spectral entraîne donc des corrélations exponentielles (dites à *courte portée*), mais la réciproque est fausse [135, 133]. Le théorème 3.5 a été démontré par Hastings [138] au moyen de la borne de Lieb-Robinson [189], qui révèle l'existence d'une vitesse maxi-

11. La présence d'un gap dans les états de volume (*bulk states*) n'entraîne pas forcément de gap pour les états de bord (*edge states*). Il convient donc de spécifier les conditions aux frontières du système. Un choix commode est de supposer que le système ne possède pas de frontière.

12. Pour les questions de complexité liées à l'identification de l'état fondamental, il est nécessaire de préciser la vitesse de convergence vers la limite commune. Le problème de simulation correspondant sera habituellement « difficile » si la séparation est $O(2^{-N})$, et « facile » si la séparation est $\Omega(1/N)$.[214]

13. Les réseaux en question sont des graphes dont tous les sommets ont même degré, mais qui, par leur construction récursive, présentent une certaine auto-similarité [91].

male de propagation dans les systèmes de spin [14]. Il s'agit donc d'une preuve faisant intervenir la dynamique du système. Plus récemment [10], une preuve combinatoire du théorème 3.5 a été formulée pour les systèmes sans frustration en terme du lemme de détectabilité [9].

Pour les systèmes *dégénérés* avec gap, les corrélations peuvent présenter des comportements variés. L'origine de la dégénérescence est déterminante pour le comportement des corrélations, et peut être identifiée à l'aide de celles-ci [296]. Des corrélateurs asymptotiquement constants dans l'espace fondamental $\{|\psi_0^j\rangle\}_{0\leq j<g}$,

$$C(\mathcal{O}_A, \mathcal{O}_B) \underset{r\to\infty}{\sim} \text{constante}, \tag{3.28}$$

où les espérances $\langle\cdot\rangle = \mathrm{Tr}(\cdot\rho)$ sont calculées par rapport à un état mixte donné $\rho = \sum_j p_j |\psi_0^j\rangle\langle\psi_0^j|$, sont un signe de symétrie brisée spontanément par les opérateurs $\mathcal{O}_A, \mathcal{O}_B$. D'un autre côté, des corrélateurs nuls pour toute densité ρ et toute séparation $r > 0$, i.e. $\xi = 0$, signalent la présence d'un ordre topologique [278], c'est à dire une dégénérescence du niveau fondamental qui ne résulte pas d'une symétrie brisée, mais qui dépend de la topologie du réseau et qui comporte des intrications à longue portée robustes face aux perturbations locales. [15] Enfin, les systèmes frustrés présentent normalement une forte dégénérescence (souvent extensive), ainsi qu'une décroissance algébrique des corrélations [145, 115]. Nous en verrons un exemple au Chapitre 5.

Les états fondamentaux *non dégénérés* et présentant des corrélations à longue portée, tels que les états fondamentaux de systèmes sans gap et de systèmes possédant une surface de Fermi, seront l'objet du Chapitre 4.

3.3 Intrication hors criticalité

Nous nous penchons maintenant sur l'intrication dans les états purs, principalement pour les états fondamentaux de systèmes unidimensionnels sur réseau, pour lesquels des théorèmes sont rigoureusement établis. Nous recenserons quelques-uns de ces résultats et mentionnerons ceux qui s'appliquent également aux dimensions supérieures. Soit $\{A, B\}$ une bipartition d'un système telle que A comporte un nombre de degrés de liberté, noté $\#A$, inférieur ou égal à ceux de B. Une conséquence immédiate de la décomposition de Schmidt est que l'entropie d'intrication d'un état pur de $\mathscr{H}_A \otimes \mathscr{H}_B$ est bornée supérieurement par une quantité proportionnelle à $\#A$,

$$S_A \leq O(1) \cdot \#A. \tag{3.29}$$

14. Dans la notation du théorème 3.5, la borne de Lieb-Robinson indique que pour un système de spins $H = \sum_i H_i$, invariant sous les translations et tel que $\|H_i\| \leq J < \infty$ pour tout i, on a $\|[e^{itH}\mathcal{O}_A e^{-itH}, \mathcal{O}_B]\| \leq c\|\mathcal{O}_A\|\,\|\mathcal{O}_B\|\, e^{v|t|-kr}$, où c, v, k sont des constantes positives. Pour des observables fermioniques, le commutateur est remplacé par un anticommutateur. Le résultat peut être étendu à des systèmes non invariants sous les translations, à des opérateurs non bornés, ainsi qu'à des systèmes dissipatifs. Voir à ce sujet le rapport [214] et les références qu'il contient.

15. Il n'existe pas d'ordre topologique intrinsèque en dimension 1. Toutefois, un système qui comporte une symétrie peut posséder un ordre SPT (*symmetry protected topological order*) qui ne se laisse pas transformer en l'état produit trivial par les transformations unitaires respectant la symétrie. Les ordres SPT ne présentent pas d'intrication à longue portée [296].

Anticipons le lien avec les théories de champs, Section 3.4, en admettant dès à présent que le pas du réseau puisse correspondre à une grandeur *physique* $\epsilon > 0$ (généralement une distance inférieure à toutes les autres échelles de longueur du système, appelée échelle de longueur à la coupure UV, en-deçà de laquelle la description en théorie de champs devient ineffective). Le volume $|A|$ de A se mesure naturellement en terme du pas du réseau, et l'on obtient

$$S_A \leq O(1) \cdot \epsilon^{-D} |A|, \tag{3.30}$$

où D est la dimension spatiale du réseau. Les inégalités générales (3.29) et (3.30) s'appellent *loi de volume*.

Nous nous intéresserons surtout aux états qui ne saturent pas les bornes (3.29), (3.30). Trivialement, les états produits ont une entropie nulle. Plus intéressants, les états fondamentaux non dégénérés d'hamiltoniens locaux et dont les corrélations sont à courte portée sont soupçonnés de ne comporter que des intrications entre A et B impliquant des degrés de liberté voisins de la frontière ∂A, entraînant une *loi d'aire* [16] :

$$S_A \leq O(1) \cdot \#\partial A \quad , \quad S_A \leq O(1) \cdot \epsilon^{-D+1} |\partial A|. \tag{3.31}$$

De nombreux hamiltoniens locaux avec gap renforcent cette intuition : modèles quasi-libres bosoniques et fermioniques [80, 97], chaines de spins [134, 98], hamiltoniens parents de MPS [17] [244] et de PEPS [18] [272]. Certains systèmes critiques satisfont également la loi d'aire [19], tandis que d'autres [20] présentent une violation logarithmique de la loi d'aire.

Mais il faut à nouveau distinguer corrélations et intrication : les *data hiding states* [142] et les *quantum expander graph states* [139] possèdent plus d'intrication que ne le laissent entrevoir leurs corrélations. En dimension spatiale $D = 1$, nous avons la solution suivante.

Théorème 3.6 (Gap et loi d'aire 1D)**.** *Pour un entier d, soit L un réseau unidimensionnel, et $H = \sum_i H_i$ un hamiltonien local sur $\otimes_{\ell \in L} \mathbb{C}^d$, tel que $\|H_i\| \leq J < \infty$ et possédant un état fondamental unique $|\psi_0\rangle$ et un gap spectral $\Delta > 0$. Alors, pour un sous-système connexe A, l'entropie d'intrication bipartite est supérieurement bornée par une quantité indépendante de la taille de A,*

$$S_A \leq c \cdot \Delta^{-1} \log^3 d, \tag{3.32}$$

où $c > 0$ dépend de J. La loi d'aire demeure valide que H soit frustré ou non.

De plus, pour un réseau à N sites, il existe un algorithme classique (déterministe) d'entrée (L, H, Δ), opérant en temps $\mathrm{poly}(N)$, et dont la sortie est une approximation de l'état fondamental de H avec une précision $\epsilon = \mathrm{poly}(1/N)$.

16. En dimension spatiale $D = 1$, $\#\partial A$ ne dépend que du nombre de points de frontière entre A et B, et non de la taille de A. La loi d'aire 1D s'exprime donc ainsi : $S \leq$ constante, où $\#\partial A$ est implicite.

17. *Matrix Product State.*

18. *Projected Entangled Pair State.*

19. Théories de champs conformes $(2+1)$-dimensionnels (CFT_3) [64] et modèles critiques de Lifshitz $(2+1)$-dimensionnels [105]. Voir Sections 4.1 et 4.2

20. Théories de champs conformes $(1+1)$-dimensionnels (CFT_2) [149, 53] et fermions critiques pourvus d'une surface de Fermi finie [285, 116, 52]. Voir Sections 4.1 et 4.3.

Ce théorème est l'aboutissement d'une série de raffinements [134, 10, 22, 21] rapprochant sa loi d'aire des bornes *inférieures* pour $S_{\max}$ atteintes dans certains modèles 1D [21]. La composante algorithmique est également le résultat de nombreux développements [243, 8, 21, 183, 154]. Voir aussi [79]. La constante c dans (3.32) dépend de l'énergie de couplage J, mais est indépendante du gap Δ, de la dimension locale d, ou de la taille du sous-système A.

Le prochain théorème généralise partiellement ce qui précède et montre que, pour un réseau unidimensionnel, les *data hiding states* ne constituent pas une obstruction à la relation entre corrélations exponentielles et loi d'aire. Noter que le théorème s'applique à des états purs quelconques, qu'ils soient ou non des états propres d'hamiltoniens locaux.

Théorème 3.7 (Corrélation exponentielles et loi d'aire 1D)**.** *Soit $|\psi\rangle$ un état pur défini sur un réseau unidimensionnel. Si $|\psi\rangle$ possède des corrélations exponentielles de longueur de corrélation (finie) $0 < \xi < \infty$, alors pour toute partie connexe A du réseau,*

$$S_A \leq c' \cdot (\log \xi) \exp c\xi + \cdots , \tag{3.33}$$

où $\cdots$ désigne des termes sous-dominants et où $c', c > 0$ [48, 47, 77].

La preuve initiale du théorème 3.7 donnait $S \leq c' l_0 \cdot \exp(c\xi \log \xi)$ sur un réseau périodique [48, 47], pour des constantes universelles $c', c > 0$ et où l_0 est la distance au-delà de laquelle les corrélations décroissent exponentiellement. La borne (3.33) est donnée dans [77] pour des constantes non universelles. Il y a lieu de croire qu'elle est essentiellement optimale et que le facteur exponentiel est inévitable [136]. Pour un système local avec gap Δ, l'inégalité (3.33) est plus forte que résultat initial de Hastings [134] $S \leq c' \cdot \xi \log \xi \exp c\xi$ avec $\xi = \Delta^{-1}$, qui fut raffiné par la suite, comme nous l'avons mentionné. Le Théorème 3.7 s'applique à une autre classe importante de modèles, soit les hamiltoniens désordonnés, qui présentent une localisation dynamique et dont les corrélations sont à courte portée dans l'état fondamental, bien que leur spectre soit généralement sans gap [135, 133]. (On parle alors de *gap de mobilité*.) On peut conclure que ces modèles satisfont également la loi d'aire [47].

La relation entre gap et loi d'aire n'est pas une caractéristique exclusive aux systèmes locaux. Le prochain théorème montre qu'elle s'obtient dans certains systèmes unidimensionnels présentant une forme modérée de non-localité.

Théorème 3.8 (Non-localité, gap et loi d'aire, [180])**.** *Soit un réseau unidimensionnel muni d'un espace de Hilbert d-dimensionnel sur chaque site, et soit $H = \sum_{i \leq j} H_{ij}$ un hamiltonien non-local tel que l'interaction H_{ij} entre des sites distants i et j satisfait*

$$\|H_{ij}\| \leq J|i-j|^{-\alpha} \tag{3.34}$$

pour des constantes $J, \alpha > 0$. Supposons H pourvu d'un gap spectral $\Delta > 0$ et d'un état fondamental unique. Si, pour toute paire d'intervalles X, Y séparés d'une

21. Voir [123] pour un modèle frustré pour lequel $S_{\max} \geq O(1) \cdot \Delta^{-1/4}$, et [156] en combinaison avec la note 18 de [22] pour un modèle sans frustration où $S_{\max} \geq O(1) \cdot \Delta^{-1/6}$. Par comparaison, les théories relativistes ont $S \leq O(1) \cdot \log(1/\Delta)$.

distance $r > 0$, il existe des constantes $\bar{J}, \bar{\alpha} > 0$ telles que

$$\| \sum_{i \in X} \sum_{j \in Y} H_{ij} \| \leq \bar{J} r^{-\bar{\alpha}}, \tag{3.35}$$

alors pour tout sous-système connexe A, l'entropie d'intrication bipartite est supérieurement bornée par une quantité indépendante de la taille de A,

$$S_A \leq c \cdot \log^2 d \cdot \mathcal{G}\left(\Delta^{-1} \log d\right), \tag{3.36}$$

où $\mathcal{G}(x) = x^{1+2/\bar{\alpha}} \log^{3+3/\bar{\alpha}} x$. La constante $c > 0$ dépendra des paramètres $J, \alpha, \bar{J}, \bar{\alpha}$, ainsi que du couplage à un potentiel local. La loi d'aire demeure valide que H soit frustré ou non.

Notons que la condition (3.35) est toujours satisfaite si $\alpha > 2$ (avec $\bar{\alpha} = \alpha - 2$), et n'est contraignante que si $\alpha \leq 2$ [180]. Typiquement, les interactions à longue portée avec $\alpha > 3$ appartiennent à la classe d'universalité du modèle à courte portée correspondant ($\alpha = \infty$) [102, 96]. Mentionnons quelques résultats qui vont au-delà des systèmes unidimensionnels.

Théorème 3.9 (Loi d'aire en dimension fractale $D < 2$, [2])**.** *Soit T un arbre à N sommets et de dimension fractale $D < 2$, muni d'un espace d-dimensionnel sur chaque sommet. Soit H un hamiltonien sur T, local, uniformément borné, pourvu d'un gap spectral Δ, et de dégénérescence g. Pour toute partie $A \subset T$ telle que $|\partial A| = O(1)$, il existe $k \geq 0$ tel que l'entropie d'intrication bipartite d'un état fondamental quelconque de H satisfait*

$$S_A \leq c \cdot \left(\log g + \Delta^{-\frac{2D(D+1)}{(2-D)^2}}\right) \log^k \left(\log g + \Delta^{-\frac{2D(D+1)}{(2-D)^2}}\right) \tag{3.37}$$

où $c > 0$ peut dépendre de la dimension locale d et de la borne uniforme pour H. La loi d'aire s'applique autant aux systèmes frustrés qu'aux systèmes sans frustration.

De plus, pour une dégénérescence polynomiale $g = N^{O(1)}$, il existe un algorithme classique (non déterministe) d'entrée (T, H, Δ, g), opérant en temps $\mathrm{poly}(N)$, et dont la sortie est, avec une probabilité élevée, une approximation d'un état fondamental de H avec une précision $\epsilon = \mathrm{poly}(1/N)$.

Théorème 3.10 (Réseaux harmoniques en dimension $D \geq 1$, [223])**.** *Les états fondamentaux de systèmes harmoniques locaux (bosoniques ou fermioniques) sur réseau de dimension spatiale $D \geq 1$, et pourvus d'un gap spectral, satisfont la loi d'aire.* [22]

Théorème 3.11 (Réseaux de spins en dimension $D \geq 1$, [76])**.** *Les états fondamentaux de systèmes de spins sur réseaux aux frontières ouvertes, de dimension spatiale $D \geq 1$, locaux et uniformément bornés, pourvus d'un gap spectral et non dégénérés,*

22. Voir également [199], qui ne requiert pas de gap, mais nécessite une décroissance (quasi)exponentielle des corrélations, et s'applique non seulement à l'état fondamental, mais également à des états faiblement excités (propres ou non). En revanche, il requiert une hypothèse supplémentaire sur le nombre d'états propres de densité d'énergie nulle.

satisfont la loi d'aire. La démonstration fait usage de deux conditions additionnelles « naturelles » du point de vue physique. [23]

Pour les réseaux de spins en dimension $D = 2$, mentionnons également la loi d'aire obtenue par [19], qui requiert pour seule condition additionnelle l'existence d'un gap *local* non nul. [24] La preuve du théorème 3.11 exige un réseau ouvert et un état fondamental unique, conditions incompatibles avec les états topologiquement ordonnés. Pour ce cas, nous avons le résultat suivant.

Théorème 3.12 (Phases topologiques en dimension $D \geq 1$, [201])**.** *Les phases topologiquement ordonnées d'hamiltoniens sur réseaux, pourvus d'un gap et sans frustration, satisfont une loi d'aire.*

Précisons que « système local avec gap » et « loi d'aire pour l'entropie d'intrication » ne sont *pas* des conditions équivalentes [11]. Il semble toutefois qu'un lien très général existe bel et bien entre les systèmes k-corps avec gap et la loi d'aire pour l'*étalement d'intrication*,

$$ES(A) = S_0(A) - S_\infty(A). \tag{3.38}$$

Le Corollaire 5 de [20] donne $ES(A) \leq c \cdot \#\partial A \log \#\partial A + \cdots$ dans l'état fondamental avec gap de tout hamiltonien k-corps, défini sur un hypergraphe quelconque, et ne requiert pas la condition plus forte de k-localité. [25] La constante c dépend du gap spectral, ainsi que d'une tolérance à l'erreur indépendante de la taille du sous-système.

Concluons avec un théorème remarquable dû à Guifré Vidal, qui démontre que la simulation classique efficiente d'un algorithme quantique à N qubits n'est possible que si l'intrication dans sa solution est largement plus faible que celle d'un état générique. L'intrication est ici mesurée par la fonction

$$E\chi = \log_2 \chi, \tag{3.39}$$

où χ est le rang de Schmidt maximal sur toutes les bipartitions $\mathcal{P}$ du système, $\chi = \max_{\mathcal{P}} R_{\mathcal{P}}$. (Voir Éq. (5.17) pour la définition du rang de Schmidt.) La fonction $E\chi$ croît linéairement avec N pour un état générique.

Théorème 3.13 (Loi de log-volume et simulation classique, [273])**.** *Soit $|\psi_N\rangle$ la solution du problème quantique $\mathcal{P}$ à N qubits. Alors $\mathcal{P}$ peut être simulé en temps polynomial* $\mathrm{poly}(N)$ *sur une machine classique si*

$$E\chi \leq \text{constante} \cdot \log N. \tag{3.40}$$

Puisque $E\chi$ est une borne supérieure pour l'entropie d'intrication bipartite [273], ce résultat démontre qu'une intrication supérieure à une loi de log-volume pour l'entropie est une ressource pour le calcul quantique.

23. Il s'agit d'hypothèses assurant la continuité de la séquence d'hamiltoniens $\{H_N\}$, où H_N agit sur un réseau de N sites. Voir la définition du *gap* à la Section 3.2.

24. Le gap local est l'infimum des gaps de sous-systèmes.

25. Précisons que [20] nomme « local » ce que nous qualifions de k-corps, et « géométriquement local » ce que nous qualifions de k-local.

3.4 Loi d'aire et théories de champs

La loi d'aire pour l'entropie de Bekenstein-Hawking d'un trou noir [34, 141] fut l'un des premiers résultats concernant l'entropie des systèmes possédant une infinité de degrés de liberté et contribua également à motiver l'étude de l'intrication dans les théories de champs quantiques (QFT) [35]. Parmi les premières analyses en ce sens, mentionnons le calcul par Srednicki [255] de l'entropie d'intrication entre une sphère de rayon R et son extérieur pour un scalaire relativiste sans masse (mais régularisé dans l'UV par un réseau de pas ϵ dans la direction radiale, et dans l'IR par un volume fini). En dimension $D+1$, $D=2,3$, le résultat présente le profil d'une loi d'aire $O(R/\epsilon)^{D-1}$, indépendamment du régulateur IR. [26] D'après Calabrese et Cardy [53], pour un intervalle semi-infini dans une QFT massive relativiste en dimension $1+1$, l'entropie d'intrication est finie :

$$S(A) \lesssim \frac{c}{6} \log \frac{\xi}{\epsilon}, \tag{3.41}$$

où ξ est la longueur de corrélation finie. [27] Le coefficient du logarithme est universel, puisqu'une modification de ϵ n'entraîne qu'un terme additif dans (3.41). L'analyse de [53] s'étend aux dimensions supérieures pour certaines géométries. Notons que, typiquement, l'entropie d'intrication d'une QFT diverge en l'absence d'un cutoff UV, car les valeurs propres de la matrice densité forment un spectre continu de densité divergente [55]. Certaines quantités peuvent avoir un comportement mieux contrôlé, telle que la différence d'entropie d'intrication entre deux états [149], ou encore l'information mutuelle (d'ordre 1) définie à l'équation (3.23),

$$I(A:B) = S(A) + S(B) - S(A \cup B). \tag{3.42}$$

Pour des intervalles A, B sans contact, la différence contenue dans (3.42) semble généralement préserver l'information mutuelle de la divergence ultraviolette [28], ce qui peut être démontré dans le cas d'une théorie relativiste [63].

3.5 Hamiltoniens non locaux

Nous avons déjà remarqué que non-localité n'est pas toujours synonyme d'état fondamental fortement intriqué, *c.f.* Théorème 3.8. Néanmoins, on connaît des systèmes unidimensionnels non locaux, pourvus d'un gap et présentant plus d'intrication qu'une simple loi d'aire [98, 97] (loi de log-volume dans ce cas précis). Dans cette section, nous décrirons brièvement un type particulier de loi de volume, que nous mentionnerons à nouveau au Chapitre 5, et qui se retrouve dans plusieurs théories de

26. Il s'agit d'une loi d'aire stricte pour un système critique. Nous y reviendrons au Chapitre 4.

27. Pour une bipartition générale, mais telle que pour tout $x, y \in \partial A$ on ait $|x-y| \gg \xi$, on suspecte $S(A) \lesssim \#\partial A \left(\frac{c}{6} \log \frac{\xi}{\epsilon}\right)$ en vertu de la *cluster decomposition property* (CDP).

28. La différence dans (3.42) supprime la contribution des intrications entre degrés de liberté séparés par une distance $\sim \epsilon$ de part et d'autre de la frontière entre $A \cup B$ et son complément. Si A et B sont en contact, l'intrication à leur frontière commune n'est pas supprimée.

champs non locales [29], comportant une échelle $\lambda > 0$ indépendante de la coupure UV et caractérisant la non-localité de la théorie. On y trouve que l'entropie d'intrication bipartite se comporte comme

$$S_A \sim \begin{cases} |A|\Lambda^D & , \quad |A|^{1/D} \ll \lambda \\ \lambda|\partial A|\Lambda^D & , \quad |A|^{1/D} \gg \lambda, \end{cases} \tag{3.43}$$

où D est la dimension spatiale de la théorie et Λ est l'échelle du momentum à la coupure UV [29, 227]. La première partie est identique à (3.30). La seconde ressemble à la loi d'aire (3.31), mais s'en distingue par la divergence $\sim \Lambda^D$. On trouve notamment cette forme non locale de loi de volume dans les théories de champs scalaires non relativistes de la forme [248]

$$H = \int d^D x \, \frac{1}{2} \left((\partial_t \phi)^2 + b\phi \cdot e^{a(-\sum_i \partial_i^2)^{w/2}} \cdot \phi \right), \tag{3.44}$$

où a, b, w sont des constantes positives. L'échelle non locale est $\lambda = a^{1/w}$ et caractérise le couplage de champs distants par le terme cinétique. La référence [166] étudie quant à elle deux déformations non locales de super-Yang-Mills $\mathcal{N} = 4$ illustrant les deux types mentionnés de lois de volume. La déformation « dipolaire » possède une échelle non locale λ indépendante de la coupure UV (loi de type (3.43)), tandis que l'échelle non locale de la déformation « non commutative » est une valeur critique $\lambda_c(\Lambda)$ qui diverge lorsque $\Lambda \to \infty$, produisant une pure loi de volume (loi de type (3.30)) dans cette limite.

29. Nous dirons qu'une théorie de champs est *locale* lorsque son action classique ne fait intervenir que des produits de champs et de leurs dérivées d'ordre $n \in \mathbb{N}$, tous évalués en un même point *spatial*. Par exemple, les actions $\int d^D x \, (\nabla\phi(x))^2$ et $\int d^D x \, \bar{\psi}(x) \frac{1}{\phi^2(x)} \psi(x)$ sont locales en ce sens, tandis que $\int d^D x d^D y \, \phi(x) V(x,y) \phi(y)$ et $\int d^D x \, \phi(x) (\Delta)^z \phi(x)$, $z \notin \mathbb{N}$, ne le sont pas.

Chapitre 4

Information dans les états fondamentaux d'hamiltoniens locaux critiques

Ce chapitre sera consacré aux systèmes quantiques critiques, i.e. dont l'état fondamental unique présente des corrélations à température nulle qui ne décroissent pas de façon exponentielle avec la séparation. [1] Il s'agit donc de systèmes sans gap (spectral ou de mobilité). Nous nous concentrerons sur les systèmes locaux.

Les théories critiques décrivent la physique des systèmes complexes au voisinage d'une transition de phase, ou dans une phase critique telle qu'un semi-métal de Dirac [293]. Lorsque le couplage g est près d'une valeur critique g_c, les propriétés à longue distance de l'état fondamental $|\Psi_0\rangle$ correspondent aux propriétés universelles de la phase correspondant à g. (Le flot du groupe de renormalisation entraîne la théorie loin de g_c.) En deçà d'une longueur de corrélation quantique ξ, par contre, $|\Psi_0\rangle$ présente des « bulles » correspondant aux caractéristiques de l'état fondamental, fortement intriqué spatialement, de la théorie critique $g = g_c$ [237]. À l'approche d'une transition continue, l'échelle ξ diverge comme $|g - g_c|^{-\nu}$ pour un ν universel et positif. On peut alors considérer une grande distance d'observation $L \to \infty$ tout en ayant $L \ll \xi$, formellement la double limite $\lim_{L\to\infty} \lim_{\xi\to\infty} Q(L, \xi)$ pour une quantité mesurée Q. La théorie critique décrit donc les propriétés universelles de la transition quantique. Il s'agit d'un point fixe (instable) du groupe de renormalisation, invariant d'échelle et aux corrélations à longues portées. Plus important encore, la théorie critique décrit le voisinage de la transition aux *basses températures*. Car pour une longueur de corrélation thermique largement inférieure à ξ, le système ne peut voir au delà de l'horizon des « bulles » de criticalité. L'état qui en résulte, appelée *état critique quantique* [146], recouvre ainsi un voisinage de g_c qui est d'autant plus grand que la température est élevée. La théorie critique et son état fondamental décrivent le comportement à faible température de cette phase critique quantique. (Les températures élevées font intervenir les états excités de la théorie critique, qui ne possèdent pas l'universalité de l'état fondamental.) La phase critique quantique ne peut être décrite par une théorie effective classique, même aux températures élevées. [2]

1. Nous éviterons le terme *critique* lorsque les corrélations à longue portée résultent d'une dégénérescence [115], comme c'est le cas pour une symétrie spontanément brisée, un ordre topologique, ou un système frustré (voir Section 3.2). Cette pratique ne fait pas consensus [145].

2. Le temps d'équilibration thermique de la phase critique quantique $\tau_{\text{eq}} \sim \hbar/k_B T$ exclue toute description classique effective, qui nécessiterait $\tau_{\text{eq}} \gg \hbar/k_B T$ [235, 237].

4.1 Théories critiques invariantes de Lorentz

Pour une théorie relativiste, une invariance d'échelle globale, s'il y a lieu, est une invariance sous les transformations d'échelle de la forme

$$\mathbf{x} \to \lambda \mathbf{x} \quad , \quad t \to \lambda t \quad , \quad \lambda > 0 \tag{4.1}$$

(accompagnée d'un changement d'échelle approprié des champs). Les théories de champs conformes (CFT) sont des représentations projectives du groupe conforme, c'est à dire du groupe de Poincaré augmenté des transformations locales d'échelle [225]. Nous nous intéresserons surtout aux CFT en dimension $1+1$ (CFT_2), qui décrivent la région critique quantique de certains modèles unidimensionnels [274]. L'algèbre conforme des CFT_2, constituée de deux copies de l'algèbre de Witt, possède un nombre infini de générateurs, ce qui procure aux CFT_2 la puissante machinerie des systèmes intégrables. De manière équivalente, une CFT_2 est une représentation vraie de deux copies de l'algèbre de Virasoro

$$\begin{aligned} [L_m, L_n] &= (m-n)L_{m+n} + \frac{c}{12}(m^3 - m)\delta_{m+n,0} \\ [\bar{L}_m, \bar{L}_n] &= (m-n)\bar{L}_{m+n} + \frac{\bar{c}}{12}(m^3 - m)\delta_{m+n,0}. \end{aligned} \tag{4.2}$$

Chaque copie est l'unique extension centrale de l'algèbre de Witt correspondante, et les constantes $c, \bar{c}$, appelées *charges centrales*, sont une mesure du nombre de degrés de liberté de chaque secteur (holomorphe et antiholomorphe) de la théorie. [3] Pour une CFT de dimension d, les opérateurs qui, sous une transformation conforme globale, se transforment comme

$$\Phi(x) \to \Phi'(x') = \left|\frac{\partial x'}{\partial x}\right|^{-\Delta/d} \Phi(x), \tag{4.4}$$

où Δ est la dimension d'échelle [4] de Φ, sont appelés opérateurs *quasi-primaires* [225]. Des opérateurs qui transforment selon (4.4) pour toute transformation conforme sont appelés opérateurs *primaires* [5]. Pour des opérateurs (quasi-)primaires Φ_1, Φ_2 et une

3. La charge centrale est une observable associée au corrélateur du tenseur énergie-impulsion

$$\langle 0|T(z)T(0)|0\rangle = c/(2z^4) \quad , \quad \langle 0|\bar{T}(\bar{z})\bar{T}(0)|0\rangle = \bar{c}/(2\bar{z}^4), \tag{4.3}$$

où $T = T_{zz} = \frac{\partial x^\mu}{\partial z}\frac{\partial x^\nu}{\partial z}T_{\mu\nu}$ avec $z = x^0 + ix^1$ et $\partial_z = (\partial_0 - i\partial_i)/2$, et similairement pour $\bar{T} = T_{\bar{z}\bar{z}}$. Pour un espace-temps (x^0, x^1) de courbure $R \neq 0$, l'anomalie conforme $-cR/12 = \langle T^\mu_\mu \rangle = -\bar{c}R/12$ requiert $c = \bar{c}$ [225]. Pour la CFT_2 d'un fermion libre de Majorana sans masse, $c = 1/2$; pour un boson libre sans masse, $c = 1$.

4. Sous une dilatation globale $(t, \mathbf{x}) \to (\lambda t, \lambda \mathbf{x})$, $\lambda > 0$, un champ classique subit la transformation

$$\Phi(\mathbf{x}) \to \Phi(\lambda \mathbf{x}) = \lambda^{-\Delta}\Phi(\mathbf{x}), \tag{4.5}$$

où Δ est la dimension d'échelle de Φ.

5. Pour les CFT_2, les opérateurs quasi-primaires sont les opérateurs annihilés par $L_1, \bar{L}_1$, tandis que les opérateurs primaires sont ceux annihilés par les $L_m, \bar{L}_m$ pour $m > 0$. Tout opérateur primaire engendre un hiérarchie de *champs descendants* obtenus par l'application des opérateurs $L_m, \bar{L}_m$ pour $m < 0$. Les corrélateurs de champs descendants peuvent être obtenus des corrélateurs de leurs champs primaires [225].

dilatation $x \to \lambda x$, il suit de (4.4) que

$$\langle \Phi_1(x_1)\Phi_2(x_2)\rangle = \lambda^{\Delta_1+\Delta_2}\langle \Phi_1(\lambda x_1)\Phi_2(\lambda x_2)\rangle. \tag{4.6}$$

L'invariance de Poincaré exige que la fonction 2-points soit une fonction de $|x_1 - x_2|$, ce qui entraîne

$$\langle \Phi_1(x_1)\Phi_2(x_2)\rangle \propto |x_1 - x_2|^{-\Delta_1-\Delta_2}. \tag{4.7}$$

On peut aussi montrer que la fonction 2-points s'annule si $\Delta_1 \neq \Delta_2$. Des corrélations en loi de puissance (avec de possibles corrections logarithmiques) sont la signature d'une théorie invariante d'échelle. Pour les CFT_2, il est utile d'introduire les coordonnées complexes

$$\begin{aligned} z = x^0 + ix^1 \qquad &, \qquad \bar{z} = x^0 - ix^1 \\ \partial = \frac{1}{2}(\partial_0 - i\partial_1) \qquad &, \qquad \bar{\partial} = \frac{1}{2}(\partial_0 + i\partial_1). \end{aligned} \tag{4.8}$$

Pour le boson libre, d'action [6]

$$S = \frac{\kappa}{2}\int dtdx\ \partial_\mu\phi\partial^\mu\phi = \kappa\int dzd\bar{z}\ \partial\phi(z,\bar{z})\bar{\partial}\phi(z,\bar{z}), \tag{4.9}$$

l'opérateur de champ scalaire n'est pas quasi-primaire [7] [225],

$$\langle \phi(z,\bar{z})\phi(w,\bar{w})\rangle = -\frac{1}{8\pi\kappa}(\log|z-w| + \log|\bar{z}-\bar{w}|), \tag{4.10}$$

mais les courants $j(z) = i\partial\phi(z,\bar{z})$ et $\bar{j}(\bar{z}) = i\bar{\partial}\phi(z,\bar{z})$ sont primaires

$$\langle j(z)j(w)\rangle = \frac{1}{8\pi\kappa}|z-w|^{-2}, \tag{4.11}$$

avec une expression analogue pour $\langle \bar{j}(\bar{z})\bar{j}(\bar{w})\rangle$.

L'entropie d'intrication bipartite dans les CFT_2 peut être obtenue en utilisant la riche structure analytique de la théorie [55, 59]. Pour un intervalle A dans une CFT_2, on a [149]

$$S(A)_{2\mathrm{d}} = \frac{c+\bar{c}}{6}\log\frac{|A|}{\epsilon}. \tag{4.12}$$

Notons que la référence [149] relie directement la divergence de l'entropie d'intrication à l'anomalie conforme résultant de la régularisation de la théorie dans l'UV. Le résultat (4.12) a été généralisé par [53] à des systèmes de taille L finie,

$$S(A)_{2\mathrm{d}} = \begin{cases} \frac{c}{6}\log\left(\frac{L}{\pi\epsilon}\sin\frac{\pi|A|}{L}\right) + O(1) & , \quad \text{(conditions Dirichlet)} \\ \frac{c}{3}\log\left(\frac{L}{\pi\epsilon}\sin\frac{\pi|A|}{L}\right) + O(1) & , \quad \text{(conditions périodiques)}, \end{cases} \tag{4.13}$$

6. On utilise la notation $\partial_\mu\phi\partial^\mu\phi = (\partial_t\phi)^2 - (\partial_x\phi)^2$. Avec $(t,x) = (ix^0, x^1)$, on trouve à l'aide de la matrice jacobienne $dzd\bar{z} = 2idx^0dx^1 = 2dtdx$.

7. La divergence du corrélateur de champ est vraisemblablement due à l'invariance du champ sous une symétrie non compacte. Voir également (4.17), de même que les théorie invariantes de Lifshitz du chapitre 6. L'auteur remercie Benjamin Doyon pour cette observation.

ainsi qu'à des systèmes dans un état thermique à température inverse β,

$$S(A)_{2\mathrm{d}} = \frac{c}{3}\log\left(\frac{\beta}{\pi\epsilon}\sinh\frac{\pi|A|}{\beta}\right) + O(1). \tag{4.14}$$

De nombreuses chaînes de spins critiques ont une CFT_2 pour théorie effective, telles que le modèle XY, le modèle XXZ et leurs cas particuliers (Ising, Heisenberg, Hubbard dans la limite d'un seul fermion par site). L'entropie d'intrication bipartite est ainsi donnée par (4.12), où ϵ est le pas du réseau et $c, \bar{c}$ sont les charges centrales (holomorphe et antiholomorphe) de la théorie de champ conforme décrivant les propriétés universelles [274, 184]. Pour ces systèmes, l'entropie d'intrication distingue clairement les régimes critique et non critique, *cf.* Théorème 3.6.

En dimension $2+1$, l'entropie d'intrication dépend fortement de la géométrie de la sous-région A. En particulier, pour un sous-système A dont la frontière comporte un coin d'angle d'ouverture θ, on trouve dans l'état fondamental

$$S(A)_{3\mathrm{d}} = B\frac{|\partial A|}{\epsilon} - a(\theta)\log\frac{|\partial A|}{\epsilon} + O(1). \tag{4.15}$$

Le terme divergent dominant est une loi d'aire. Nous avons déjà rencontré l'exemple du scalaire relativiste à la Section 3.4. La partie logarithmique de (4.15) est appelée intrication de coin (*corner entanglement*). Le coefficient $a(\theta)$ est un nombre positif indépendant du régulateur UV et tel que $a(2\pi-\theta) = a(\theta)$ dû à la pureté de l'état [64, 65]. Comme elle est universelle, la fonction $a(\theta)$ est une caractéristique de la CFT_3 et fournit, pour plusieurs modèles critiques, une mesure du « nombre de degrés de liberté » de leur CFT_3 effective [105, 164, 261].

4.2 Théories critiques invariantes de Lifshitz

En un point critique quantique, la physique est invariante d'échelle, mais pas nécessairement invariante de Lorentz [23]. Une théorie est dite invariante de Lifshitz lorsqu'elle est invariante sous les transformation globales d'échelle

$$\mathbf{x} \to \lambda\mathbf{x} \quad , \quad t \to \lambda^z t \quad , \quad \lambda > 0, \tag{4.16}$$

où $z > 0$ est appelé *exposant dynamique*. (On réserve généralement le terme *Lifshitz* au cas anisotrope $z \neq 1$.) Les corrélations et l'entropie d'intrication peuvent être obtenus analytiquement pour un type particulier de théories de champs invariantes de Lifshitz (LFT), soit celles possédant une structure de Rokhsar-Kivelson (RK) [8], qui sera l'objet de la Section 4.4. Mentionnons d'ores et déjà que la structure RK implique que, dans l'état fondamental, les corrélations à temps égal de la théorie Lifshitz $(D+1)$-dimensionnelle sont reproduites par les propagateurs d'une CFT D-dimensionnelle (à dérivées supérieures si $z > 2$). Lorsque $D = 2$, en particulier,

8. Les LFT pour lesquelles un dual holographique est connu constituent un autre type important de théories se prêtant à l'analyse [163, 169].

la riche structure des CFT_2 est mise à profit. Pour la CFT_2 bosonique, Éq.(4.9), la LFT_{2+1} parente a pour corrélateurs de ses opérateurs de champ [9]

$$\langle \phi(\mathbf{x},t), \phi(\mathbf{x}',t')\rangle = \begin{cases} -\frac{1}{4\pi\kappa}\log\frac{|\mathbf{x}'-\mathbf{x}|}{\epsilon} & , \quad |t'-t| \to 0 \\ -\frac{1}{8\pi\kappa}\log\frac{4\kappa|t'-t|}{\epsilon^2\gamma} & , \quad |\mathbf{x}'-\mathbf{x}| \to \epsilon, \end{cases} \tag{4.17}$$

où $\log\gamma$ est la constante d'Euler. L'éq. (4.17) correspond à un exposant dynamique $z = 2$. Le corrélateur de l'opérateur de champs à temps fixe $t' = t$ reproduit celui de la CFT, Éq. (4.10). En outre, les opérateurs de charge $\mathcal{O}_n(\mathbf{x}) = e^{-in\phi(\mathbf{x})}$, $n \in \mathbb{Z}$, qui créent un état cohérent bosonique de charge n [23], présentent des corrélations en loi de puissance

$$\langle \mathcal{O}_n(\mathbf{x},t)\mathcal{O}_n(\mathbf{x}',t')\rangle = \begin{cases} \left(\frac{\epsilon}{|\mathbf{x}'-\mathbf{x}|}\right)^{\frac{n^2}{4\pi\kappa}} & , \quad |t'-t| \to 0 \\ \left(\frac{\epsilon^2\gamma}{4\kappa|t'-t|}\right)^{\frac{n^2}{8\pi\kappa}} & , \quad |\mathbf{x}'-\mathbf{x}| \to \epsilon, \end{cases} \tag{4.18}$$

caractéristiques d'une théorie invariante d'échelle.

La symétrie conforme *spatiale* de l'état fondamental d'une LFT_{2+1} munie de la structure RK procure également le levier nécessaire pour déterminer son intrication bipartite. La formule de Fradkin-Moore [105] donne, pour des champs *non compacts*, l'entropie d'intrication bipartite

$$S(A) = -\log\frac{Z_D^A Z_D^B}{Z_F}, \tag{4.19}$$

où Z_D^A et Z_D^B sont les fonctions de partition de la CFT_2 sur A et B, respectivement, pourvues de conditions de Dirichlet (conformes), tandis que Z_F est la fonction de partition libre. Pour un sous-système A dont la frontière est lisse sauf en un nombre fini de coins d'angles intérieurs θ_i, on obtient [105]

$$S(A)_{\mathrm{LFT}} = B\frac{|\partial A|}{\epsilon} - \sum_{\theta_i} a(\theta_i)\log\frac{|\partial A|}{\epsilon} + O(1), \tag{4.20}$$

avec

$$a(\theta) = \frac{c(\pi-\theta)^2}{12\theta(2\pi-\theta)}. \tag{4.21}$$

La comparaison avec l'Éq. (4.15) d'une CFT_3 est frappante, mais il faut rappeler que les équations ci-dessus proviennent des propriétés d'une CFT_2, qui permettent le calcul explicite de la fonction $a(\theta)$ [61, 105].

Certaines QFT invariantes de Lifshitz décrivent les classes d'universalité de systèmes critiques, notamment en dimension $1+1$ pour des chaînes de rotors quantiques [238] et pour la transition ferromagnétique d'électrons itinérants [289], et en dimension $2+1$ pour les modèles de dimères quantiques [231, 203], la théorie de jauge

9. Ici, les corrélateurs sont régularisés en leur soustrayant $\langle \phi(\epsilon,t), \phi(0,t)\rangle$ [23].

$\mathbb{Z}_2$ [203] et le modèle quantique à huit sommets (*quantum eight-vertex model*) [23] [10]. Tous ces exemples ont un exposant dynamique $z = 2$. Les exemples cités en dimension $2+1$ se démarquent cependant par le fait qu'elles possèdent la structure RK [23] sur laquelle nous reviendrons à la Section 4.4.

4.3 Chaînes de spins critiques et systèmes critiques sur réseau

Nous avons mentionné que pour de nombreuses chaînes de spins critiques, la loi d'aire n'est que légèrement mise en défaut par une violation logarithmique dans la taille du sous-système. Récemment, toutefois, plusieurs modèles sur réseau unidimensionnel ont réfuté la validité générale de cette observation en présentant des violations en loi de puissance, voire une entropie d'intrication en loi de volume [156, 276, 119, 204, 86, 87, 297, 298, 299] [11].

Les systèmes critiques sur réseau D-dimensionnel ont également un comportement varié. Les systèmes harmoniques sur réseau (bosoniques ou fermioniques) appartenant à la classe d'universalité d'une CFT respectent la loi d'aire si $D = 2$, *cf.* (4.15), et y dérogent par un facteur logarithmique pour $D = 1$, *cf.* (4.12). Il en va de même des théories appartenant à la classe d'universalité d'une LFT munie de la structure RK, tel qu'abordé à la Section 4.2. Les fermions critiques sur un réseau D-dimensionnel et pourvus d'une surface de Fermi de mesure finie (mesure non nulle, dimension non fractale [12]) constituent le prototype de la violation de la loi d'aire en dimension supérieure. On trouve alors

$$S(A) = \left(\frac{\ell}{\epsilon}\right)^{D-1} \log \ell, \tag{4.22}$$

où ℓ est la longueur caractéristique de A et ϵ est le pas du réseau [285, 116, 52]. Ce résultat ne s'applique pas aux CFT fermioniques, qui ne possèdent pas de surface de Fermi [97].

4.4 Hamiltoniens de type Rokhsar-Kivelson

Nous allons décrire la structure de Rokhsar-Kivelson (RK). Notre présentation doit beaucoup aux références [68, 241, 23]. À la connaissance de l'auteur, le passage aux théories de champs de type RK, tel que nous le ferons à la Section 4.4.2,

10. L'action classique correspondante jour aussi un rôle central dans les transitions de phase associées à une brisure spontanée d'isotropie ou d'invariance sous les translations de cristaux liquides en 3 dimensions [23].

11. Notons que les références [276, 156, 119] présentent toutes un défaut de localité : résultat dépendant des conditions aux frontières [276], termes locaux dépendants de la taille du système [156], interactions à longue portée [119]. Les autres références sont véritablement locales et concernent des chaînes de spin entier $s \geq 2$ [204] et demi-entier $s \geq 3/2$ [87] présentant une loi de puissance pour l'entropie d'intrication, accompagnée d'une violation de la *Cluster Decomposition Property* [86], et pouvant être déformées jusqu'à présenter une entropie d'intrication extensive [297, 298, 299].

12. Voir [119] pour un exemple de fermions critiques pourvus d'une surface de Fermi fractale et présentant une loi de volume pour l'entropie d'intrication.

n'est pas traité explicitement dans la littérature. De nombreux systèmes quantiques (voir les références de [68]) en dimension $D+1$ possèdent une base privilégiée $\mathscr{B}$ dans laquelle l'hamiltonien consiste en une somme dénombrable d'hamiltoniens 2×2. (Chaque hamiltonien 2×2 agit de façon non triviale sur un sous-espace de dimension 2, et s'annule sur les kets restants de $\mathscr{B}$.) Ces hamiltoniens 2×2 sont constitués chacun d'un terme d'énergie potentielle favorisant l'ordre local dans la base $\mathscr{B}$, et d'un terme cinétique favorisant la superposition des vecteurs de $\mathscr{B}$. Pour une valeur particulière du rapport entre les termes potentiels et cinétiques, appelée *point de Rokhsar-Kivelson*, les hamiltoniens locaux deviennent semi-définis positifs. Un état fondamental sans frustration (d'énergie zéro) est obtenu, dont la constante de normalisation correspond à la fonction de partition d'un système classique D-dimensionnel. Cette structure particulière de l'hamiltonien et de son état fondamental est appelée *structure de Rokhsar-Kivelson.*

Définition 4.1 (Structure RK)**.** *Trois propriétés définissent la structure RK d'un hamiltonien quantique :*

1. *Il existe une base dénombrable $\mathscr{B}$ pour l'espace de Hilbert $\mathscr{H}$ telle que l'hamiltonien se décompose dans $\mathscr{B}$ en une somme d'hamiltoniens 2×2 semi-définis positifs (i.e. des projecteurs, à un facteur près).*
2. *Il existe un état fondamental sans frustration, d'énergie zéro, annihilé par tous les projecteurs de la propriété 1.*
3. *Pour l'état fondamental de la propriété 2, le facteur de normalisation correspond à la fonction de partition thermique d'un système classique dont l'espace de configuration $\mathscr{C}$ permet d'indexer $\mathscr{B}$, i.e. $\mathscr{B}=\{|s\rangle \mid s\in\mathscr{C}\}$.*

Par un argument élémentaire mais fastidieux [68], tout hamiltonien de type RK peut être ramené à la *forme en matrices stochastiques* (SMF)

$$H=\frac{1}{2}\sum_{s\neq s'}\omega_{ss'}P_{ss'} \quad , \quad \omega_{ss'}\in(0,\infty), \tag{4.23}$$

pour des opérateurs hermitiens

$$\begin{aligned} P_{ss'} &= \begin{pmatrix} e^{\frac{\beta}{2}(E(s)-E(s'))} & -1 \\ -1 & e^{\frac{\beta}{2}(E(s')-E(s))} \end{pmatrix}_{ss'} \\ &= e^{\frac{\beta}{2}(E(s)-E(s'))}|s\rangle\langle s| - |s\rangle\langle s'| - |s'\rangle\langle s| + e^{\frac{\beta}{2}(E(s')-E(s))}|s'\rangle\langle s'|, \end{aligned} \tag{4.24}$$

de valeurs propres 0 et $2\cosh(\frac{\beta}{2}(E(s')-E(s))$. Ici, $\beta\in\mathbb{R}$ et $E:\mathscr{C}\to\mathbb{R}$. Rappelons que les $s\in\mathscr{C}$ sont les configurations d'un système classique et qu'elles permettent d'indexer les états de la base privilégiée, $\mathscr{B}=\{|s\rangle \mid s\in\mathscr{C}\}$. On a donc

$$\langle s|s'\rangle=\delta_{s,s'} \quad , \quad \mathbb{1}=\sum_{s\in\mathscr{C}}|s\rangle\langle s|. \tag{4.25}$$

L'état

$$|\psi_0\rangle=\frac{1}{\sqrt{Z(\beta)}}\sum_{s\in\mathscr{C}}e^{-\frac{\beta}{2}E(s)}|s\rangle \tag{4.26}$$

satisfait $P_{ss'}|\psi_0\rangle = 0$ pour tout $(s, s') \in \mathscr{C}^2$, et constitue un état fondamental de H (pour toutes valeurs positives des $\omega_{ss'}$), sans frustration et d'énergie nulle. On reconnait dans la constante de normalisation,

$$Z(\beta) = \sum_{s\in\mathscr{C}} e^{-\beta E(s)}, \tag{4.27}$$

la fonction de partition à température inverse β d'un système classique défini sur $\mathscr{C}$ et d'énergie $E : \mathscr{C} \to \mathbb{R}$.

4.4.1 Hamiltoniens quantiques RK et systèmes classiques stochastiques

L'équation de Schrödinger (Euclidienne) pour H est équivalente à l'équation maîtresse d'un système classique stochastique. À l'aide de l'opérateur $\mathcal{E}|s\rangle = E(s)|s\rangle$, on définit la transformation (non-unitaire)

$$|p\rangle = e^{-\frac{\beta}{2}\mathcal{E}}|\psi\rangle \quad , \quad M = -e^{-\frac{\beta}{2}\mathcal{E}} H e^{\frac{\beta}{2}\mathcal{E}} = -SHS^{-1}. \tag{4.28}$$

La relation de similarité entre $H = \sum_n \varepsilon_n |\psi_n\rangle\langle\psi_n|$ et $-M = -\sum_n \lambda_n |\zeta_n\rangle\langle\zeta_n|$ entraîne un isomorphisme de leurs spectres et de leurs états propres :

$$\begin{aligned} M(S|\psi_n\rangle) &= -SHS^{-1}S|\psi_n\rangle = -\varepsilon_n S|\psi_n\rangle \\ \Rightarrow \lambda_n = -\varepsilon_n \qquad &, \qquad |\zeta_n\rangle \propto S|\psi_n\rangle. \end{aligned} \tag{4.29}$$

L'application de (4.28) sur $\langle s|\frac{d}{d\tau}|\psi\rangle = -\langle s|H|\psi\rangle$ donne

$$\frac{dp_s}{d\tau} = \sum_s M_{ss'} p_{s'}, \tag{4.30}$$

où $p_s = \langle s|p\rangle$. Crucialement, la forme RK de l'hamiltonien implique $M_{s\neq s'} > 0$ (positivité des taux de transition), $M_{ss} = -\sum_{s'\neq s} M_{s's}$ (conservation de la probabilité), ainsi que la condition de balance détaillée

$$e^{-\frac{\beta}{2}E(s')} M_{ss'} = e^{-\frac{\beta}{2}E(s)} M_{s's}, \tag{4.31}$$

faisant de (4.30) une équation maîtresse *bona fide* pour les probabilités $p_s(\tau)$, décrivant l'approche du système stochastique vers l'équilibre. Puisque $\varepsilon_n = -\lambda_n$, l'hamiltonien H est pourvu d'un gap spectral au-dessus de $\varepsilon_0 = 0$ si et seulement si les temps caractéristiques d'équilibration du système stochastique, $|\lambda_n|^{-1}$ $(n \neq 0)$, sont bornés supérieurement.

4.4.2 Hamiltoniens RK de champs quantiques

Au Chapitre 6, nous rencontrerons des hamiltoniens de champs scalaires réels dont l'état fondamental est de type RK, Éq. (4.26). Afin d'obtenir une formulation mieux adaptée au traitement habituel des théories de champs, nous présentons un passage au continuum pour les hamiltoniens RK au cours duquel les opérateurs de

type projecteurs deviennent des opérateurs différentiels semi-définis positifs. Pour un champ scalaire réel en dimension $D+1$, la base privilégiée $\mathscr{B}$ sera indexée par les configurations [13] $\phi : \mathbb{R}^D \to \mathbb{R}$. L'hamiltonien (4.23) devient

$$H = \frac{1}{2}\int_{\phi'\neq\phi} \mathcal{D}\phi\mathcal{D}\phi'\ \omega_{\phi\phi'}P_{\phi\phi'} \quad , \quad \omega_{\phi\phi'} \in (0,\infty), \tag{4.32}$$

avec les opérateurs de type projecteurs

$$\begin{aligned} P_{\phi\phi'} &= \begin{pmatrix} e^{\frac{\beta}{2}E_{\phi\phi'}} & -1 \\ -1 & e^{\frac{\beta}{2}E_{\phi'\phi}} \end{pmatrix}_{\phi\phi'} \\ &= e^{\frac{\beta}{2}(E[\phi]-E[\phi'])}|\phi\rangle\langle\phi| - |\phi\rangle\langle\phi'| - |\phi'\rangle\langle\phi| + e^{\frac{\beta}{2}(E[\phi']-E[\phi])}|\phi'\rangle\langle\phi'|, \end{aligned} \tag{4.33}$$

où nous avons introduit la notation $E_{\phi'\phi} = E[\phi'] - E[\phi]$. Il est utile de débuter par l'hamiltonien de « température infinie » $\beta = 0$,

$$H^0 = \frac{1}{2}\int_{\phi'\neq\phi} \mathcal{D}\phi\mathcal{D}\phi'\omega_{\phi\phi'}\begin{pmatrix} 1 & -1 \\ -1 & 1 \end{pmatrix}_{\phi\phi'}. \tag{4.34}$$

Il nous est permis de fixer les valeurs (positives) de la fonction $\omega_{\phi\phi'}$ sans affecter l'état fondamental de H^0 (ce qui demeure vrai pour $\beta > 0$). Avec le delta de Dirac $\delta_x(y) = \delta(x-y)$, et pour $\epsilon > 0$, nous choisirons

$$\omega_{\phi\phi'} = \begin{cases} 1/\epsilon^2 & , \quad \text{si } \exists x \in \mathbb{R}^D \text{ tel que } \phi' = \phi + \epsilon\delta_x \\ \epsilon & , \quad \text{autrement.} \end{cases} \tag{4.35}$$

Lors du passage $\epsilon \to 0^+$, seuls survivront les termes couplant des configurations classiques qui diffèrent en un seul point par un delta de Dirac. Ce choix semble indiqué pour obtenir le terme cinétique habituel, $\Pi^2 = (-i\delta/\delta\phi)^2$, puisque $\delta\eta/\delta\phi(x) = \lim_{\epsilon\to 0}(\eta[\phi+\epsilon\delta_x] - \eta[\phi])/\epsilon$. Définissons $\phi_x = \phi + \epsilon\delta_x$, notation que nous utiliserons par la suite. De plus, nous écrirons $\langle\phi|\Psi\rangle$ sous sa forme fonctionnelle $\Psi[\phi]$, ou encore Ψ_ϕ. Pour $\epsilon \to 0^+$,

$$\begin{aligned} \frac{1}{\epsilon^2}\langle\Phi|\int \mathcal{D}\phi \left(\begin{smallmatrix} 1 & -1 \\ -1 & 1 \end{smallmatrix}\right)_{\phi\phi_x}|\Psi\rangle &= \frac{1}{\epsilon^2}\int \mathcal{D}\phi(\Phi[\phi]^* \quad \Phi[\phi_x]^*)\begin{pmatrix} 1 & -1 \\ -1 & 1 \end{pmatrix}\begin{pmatrix} \Psi[\phi] \\ \Psi[\phi_x] \end{pmatrix} \\ &= \langle\tfrac{\delta\Phi}{\delta\phi(x)}|\tfrac{\delta\Psi}{\delta\phi(x)}\rangle \\ &= -\langle\Phi|\tfrac{\delta^2\Psi}{\delta\phi(x)^2}\rangle + \text{terme frontière.} \end{aligned} \tag{4.36}$$

Les termes de frontière seront désormais implicites. Par le choix des fonctions $\omega_{\phi\phi'}$, Éq.(4.35), seuls demeurent dans l'expression pour H^0, (4.34), les ϕ' de la forme $\phi_x = \phi + \epsilon\delta_x$ et l'intégrale sur ϕ' devient une simple intégrale spatiale. On obtient la représentation de Schrödinger de l'hamiltonien,

$$H^0_{\text{Sch}} = \frac{1}{2}\int dx \left(-\frac{\delta^2}{\delta\phi(x)^2}\right). \tag{4.37}$$

13. Ou un sous-ensemble dense et dénombrable de ces configurations, un ensemble de polynômes, par exemple.

On définit maintenant les opérateurs non hermitiens

$$A(x) = \frac{1}{2\sqrt{2}\epsilon} \int \mathcal{D}\phi \left(\begin{smallmatrix} -1 & 1 \\ -1 & 1 \end{smallmatrix}\right)_{\phi\phi_x} \quad , \quad A^\dagger(x) = \frac{1}{2\sqrt{2}\epsilon} \int \mathcal{D}\phi \left(\begin{smallmatrix} -1 & -1 \\ 1 & 1 \end{smallmatrix}\right)_{\phi\phi_x}, \tag{4.38}$$

de sorte que [14]

$$A(x)_{\rm Sch} = \frac{1}{\sqrt{2}} \frac{\delta}{\delta\phi(x)} \quad , \quad A(x)^\dagger_{\rm Sch} = -\frac{1}{\sqrt{2}} \frac{\delta}{\delta\phi(x)}. \tag{4.39}$$

Ainsi, l'hamiltonien H^0 est manifestement semi-défini positif,

$$H^0_{\rm Sch} = \int dx\ A(x)^\dagger_{\rm Sch} A(x)_{\rm Sch}, \tag{4.40}$$

et possède un état fondamental de la forme (4.26) avec $\beta = 0$. En effet, pour tout $x \in \mathbb{R}^D$, pour Ψ quelconque et pour $\Psi_0[\phi] =$ constante,

$$\langle\Psi|A^\dagger(x)_{\rm Sch} A(x)_{\rm Sch}|\Psi\rangle = \|A(x)_{\rm Sch}\Psi\|^2 \geq 0 \quad , \quad A(x)_{\rm Sch}|\Psi_0\rangle = 0. \tag{4.41}$$

Une construction similaire s'applique à l'hamiltonien RK général, défini aux Éqs.(4.32) et (4.33), pour $\beta > 0$. On fixe les valeurs (positives) de la fonction $\omega_{\phi\phi'}$ comme à l'Éq.(4.35), puis on évalue

$$\begin{aligned} &\frac{1}{\epsilon^2}\langle\Phi| \int \mathcal{D}\phi\ P_{\phi\phi_x}|\Psi\rangle \\ &= \int \tfrac{\mathcal{D}\phi}{\epsilon^2}\ e^{\frac{\beta}{2}E_{\phi_x\phi}} (\Phi^*_{\phi_x} - \Phi^*_\phi + (1 - e^{\frac{\beta}{2}E_{\phi\phi_x}})\Phi^*_\phi)(\Psi_{\phi_x} - \Psi_\phi + (1 - e^{\frac{\beta}{2}E_{\phi\phi_x}})\Psi_\phi) \\ &= \left\langle \left(\tfrac{\delta}{\delta\phi(x)} + \tfrac{\delta(\beta E/2)}{\delta\phi(x)}\right)\Phi \middle| \left(\tfrac{\delta}{\delta\phi(x)} + \tfrac{\delta(\beta E/2)}{\delta\phi(x)}\right)\Psi \right\rangle, \end{aligned} \tag{4.42}$$

ce qui, à un terme de frontière près, donne

$$H_{\rm Sch} = \frac{1}{2}\int dx \left(-\tfrac{\delta}{\delta\phi(x)} + \tfrac{\delta(\beta E/2)}{\delta\phi(x)}\right)\left(\tfrac{\delta}{\delta\phi(x)} + \tfrac{\delta(\beta E/2)}{\delta\phi(x)}\right). \tag{4.43}$$

H est explicitement semi-défini positif et possède l'état fondamental

$$|\Psi_0\rangle = \frac{1}{\sqrt{Z(\beta)}} \int \mathcal{D}\phi\ e^{-\frac{\beta}{2}E[\phi]}|\phi\rangle. \tag{4.44}$$

14. En effet,

$$\langle\Phi|A\Psi\rangle \to \frac{1}{\sqrt{2}}\langle\Phi|\tfrac{\delta\Psi}{\delta\phi}\rangle \quad , \quad \langle\Phi|A^\dagger\Psi\rangle \to \frac{1}{\sqrt{2}}\langle\tfrac{\delta\Phi}{\delta\phi}|\Psi\rangle = -\frac{1}{\sqrt{2}}\langle\Phi|\tfrac{\delta\Psi}{\delta\phi}\rangle.$$

On évitera d'écrire $\langle\Phi|A|\Psi\rangle$ et $\langle\Phi|A^\dagger|\Psi\rangle$, puisque A et $A^\dagger$ ne sont pas hermitiens. Par définition, $\langle\Phi|A^\dagger\Psi\rangle = \langle A\Phi|\Psi\rangle$. Notons également que

$$A^\dagger A = \frac{1}{2\epsilon^2}\int \mathcal{D}\phi \left(\begin{smallmatrix} 1 & -1 \\ -1 & 1 \end{smallmatrix}\right) \quad , \quad AA^\dagger = \frac{1}{2\epsilon^2}\int \mathcal{D}\phi \left(\begin{smallmatrix} 1 & 1 \\ 1 & 1 \end{smallmatrix}\right).$$

Ainsi $(A^\dagger A)_{\rm Sch} = A^\dagger_{\rm Sch} A_{\rm Sch}$, tandis que $(AA^\dagger)_{\rm Sch}$ diverge comme $1/\epsilon^2$, car $\langle\Phi|AA^\dagger\Psi\rangle = 2\langle\Phi|\Psi\rangle/\epsilon^2$.

Si $E[\phi]$ est une fonctionnelle locale, la constante de normalisation $Z(\beta)$ correspond à la fonction de partition d'une théorie classique à température inverse β, dont les corrélations à temps égal reproduisent celles de l'hamiltonien (4.43) pour des opérateurs diagonaux dans la base $\{|\phi\rangle\}$,

$$\langle\Psi_0|\hat{\mathcal{O}}_1\hat{\mathcal{O}}_2|\Psi_0\rangle = \int \mathcal{D}\phi\ \mathcal{O}_1[\phi]\mathcal{O}_2[\phi]\frac{e^{-\beta E[\phi]}}{Z(\beta)}. \tag{4.45}$$

Dans certains cas, dont ceux que nous rencontrerons au Chapitre 6, la fonctionnelle $E[\phi]$ peut également correspondre à l'action euclidienne d'une théorie quantique en dimension spatiale $D-1$. Les propagateurs de cette théorie reproduisent alors les corrélations à temps égal de l'hamiltonien (4.43). Puisqu'on a imposé peu de contraintes sur la fonctionnelle $E[\phi]$, la variation d'un paramètre g dans la famille de fonctionnelles $E_g[\phi]$ permettra d'étudier certaines transitions de phase quantiques de manière analytique [23]. (Voir également le Chapitre 6.) Terminons en observant qu'on peut définir l'opérateur non hermitien

$$A(x) = \frac{1}{2\sqrt{2}\epsilon}\int \mathcal{D}\phi \left[\begin{pmatrix} -1 & 1 \\ -1 & 1 \end{pmatrix} + \begin{pmatrix} e^{\beta E_{\phi_x\phi}/2} & 0 \\ 0 & e^{\beta E_{\phi_{xx}\phi_x}/2} \end{pmatrix}\right]_{\phi\phi_x}, \tag{4.46}$$

où $\phi_{xx} = (\phi_x)_x = \phi + 2\epsilon\delta_x$. Sa représentation de Schrödinger est

$$A(x)_{\text{Sch}} = \frac{1}{\sqrt{2}}\left(\frac{\delta}{\delta\phi(x)} + \frac{\delta(\beta E/2)}{\delta\phi(x)}\right), \tag{4.47}$$

d'où [15]

$$H_{\text{Sch}} = \int dx\ A(x)^\dagger_{\text{Sch}} A(x)_{\text{Sch}}. \tag{4.48}$$

15. En général, cependant, $A(x)|\Psi_0\rangle = 0$ seulement dans la limite $\epsilon \to 0$. De même, $\int dx\ A^\dagger(x)A(x) = H$ seulement lorsque $\epsilon \to 0$:

$$A^\dagger(x)A(x) = \frac{1}{2\epsilon^2}\int \mathcal{D}\phi\Bigg[\begin{pmatrix} 1 & -1 \\ -1 & 1 \end{pmatrix} + \frac{1}{2}\begin{pmatrix} (e^{\beta E_{\phi_x\phi}/2}-1)^2 & 0 \\ 0 & (e^{\beta E_{\phi_{xx}\phi_x}/2}-1)^2 \end{pmatrix}$$
$$-\frac{1}{2}\begin{pmatrix} 0 & e^{\beta E_{\phi_{xx}\phi_x}/2} - e^{\beta E_{\phi_x\phi}/2} \\ e^{\beta E_{\phi_{xx}\phi_x}/2} - e^{\beta E_{\phi_x\phi}/2} & 0 \end{pmatrix} + \begin{pmatrix} e^{-\beta E_{\phi_x\phi}/2} & 0 \\ 0 & e^{\beta E_{\phi_{xx}\phi_x}/2} \end{pmatrix}\Bigg],$$

qui n'est pas de la forme (4.33) pour β et E génériques. Dans la limite $\epsilon \to 0$, le dernier terme $\mathcal{K}(x)$ correspond à une dérivée totale,

$$\langle\Phi|\mathcal{K}(x)|\Psi\rangle = \tfrac{1}{2}\tfrac{\delta}{\delta\phi(x)}\left(\Phi\tfrac{\delta(\beta E/2)}{\delta\phi(x)}\Psi\right),$$

et on retrouve

$$(A^\dagger(x)A(x))_{\text{Sch}} = \tfrac{1}{2}\left[\left(-\tfrac{\delta^2}{\delta\phi(x)^2}\right) + \left(\tfrac{\delta(\beta E/2)}{\delta\phi(x)}\right)^2 - \tfrac{\delta^2(\beta E/2)}{\delta\phi(x)^2}\right],$$

en accord avec (4.43).

Chapitre 5

Deuxième article.

Frustration, solitons, and entanglement in spin chains

par

Christian Boudreault[1,2], Solomon A. Owerre[2,3], Manu B. Paranjape[2,3]

[1]Département des sciences de la nature, Collège militaire royal de Saint-Jean, Saint-Jean-sur-Richelieu, QC, Canada, J3B 8R8

[2]Département de physique, Université de Montréal, C.P. 6128, succursale Centre-ville, Montréal, QC, Canada, H3C 3J7

[3]Perimeter Institute for Theoretical Physics, 31 Caroline Street North Waterloo, Ontario, Canada N2L 2Y5

Cet article a été soumis pour publication dans Journal of Physics A : Mathematical and Theoretical.

Contribution du candidat et des coauteurs :
Christian Boudreault a contribué à la conceptualisation, a effectué la majorité des calculs et a rédigé l'essentiel de l'article. Solomon Owerre a contribué à la conceptualisation initiale. Manu Paranjape a supervisé le projet, contribué à sa conceptualisation et participé à la mise en forme définitive de l'article.

Résumé. Les défauts de chaînes de spins antiferromagnétiques frustrées sont universellement présents dans les systèmes géométriquement frustrés [265, 270, 114, 198]. Nous considérons les défauts du modèle XXZ unidimensionnel de spins s avec anisotropie à ion unique sur une chaîne périodique de N sites, tel qu'étudié par Haldane [131]. L'hamiltonien est $H = |J| \sum_{i=1}^{N} \left(\vec{S}_i \cdot \vec{S}_{i+1} + \lambda S_i^z S_{i+1}^z + \mu (S_i^z)^2 \right)$. Dans la limite $\lambda, \mu \gg 1$, le terme de Heisenberg peut être traité en perturbativement et l'hamiltonien (classique) restant est trivialement diagonal, ses états propres correspondant à ceux de S^z, indépendamment des paramètres λ et μ. Nous identifions l'état fondamental pour toutes valeurs de λ, μ et N, déterminant ainsi le diagramme de phase du modèle classique. Le modèle classique pour $\lambda = \mu$ est un point critique pour une transition de phase de second ordre, et le spectre contient des excitations sans gap. Pour N impair et $\lambda > 0$, le système classique est antiferromagnétique mais frustré, et l'état fondamental doit inclure un défaut solitonique. Le soliton sera une excitation physique pour toutes valeurs de N paire ou impaire. Nous montrons que la taille du soliton dépend uniquement du rapport μ/λ et non du nombre de sites N. Nous calculons le profile explicite du soliton et l'illustrons pour quelques valeurs quantifiées du spin. Nous considérons ensuite l'interaction de Heisenberg perturbativement et déterminons l'état fondamental solitonique perturbatif du modèle frustré. Nous identifions le spectre d'intrication, l'entropie d'intrication (EE) et la capacité d'intrication (CE) de l'état fondamental solitonique. Nous observons une violation algébrique de la loi d'aire pour l'EE [149, 274, 53, 134], en accord avec des résultats récents pour les chaînes faiblement frustrées [115]. Notre analyse va toutefois au-delà le régime de faible frustration et nous obtenons une EE extensive dans la taille du sous-système lorsque la frustration forte prévaut.
Mots-clés : Frustration géométrique, chaînes de spins quantiques, solitons, entropie d'intrication, capacité d'intrication, violation de la loi d'aire

Abstract. Defects in frustrated antiferromagnetic spin chains are universally present in geometrically frustrated systems [265, 270, 114, 198]. We consider the defects of the one-dimensional, spin-s XXZ model with single-ion anisotropy on a periodic chain with N sites that was famously studied by Haldane [131]. The Hamiltonian is given by $H = |J| \sum_{i=1}^{N} \left(\vec{S}_i \cdot \vec{S}_{i+1} + \lambda S_i^z S_{i+1}^z + \mu (S_i^z)^2 \right)$. In the limit $\lambda, \mu \gg 1$, the Heisenberg term can be treated perturbatively, the remaining (classical) Hamiltonian is trivially diagonal, with eigenstates simply given by the eigenstates of S^z, independent of the parameters λ and μ. We determine the ground state for all values of λ and μ and N and thus determine the phase diagram of the classical model. The classical model for $\lambda = \mu$ is a critical point for a second-order phase transition, and the spectrum contains gapless excitations. For N odd and $\lambda > 0$ the classical system is antiferromagnetic but frustrated, and the ground state must include a soliton defect. This soliton will be a physical excitation for all values of N odd or even. We show that the size of the soliton depends only on the ratio μ/λ and not on the number of sites N. We compute the explicit profile of the soliton and illustrate it for some exemplary discrete quantum values. Next we consider the Heisenberg interaction perturbatively and determine the corresponding perturbative solitonic ground state for the frustrated model. Then we compute the entanglement spectrum, entanglement entropy (EE), and capacity of entanglement (CE) of the solitonic ground state. We find an algebraic violation of the area law for the EE [149, 274, 53, 134] consistent with recent results on weakly frustrated chains [115]. Our analysis then moves beyond the weak frustration regime, and we obtain

an extensive scaling of the EE when strong frustration prevails.

Keywords : Geometrical frustration, quantum spin chains, solitons, entanglement entropy, capacity of entanglement, violation of the area law

5.1 Introduction

The study of phase transitions and entanglement properties of frustrated systems is a venerable subject [99, 265, 270, 103, 42] which has attracted renewed interest in recent years [46, 114, 286, 198, 113, 115, 195, 194]. Frustration refers to the impossibility for the ground state of a many-body system to locally minimize energy. In classical systems, frustration can only arise because of topological obstructions. For instance, the (classical) antiferromagnetic (AF) Ising chain $|J|\sum_i S_i^z S_{i+1}^z$ minimizes the energy of the local interaction terms $|J|S_i^z S_{i+1}^z$ with the Néel order. On a periodic chain of odd length, however, the Néel order cannot be realized and a defect must be present which causes frustration for one or more local terms. This example of a *geometric* frustration is prototypical : a theorem by Toulouse implies that a classical system in any dimension is frustrated if and only if it contains loops of odd length that can be mapped to a (frustrated) AF Ising chain [265, 270]. Quantum criteria that reduce to the Toulouse condition in the classical case have been obtained in [114, 198]. Odd-numbered periodic AF chains are thus the elementary building blocks of geometric frustration, classical or quantum. Contrary to common belief, these systems are known to display boundary-induced orders and transitions *in the bulk* of large chains [195, 194]. We stress that these effects of frustration and their corresponding degeneracies can be altered dramatically by adding a single site, thus revealing their nonperturbative nature [115]. Quantum systems can feature another type of frustration due to the impossibility of realizing certain structures of local entanglement on a global scale. An example is the AF Heisenberg chain $|J|\sum_{i=1}\vec{S}_i\cdot\vec{S}_{i+1}$ whose local interaction terms have singlet ground state $(|\uparrow_i\downarrow_{i+1}\rangle - |\downarrow_i\uparrow_{i+1}\rangle)/\sqrt{2}$. No global state can possess such local entanglement on every pair of nearest-neighbours, and the system is frustrated. This *quantum* frustration has of course no classical equivalent.

In this work, we are concerned with the geometric frustration of a quantum spin chain, especially when frustration becomes strong. To define strong frustration, we use the measure of local frustration proposed in [114, 198]. For a many-body Hamiltonian $H = \sum_S h_S$, frustration of the interactions h_S on subsystem S is a number $f_S \in [0,1]$ quantifying how much a ground state of H is failing to overlap with the ground state of h_S. (It will be precisely explained in Section 5.4.1.) No frustration corresponds to $f_S = 0$, while maximal frustration implies $f_S = 1$. We define *weak* ($f_S \sim 0$) and *strong* ($f_S \sim 1$) frustration accordingly. Geometric frustration can also be *extensive*. For instance, it is extensive in the AF Ising model on the triangular lattice because the number of frustrated rings (triangles) scales like system size. The systems that we consider in this work have non-extensive frustration, but most have strong frustration. (That is, we distinguish between *weak* and *non-extensive* frustration, contrary to [115].) We will study aspects of ground state entanglement in geometrically frustrated chains, mostly when frustration is strong. Our results

will be obtained by high-order perturbation theory. Combinations of analytical and numerical approaches indicate that the perturbative picture, in which the frustrated ground state is analyzed in terms of single-particle excitations (defects) over the non-frustrated ground state, sometimes persists beyond the perturbative regime [115].

Haldane [131] considered the Heisenberg model with an anisotropy corresponding to the Hamiltonian

$$H = |J| \left(\sum_{i=1}^{N} \vec{S}_i \cdot \vec{S}_{i+1} + \lambda S_i^z S_{i+1}^z + \mu (S_i^z)^2 \right) \tag{5.1}$$

(with periodic boundary conditions, $\vec{S}_{N+1} = \vec{S}_1$), for large spin $|\vec{S}| = s \gg 1$ but for small anisotropy $0 < (\lambda - \mu)^{1/2} \ll 1$, $\lambda > \mu$. However the complete phase diagram of the model, for all values of the couplings is still of much interest. We will consider the model in the large anisotropy limit, the opposite limit to that considered by Haldane. We define $a = |J|\mu$ and $b = |J|\lambda$, and consider the model perturbatively for $|J| \to 0$ but a and b finite. Thus we write the Hamiltonian as

$$\begin{aligned} H(\vec{S}_1, \ldots, \vec{S}_N) &= H_0(S_1^z, \ldots, S_N^z) + |J| \sum_{i=1}^{N} \vec{S}_i \cdot \vec{S}_{i+1}, \\ H_0(S_1^z, \ldots, S_N^z) &= \sum_{i=1}^{N} \Big(a(S_i^z)^2 + b S_i^z S_{i+1}^z \Big) \end{aligned} \tag{5.2}$$

and treat $|J|$ perturbatively. This limit is still of import to Haldane's considerations. The anisotropy, however small in Haldane's work, picks the antiferromagnetic Néel ordered ground state that is aligned in the z direction. For different parts of the parameter space in the anisotropy, it is possible and indeed true that a different ground state is indicated. The anisotropic term in the Hamiltonian only involves the z component of the spin thus, considering it alone, it is essentially an Ising [158] model. In fact it corresponds exactly to the model studied by Blume and Capel (for spin 1) [45, 57, 56, 58], albeit here, it is for arbitrary and large spin. Therefore we will call the limiting model defined by $H_0(S_1^z, \ldots, S_N^z)$ the Blume-Capel-Haldane-Ising (BCHI) model.

Being a sum of mutually commuting operators, the BCHI Hamiltonian H_0 is fully classical. The eigenstates of $H_0(S_1^z, \ldots, S_N^z)$ are obvious and independent of the parameters, a and b, and can be labelled as $|s_1, \ldots, s_N\rangle$, where s_i is the z component of the ith spin and as usual $s_i \in \{-s, -s+1, \ldots, s-1, s\}$. The corresponding energy eigenvalue is $E(s_1, \ldots, s_N) = \sum_{i=1}^{N} \Big(a(s_i)^2 + b s_i s_{i+1} \Big)$. Which eigenstate has the minimum energy, i.e. which state is the ground state, is not always obvious.

For antiferromagnetic coupling, with odd N, there must be a defect in the Néel state on a periodic chain. The defect is localized between two adjacent spins for easy-axis coupling, $a < 0$. However, for easy-plane coupling, $a > 0$, we find that the defect spreads out to maximal size as the antiferromagnetic coupling is weakened. The defect is a soliton in the Néel state, and corresponds to a finite energy excitation. We calculate the size of the soliton and find that it is independent of the number of

sites N but depends on the ratio a/b. Hence the size is a characteristic that is not an artefact of the odd number of sites, and the same solitons can be excited in the periodic chain with an even number of spins or the finite or infinite, open chain.

In Section 5.2 we will summarize the main features of the BCHI theory's soliton. In Section 5.3 we turn the Heisenberg interaction on, and perform high-order perturbation to determine the perturbative ground state when the soliton must be present due to frustration. In Section 5.4 we study entanglement in the perturbative solitonic ground state, and find our main results.

5.2 Solitons of the classical theory

To prepare the stage, let us first consider a closed chain of *even* length N, equipped with a globally defined z axis. (From now on, a closed chain will be called *orientable* if it comes equipped with a globally defined z axis.) Each site hosts a system of spin s, coupled to its nearest neighbours by the (classical) BCHI Hamiltonian

$$H_0(S_1^z, \ldots, S_N^z) = \sum_{j=1}^{N} \Big(a(S_j^z)^2 + b S_j^z S_{j+1}^z \Big). \tag{5.3}$$

It is an easy exercise to find the exact ground state for all values of a and b. (See Appendix 5.6.1.1.) The result is given in Fig. 5.1. Wherever the ground state is

FIGURE 5.1 – Ground state of the orientable chain, with N even, and arbitrary spin s

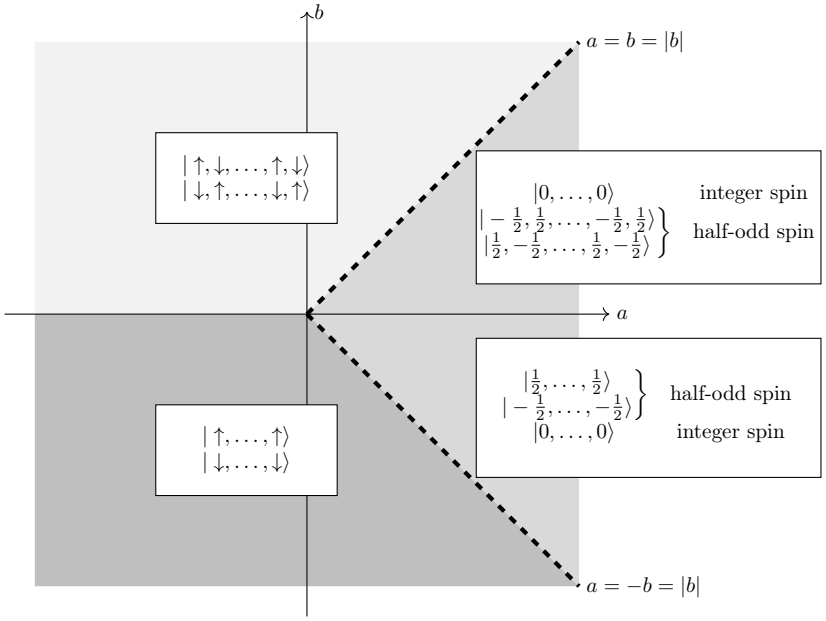

$\mathbb{Z}_2$-degenerate, there exists a soliton solution interpolating between the two degenerate vacua with minimal energy cost. When the spin is not restricted to quantized values of s^z, the soliton is found by quadratic optimization to have finite energy,

low degeneracy, and a profile entirely determined by the dynamical ratio $a/|b|$. (See Appendix 5.6.1.2.) This is summarized in Fig. 5.2, where defects are made of spin components $\pm s$, "little" defects are made of spin components $\pm\frac{1}{2}$, while s_j^M and $\bar{s}_j^M$ are solitons of length $M \geq 1$ in the ferromagnetic ($b < 0$) and antiferromagnetic ($b > 0$) regions, respectively. Their profile is found to be

FIGURE 5.2 – Soliton in parameter space

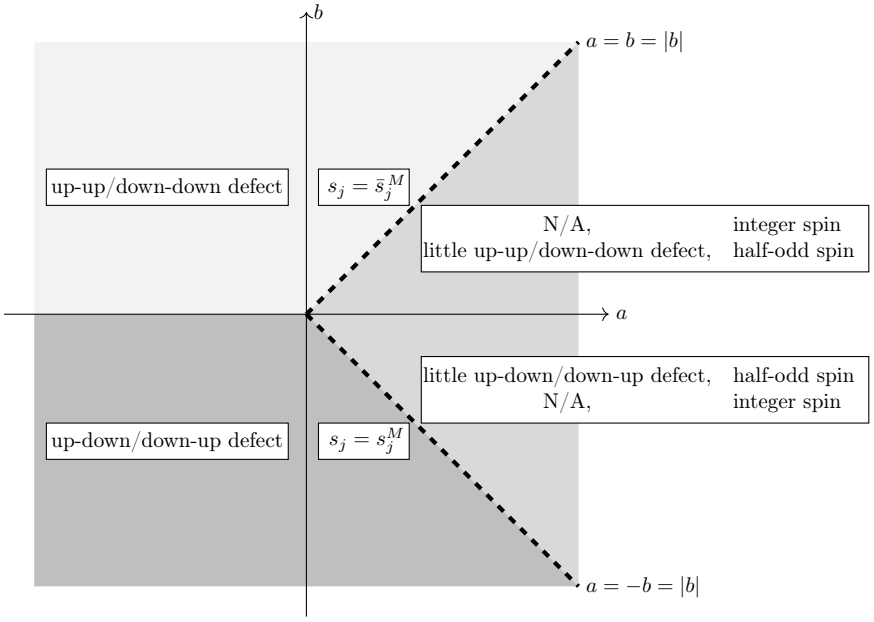

$$s_j = \begin{cases} s_j^M & = \frac{s}{\sin(M+1)\theta/2}\ \sin\left(\frac{M+1}{2} - j\right)\theta, \qquad b < 0 \text{ (ferromagnetic)}, \\ \bar{s}_j^M & = \frac{(-1)^j s}{\sin(M+1)\theta/2}\ \sin\left(\frac{M+1}{2} - j\right)\theta, \qquad b > 0 \text{ (antiferromagnetic)}, \end{cases} \tag{5.4}$$

where $\cos\theta = \frac{a}{|b|}$, and $M \geq 1$ is the unique integer such that $\cos\frac{\pi}{M+1} < \frac{a}{|b|} < \cos\frac{\pi}{M+2}$. The soliton corresponds to a rotation of the spin components (staggered if $b > 0$) by π radians over the sites labelled by $j = 1, \ldots, M$, interpolating smoothly from one ground state to the other. In some cases, however, the presence of the soliton is dictated by a global (topological) property. Such is the case when b is positive (antiferromagnetic) and N is odd, for then the would-be Néel order cannot be realized without frustration. A global property (the parity of N) enforces the existence of the defect, while local interactions give it its form, given again by Eq.(5.4). The topological nature of the phenomenon is even more obvious by noticing that the Néel order is restored if one is allowed to change the periodic condition on the global z axis to an antiperiodic condition, such that the z axis is sent to $-z$ after one world trip. (We will call it the *non-orientable* chain, effectively a Möbius strip. Although the z direction cannot be defined globally on the non-orientable chain, it is defined locally so that the quadratic, nearest neighbour interactions in H_0 still make sense, and are independent of the local gauge $\pm z$.)

When the z component of the spin is quantized, the expressions above are only approximations to the soliton, but are already in good qualitative agreement with numerically obtained solitons of moderate spin. In Fig.5.3 and Fig.5.4, the soliton is shown with different lengths for spin 20, and spin $41/2$, respectively. We observe that the length, the overall symmetry, and the degeneracy of the soliton are quite close to those of the unquantized version. (The quantized antiferromagnetic solitons for spin 1 to $7/2$ are provided in the Appendices. See Section 5.6.1.2.)

On any type of chain, the energy cost of producing a non-topological soliton between the two degenerate vacua is

$$\Delta\big(\tfrac{a}{|b|}\big) = |b|s^2\,\tfrac{\pi}{\sqrt{2}}\left(1-\tfrac{a}{|b|}\right)^{1/2}. \tag{5.5}$$

This expression is valid when $a/|b| \lesssim 1$, so that the soliton's length M is large. Solitons become massless as $a \to |b|$, with critical exponent $z\nu = 1/2$. (The critical theory is the free relativistic scalar, with dynamical exponent $z = 1$. See below.) And although the spin required to realize long lightweight solitons diverges, it does so only slowly as $s = O(1-a/|b|)^{-1/2}$. This is illustrated in Fig.5.5, showing a nearly massless soliton at the transition line $a = b$ for spin 20. Non-topological solitons, however, necessarily come in deconfined pairs of energy 2Δ, overturning the fully (anti)polarized segment between them. Near the transition lines $a = |b|$, instability against pairs of soliton excitations destroys the possibility of a long-range order in the ground state. Spin waves, on the other hand, are directly found to have mass $\Delta_{\rm SW} = a + 2|b|s\big(1-\tfrac{a}{|b|}\big)$. At the transition lines, a mass gap $\Delta_{\rm SW} = a = |b|$ remains and spin waves will be frozen at low temperatures. The correlation function in the region $a \lesssim |b|$ with thermal soliton pairs as low-lying excitations is found to be

$$\langle S_i S_j\rangle_\beta \sim \begin{cases} \frac{M}{2}s^2|i-j|^{-1} & \text{for } \beta\Delta \ll |i-j|/N, \\ s^2 e^{-|i-j|/N\xi} & \text{for } \beta\Delta > 2|i-j|/N. \end{cases} \tag{5.6}$$

Here β is the inverse temperature, and we have assumed $M \ll |i-j| \ll N$. At quantum criticality, $\beta\Delta \sim 0$, correlations have a power-law decay $\propto |i-j|^{-(d-2+\eta)}$ with critical exponent $\eta = 2$, but the smallness of $M/|i-j|$ indicates that lightweight solitons melt the fully (anti)polarized order. Away from quantum criticality, the correlation length $\xi = \frac{1}{2}(e^{\beta\Delta}-1)$ is finite, except at the other critical point, the zero-temperature limit $\beta\Delta \to \infty$. In the continuous limit effective at criticality, we may rescale the spin components as usual,

$$s^z_{x/\epsilon} = (\epsilon|b|)^{-1/2}(-\text{sgn } b)^{x/\epsilon}\psi(x), \tag{5.7}$$

where ϵ is the lattice constant and $\frac{x}{\epsilon} \in [-\frac{N}{2}, \frac{N}{2}]$, the length of the lattice being $L = N\epsilon$. The partition function of the classical model, $Z = \text{Tr}\exp(-\beta H_0) = \sum_{s^z_1,\ldots,s^z_N} \exp\left(-S[\{s^z_i\}]\right)$, naturally corresponds to a Euclidean action whose continuum version is

$$S[\psi] = \int_0^\beta d\tau \int dx\; \tfrac{1}{2}\psi(x)\left[k^2 - \partial_x^2\right]\psi(x) + \mathcal{O}(\epsilon^2), \tag{5.8}$$

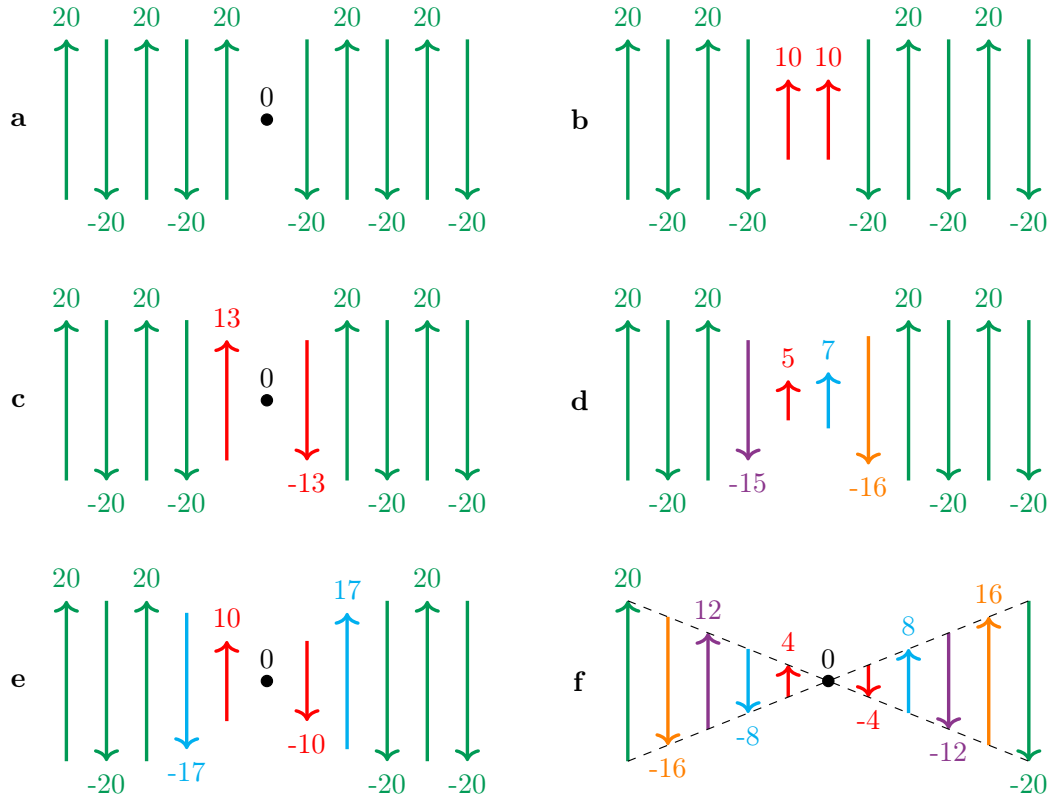

FIGURE 5.3 – (Color online) The soliton of spin 20 on a chain of length $N = 11$ for different chosen values of a/b. The values of s^z are given in units of $\hbar$. (Numerically evaluated with the Mathematica function NMinimize, with up to 350 iterations using the methods DifferentialEvolution and SimulatedAnnealing.) **a.** $a/b = 0.498$. **b.** $a/b = 0.503$. **c.** $a/b = 0.769$. **d.** $a/b = 0.833$. (Degeneracies are not shown.) **e.** $a/b = 0.870$. **f.** $a/b = 0.999$. The soliton's length is numerically observed to change from M to $M+1$ at $a/b \sim \cos \pi/(M+2)$, in agreement with the large spin calculation. Solitons of odd length have total spin 0. Solitons of even length have (close to) maximal total spin.

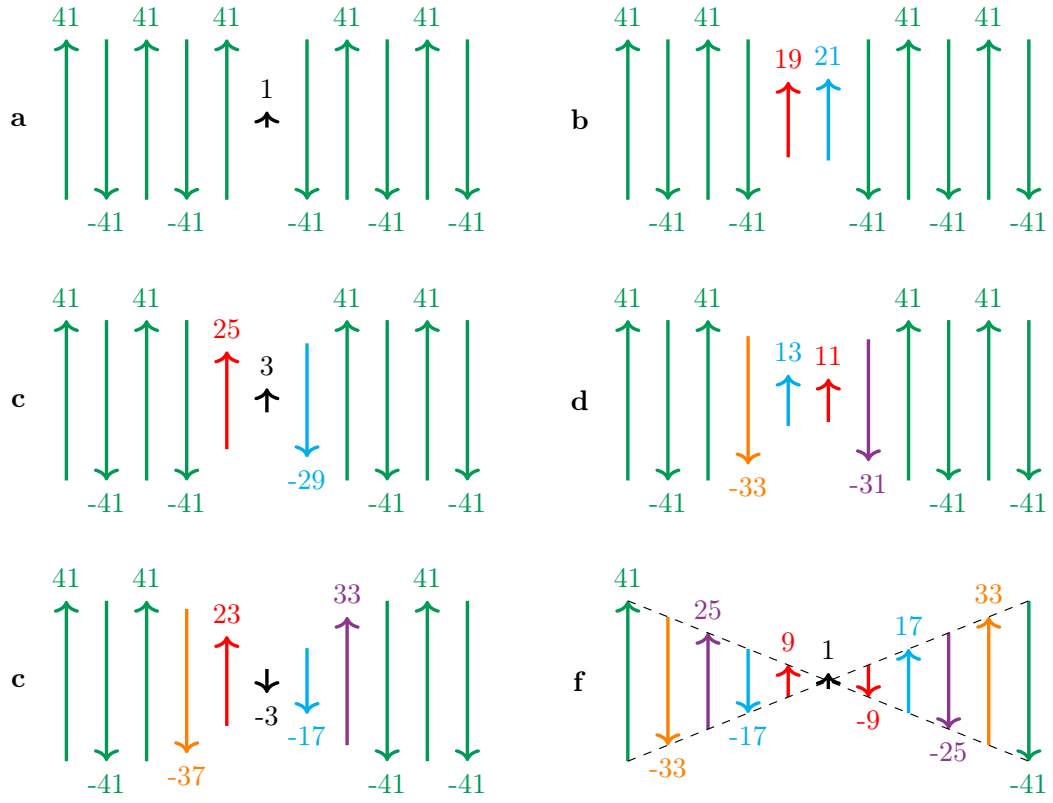

FIGURE 5.4 – (Color online) The soliton of spin 41/2 on a chain of length $N = 11$ for different chosen values of a/b. The values of s^z are given in units of $\hbar/2$. (Numerically evaluated with the Mathematica function NMinimize, with up to 350 iterations using the methods DifferentialEvolution and SimulatedAnnealing.) **a.** $a/b = 0.498$. **b.** $a/b = 0.503$. **c.** $a/b = 0.769$. **d.** $a/b = 0.833$. (Degeneracies are not shown.) **e.** $a/b = 0.870$. **f.** $a/b = 0.999$. The soliton's length is numerically observed to change from M to $M+1$ at $a/b \sim \cos \pi/(M+2)$, in agreement with the large spin calculation. Solitons of odd length have total spin 1/2. Solitons of even length have (close to) maximal total spin.

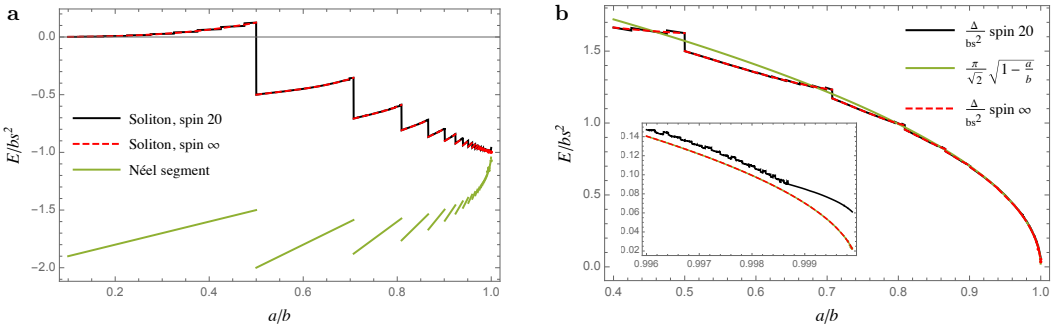

FIGURE 5.5 – (Color online) **a** Dimensionless energy of the large spin AF soliton (upper curve, dashed), and of the AF soliton of spin 20 (upper curve, solid), compared to the dimensionless energy of the Néel segment of the same length (lower curve), all given as functions of the dimensionless parameter a/b. Curves breaking correspond to transitions in the length of the soliton. Here, the spin-20 soliton is obtained approximately from the unquantized soliton by restricting the $\bar{s}_j^M$ to the closest integers. The cost of replacing a Néel segment by a soliton becomes vanishingly small in the limit $a/b \to 1$, even for moderate values of the spin. **b** Dimensionless energy difference $\Delta = E_{\text{soliton}} - E_{\text{Néel}}$ for the large spin soliton (dashed), and the spin-20 soliton (irregular, solid), compared to the asymptotic behaviour (smooth, solid) Eq. (5.59). **Inset** Zoom-in around $a \lesssim b$, showing the small but non-zero mass $\Delta = O(s^{-1})$ of the spin-20 soliton, due to its finite length.

where we have defined the squared mass $k^2 = \frac{2}{\epsilon^2}\left(\frac{a}{|b|} - 1\right)$ of a one-dimensional relativistic scalar field. If ψ is unbounded, the model is stable only for nonnegative k^2, i.e. $a \geq |b|$. But for negative k^2, it can be stabilized by forcing $|\psi(x)| \leq s < \infty$. In this case, a kink interpolating between the degenerate ground states $\psi(x) \equiv s$ for $x < 0$, and $\psi(x) \equiv -s$ for $x > \pi/|k|$, is

$$\psi(x) = s \cos |k|x \qquad \text{for} \qquad |k|x \in [0, \pi], \tag{5.9}$$

which satisfies the equation of motion with boundary conditions $\lim_{|x|\to\infty} \psi(x) = -\text{sgn}(x)s$. This is just the continuous version of the soliton of length $M = \pi/|k|\epsilon$. From Eq.(5.5), this excitation becomes massless as $O(|k|)$ in the limit $a \to |b|$. Spin waves, on the other hand, have mass $\Delta_{\text{SW}} = a + c|k|^2$, as usual. The qualitative change in the symmetries of the ground state occurring at $k^2 = 0$ or equivalently at $a = |b|$ (the potential going from concave to convex), gives clearly a second-order phase transition. All calculations for this overview can be found in the Appendices, where we also determine the magnetic form factor of the soliton, which in principle is observable through neutron scattering.

5.3 Solitons of the interacting theory

5.3.1 Semi-classical picture

Up to now we have assumed that exchange interaction was absent. If a small Heisenberg exchange term is added, the states $|s_1^z, \ldots, s_N^z\rangle$ are not eigenstates anymore, and the partition function is more tractable when traced over spin coherent states. The scalar field ψ (now a function of x *and* τ) becomes the z component of a vector field $\vec{l}(x,\tau) = (s\sin\theta\cos\phi, s\sin\theta\sin\phi, s\cos\theta)$, and the non-orthogonality of spin coherent states $\bigotimes_x |\vec{l}(x,\tau)\rangle$ results in the appearance of an observable, gauge invariant Berry phase on states labelled by periodic fields $\vec{l}(x,\tau+\hbar\beta) = \vec{l}(x,\tau)$. The semi-classical energy of $\vec{s}(x_j,\tau) = (-\text{ sgn } b)^j \vec{l}(x_j,\tau)$ is

$$\begin{aligned} E_{\text{cl}} &= a\sum_j (l_j^z)^2 - |b|\sum_j l_j^z l_{j+1}^z - \frac{|J|}{b}|b|\sum_j \vec{l}_j\cdot\vec{l}_{j+1} \\ &= as^2\sum_j \cos^2\theta_j - |b|s^2\sum_j \cos\theta_j\cos\theta_{j+1} \\ &\quad - \frac{|J|}{b}|b|s^2\sum_j \left(\sin\theta_j\sin\theta_{j+1}\cos(\phi_j-\phi_{j+1}) + \cos\theta_j\cos\theta_{j+1}\right). \end{aligned} \tag{5.10}$$

In the region $a < |b|$, the dominant BCHI energy is (locally) minimized by the (anti)ferromagnetic states $\vec{l}_\pm(x_j,\tau) \equiv \pm(0,0,s)$, with constant $\theta(x_j) \equiv 0$, and undefined $\phi(x_j)$. The classical exchange energy is the same on both states, spontaneously breaking $\mathbb{Z}_2$. On the lines $a = |b|$, the BCHI energy is (locally) minimized by the states with $l^z(x_j,\tau) \equiv m$, $-s \le m \le s$, hence constant $\theta(x_j) \equiv \theta_0$. The classical exchange energy for these states is

$$E_{\text{ex}} = -\frac{|J|}{b}|b|s^2\sum_j \left(\sin^2\theta_0\cos(\phi_j-\phi_{j+1}) + \cos^2\theta_0\right). \tag{5.11}$$

When $|J|b > 0$, E_{ex} is minimal for $\phi(x_j) \equiv \phi_0$, and arbitrary θ_0 and ϕ_0. The corresponding classical ground space consists of all the states of the form $\vec{l}_m(x) \equiv (\sqrt{s^2-m^2}\cos\phi_0, \sqrt{s^2-m^2}\sin\phi_0, m)$, $-s \le m \le s$. This space is closed under the action of $O(3)$. The spontaneous breaking of $O(3)$ to $U(1)$ by a choice of m generates a gapless Goldstone mode, which is the semi-classical soliton. Consequently, and following (5.9), semi-classical solitons are states $\bigotimes_x |\vec{L}_\kappa(x,\tau)\rangle$, labelled by

$$\begin{aligned} \vec{L}_\kappa(x,\tau) &= \pm(\sqrt{s^2-\psi^2(x)}\cos\phi_0, \sqrt{s^2-\psi^2(x)}\sin\phi_0, \psi(x)) \\ &= \pm(s\sin\kappa x\cos\phi_0(\tau), s\sin\kappa x\sin\phi_0(\tau), s\cos\kappa x), \end{aligned} \tag{5.12}$$

with vanishing mass as $\kappa \to 0$. A second, $U(1)$ Goldstone mode is expected to carry modulations of ϕ_0 along x. When $|J|b < 0$, E_{ex} is minimal for $\phi(x_j) = \phi_0 + (-1)^j\pi/2$, $\theta_0 = \pi/2$, and arbitrary ϕ_0. The classical ground space then consists of the states $\vec{l}_0(x_j) = (-1)^j(-s\sin\phi_0, s\cos\phi_0, 0)$, and only the $U(1)$ spin wave mode is gapless. We will assume from now on that $|J|b > 0$. When $a \lesssim |b|$, the soliton and $U(1)$ waves

are pseudo-Goldstone. The approximate $O(3)$ symmetry opens a gap in the values of κ, giving mass to the soliton, and the finite length of the soliton constitutes an upper bound on the length of the $U(1)$ waves.

5.3.2 Perturbative soliton tunneling

We now study the solitonic ground state of the frustrated chain perturbatively by allowing soliton translations to restore the translation invariance of the ground state. For this purpose, we will neglect quantum degeneracies not present in the semi-classical picture. For most values of a/b, these degeneracies will result from the breaking of a symmetry in the semi-classical expressions, and will be related by the corresponding operators. We thus overlook a number G_M of quantum degeneracies expected to depend on the soliton length M, but *not* on the length N of the chain. Specifically, we expect G_M to be upper bounded by the number of quantized configurations within a small distance δ from the semi-classical soliton in space $[-s, s]^M$, that is $G_M = O(\delta^M)$. One should keep in mind that for any given soliton length M, all degeneracies mentioned in the following sections must be multiplied by the corresponding factor G_M. While in the thermodynamic limit $N \to \infty$ the perturbative energy band arising from soliton translations will become gapless, the splitting resulting from the lifting of the G_M-fold degeneracy depends only on M (i.e. on a/b), and will remain finite.

In order to perform the perturbative level splitting of the semi-classical soliton ground space, we need to translate the now interacting solitons by tunnelling. Define the operators

$$(S_i^+ S_{i+1}^-)^\alpha = \begin{cases} (S_i^+ S_{i+1}^-)^{|\alpha|} & , \quad \text{if } \alpha \geq 0 \\ (S_i^- S_{i+1}^+)^{|\alpha|} & , \quad \text{if } \alpha < 0. \end{cases} \tag{5.13}$$

Then, for any s_i, s_{i+1}, we have

$$(S_i^+ S_{i+1}^-)^{s_{i+1}-s_i} |\ldots, s_i, s_{i+1}, \ldots\rangle \propto |\ldots, s_{i+1}, s_i, \ldots\rangle. \tag{5.14}$$

It is a known fact that adjacent transpositions generate the permutation groups. In fact, any permutation of N elements can be decomposed into at most $\lfloor N^2/4 \rfloor$ *cyclically* adjacent transpositions, i.e. including swapping the first and last elements [269]. With N sites of spin s, and provided that the exact spectrum of the full Hamiltonian $H_0 + |J| \sum_k \mathbf{S}_k \cdot \mathbf{S}_{k+1}$ is analytic at $|J| = 0$, the group of component permutations $|s_1, \ldots, s_N\rangle \xrightarrow{\sigma} |s_{\sigma(1)}, \ldots, s_{\sigma(N)}\rangle$ is reached at perturbative order $2s\lfloor N^2/4 \rfloor$ or less. General automorphisms $|s_1, \ldots, s_N\rangle \to |s'_1, \ldots, s'_N\rangle$ between states of equal total spin $\sum_k s_k = \sum_k s'_k$ must occur at perturbative order $\sim sN^2$ or less. All the transitions that we will study below occur much earlier, with perturbative orders of size $\sim sN$, or even $\sim s$.

We have relegated to Appendix(5.6.4) the technical details of the calculations establishing the properties of solitons of minimal size (*i.e.* of length one), solitons of intermediate size, and solitons of large size (meaning a size comparable to the total number of sites), and the corresponding ground state.

We summarize the results as follows. The ground state corresponds to the superposition of the soliton translated to all positions around spin chain, which yields

a translationally invariant ground state (except for half-odd values of s and a soliton of length one, for which translation invariance is broken in accordance with the Lieb-Schultz-Mattis theorem [202]). For the solitons of length one, the translation by one site is achieved by flipping two spins adjacent to the solitons, which occurs at order s in perturbation. For intermediate solitons of length $M > 1$, the translation by two sites is achieved at low order, while for a single-site translation, one has to flip the remaining Néel state to achieve the translation, a costly operation. For the large solitons, it is energetically more efficient to translate by a single site, along with the remaining Néel part of the chain.

5.4 Solitons, frustration, and entanglement

We now develop the arguments leading to our main results. We consider the region $0 < b/2 < a < b$ where the perturbative ground state of the AF chain of odd length N is of the form

$$|\psi_0\rangle = \frac{1}{\sqrt{N}} \sum_{\mu=1}^{N} \omega^\mu |\mu\rangle, \tag{5.15}$$

where $\omega^4 = 1$, and $|\mu\rangle$ is a normal vector parameterized by a classical configuration with soliton at position μ and Néel background. In the above expression, we have neglected a small number of classical $\mathbb{Z}_2$-degeneracies, as well as a number G_M of quantum degeneracies, expected as before to depend of the soliton length M, but *not* on the length N of the chain. Specifically, we expect G_M to be upper bounded by the number of quantized configurations within a small distance δ from the classical soliton in space $[-s, s]^M$, that is $G_M = O(\delta^M)$. As long as transition amplitudes between degenerate states are sufficiently small, the effect of the degeneracies on the entanglement entropy will be a subleading additional term $\log G_M = O(M \log \delta)$, plus a small integer multiple of $\log 2$. In the next section (section 5.4.1) we describe the measure of frustration that we will use. In the sections that follow (sections 5.4.2 to 5.4.6), we consider a single-interval subsystem of any size, and find the corresponding Schmidt decomposition, entanglement spectrum, entanglement entropy, and capacity of entanglement, and compare with results from the literature.

5.4.1 Frustration

In [114, 198], a measure of frustration is proposed for a many-body system $H = \sum_S h_S$ with ground state $|\mathrm{GS}\rangle$, and local interactions h_S on subsystem S. Let $\rho = |\mathrm{GS}\rangle\langle\mathrm{GS}|$, and let $\Pi_S \otimes 1_R$ be the projector onto the ground space of h_S, and the identity on the rest of the system R. Then $f_S = 1 - \mathrm{Tr}(\rho \Pi_S \otimes 1_R)$ quantifies how much ρ fails to overlap with the local subspace selected by $\Pi_S \otimes 1_R$, and constitutes an unambiguous measure of the frustration of h_S [114]. For our Hamiltonian (5.1), the subsystems are neighbour pairs $i, i+1$, and the local interaction terms $h_{i,i+1}$ have ground state $|GS\rangle_i = (|\uparrow\downarrow\rangle \pm |\downarrow\uparrow\rangle)/\sqrt{2}$, up to perturbative corrections [216]. Here, the arrows $\uparrow$ / $\downarrow$ denote maximal/minimal z-components of spin, $S^z = \pm s$,

and the sign in $|GS\rangle_i$ depends on the parity of $2s$. From (5.15) we find for all sites i

$$f_{i,i+1} = 1 - \mathrm{Tr}(|\psi_0\rangle\langle\psi_0|\Pi_{i,i+1} \otimes 1_R) = \frac{M+1}{N}, \tag{5.16}$$

where the number M of non-maximal spins in the soliton satisfies $2 \leq M \leq N-2$. We see that frustration is weak for small solitons, and strong for large solitons, tending to the maximal value 1 when $M/N \to 1$. In the thermodynamic limit, by varying the ratio a/b in the Hamiltonian, frustration covers its entire range of values $(0, 1)$.

5.4.2 Schmidt decomposition

Let A and B be two intervals such that $\{A, B\}$ is a bipartition of the chain. Define I which we call the seam set, such that $\mu \in I$ iff the soliton $|\mu\rangle$ has (non Néel) components in *both* A and B. Let A° stand for the interior of A : $\mu \in A^\circ$ iff the soliton part of $|\mu\rangle$ lies entirely within A. Define B° similarly. Partitioning the sum in Eqn.(5.15) as $\sum_I + \sum_{A^\circ} + \sum_{B^\circ}$, we obtain the Schmidt decomposition of $|\psi_0\rangle$ with respect to partition $\{A, B\}$,

$$|\psi_0\rangle = \frac{1}{\sqrt{N}} \left(\Big(\sum_{\mu \in I} \omega^\mu |\mu\rangle_A |\mu\rangle_B \Big) + \sqrt{|A^\circ|}|A^\circ\rangle|\text{Néel}\rangle_B + \sqrt{|B^\circ|}|\text{Néel}\rangle_A|B^\circ\rangle \right). \tag{5.17}$$

Let us explain the notation. The state $|\mu\rangle$ in (5.15) is a tensor product of the states for each spin in the chain. Here $|\cdot\rangle_{A,B}$ naturally stands for the restriction to A's or B's subspace, so that $|\mu\rangle_A$ and $|\text{Néel}\rangle_A$ are vectors that are the tensor product of the spins in the subset A (and similar for B). Then, $|A^\circ\rangle$ is obtained from $\sum_{\mu=1}^N \omega^\mu |\mu\rangle_A$ by restricting the sum to $\mu \in A^\circ$, and normalizing : $|A^\circ\rangle = |A^\circ|^{-1/2} \sum_{\mu \in A^\circ} \omega^\mu |\mu\rangle_A$. (Here and in what follows, the cardinality of a set X is written $|X|$.) The vector $|B^\circ\rangle$ is obtained similarly. Eqn.(5.17) is formally invariant under the exchange $A \leftrightarrow B$. States corresponding to different classical configurations have vanishingly small overlap, $\langle\eta|\eta'\rangle \sim |J|^\gamma$, where as before $|J| \ll 1$ is the coupling constant, and γ is the perturbative order at which soliton translations are reached. Thus, the vectors in (5.17) effectively constitute an orthonormal Schmidt basis.

The Schmidt rank is defined as the number of terms appearing in Eqn.(5.17). Without loss of generality we assume that A is smaller than B. Let R be the size of A (so $R < N/2$), and M be the length of the soliton. We must distinguish the cases $M \leq R$ and $M > R$, and the subcases of the latter $M + R \leq N$ and $M + R > N$.

Case $M \leq R$. The seam set I in (5.17) has $2M - 2$ elements, so the Schmidt rank is $2M$. In particular when $M = 1$ (Néel defect or minimal soliton), the Schmidt decomposition is seamless ($I = \varnothing$) and the rank is 2. The other extreme subcase is when $M = R$ and R is maximal, $R = (N-1)/2$: then I has $N - 3$ elements, and the Schmidt rank is $N - 1$.

Case $M > R$. The set A° is empty so $|A^\circ\rangle = 0$. The set I has $M + R - 1$ element,

with a maximum of N :

$$|I| = \begin{cases} M+R-1 & , \quad M+R \leq N \\ N & , \quad M+R > N. \end{cases} \tag{5.18}$$

When I has size N, the state $|\text{Néel}\rangle_A$ is void as well. The Schmidt rank is $M+R$ (for $M+R \leq N$) with a maximum of N (for $M+R \geq N$).

5.4.3 Reduced density

The reduced density matrix $\rho_A = \text{Tr}_B |\psi_0\rangle\langle\psi_0|$ is

$$\rho_A = \frac{1}{N} \left(\sum_{\mu \in I} |\mu\rangle_{AA}\langle\mu| + |A^\circ|\, |A^\circ\rangle\langle A^\circ| + |B^\circ|\, |\text{Néel}\rangle_{AA}\langle\text{Néel}| \right), \tag{5.19}$$

with

$$\begin{cases} |A^\circ| = R-M+1 & , \quad |B^\circ| = N-M-R+1 & \text{when } M \leq R; \\ |A^\circ| = 0 & , \quad |B^\circ| = N-M-R+1 & \text{when } M > R \text{ and } M+R \leq N; \\ |A^\circ| = 0 & , \quad |B^\circ| = 0 & \text{when } M > R \text{ and } M+R > N. \end{cases} \tag{5.20}$$

Let us verify proper normalization. In all cases, $\text{Tr}_A\, \rho_A = |I| + |A^\circ| + |B^\circ|$.

Case $M \leq R$. Then $\text{Tr}_A\, \rho_A = \frac{1}{N}\left((2M-2) + (R-M+1) + (N-M-R+1)\right) = 1$.

Case $M > R$. If $M+R \leq N$, we have $|A^\circ| = 0$ and the trace reduces to $\text{Tr}_A\, \rho_A = \frac{1}{N}\left((M+R-1) + (N-M-R+1)\right) = 1$. If $M+R > N$, we have $|A^\circ| = 0, |B^\circ| = 0$, and $\text{Tr}_A\, \rho_A = \frac{1}{N}(N) = 1$.

5.4.4 Entanglement spectrum

The reduced density (5.19) may be recast as the partition function at unit temperature ($\beta = 1$) of an entanglement spectrum Hamiltonian (or modular Hamiltonian) H_A,

$$\rho_A = \sum_n e^{-\xi_n} |n\rangle_{AA}\langle n| = e^{-H_A} \quad , \tag{5.21}$$

whose eigensystem is

$$\begin{aligned} H_A\, |\mu\rangle_A &= \ln N\, |\mu\rangle_A && (\mu \in I) \\ H_A\, |A^\circ\rangle &= \ln \tfrac{N}{R-M+1}\, |A^\circ\rangle && (M \leq R, \text{ void otherwise}) \\ H_A\, |\text{Néel}\rangle_A &= \ln \tfrac{N}{N-M-R+1}\, |\text{Néel}\rangle_A && (M+R \leq N, \text{ void otherwise}) \end{aligned} \tag{5.22}$$

The ground state of H_A is $|\text{Néel}\rangle_A$, and is gapped from the low-lying state $|A^\circ\rangle$. The higher excited states $|\mu\rangle_A$ form a level with degeneracy $g_{M,R} = |I| = O(M)$,

$$g_{M,R} = \begin{cases} 2M-2 & , \quad M \leq R \\ M+R-1 & , \quad M > R,\ M+R \leq N \\ N & , \quad M > R,\ M+R > N. \end{cases} \tag{5.23}$$

We will label entanglement energies as follows

$$\xi_0 = \ln \tfrac{N}{N-M-R+1} \quad \leq \quad \xi_1 = \ln \tfrac{N}{R-M+1} \quad \leq \quad \xi_2 = \ln N. \tag{5.24}$$

A 'phase transition of entanglement' of geometrical origin occurs as $R \nearrow N/2$, which closes the gap between ξ_0 and ξ_1 as the roles of A and B get exchanged. The energy gap $|\xi_1 - \xi_0|$ is a measure of the size difference between A and B. Another more physical transition occurs as $M \nearrow R$, at which point the lower excited level ξ_1 merges with the upper level ξ_2. When $R < M$, all solitons belong to the set I, whose size grows with R, resulting in entanglement being highly sensitive to R. (See the extensive stage of the small-soliton phase, eq. (5.29).) When $R > M$, the size of I plateaus, and so does entanglement entropy. (See the plateaued stage of the small-soliton phase, eq. (5.29).) A third transition is observed as $M + R \nearrow N$, and ξ_0 merges with ξ_2. Beyond this point, a pure Néel state within A ceases to be a possibility, resulting in all N states within I, and saturated entanglement with B. (See the saturated stage of the large soliton phase, eq. (5.30).)

5.4.5 Entanglement entropy

The entanglement entropy (EE), or modular thermal average energy (at unit temperature), of subsystem A is defined as

$$S_A = -\mathrm{Tr}_A\, \rho_A \ln \rho_A = \sum_n \xi_n e^{-\xi_n} = \langle H_A \rangle_{\beta=1}. \tag{5.25}$$

Considering multiplicities we have

$$S_A = \begin{cases} \xi_0 e^{-\xi_0} + \xi_1 e^{-\xi_1} + g_{M,R}\, \xi_2 e^{-\xi_2} & , \quad M \leq R \\ \xi_0 e^{-\xi_0} + g_{M,R}\, \xi_2 e^{-\xi_2} & , \quad M > R,\ M + R \leq N \\ g_{M,R}\, \xi_2 e^{-\xi_2} & , \quad M > R,\ M + R > N. \end{cases} \tag{5.26}$$

From (5.23) and (5.24) we get

$$S_A = \begin{cases} \frac{N-M-R+1}{N} \ln \frac{N}{N-M-R+1} + \frac{R-M+1}{N} \ln \frac{N}{R-M+1} + \frac{2M-2}{N} \ln N & , \quad \text{region I} \\ \frac{N-M-R+1}{N} \ln \frac{N}{N-M-R+1} + \frac{M+R-1}{N} \ln N & , \quad \text{region II} \\ \ln N & , \quad \text{region III,} \end{cases} \tag{5.27}$$

with regions I, II, and III as represented in Fig. 5.6. The EE has bound $O(\ln N)$, which is much less than the entanglement entropy $O(N \ln(2s+1))$ found in a generic state of N coupled s-spins. This is because the perturbative low-lying subspace has dimension N. The entropy is represented in Figs. 5.7 and 5.8 for multiple subsystem sizes and soliton sizes. If the thermodynamic limit $N \to \infty$ is reached while M is fixed, we get the *binary entropy* function $S_A = -\frac{R}{N} \ln \frac{R}{N} - \left(1 - \frac{R}{N}\right) \ln \left(1 - \frac{R}{N}\right)$ corresponding to a randomly positioned soliton being in A with probability $\frac{R}{N}$, and outside of A with probability $\left(1 - \frac{R}{N}\right)$. This weak frustration scenario, $M = O(1)$, is in good qualitative agreement with the results obtained for the (weakly) frustrated

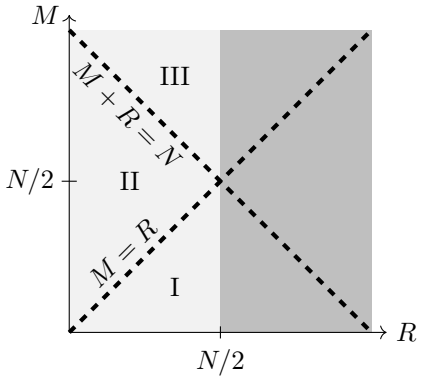

FIGURE 5.6 – The (R, M)-space for subsystem length R and soliton length M. In the light gray region ($R \leq N/2$) the EE is given by (5.27). In the dark gray region ($R > N/2$) the EE is obtained by the symmetry $S_{A^c}(R) = S_A(N - R)$, where A^c is the complement of A. The entanglement entropy has qualitatively distinct behaviours on regions I, II, and III.

chains of Ref.[115], namely : (i) a bulk violation of the area law [149, 274, 53, 134] $S_A = a(N)R^{b(N)}$, where $b(N) \approx 0.22(2)$ (sub-extensive) for N chosen between 201 and 901, and (ii) the saturation of the EE in the limit of large N. The universal EE curve that the authors of [115] identify in the scaling thermodynamic limit of their models is the binary entropy function mentioned above, in agreement with the single-particle interpretation described by these authors as well as in this paragraph. (See also [70, 69] for a more general quasiparticle interpretation of EE.) When both M and R are fixed as $N \to \infty$, the dependence on boundary conditions disappears and $S_A \to 0$, in agreement with the non-frustrated chain (open or closed) and its Néel ground state, a product state without entanglement.

We now turn to strong frustration, i.e. $M = O(N)$. If M, R, and N all grow at the same rate as the thermodynamic limit is reached, we drop the bounded terms in Eqn.(5.27), and find

$$S_A \sim \begin{cases} \frac{2M}{N} \ln N & , \quad \text{region I} \\ \frac{R+M}{N} \ln N & , \quad \text{region II} \\ \ln N & , \quad \text{region III.} \end{cases} \tag{5.28}$$

This entanglement behaviour is strikingly different from the one found in the weakly frustrated case. On the one hand, the EE is extensive in subsystem size when R is smaller than the soliton length M (region II), then plateaus as R becomes larger than M (region I). On the other hand, the EE is nonfinite as $N \to \infty$, diverging like $\ln N$ in all regions. This behavior appears irreconcilable with a quasiparticle interpretation as given in [70, 69]. Interestingly, even though the soliton ground state $|\psi_0\rangle$ has arguably large entanglement when $M \gg 1$ (being extensive in subsystem size), it is also arguably slightly entangled in the sense of algorithm theory. Because the EE diverges no more than $O(\ln N)$, if the solution of a quantum N-qubit problem is encoded in $|\psi_0\rangle$, a theorem by Vidal shows that this problem is likely to be efficiently

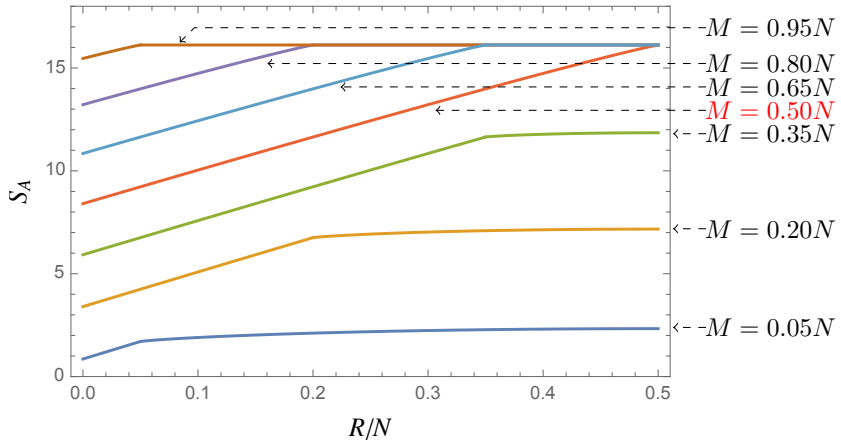

FIGURE 5.7 – (Color online) Entanglement entropy S_A of a connected interval A of size R for the perturbative ground state of the frustrated anisotropic XXZ chain with strong BCHI, and weak Heisenberg. The system size is $N \sim 10^7$, the soliton length ranges from $M = 0.05N$ to $M = 0.95N$. Observe the different properties corresponding to $M < 0.5N$ (small-soliton phase) and $M > 0.5N$ (large-soliton phase).

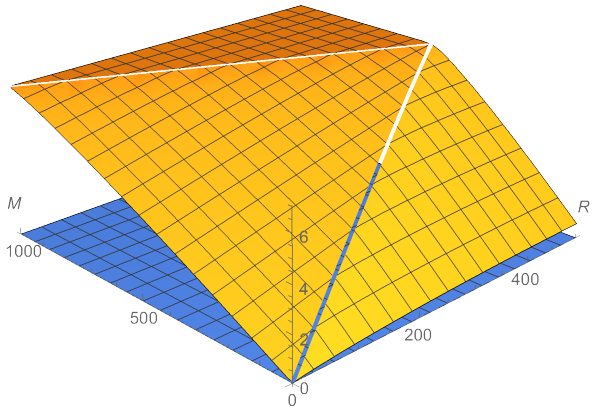

FIGURE 5.8 – Entanglement entropy S_A in the solitonic ground state, for subsystem lengths $R \in [1, N/2]$ and soliton lengths $M \in [2, N-2]$. Here we have used system size $N = 1001$. The behaviour is qualitatively different in regions I (right), II (front), and III (top). The EE is extensive in region II.

simulatable classically [273].

We note that the strongly frustrated chain cannot admit a long-distance effective field theory which is scale invariant because the soliton length is a macroscopic physical scale of the system. This is also seen, for weak and strong frustrations, at the level of EE scaling with respect to subsystem length, where we observe algebraic scaling in the frustrated chain, as opposed to logarithmic scaling in CFT_2's [149, 274, 53] and $(1+1)D$ Lifshitz theories [23, 72]. Anticipating the results of the next section, let us mention that the capacity of entanglement can also diagnose the impossibility of a conformal scale-invariant effective limit. An aspect of the right effective theory might be found in Fig. 5.7, where we observed a duality between solitons lengths M and $N-M$ in the plateauing of EE. We have identified two perturbative quantum phases, depending on the couplings through the soliton length M. The *small-soliton* phase corresponds to $M < N/2$:

$$S_A(r) \sim \begin{cases} \frac{R+M}{N} \ln N & , \quad R < M \quad \text{(extensive)} \\ \frac{2M}{N} \ln N & , \quad R > M \quad \text{(plateaued)}. \end{cases} \tag{5.29}$$

In perturbation theory, this phase corresponds to soliton translations over two lattice constants. (See Section 5.6.4.2.) The *large-soliton* phase corresponds to $M > N/2$:

$$S_A(r) \sim \begin{cases} \frac{R+M}{L} \ln N & , \quad R < N-M \quad \text{(extensive)} \\ \ln N & , \quad R > N-M \quad \text{(plateaued)}. \end{cases} \tag{5.30}$$

In perturbation theory, this phase corresponds to soliton (and Néel background) translations over a single lattice constant. (See Section 5.6.4.3.) These equations can be brought into a unique form by considering the *relative* entanglement entropy $S'_A(R) = S_A(R) - S_A(0)$, where $S_A(0) = \frac{M}{N} \ln N$ is the EE of a interval of length $O(1)$ in the limit $N, M \to \infty$. (Corresponding to a divergent single-point entropy in the continuous limit.) We find

$$S'_A(R) \sim \begin{cases} \frac{R}{N} \ln N & , \quad R < \lambda \quad \text{(extensive)}, \\ \frac{\lambda}{N} \ln N & , \quad R > \lambda \quad \text{(plateaued)}, \end{cases} \tag{5.31}$$

where the length scale λ is the soliton length M in the small-soliton phase ($M < N/2$), and the soliton colength $N-M$ in the large-soliton phase ($M > N/2$). Intriguingly, some strongly coupled nonlocal field theories [248, 206], as well as some local lattice models with broken translation invariance [276], present a particular volume-law scaling of the EE that has recently attracted interest. These theories possess a nonlocal scale λ, and the leading divergence in entanglement entropy has the form

$$S_A \sim \begin{cases} |A|\Lambda^D & \text{(subsystem scale much smaller than } \lambda) \\ \lambda|\partial A|\Lambda^D & \text{(subsystem scale much larger than } \lambda), \end{cases} \tag{5.32}$$

where $|A|$ is the volume of A, $|\partial A|$ is area the boundary, and Λ is the momentum scale at the cutoff [227]. The coefficients are reminiscent of what we found in Eqn.(5.31),

but with a crucial difference in the respective divergences. The volume law has a pure UV divergence $O(\Lambda^D)$, whereas the continuous version of (5.31) has a logarithmic UV/IR mixing divergence $O(\ln \Lambda L)$, where $\Lambda L = N$. Could it still be an indication that perhaps the effective field theory over the soliton ground state is nonlocal? Whether or not this similarity is fortuitous is beyond the scope of the present work.

5.4.6 Capacity of entanglement

The capacity of entanglement (CE) is another quantity associated to a reduced density matrix, defined in the same way as one defines heat capacity for thermal systems [291, 85]. From the modular Hamiltonian H_A defined in Eqn.(5.21), with eigenvalues ξ_n, we define the capacity of entanglement of subsystem A as the variance of H_A,

$$CE_A = \left(\sum_n \xi_n^2 \, e^{-\xi_n} \right) - S_A^2 = \langle H_A^2 \rangle - \langle H_A \rangle^2 = \mathrm{var}(H_A). \tag{5.33}$$

The CE is therefore a measure of the width of the eigenvalue distribution for the modular Hamiltonian, and for the reduced density matrix. Because we have explicitly calculated the modular Hamiltonian of the soliton ground state, Eqn.(5.22), we may compute de CE of any single-interval A. We find

$$CE_A \sim \begin{cases} \frac{N-M-R+1}{N}(\ln \frac{N}{N-M-R+1})^2 + \frac{R-M+1}{N}(\ln \frac{N}{R-M+1})^2 + \frac{2M-2}{N}(\ln N)^2 - S_A^2, \\ \frac{N-M-R+1}{N}(\ln \frac{N}{N-M-R+1})^2 + \frac{R+M-1}{N}(\ln N)^2 - S_A^2, \\ 0, \end{cases} \tag{5.34}$$

in regions I, II, and III, respectively, as defined in Fig. 5.6. Note that CE_A is identically zero in region III because all eigenvalues of the reduced density matrix are equal to $1/N$. In this region, the soliton ground state has the EE and CE of the generalized GHZ state $N^{-1/2} \sum_{i=1}^{N} |i\rangle^{\otimes N}$. We provide a plot of the CE in Fig. 5.9. In CFTs, the capacity of entanglement is found to scale like the entanglement entropy [85]. Moreover, there is convincing evidence that such a scaling $CE_A \sim S_A$ can detect criticality in many models [291, 85]. For the soliton ground state, we observe in Fig. 5.10 that $CE_A \not\sim S_A$ everywhere, except for $M = O(1)$, for which case we have already found a super-logarithmic violation of the area law, not consistent with a low-energy CFT limit. The capacity of entanglement confirms that the frustrated system has no conformal effective theory.

5.5 Conclusion

In this paper, we have studied a large-spin Haldane-like anisotropic XXZ model in the limit of large anisotropy which we call the (classical) Blume-Capel-Haldane-Ising limit. We find that solitons interpolating between different Néel or ferromagnetic segments are the low energy excitations in this limit. We observe a rich spectrum of ground states in the limiting model, especially when solitons are present due to

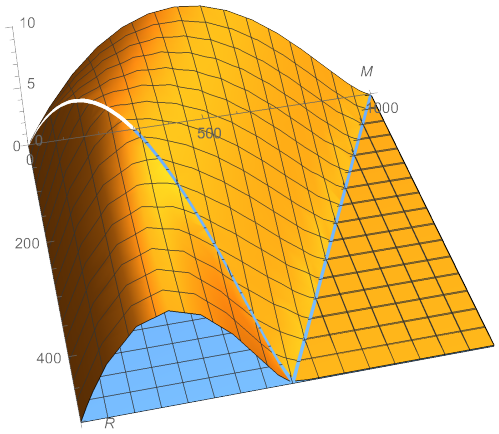

FIGURE 5.9 – The capacity of entanglement CE_A in the solitonic ground state, for subsystem lengths $R \in [1, N/2]$ and soliton lengths $M \in [2, N-2]$. The system size is $N = 1001$. The behaviour is qualitatively different in regions I (left), II (top), and III (right). The CE vanishes in region III.

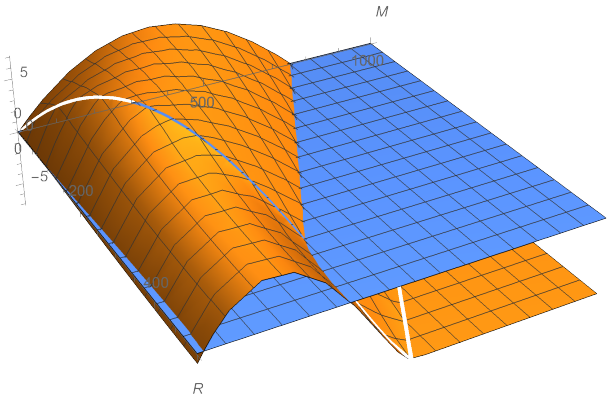

FIGURE 5.10 – The difference $CE_A - S_A$ in the solitonic ground state, for subsystem lengths $R \in [1, N/2]$ and soliton lengths $M \in [2, N-2]$. The system size is $N = 1001$. We see that $CE_A \sim S_A$ (i.e. $CE_A - S_A \sim 0$ for all A and fixed M) only when $M \sim O(1)$, confirming that the frustrated system has no conformal low-energy limit.

frustration, and we compute the perturbative corrections due to the Heisenberg interaction. In this way, we find the perturbative solitonic ground state of the chain with frustration, along with a continuous band of excited states. We determine the entanglement spectrum, entanglement entropy (EE), and capacity of entanglement (CE) in the solitonic ground state. We find an algebraic violation of the area law for the EE consistent with recent results on weakly frustrated chains [115]. Moving beyond the weak frustration regime, we are able to reveal that the EE has extensive scaling in subsystem size when frustration is strong. In that regime, we also observe that the EE scales logarithmically with the length N of the chain. In a future work, we intend to numerically study the entanglement in randomly generated 3D configurations of spin-s XXZ chains hosting a soliton, using the results obtained in the present work. It will be interesting to determine how the EE of this 3D system scales with subsystem size, soliton length M, average length $\langle N \rangle$ of the chains, and chain density. It would also be stimulating to identify frustrated 3D systems hosting the BCHI soliton. These results could shed light on the physics of geometrically frustrated 3D systems, where frustrated AF chains are bound to be found.

Frustration is likely to be very common in nature. Remarkably, non-extensively frustrated antiferromagnetic 1D chains are universally present in systems with geometric frustration, even in higher dimensions, and whether frustration is extensive or not [115]. Systems with extensive frustration, including the ANNNI model [99, 103], spin ices [46], and spin glasses [42], possess properties strikingly different from those of unfrustrated systems, and the physics of frustrated 1D chains is a promising avenue to better understand this fascinating subject.

5.6 Appendices

5.6.1 BCHI model with arbitrary spin s

The one dimensional BCHI model with $N \geq 2$ sites with the Hamiltonian, Eqn.(5.2) can be written as

$$H = \frac{1}{2}\mathbf{S}^T A \mathbf{S} \tag{5.35}$$

where $\mathbf{S}^T = (S_1^z, S_2^z, \cdots, S_N^z)$ and A is the circulant matrix with first row given by $(2a, b, 0, \ldots, 0, b)$. Because the Hamiltonian is quadratic and local, it can be defined on one-dimensional lattices of period 1 and 2. Specifically, the labels of the eigenstates $|s_1, \ldots, s_N\rangle$ should define a section $\sigma(i) = s_i$ on the orientable closed strip, the trivial fiber bundle $[-s, s] \times S^1$, on which the z axis is sent to itself after one world trip. Alternatively, they could define a section on the Möbius strip, the (unique) non-orientable bundle that looks locally like the product $[-s, s] \times S^1$, on which the z axis is sent to $-z$ after one world trip. Although the z direction cannot be defined globally on the Möbius strip, it is defined locally so that nearest neighbour interactions $S_i^z S_{i+1}^z$ make sense and are independent of the local gauge $\pm z$. We will eventually find the phase diagram for all periodic chains. Since, in the thermodynamic limit, Landau's theorem precludes the existence of a phase transition in this system at any positive temperature, we study the phase diagram at $T = 0$.

5.6.1.1 The ground state on the orientable lattice with N even.

On the orientable periodic lattice with an even number of sites, the staggered spin operators $\bar{S}_j \equiv (-1)^j S_j$ are globally well-defined, and we find the usual mapping between the ferromagnetic ($b < 0$) and the antiferromagnetic ($b > 0$) cases

$$H^{b>0}(\bar{S}_1, \ldots, \bar{S}_N) = H^{b<0}(S_1, \ldots, S_N) \tag{5.36}$$

and vice versa. For definiteness we will find the ferromagnetic ground state, and then obtain the antiferromagnetic one by the above duality. Note that staggered operators are locally defined when N is odd, if not globally, and the equivalence Eqn.(5.36) remains locally valid.

The ferromagnetic case is easily dealt with. We write the state $|s_1, \ldots, s_N\rangle$ as $|r(\alpha_1, \ldots, \alpha_N)\rangle$ where $r = \sqrt{\sum_k s_k^2}$ and $\sum_k \alpha_k^2 = 1$. Then the energy is given as

$$E(s_1, \ldots, s_N) = \big(a + b \textstyle\sum_k \alpha_k \alpha_{k+1}\big) r^2 = C(\hat{\boldsymbol{\alpha}}) r^2 \tag{5.37}$$

where explicitly,

$$C(\hat{\boldsymbol{\alpha}}) = \big(a + b \textstyle\sum_k \alpha_k \alpha_{k+1}\big). \tag{5.38}$$

As $\sum_k (\alpha_k \pm \alpha_{k+1})^2 \geq 0$, we have

$$-1 \leq \sum_k \alpha_k \alpha_{k+1} \leq 1. \tag{5.39}$$

Thus for $|b| < a$, using Eqn.(5.39) in Eqn.(5.38), we have $C(\hat{\boldsymbol{\alpha}}) > 0$ and hence the minimum energy configuration is realized exactly for $r = 0$ corresponding to the state $|0, \ldots, 0\rangle$ with corresponding energy $E_0 = 0$. For half odd integer spin, the state $|0, \ldots, 0\rangle$ is not permitted. Then in this case, one of the states closest to the origin, $|\pm 1/2, \ldots, \pm 1/2\rangle$ (with uncorrelated $\pm$ signs) will be the minimal energy configuration. Since the first term in the energy does not care whether the spin is $\pm 1/2$ and since $b < 0$, the energy is minimized at the "little" ferromagnetic states

$$|1/2, \ldots, 1/2\rangle \quad \text{or} \quad |-1/2, \ldots, -1/2\rangle \tag{5.40}$$

with energy $E_0 = (1/4)N^2(a - |b|)$.

For all other cases, $|b| > a$ (including a negative), the factor $C(\hat{\boldsymbol{\alpha}})$ becomes negative for certain directions, and in particular for $\hat{\boldsymbol{\alpha}}^T = \pm \frac{1}{\sqrt{N}}(1, \ldots, 1)$ the upper bound Eqn.(5.39), for the sum $\sum_k \alpha_k \alpha_{k+1}$ is saturated. These are the only two states for which the bound is saturated, and here $C(\hat{\boldsymbol{\alpha}}) = a + b = a - |b|$. $C(\hat{\boldsymbol{\alpha}})$ is negative and minimal for this direction. The extreme corners $\pm(s, \ldots, s)$ of the hypercube $[-s, s]^N$ are attained along this direction. Hence r is maximal, and correspondingly, the energy is minimal at the two corners. Thus the two corresponding ferromagnetic states, which we will write as $|\uparrow, \ldots, \uparrow\rangle$ and $|\downarrow, \ldots, \downarrow\rangle$, are the ground states in the regime $|b| > a$ (and we will use the notation $\uparrow$ and $\downarrow$ when the corresponding spin is maximally up, s, or maximally down, $-s$, respectively).

When expressed as a function of the non-thermal parameter $a/|b|$ the ground state energy is non-analytic at $a = |b|$, so this is a quantum phase transition [236].

For $a = |b|$ the states $|\pm(m, \ldots, m)\rangle$ are degenerate for any $m \in \{-s, -s+1, \ldots, s\}$ thus the ground state is $2s+1$ fold degenerate with $E_0 = 0$, and the system passes through a highly degenerate critical point. In the large s limit this is veritably a massless continuum.

With the duality, Eqn.(5.36) we obtain the antiferromagnetic ground state, and plot the result in Fig.(5.1). The ground state is everywhere doubly degenerate, except on the critical lines $a = |b|$, as well as for the particular case $a > |b|$ and integer spin s, for which the ground state $|0, \ldots, 0\rangle$ trivially possesses the $\mathbb{Z}_2$ symmetry of the Hamiltonian. We now find, for all values of a and b, the soliton interpolating between the two degenerate vacua, if applicable.

5.6.1.2 The BCHI soliton

The profile of the soliton will be seen to depend only on the ratio $a/|b|$, and not on the size N of the lattice nor on the boundary conditions. The calculation and results are local, and will apply equally well to any periodic lattice, whether or not the degenerate ground states identified in Fig.(5.1) can be realized globally. For definiteness, let us begin with the antiferromagnetic case ($b > 0$).

Antiferromagnetic soliton When $0 < b < a$, a straightforward induction shows that the soliton (for half-odd spin s) is the "little" defect comprising two adjacent $+1/2$ or two adjacent $-1/2$ spin components.

For $0 < a < b$, the soliton is found by minimizing the energy functional subject to the boundary conditions, $s_0 = s$ and $s_{n+1} = (-1)^n s$, connecting the two Néel ground states. For now n is at least as large as the size of the soliton, but otherwise arbitrary. With these boundary conditions, the energy of the generic state $|s_0, \ldots, s_{n+1}\rangle$ is

$$E = \frac{1}{2}\mathbf{s}^{\mathrm{T}} B_n \mathbf{s} + 2as^2 + b\mathbf{s}^{\mathrm{T}}\mathbf{t}\ , \tag{5.41}$$

where B_n is the tridiagonal Toeplitz matrix of dimension $n \times n$ with the three non-zero diagonals given by

$$B_n = \begin{pmatrix} 2a & b & & & & & & \\ b & 2a & b & & & & & \\ & b & 2a & b & & & & \\ & & \cdot & \cdot & \cdot & & & \\ & & & \cdot & \cdot & \cdot & & \\ & & & & \cdot & \cdot & \cdot & \\ & & & & & b & 2a & b \\ & & & & & & b & 2a \end{pmatrix}_{n\times n} \tag{5.42}$$

and where $\mathbf{s} = (s_1, s_2, \ldots, s_n)^T$ and $\mathbf{t} = (s, 0, \ldots, 0, (-1)^n s)^T$. The critical points of the energy form are given by

$$B_n \mathbf{s} = -b\mathbf{t}. \tag{5.43}$$

The Hessian matrix of the energy quadratic form is B_n, whose eigenvalues and eigenvectors are easily found. The eigenvalues are $\lambda_k = 2\big(a + b\cos\frac{k\pi}{n+1}\big)$, $k = 1, 2, \ldots, n$.

Now the Hessian is positive definite for $\cos\frac{\pi}{n+1} < \frac{a}{b}$, therefore in this range the unique critical point, Eqn. (5.43), is the minimum energy configuration for the boundary problem $s_0 = s$, $s_{n+1} = (-1)^n s$. The solution is obtained by inverting the Toeplitz matrix B_n, $\mathbf{s} = -b(B_n)^{-1}\mathbf{t}$, explicitly from [89, 83]

$$s_k = \bar{s}_k^n \stackrel{\text{def}}{=} (-1)^k s\left(\frac{\sin(n+1-k)\theta - \sin k\theta}{\sin(n+1)\theta}\right), \qquad k = 1, \ldots, n, \tag{5.44}$$

where $\cos\theta = a/b$. Equivalently, the solution can be written as

$$\bar{s}_k^n = \frac{(-1)^k s}{\sin(n+1)\theta/2}\ \sin\left(\tfrac{n+1}{2} - k\right)\theta, \qquad k = 1, \ldots, n. \tag{5.45}$$

From this expression it is easily seen that $|\bar{s}_k^n| < s$, so the solution is inside the hypercube $[-s, s]^n$ of acceptable solutions. One also recognizes a rotation of the spin components by π, interpolating smoothly from one Néel ground state to the other over the sites labelled by $k = 1, \ldots, n$. The soliton we are after must therefore be found among these functions $\bar{s}_k^n$, with integer n such that $\cos\frac{\pi}{n+1} < \frac{a}{b} < 1$, since they are the minimum energy solutions to the boundary problems $s_0 = s$, $s_{n+1} = (-1)^n s$. It is clear that the corresponding energies decrease with n, $E_n > E_{n+1}$, since the nth problem is subsumed in the $(n+1)$st. This implies that the soliton has maximal such n. We conclude that the antiferromagnetic ($b > 0$) soliton for $a > 0$ is given by Eqn.(5.45) :

$$s_k = \bar{s}_k^M = \frac{(-1)^k s}{\sin(M+1)\theta/2}\ \sin\left(\tfrac{M+1}{2} - k\right)\theta, \qquad k = 1, \ldots, M, \tag{5.46}$$

where $\cos\theta = \frac{a}{b}$ and $M \geq 1$ is the unique integer such that $\cos\frac{\pi}{M+1} < \frac{a}{b} < \cos\frac{\pi}{M+2}$. The soliton corresponds to a rotation of the spin components by π over the sites labelled by $k = 1, \ldots, M$, interpolating smoothly from one Néel ground state to the other, and has minimal energy among such interpolations. As a is decreased towards zero, the soliton is shortened until it reaches the trivial $\bar{s}_1^1 = 0$ in the range $0 < a < \cos\frac{\pi}{3}$.

As a becomes negative one can guess, and prove by an easy induction, that the domain-wall soliton collapses to a simple "up-up" or "down-down" defect.

Ferromagnetic soliton In the ferromagnetic case $b < 0$, the problem can be solved by an essentially identical analysis or more simply by the exact local equivalence, Eqn.(5.36). In places where the antiferromagnetic case had "up-up" or "down-down" defects (or little defects), the ferromagnetic case has "up-down" or "down-up" defects (or little defects). Where the antiferromagnetic ground state is non-degenerate, so is the ferromagnetic one. Where the antiferromagnetic soliton is $s_k = \bar{s}_k^M$, Eqn.(5.46), the ferromagnetic soliton is

$$s_k = s_k^M = \frac{s}{\sin(M+1)\theta/2}\ \sin\left(\tfrac{M+1}{2} - k\right)\theta, \qquad k = 1, \ldots, M, \tag{5.47}$$

with $\cos\theta = \frac{a}{|b|}$ and $M \geq 1$ is the unique integer such that $\cos\frac{\pi}{M+1} < \frac{a}{|b|} < \cos\frac{\pi}{M+2}$.

Explict, discrete-spin soliton profile The expressions found above in Eqns.(5.46, 5.47) for the soliton profile are expressed as continuous functions of the parameters and hence do not actually correspond to the discrete values that are allowed for the z components of the spin. However it is an easy numerical exercise to find the actual discrete soliton profiles. Using Mathematica we find a few examples for the antiferromagnetic case. See Tables 5.1, 5.2, 5.3, 5.4, 5.5, 5.6. For small values of the spin we observe that the exact, discrete soliton changes size at rational values of $\frac{a}{b} \sim \frac{n}{n+1}$. At the present time we only have a numerical observation of this phenomenon, and we think this is only for small values of the spin, as it no longer seems to be the case already at spin 20 and spin 41/2. (See Figs.5.3, 5.4 of the main text.) For these values, the soliton's length is numerically observed to change from M to $M+1$ at $a/b \sim \cos \pi/(M+2)$, in agreement with the large spin calculation.

5.6.1.3 The ground state for all periodic lattices

There is a duality between orientable and non-orientable periodic chains reflected in the parity of the allowed number of solitons. On the orientable chain of length N, the number of solitons must be even, except for N odd and $b > 0$ (antiferromagnetic). In this case, it is clearly impossible to have all spins coupled in up-down pairs, and a topological defect must be present. The exact opposite happens on the Möbius strip where only this case, $b > 0$ and odd N, can close up smoothly under the additional twist of the strip. In all cases where a defect is imposed by topology, the periodic conditions simply force two degenerate configurations from Fig.(5.1) to meet. Consequently, the shape of the defect is determined by the appropriate boundary value problem from Section 5.6.1.2 when $b > 0$, or Section 5.6.1.2 when $b < 0$, and the semi-classical solution is provided by Eqn.(5.46), or Eqn.(5.47), respectively. Thus we have the following Table 5.7. The difference between the ferromagnetic and antiferromagnetic cases when N is odd reflects the fact the the equivalence Eqn.(5.36) is not globally well-defined on a periodic chain of odd length. One can immediately read the ground state of any given periodic chain from Table 5.7 and Figs.(5.1), (5.2) from the main text. Whenever the table indicates an even number of solitons, the ground state has no soliton and is as in Fig.(5.1). It is either doubly degenerate or non-degenerate (integer s, $a > |b|$). When the table indicates an odd number of solitons, the ground state has a unique soliton (if applicable) whose length and semi-classical shape are found from Fig.(5.2) and Eqns.(5.46), (5.47). The rest of the chain is as in Fig.(5.1). These semi-classical single-soliton states are $2N$-fold ($2s$ even) or $4N$-fold ($2s$ odd) degenerate. The special case $s \in \mathbb{N}$, $a > |b|$ has no soliton since the corresponding ground state is non-degenerate.

5.6.2 The critical lines $a = |b|$

5.6.2.1 Solitons as excitations

We will study the part played by soliton excitations in destroying the fully polarized or anti-polarized order of the BCHI chains (with a possible additional soliton defect of topological origin) as $a \to |b|$. In this limit, the magnetic order will be

TABLE 5.1 – Spin 1

$\uparrow \leftrightarrow s_z = 1; \quad 0 \leftrightarrow s_z = 0$	
$\vert \ldots, \downarrow, \uparrow, 0, \downarrow, \uparrow, \ldots \rangle$	$\vert \ldots, 0, 0, 0, 0, 0, \ldots \rangle$
$\frac{a}{b} < 1$	$\frac{a}{b} > 1$

TABLE 5.2 – Spin 2

$\uparrow \leftrightarrow s_z = 2; \quad \uparrow \leftrightarrow s_z = 1; \quad 0 \leftrightarrow s_z = 0$			
$\vert \ldots, \downarrow, \uparrow, 0, \downarrow, \uparrow, \ldots \rangle$	$\vert \ldots, \downarrow, \uparrow, \downarrow, \downarrow, \uparrow, \downarrow, \ldots \rangle$	$\vert \ldots, \downarrow, \uparrow, \downarrow, 0, \uparrow, \downarrow, \uparrow, \ldots \rangle$	$\vert \ldots, 0, 0, 0, 0, 0, \ldots \rangle$
$\frac{a}{b} < \frac{1}{2}$	$\frac{1}{2} < \frac{a}{b} < \frac{3}{4}$	$\frac{3}{4} < \frac{a}{b} < 1$	$\frac{a}{b} > 1$

TABLE 5.3 – Spin 3

$\uparrow \leftrightarrow s_z = 3; \quad \uparrow \leftrightarrow s_z = 2; \quad \uparrow \leftrightarrow s_z = 1; \quad 0 \leftrightarrow s_z = 0$					
$\vert \ldots, \downarrow, \uparrow, 0, \downarrow, \uparrow, \ldots \rangle$	$\vert \ldots, \downarrow, \uparrow, \downarrow, \downarrow, \uparrow, \downarrow, \ldots \rangle$ $\vert \ldots, \downarrow, \uparrow, \downarrow, \downarrow, \uparrow, \downarrow, \ldots \rangle$	$\vert \ldots, \downarrow, \uparrow, \downarrow, 0, \uparrow, \downarrow, \uparrow, \ldots \rangle$	$\vert \ldots, \downarrow, \uparrow, \downarrow, \uparrow, \uparrow, \downarrow, \uparrow, \downarrow, \ldots \rangle$	$\vert \ldots, \downarrow, \uparrow, \downarrow, \uparrow, 0, \downarrow, \uparrow, \downarrow, \uparrow, \ldots \rangle$	$\vert \ldots, 0, 0, 0, \ldots \rangle$
$\frac{a}{b} < \frac{1}{2}$	$\frac{1}{2} < \frac{a}{b} < \frac{2}{3}$	$\frac{2}{3} < \frac{a}{b} < \frac{6}{7}$	$\frac{6}{7} < \frac{a}{b} < \frac{8}{9}$	$\frac{8}{9} < \frac{a}{b} < 1$	$\frac{a}{b} > 1$

TABLE 5.4 – Spin $\frac{3}{2}$

$\uparrow \leftrightarrow s_z = \frac{3}{2}; \quad \uparrow \leftrightarrow s_z = \frac{1}{2}$		
$\vert \ldots, \downarrow, \uparrow, \uparrow, \downarrow, \uparrow, \ldots \rangle$	$\vert \ldots, \downarrow, \uparrow, \downarrow, \downarrow, \uparrow, \downarrow, \ldots \rangle$	$\vert \ldots, \downarrow, \uparrow, \downarrow, \downarrow, \uparrow, \downarrow, \uparrow, \ldots \rangle$
$\frac{a}{b} < \frac{1}{2}$	$\frac{1}{2} < \frac{a}{b} < 1$	$\frac{a}{b} > 1$

TABLE 5.5 – Spin $\frac{5}{2}$

$\uparrow \leftrightarrow s_z = \frac{5}{2}; \quad \uparrow \leftrightarrow s_z = \frac{3}{2}; \quad \uparrow \leftrightarrow s_z = \frac{1}{2}$				
$\vert \ldots, \downarrow, \uparrow, \uparrow, \downarrow, \uparrow, \ldots \rangle$	$\vert \ldots, \downarrow, \uparrow, \downarrow, \downarrow, \uparrow, \downarrow, \ldots \rangle$ $\vert \ldots, \downarrow, \uparrow, \downarrow, \downarrow, \downarrow, \uparrow, \ldots \rangle$	$\vert \ldots, \downarrow, \uparrow, \downarrow, \uparrow, \uparrow, \downarrow, \uparrow, \ldots \rangle$	$\vert \ldots, \downarrow, \uparrow, \downarrow, \uparrow, \uparrow, \downarrow, \uparrow, \downarrow, \ldots \rangle$	$\vert \ldots, \downarrow, \uparrow, \downarrow, \downarrow, \uparrow, \downarrow, \uparrow, \ldots \rangle$
$\frac{a}{b} < \frac{1}{2}$	$\frac{1}{2} < \frac{a}{b} < \frac{3}{4}$	$\frac{3}{4} < \frac{a}{b} < \frac{5}{6}$	$\frac{5}{6} < \frac{a}{b} < 1$	$\frac{a}{b} > 1$

TABLE 5.6 – Spin $\frac{7}{2}$

$\uparrow \leftrightarrow s_z = \frac{7}{2}; \quad \uparrow \leftrightarrow s_z = \frac{5}{2}; \quad \uparrow \leftrightarrow s_z = \frac{3}{2}; \quad \uparrow \leftrightarrow s_z = \frac{1}{2}; \quad 0 \leftrightarrow s_z = 0$						
$\vert \ldots, \downarrow, \uparrow, \uparrow, \downarrow, \uparrow, \ldots \rangle$	$\vert \ldots, \downarrow, \uparrow, \downarrow, \downarrow, \uparrow, \ldots \rangle$	$\vert \ldots, \downarrow, \uparrow, \downarrow, \uparrow, \uparrow, \downarrow, \uparrow, \ldots \rangle$ $\vert \ldots, \downarrow, \uparrow, \downarrow, \downarrow, \downarrow, \uparrow, \ldots \rangle$	$\vert \ldots, \downarrow, \uparrow, \downarrow, \uparrow, \uparrow, \downarrow, \uparrow, \downarrow, \ldots \rangle$ $\vert \ldots, \downarrow, \uparrow, \downarrow, \uparrow, \uparrow, \downarrow, \uparrow, \ldots \rangle$	$\vert \ldots, \downarrow, \uparrow, \downarrow, \uparrow, \uparrow, \downarrow, \uparrow, \downarrow, \uparrow, \ldots \rangle$	$\vert \ldots, \downarrow, \uparrow, \downarrow, \uparrow, \downarrow, \downarrow, \uparrow, \downarrow, \uparrow, \ldots \rangle$	$\vert \ldots, 0, 0, 0, \ldots \rangle$
$\frac{a}{b} < \frac{1}{2}$	$\frac{1}{2} < \frac{a}{b} < \frac{3}{4}$	$\frac{3}{4} < \frac{a}{b} < \frac{5}{6}$	$\frac{5}{6} < \frac{a}{b} < \frac{9}{10}$	$\frac{9}{10} < \frac{a}{b} < \frac{11}{12}$	$\frac{11}{12} < \frac{a}{b} < 1$	$\frac{a}{b} > 1$

TABLE 5.7 – Number of allowed solitons on periodic chains of length $N \geq 2$.

	Orientable chain		Non-orientable chain	
	F ($b < 0$)	AF ($b > 0$)	F ($b < 0$)	AF ($b > 0$)
N even	Even	Even	Odd*	Odd*
N odd	Even	Odd*	Odd*	Even

* : Does not apply to the non-degenerate case $s \in \mathbb{N}$, $a > |b|$.

affected by the creation of soliton pairs resulting in the complete overturn of all spin components in the finite interval between the solitons. The energy of such an excitation is confined to the solitons themselves, since flipping spins leaves the Hamiltonian invariant. We compute that energy in the region $a \lesssim |b|$, where solitons are long, just before the transition. For simplicity, we consider ferromagnetic solitons. The results will hold for antiferromagnetic solitons since the equivalence Eqn.(5.36) is always locally well-defined, although it might fail to be defined globally. The ferromagnetic soliton, Eqn.(5.47), of angle parameter θ (and corresponding integer length $M \geq 1$ such that $\frac{\pi}{M+2} < \theta < \frac{\pi}{M+1}$), located at position 1, is

$$s_k(\theta) = \frac{s}{\sin(M+1)\theta/2} \sin\big(\tfrac{M+1}{2} - k\big)\theta, \qquad 1 \leq k \leq M. \tag{5.48}$$

It interpolates smoothly from $s_0 = s$ to $s_{M+1} = -s$. Here θ is considered a free parameter of the soliton, and the θ-soliton will minimize energy only when $\cos\theta$ is tuned to $\cos\theta_0 \stackrel{\text{def}}{=} \frac{a}{|b|}$. In the limit $M \to \infty$, we have

$$s_k(\theta) = s\cos k\theta, \qquad 1 \leq k \leq M. \tag{5.49}$$

The energy of this soliton, including interactions with sites 0 and $M+1$, is

$$E(\tfrac{a}{|b|}, \theta) = as^2 \textstyle\sum_{k=1}^{M} \cos^2 k\theta - |b|s^2 \left(\cos\theta - \cos M\theta + \sum_{k=1}^{M-1} \cos k\theta \cos(k+1)\theta\right). \tag{5.50}$$

This expression is valid for any θ and $\frac{a}{b}$ whether or not the soliton is "minimal", i.e. minimizes energy. Using the identity $\sum_{j=0}^{n} \cos(\phi + ja) = \frac{\sin((n+1)\frac{a}{2})\cos(\phi + \frac{na}{2})}{\sin a/2}$ on each sum, the energy expression can be manipulated into the form

$$E(\tfrac{a}{|b|}, \theta) = |b|s^2\Big(\epsilon(\theta) + \delta(\theta)\big(\tfrac{a}{|b|} - \cos\theta\big)\Big), \tag{5.51}$$

where specifically

$$\epsilon(\theta) = \Big(\tfrac{1}{2}\sin M\theta \sin(M-1)\theta + \cos M\theta(\cos\theta\cos M\theta + 1) - \cos\theta\Big), \tag{5.52}$$

$$\delta(\theta) = \frac{M-1}{2} + \frac{\sin(M-1)\theta\cos M\theta}{2\sin\theta}. \tag{5.53}$$

The second term in Eqn.(5.51) vanishes identically for minimal solitons, $\cos\theta = \cos\theta_0 \stackrel{\text{def}}{=} \frac{a}{|b|}$, and is negligible for general solitons of the large-M limit because both $\frac{a}{|b|}$ and $\cos\theta$ are comprised in the interval $\big(\cos\frac{\pi}{M+1}\ ,\ \cos\frac{\pi}{M+2}\big)$. In fact, $\frac{a}{|b|}$, $\cos\theta$, and $\cos\frac{\pi}{M}$ can be used interchangeably in this limit :

$$\cos\theta \sim \cos\frac{\pi}{M} \sim \frac{a}{|b|}. \tag{5.54}$$

Thus

$$E\big(\tfrac{a}{|b|},\theta\big) = E(M) \sim -|b|s^2\cos\tfrac{\pi}{M}. \tag{5.55}$$

The energy of the fully polarized segment of length M, including interactions with sites 0 and $M+1$, is

$$E_0(M) = Mas^2 - (M+1)|b|s^2 \sim -|b|s^2\Big(M+1-M\cos\tfrac{\pi}{M}\Big). \tag{5.56}$$

The excitation energy of the soliton with respect to the fully polarized chain is thus, in the large-M limit,

$$\Delta(M) = E(M) - E_0(M) \sim |b|s^2(M+1)\big(1-\cos\tfrac{\pi}{M}\big). \tag{5.57}$$

To lowest order in $1/M$,

$$\Delta(M) = E(M) - E_0(M) \sim |b|s^2\,\frac{\pi^2}{2}\left(\frac{1}{M}\right), \tag{5.58}$$

or equivalently

$$\Delta\big(\tfrac{a}{|b|}\big) \sim |b|s^2\,\frac{\pi}{2}\arccos\frac{a}{|b|} \sim |b|s^2\,\frac{\pi}{\sqrt{2}}\left(1-\tfrac{a}{|b|}\right)^{1/2}. \tag{5.59}$$

The creation energy of a pair of solitons, overturning a chain segment from one degenerate ground state to the other, is thus

$$\Delta_{\text{pair}}\big(\tfrac{a}{|b|}\big) \sim |b|s^2\pi\sqrt{2}\left(1-\tfrac{a}{|b|}\right)^{1/2}. \tag{5.60}$$

They become massless as $a \to |b|$, with critical exponent $z\nu = 1/2$. (The critical theory is the free relativistic scalar, with dynamical exponent $z = 1$. See below.) The spin required to realize long lightweight solitons diverges slowly as $s = O(1 - a/|b|)^{-1/2}$. In this limit, instability against pairs of soliton excitations destroys the possibility of a long range order in the ground state. Spin waves $|k\rangle = \sum_j e^{ikj}S_j^-|0\rangle$ on the fully polarized state $|0\rangle$ when $b < 0$ (or their staggered version on the anti-polarized state when $b > 0$) are directly found to have mass $\Delta_{\text{SW}} = a + 2|b|s\big(1-\frac{a}{|b|}\big)$. At the transition lines $a = |b|$, a mass gap $\Delta_{\text{SW}} = a = |b|$ remains and spin waves will be frozen at low temperatures.

5.6.2.2 Correlations in the ground state at criticality

We calculate the correlation between s_i^z and s_j^z in the region $a \lesssim |b|$ with thermal soliton pairs as low-lying excitations. Throughout, sites i and j are considered close compared to the total length N of the chain, $|i-j| \ll N$, and we assume that the separation $|i-j|$ is much larger than the soliton length M. By Landau's argument for one-dimensional local systems [159], we expect a finite correlation length at all positive temperatures, except at quantum criticality where solitons become massless. An infinite correlation length is expected also at zero temperature.

We consider the ferromagnetic transition ($b < 0$) for simplicity. The equivalence (5.36), locally valid in all cases, immediately entails the corresponding antiferromagnetic results. In the thermally excited ferromagnetic ground state, the value of $s_i^z s_j^z$ will depend on how many solitons (or antisolitons) are interspersed between site i and site j :

$$s_i^z s_j^z = (-1)^q s^2, \tag{5.61}$$

where q is the number of solitons between site i and site j. With the size M of the solitons provided by Eqn.(5.54), the maximum number of solitons on the entire chain is of order N/M. In a thermal bath with inverse temperature β the Boltzmann factor for having k solitons on the chain is $e^{-\beta k\Delta}$, where Δ is given by Eqns.(5.58) and (5.59). The probability that q solitons among k are between sites i and j is $\binom{k}{q} x^q (1-x)^{k-q}$, where $x = |i-j|/N \ll 1$. Thus

$$\langle S_i S_j \rangle_\beta = \frac{1}{Z} \sum_{k=0}^{N/M} e^{-\beta k\Delta} \left(\sum_{q=0}^{k} (-1)^q s^2 \binom{k}{q} x^q (1-x)^{k-q} \right). \tag{5.62}$$

The partition function is trivially evaluated :

$$Z = \sum_{k=0}^{N/M} e^{-\beta k\Delta} = \left(1 - e^{-\beta\Delta}\right)^{-1}, \tag{5.63}$$

where for the last equality we have considered the large N limit with fixed β, Δ, and M (i.e. fixed $a/|b|$). Similarly,

$$\begin{aligned}
\langle S_i S_j \rangle_\beta &= \frac{1}{Z} \sum_{k=0}^{N/M} e^{-\beta k\Delta} \left(\sum_{q=0}^{k} (-1)^q s^2 \binom{k}{q} x^q (1-x)^{k-q} \right) \\
&= \frac{s^2}{Z} \sum_{k=0}^{N/M} e^{-\beta k\Delta} \left(\sum_{q=0}^{k} \binom{k}{q} (-x)^q (1-x)^{k-q} \right) \\
&= \frac{s^2}{Z} \sum_{k=0}^{N/M} e^{-\beta k\Delta} (1-2x)^k \\
&= \frac{s^2}{Z} \left(1 - e^{-\beta\Delta}(1-2x)\right)^{-1},
\end{aligned} \tag{5.64}$$

where use has been made of the binomial theorem in the third equality, and of the large N limit in the last equality. Putting together Eqns.(6.9) and (5.64), and using $x = |i-j|/N \ll 1$ again, we find

$$\langle S_i S_j \rangle_\beta \sim \begin{cases} \frac{M}{2} s^2 |i-j|^{-1} & \text{for } \beta\Delta \ll |i-j|/N, \\ s^2 e^{-|i-j|/N\xi} & \text{for } \beta\Delta > 2|i-j|/N. \end{cases} \tag{5.65}$$

At quantum criticality, $\beta\Delta \sim 0$, correlations have a power-law decay $\propto |i-j|^{-(d-2+\eta)}$ with critical exponent $\eta = 2$. The long range of critical correlations signals a scale invariance in the distribution of the solitons, but the smallness of $M/|i-j|$ indicates that lightweight solitons melt the ferromagnetic order. Away from quantum criticality, the correlation length $\xi = \frac{1}{2}(e^{\beta\Delta} - 1)$ is finite, except in the zero-temperature limit $\beta\Delta \to \infty$, the only other critical point.

5.6.2.3 1st- and 2nd order transitions in the ground state

We have found a non-analyticity in the ground-state energy and correlations as a function of the non-thermal parameter $a/|b|$, a quantum phase transition. The effect of a longitudinal field h_z establishes the existence of a first-order transition at $h_z = 0$ in the regime $a < |b|$. This first-order line terminates at the critical point $a = |b|$, and the transition there looks increasingly like a second-order transition in the limit of large spin s, although strictly speaking it is a simple level crossing. (See the continuum field theory in Section 5.2.) We illustrate this with the $T = 0$ phase diagram of the orientable ferromagnetic model in a longitudinal field, Fig.(5.11).

The lines $h_z = \pm 2s(a - |b|)$ separate the maximally polarized region (medium gray) from the region where the ground state is polarized with non-maximal total spin (light gray). The ground state is then $|m, \ldots, m\rangle$, with $|m| < s$, and m increases as we move away from the a axis. The neighbourhood of the critical point $a = |b|$ is where a continuous field theory is effective (dark gray). Soliton pairs are effectively suppressed outside this region by tunneling events from false vacua to the true vacuum.

5.6.3 Magnetic form factor

The soliton is in principle observable through neutron scattering. We calculate the magnetic form factor of the semi-classical antiferromagnetic soliton of length M and angle parameter θ. Again θ is just a parameter of the soliton comprised in the interval $(\frac{\pi}{M+2}, \frac{\pi}{M+1})$, and is not necessarily equal to $\cos^{-1} a/|b|$. The form factor is the (discrete) Fourier transform of the soliton :

$$\begin{aligned} \tilde{s}(\xi) &= \sum_{k=0}^{M-1} s_k \, e^{ik\xi} \, , \qquad \xi = 2\pi j/N \, , \; j = 0, 1, \ldots, N-1 \\ &= \sum_{k=0}^{M-1} (-1)^{k+1} \sigma \sin\left[\left(\tfrac{M-1}{2} - k\right)\theta\right] \, e^{ik\xi} \end{aligned}$$

FIGURE 5.11 – $T = 0$ phase diagram for the orientable ferromagnetic case in a longitudinal field h_z

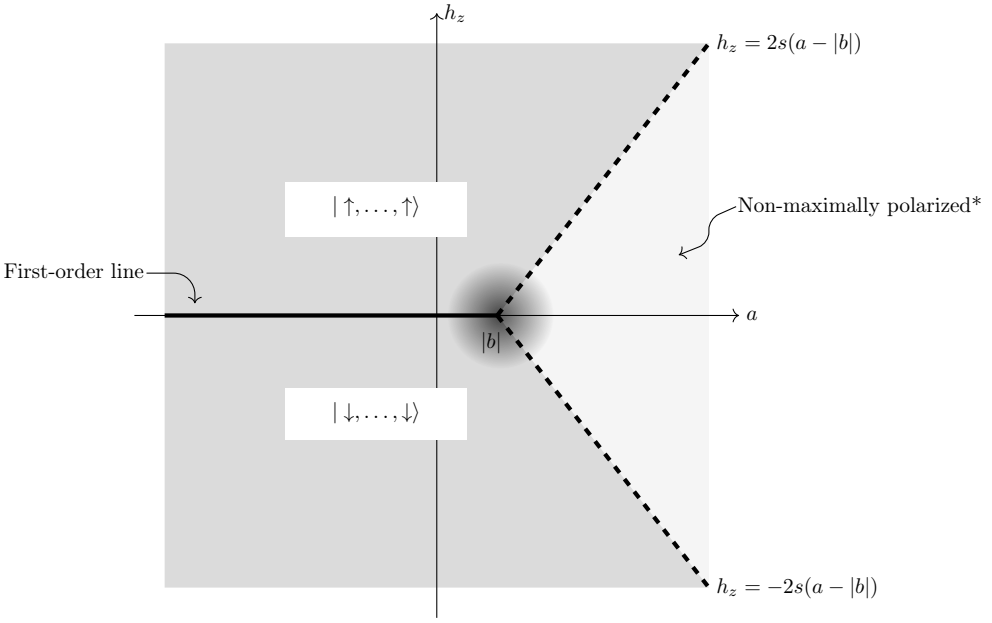

* : Does not apply to the case $s = 1/2$. In this case the anisotropy term $a \sum_j s_j^2$ is constant, and BCHI = Ising.

where $\sigma = \frac{s}{\sin(M+1)\theta/2}$. The sum can be written as

$$-\sigma \sum_{k=0}^{M-1} \left(\sin(\tfrac{M-1}{2}\theta) \cos k\theta - \cos(\tfrac{M-1}{2}\theta) \sin k\theta \right) e^{ik(\pi+\xi)}$$

and separated into real and imaginary parts. The real part is

$$-\sigma \sin(\tfrac{M-1}{2}\theta) \textstyle\sum_{k=0}^{M-1} \cos k\theta \cos k(\pi + \xi) + \sigma \cos(\tfrac{M-1}{2}\theta) \sum_{k=0}^{M-1} \sin k\theta \cos k(\pi + \xi)$$

and can be rearranged as

$$-\tfrac{\sigma}{2} \sin(\tfrac{M-1}{2}\theta) \textstyle\sum_{k=0}^{M-1} \left[\cos 2k\alpha_- + \cos 2k\alpha_+ \right] + \tfrac{\sigma}{2} \cos(\tfrac{M-1}{2}\theta) \sum_{k=0}^{M-1} \left[\sin 2k\alpha_- + \sin 2k\alpha_+ \right]$$

where $\alpha_\pm = \frac{1}{2}(\theta \pm \pi \pm \xi)$. Using the identities

$$\sum_{j=0}^{n} \sin(\phi + ja) = \frac{\sin((n+1)\frac{a}{2}) \sin(\phi + \frac{na}{2})}{\sin a/2},$$

and

$$\sum_{j=0}^{n} \cos(\phi + ja) = \frac{\sin((n+1)\frac{a}{2}) \cos(\phi + \frac{na}{2})}{\sin a/2},$$

and after some easy manipulations, this becomes

$$\frac{\sigma}{2}\left[\frac{\sin M\alpha_+}{\sin\alpha_+} - \frac{\sin M\alpha_-}{\sin\alpha_-}\right]\sin\Big((M-1)(\tfrac{\alpha_+-\alpha_-}{2})\Big). \tag{5.66}$$

The imaginary part is dealt with in a completely analogous manner and yields

$$-\frac{\sigma}{2}\left[\frac{\sin M\alpha_+}{\sin\alpha_+} - \frac{\sin M\alpha_-}{\sin\alpha_-}\right]\cos\Big((M-1)(\tfrac{\alpha_+-\alpha_-}{2})\Big). \tag{5.67}$$

The form factor of the soliton can thus be written

$$\tilde{s}(\xi) = \Lambda(\sin\Phi - i\cos\Phi) = \Lambda\, e^{i(\Phi-\frac{\pi}{2})}, \tag{5.68}$$

where $\Lambda = \frac{\sigma}{2}[\frac{\sin M\alpha_+}{\sin\alpha_+} - \frac{\sin M\alpha_-}{\sin\alpha_-}]$, and $\Phi = (M-1)(\frac{\alpha_+-\alpha_-}{2})$. We can reintroduce the original parameters θ and ξ by noticing that

$$\sin\tfrac{M}{2}(\theta\pm\pi\pm\xi) = \begin{cases}(-1)^q\sin\frac{M}{2}(\theta\pm\xi), & \text{if } M=2q\,;\\ \pm(-1)^q\cos\frac{M}{2}(\theta\pm\xi), & \text{if } M=2q+1.\end{cases}$$

We get our final result

$$\begin{aligned}\tilde{s}(\xi) &= \Lambda(M,\theta,\xi)\exp i\big(\Phi(M,\xi)-\tfrac{\pi}{2}\big)\\ \mathrm{Re}\,\tilde{s}(\xi) &= \Lambda(M,\theta,\xi)\sin\Phi(M,\xi)\\ \mathrm{Im}\,\tilde{s}(\xi) &= -\Lambda(M,\theta,\xi)\cos\Phi(M,\xi)\end{aligned} \tag{5.69}$$

where

$$\Lambda(M,\theta,\xi) = \begin{cases}\frac{(-1)^q s}{2\sin(M+1)\theta/2}\Big(\frac{\sin M(\theta+\xi)/2}{\cos(\theta+\xi)/2} + \frac{\sin M(\theta-\xi)/2}{\cos(\theta-\xi)/2}\Big), & \text{if } M=2q\,;\\ \frac{(-1)^q s}{2\sin(M+1)\theta/2}\Big(\frac{\cos M(\theta+\xi)/2}{\cos(\theta+\xi)/2} - \frac{\cos M(\theta-\xi)/2}{\cos(\theta-\xi)/2}\Big), & \text{if } M=2q+1,\end{cases} \tag{5.70}$$

and

$$\Phi(M,\xi) = \tfrac{M-1}{2}(\pi+\xi). \tag{5.71}$$

It is immediate from Eqn.(5.70) that $\Lambda(M,\theta,-\xi) = (-1)^M\Lambda(M,\theta,\xi)$. We can thus check directly from Eqns.(5.69) and (5.71) that $\mathrm{Re}\tilde{s}(-\xi) = \mathrm{Re}\tilde{s}(\xi)$ and that $\mathrm{Im}\tilde{s}(-\xi) = -\mathrm{Im}\,\tilde{s}(\xi)$. This is the reality condition for the Fourier transform : $\tilde{s}(-\xi) = \tilde{s}(\xi)^*$.

Since $\tilde{s}(0)$ is just the total angular momentum, we set $\xi = 0$ in Eqn.(5.69) and obtain

$$\sum_{k=0}^{M-1} s_k = \begin{cases}\frac{-s\sin M\theta/2}{\cos\frac{\theta}{2}\sin(M+1)\frac{\theta}{2}}\,, & \text{if } M=2q\,;\\ 0\,, & \text{if } M=2q+1.\end{cases} \tag{5.72}$$

This is the total angular momentum of the semi-classical antiferromagnetic soliton of length M and angle parameter θ, whether or not $\cos\theta = a/b$. When M is odd, $\sum s_k$ is identically zero, in contrast to the Néel segment of odd length and total spin $\pm s$ that it replaces. The corresponding quantum soliton will have minimal total spin and belong to the spin singlet for integer s, and to the doublet for half-odd s. When M is even, $\sum s_k$ approaches $\pm s$ in the limit $M\to\infty$, whereas the Néel segment of even length that it replaces has minimal total spin. In either case, an excitation event (i.e. the formation of a soliton pair overturning the Néel segment between them) is possible that leaves the spin of the chain and the spin of the scattered electron unchanged. The excitation of a spin wave, on the other hand, demands a change of $\pm\hbar$ in the spin of the scattered neutron.

5.6.4 Solitons of various sizes with the perturbative Heisenberg term

5.6.4.1 Solitons of length one

We now specialize the the region $0 < a < \frac{b}{2}$ of parameter space, where the soliton has size one (one non-maximal spin z component). This case deserves special treatment because small-soliton translations by one lattice constant occur at low perturbative order only for solitons of length one. For other intermediate soliton lengths, translations by *two* lattice constants occur earlier in the perturbative development than translations by one lattice constant. (See Sec. 5.6.4.2.) We compute the perturbative energy splitting in the soliton degenerate subspace due to translations by one lattice constant on the periodic chain of odd length N. On the *open* chain, length-one solitons are massive excitations and will be seen not to destroy the Néel order.

Integer spin When $s \in \mathbb{N}$, the soliton has total spin zero, and the soliton degenerate subspace has dimension $2N$. For each soliton $|\nu\rangle$, define the projector $P_\nu = \sum_{\mu \neq \nu} |\mu\rangle\langle\mu|$. Let $|1\rangle$ have z component representation

$$|\ldots, \uparrow, \downarrow, \uparrow, \underbrace{0, \downarrow}_{\text{sites 1 and 2}}, \uparrow, \downarrow, \ldots\rangle, \tag{5.73}$$

where arrows denote maximal components $\pm s$. (The soliton with Néel background reversed, denoted $|\overline{1}\rangle$, is also one of the $|\nu\rangle$'s.) Applying $P_1(S_1^- S_2^+ + S_1^+ S_2^-)^s$ to $|1\rangle$ will produce the state with z component representation

$$|\ldots, \uparrow, \downarrow, \uparrow, \underbrace{\downarrow, 0}_{\text{sites 1 and 2}}, \uparrow, \downarrow, \ldots\rangle. \tag{5.74}$$

It seems natural to denote it $|2\rangle$. It is clear that the transition $|1\rangle \to |2\rangle$ occurs at perturbative order s, and not earlier, because a minimal amount s of spin must be exchanged between sites 1 and 2, no matter what. Note also that $P_2(S_1^- S_2^+ + S_1^+ S_2^-)^s$ will operate the inverse transition $|2\rangle \to |1\rangle$ when applied on $|2\rangle$. The soliton $|\mu + 1\rangle$ is defined recursively as

$$|\mu + 1\rangle \propto P_\mu (S_\mu^- S_{\mu+1}^+ + S_\mu^+ S_{\mu+1}^-)^s |\mu\rangle, \tag{5.75}$$

where $S_\mu^\pm$ is shorthand for $S_{(\mu \bmod N)}^\pm$. One easily convinces oneself that $|N + 1\rangle$ thus defined is actually $|\overline{1}\rangle$, and that $|2N + 1\rangle = |\overline{N + 1}\rangle = |1\rangle$. All translations are reversible at order s, since

$$|\mu\rangle \propto P_{\mu+1} (S_\mu^- S_{\mu+1}^+ + S_\mu^+ S_{\mu+1}^-)^s |\mu + 1\rangle. \tag{5.76}$$

Translations over more than one lattice constant will require more adjacent transpositions of spin components, and will occur at higher orders. Brillouin-Wigner perturbation theory tells us that the level splitting is given to lowest order by the eigenvalues of the matrix w with (off-diagonal) components

$$w_{\mu\nu} = \langle\mu| V \left(R_\nu V\right)^{s-1} |\nu\rangle, \qquad \mu, \nu = 1, 2, \ldots, 2N, \tag{5.77}$$

where

$$R_\nu = (E_\nu - H_0)^{-1} Q = (E_\nu - H_0)^{-1} \left(1 - \sum_\mu |\mu\rangle\langle\mu| \right), \tag{5.78}$$

and E_ν is the exact energy of the perturbed soliton of quantum number ν. Translation invariance of the translation operators from Eqns. (5.75)-(5.76) implies that w is a circulant matrix,

$$w = \mathrm{circ}(a_1, \ldots, a_{2N}) = \begin{pmatrix} a_1 & a_2 & \cdots & a_{2N} \\ a_{2N} & a_1 & \cdots & a_{2N-1} \\ \vdots & \vdots & \ddots & \vdots \\ a_2 & a_3 & \cdots & a_1 \end{pmatrix}. \tag{5.79}$$

It is clear that w is symmetric, and that its first column has only two nonzero (off-diagonal) entries, $w_{2,1}$ and $w_{2N,1}$, which must be equal by the combination of circulation and symmetry. So it suffices to find the constant C such that $w = C\,\mathrm{circ}(0, 1, 0, \ldots, 0, 1)$. We have

$$C = w_{2,1} = \left(\frac{|J|}{2} \right)^s \langle 2| S_1^- S_2^+ \left(\tfrac{Q}{E_1 - H_0}\, S_1^- S_2^+ \right)^{s-1} |1\rangle = \left(\frac{|J|}{2} \right)^s \frac{\langle 2|(S_1^- S_2^+)^s|1\rangle}{\prod_{m=1}^{s-1}(E_1 - e_m)}, \tag{5.80}$$

where e_m is the unperturbed energy of the state

$$(S_1^- S_2^+)^m |1\rangle \propto |\ldots, \uparrow, \downarrow, \uparrow, \underbrace{-m, -s+m}_{\text{sites 1 and 2}}, \uparrow, \downarrow, \ldots\rangle. \tag{5.81}$$

Approximating E_1 as $E_1(|J| = 0)$, the energy denominators are easily computed to be

$$E_1 - e_m = (2a - b)(s - m)m. \tag{5.82}$$

The amplitude $\langle 2|(S_1^- S_2^+)^s|1\rangle$ in (5.80) is obtained by inserting identity resolutions

$$\begin{aligned} &\langle 2|(S_1^- S_2^+)^s|1\rangle \\ &= \prod_{m=0}^{s-1} \langle \ldots, \downarrow, \uparrow, \underbrace{-m-1, -s+m+1}_{\text{sites 1 and 2}}, \uparrow, \downarrow, \ldots | S_1^- S_2^+ | \ldots, \downarrow, \uparrow, \underbrace{-m, -s+m}_{\text{sites 1 and 2}}, \uparrow, \downarrow, \ldots \rangle \\ &= \prod_{m=0}^{s-1} \sqrt{(s-m)(s+1+m)(2s-m)(m+1)} \\ &= \prod_{m=0}^{s-1} (2s-m)(s-m). \end{aligned} \tag{5.83}$$

Hence

$$C = \left(\frac{|J|}{2} \right)^s \frac{\prod_{m=0}^{s-1}(2s-m)(s-m)}{\prod_{m=1}^{s-1}(2a-b)(s-m)m} = (-1)^{s-1} K s^2 \frac{(2s)!}{(s!)^2} \left(\frac{|J|}{2K} \right)^s, \tag{5.84}$$

where we have introduced $K = b - 2a > 0$. The factor $(-1)^{s-1}$ is due to the presence of $s-1$ negative energy denominators. Circulant matrices $\mathrm{circ}(a_1, \ldots, a_{2N})$ are diagonalized by discrete Fourier transforms, and have eigenvalues

$$\epsilon_j = a_1 + a_2\omega_j + a_3\omega_j^2 + \cdots + a_{2N}\omega_j^{2N-1}, \qquad j = 0, \ldots, 2N-1, \tag{5.85}$$

and corresponding eigenvectors $\frac{1}{\sqrt{2N}}(1, \omega_j, \omega_j^2, \ldots, \omega_j^{2N-1})^{\mathrm{T}}$, with $\omega_j = \exp(ij\pi/N)$. As the matrix w from (5.77) has the form $w = C\,\mathrm{circ}(0, 1, 0, \ldots, 0, 1)$, its eigenvalues are

$$\epsilon_j = C(\omega_j + \omega_j^{2N-1}) = 2C\cos\frac{j\pi}{N}, \qquad j = 0, \ldots, 2N-1. \tag{5.86}$$

The spectrum is doubly degenerate for all values of j except $j = 0$ and $j = N$. From (5.84) the ground state of the periodic chain corresponds to $j = 0$ when s is even, and to $j = N$ when s is odd :

$$|\Omega\rangle = \begin{cases} \frac{1}{\sqrt{2N}} \sum_\mu |\mu\rangle & , \quad s \text{ even;} \\ \frac{1}{\sqrt{2N}} \sum_\mu (-1)^\mu |\mu\rangle & , \quad s \text{ odd.} \end{cases} \tag{5.87}$$

In the thermodynamic limit of the *open* chain, solitons have a gap $\Delta - |C| = (2\,(b + |J|) - a)\,s^2 - |C|$, and will not disorder the ground state, except possibly when $a \to b/2$ (hence $K \to 0$), and $|C|$ becomes larger than Δ. This limit corresponds to the level crossing with solitons of length two. Around that point, Brillouin-Wigner perturbation theory may fail to converge due to the presence of small energy denominators in (5.80). But refining our expression for the energy denominators (5.82) by using the classical energy, Eq. (5.10), we get instead

$$E_1 - e_m = (2a - b - |J|)(s - m)m, \tag{5.88}$$

and $K = b + |J| - 2a$ in Eq. (5.84). When $a \to b/2$ (hence $K \to |J|$), we find that $|C|$ is of order $|J|$, and we conclude again that length-one solitons do not disorder the ground state.

Half-odd spin When $s - \frac{1}{2} \in \mathbb{N}$, the soliton has total spin $\pm\frac{1}{2}$, and the soliton degenerate subspace has dimension $4N$. To compute the perturbative level splitting due to soliton translations, we need to diagonalize a $4N \times 4N$ Brillouin-Wigner matrix W, analogous to the matrix w from the previous section, Eq. (5.77). But since the Hamiltonian conserves total spin, that matrix is block diagonal

$$W = \begin{pmatrix} w^+ & 0 \\ 0 & w^- \end{pmatrix}, \tag{5.89}$$

and we need only to diagonalize each $2N \times 2N$ superselection sector separately. Define the projectors $P_\nu^\pm = \sum_{\mu \neq \nu} |\mu\rangle_{\pm\,\pm}\langle\mu|$ into the degenerate soliton subspaces of total spin $\pm\frac{1}{2}$, respectively, and let

$$|1\rangle_\pm = |\ldots, \uparrow, \downarrow, \uparrow, \underbrace{\pm\tfrac{1}{2}, \downarrow}_{\text{sites 1 and 2}}, \uparrow, \downarrow, \ldots\rangle. \tag{5.90}$$

(The solitons with all components reversed, denoted $|\overline{1}\rangle_{\pm}$, are part of the $|\nu\rangle_{\mp}$'s.) Now

$$P_1^-(S_1^-S_2^+ + S_1^+S_2^-)^{s-\frac{1}{2}}|1\rangle_- \quad \propto \quad |\ldots,\uparrow,\downarrow,\uparrow,\underbrace{\downarrow,-\tfrac{1}{2}}_{\text{sites 1 and 2}},\uparrow,\downarrow,\ldots\rangle. \tag{5.91}$$

Like in the previous section, we call the righthand side $|2\rangle_-$. The transition $|1\rangle_- \to |2\rangle_-$ and its inverse occur at perturbative order $s-\frac{1}{2}$, and not earlier. The transition $|2\rangle_- \to |3\rangle_-$, however, occurs only at the *next* order in perturbation, $s+\frac{1}{2}$. Indeed, transposing spin components $s_2 = -\frac{1}{2}$ and $s_3 = +s$ requires at least $|s_2 - s_3|$ instances of $S_2^-S_3^+ + S_2^+S_3^-$. At minimal perturbative order $s-\frac{1}{2}$, the spin $-\frac{1}{2}$ sector only has translations of the type

$$|2k-1\rangle_- \longleftrightarrow |2k\rangle_- \qquad , \qquad k = 1, 2, \ldots, N. \tag{5.92}$$

As before, $|N+1\rangle_- = |\overline{1}\rangle_-$. The Brillouin-Wigner matrix for this sector of soliton subspace has components

$$w^-_{\mu\nu} = {}_-\langle\mu|V\left(R^-_\nu V\right)^{s-\frac{3}{2}}|\nu\rangle_- \qquad , \qquad \mu,\nu = 1, 2, \ldots, 2N, \tag{5.93}$$

where

$$R^-_\nu = (E^-_\nu - H_0)^{-1}Q_- = (E^-_\nu - H_0)^{-1}\left(1 - \sum_\mu |\mu\rangle_-\,{}_-\langle\mu|\right), \tag{5.94}$$

and E^-_ν is the exact energy of the perturbed soliton of quantum number ν and total spin $-\frac{1}{2}$. According to (5.92), the matrix w^- is block diagonal, with N blocks of dimension 2×2 along the diagonal. The blocks are symmetric, and they must be identical by the two-site translation invariance of the Néel background. What we need to diagonalize is thus a 2×2 matrix $C^-\left(\begin{smallmatrix}0&1\\1&0\end{smallmatrix}\right)$, with eigenvalues

$$\epsilon_\pm = \pm C^-, \tag{5.95}$$

and corresponding eigenvectors $\frac{1}{\sqrt{2}}(1,\pm 1)^{\mathrm{T}}$, respectively. At this minimal perturbative order, the spectrum of the spin $-\frac{1}{2}$ sector is N-fold degenerate, and has a mass gap of $2|C^-|$. The constant C^- is

$$\begin{aligned} C^- = w^-_{2,1} &= \left(\frac{|J|}{2}\right)^{s-\frac{1}{2}} {}_-\langle 2|S_1^-S_2^+\left(\tfrac{Q}{E_1^- - H_0}\,S_1^-S_2^+\right)^{s-\frac{3}{2}}|1\rangle_- \\ &= \left(\frac{|J|}{2}\right)^{s-\frac{1}{2}} \frac{{}_-\langle 2|(S_1^-S_2^+)^{s-1/2}|1\rangle_-}{\prod_{m=1}^{s-3/2}(E_1^- - e_m)}, \end{aligned} \tag{5.96}$$

where

$$E_1^- - e_m = (2a-b)(s-m-\tfrac{1}{2})m. \tag{5.97}$$

The amplitude ${}_-\langle 2|(S_1^- S_2^+)^{s-\frac{1}{2}}|1\rangle_-$ in (5.96) is obtained by introducing identity resolutions, and the result is

$$\begin{aligned} {}_-\langle 2|(S_1^- S_2^+)^{s-\frac{1}{2}}|1\rangle_- &= \prod_{m=0}^{s-\frac{3}{2}} \sqrt{(s-m-\tfrac{1}{2})(s+m+\tfrac{3}{2})(2s-m)(m+1)} \\ &= \prod_{m=0}^{s-\frac{3}{2}} (2s-m)(s-m-\tfrac{1}{2}). \end{aligned} \tag{5.98}$$

Hence

$$\begin{aligned} C^- &= \left(\frac{|J|}{2}\right)^{s-\frac{1}{2}} \frac{\prod_{m=0}^{s-\frac{3}{2}}(2s-m)(s-m-\frac{1}{2})}{\prod_{m=1}^{s-\frac{3}{2}}(2a-b)(s-m-\frac{1}{2})m} \\ &= (-1)^{s-\frac{3}{2}} \frac{K}{2} \left(s-\tfrac{1}{2}\right)^2 \frac{(2s+1)!}{\left((s+\frac{1}{2})!\right)^2} \left(\frac{|J|}{2K}\right)^{s-\frac{1}{2}}, \end{aligned} \tag{5.99}$$

where $K = b - 2a > 0$. The N-fold degenerate ground states are

$$|\Omega\rangle_- = \begin{cases} \frac{1}{\sqrt{2}}(|2k-1\rangle_- - |2k\rangle_-) & , \quad s-\frac{1}{2} \text{ odd}; \\ \frac{1}{\sqrt{2}}(|2k-1\rangle_- + |2k\rangle_-) & , \quad s-\frac{1}{2} \text{ even}, \end{cases} \tag{5.100}$$

for $k = 1, 2, \ldots, N$. The spontaneous breaking of translation invariance is consistent with the Lieb-Schultz-Mattis theorem, which says that the ground state of a translation invariant s-spin chain can be gapped *and* translation invariant only if $s - m_0$ is integer, where m_0 is the magnetization per site in the ground state [202]. For the soliton of length one, the magnetization per site tends to zero in the thermodynamic limit, so $s - m_0$ is noninteger in this limit.

The calculation for the total spin $\frac{1}{2}$ sector is virtually identical, the only difference being that at minimal perturbative order $s-\frac{1}{2}$, the spin $\frac{1}{2}$ sector only has translations of the type

$$|2k\rangle_+ \longleftrightarrow |2k+1\rangle_+ \qquad , \qquad k = 1, 2, \ldots, N, \tag{5.101}$$

with $|N+1\rangle_+ = |\bar{1}\rangle_+$ and $|2N+1\rangle_+ = |1\rangle_+$. (Compare with (5.92).) The perturbative mass gap is $2|C^+| = 2|C^-|$, and the N-fold degenerate ground states are

$$|\Omega\rangle_+ = \begin{cases} \frac{1}{\sqrt{2}}(|2k\rangle_+ - |2k+1\rangle_+) & , \quad s-\frac{1}{2} \text{ odd}; \\ \frac{1}{\sqrt{2}}(|2k\rangle_+ + |2k+1\rangle_+) & , \quad s-\frac{1}{2} \text{ even}, \end{cases} \tag{5.102}$$

for $k = 1, 2, \ldots, N$.

On the *open* chain, the low-lying states are gapped from the Néel ground state by $\Delta - |C| = \frac{1}{4}a + (2b-a)s^2 - |C|$, and will not disorder it. The only possible exception is again when $a \to \frac{b}{2}$, at the level crossing with solitons of length two. But, as before, refining our energy denominators to include a first-order $|J|$ term shows that $|C|$ is of order $|J|$ in that limit, so that perturbative theory should converge after all.

5.6.4.2 Solitons of intermediate length

For solitons of intermediate length $M > 1$, translations by one lattice constant occur at relatively high perturbative order. Due to the alternating character of the Néel order, moving the soliton over one site in a *fixed* Néel background cannot result in a translated soliton. (Unless $M = 1$, Sec. 5.6.4.1.) Solitons of even length, on the one hand, have the following general form

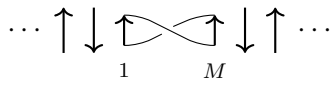

(5.103)

where the longest arrows represent maximal spin components of the Néel background. To preserve the right anti-alignment of s_1 and s_M with their respective neighbour, translations by one lattice constant require translating the Néel background along, a costly operation. (Unless the soliton's length is larger than the remaining Néel segment, a situation to be discussed in Sec. 5.6.4.3.) Similarly, solitons of odd length $M > 1$ have the general form

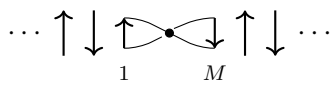

(5.104)

where the central dot represents component 0 ($2s$ even) or $\pm\frac{1}{2}$ ($2s$ odd). Again, the Néel background must be brought along to preserve the right anti-alignment of s_1 and s_M with their respective neighbour. For integer spin solitons, of total spin zero, another possibility is to move the soliton by one site in a fixed Néel background, and invert all soliton components. All these transitions occur at relatively high perturbative order.

Obviously, moving the soliton over *two* lattice constants in a fixed Néel background conserves total spin and results in a translated soliton. Such transitions can be performed at comparatively low perturbative order. (See Sec. 5.6.4.3 for comparison.) Because the chain has odd length N, the soliton will visit all positions after N steps, and two trips around the chain :

$$|\mu\rangle \to |\mu+2\rangle \to \cdots \to |\mu-1\rangle \to |\mu+1\rangle \to \cdots \to |\mu\rangle. \tag{5.105}$$

At the lowest perturbative order where these translations occur, there are two orthogonal superselection sectors corresponding to the two Néel backgrounds. (If $2s$ is odd and the soliton has odd length, there are four sectors as the central component can be $\pm\frac{1}{2}$.) For each sector, we need to diagonalize a Brillouin-Wigner matrix w analogous to Eq. (5.77). The matrix w is $N \times N$, circulant, of the form

$$w = \mathrm{circ}(a_1, a_2, \ldots, a_N) = C_s \mathrm{circ}(0, 0, 1, 0, \ldots, 0, 1, 0). \tag{5.106}$$

Its eigenvalues are

$$\epsilon_j = a_1 + a_2\omega_j + a_3\omega_j^2 + \cdots + a_N\omega_j^{N-1}, \qquad j = 0, \ldots, N-1, \tag{5.107}$$

with corresponding eigenvectors $\frac{1}{\sqrt{N}}(1, \omega_j, \omega_j^2, \ldots, \omega_j^{N-1})^{\mathrm{T}}$, where $\omega_j = \exp(i2\pi j/N)$. We find

$$\epsilon_j = C_s(\omega_j^2 + \omega_j^{N-2}) = 2C_s \cos\frac{4\pi j}{N}, \qquad j = 0, \ldots, N-1. \tag{5.108}$$

We will not attempt to compute C_s explicitly, but only whether it is positive or negative for any given s, since this is enough to determine the perturbative ground space. The difficulty in calculating C_s explicitly lies in the number of ways in which the transposition operators $S_i^+ S_{i+1}^- + S_i^- S_{i+1}^+$ can be ordered. C_s is a sum over all these different orderings. Each term in that sum is analogous to Eq. (5.80), with a positive amplitude in the numerator, and a product of negative energy denominators. The number of energy denominators is the same in all terms, namely one less than the perturbative order. The sign of C_s is thus determined by the *parity* of the order of perturbation at which the transition occurs

$$C_s \begin{cases} > 0 & , \quad \text{odd perturbative order;} \\ < 0 & , \quad \text{even perturbative order.} \end{cases} \tag{5.109}$$

It is possible that the parity of the minimal perturbative order, and by extension the degenerescence of the ground space, delicately depends on the fine details of the quantum soliton. We assume, however, that on average (including soliton degeneracies) it will be a robust property attached to symmetries which our semiclassical expression is likely to possess as well.

Minimal perturbative order In order for a soliton to transit over one lattice constant, an amount $\pm s$ of spin from the Néel background must tunnel across it. Let the soliton have arbitrary length M, and components $s_1, \ldots, s_M$. From Eq. (5.14), the minimal perturbative order at which the component $\pm s$ will transfer is

$$\sum_{i=1}^{M} |\pm s - s_i| = Ms \mp \sum_{i=1}^{M} s_i \ . \tag{5.110}$$

An up-down or down-up pair from the Néel background will therefore transit across a soliton of length M at minimal perturbative order $2Ms$.

Solitons of even intermediate length Solitons of even length have two symmetric halves. As an illustration, consider the soliton of length four, and arbitrary spin s :

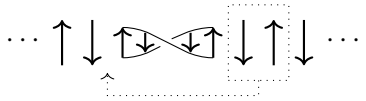

By Eq. (5.110), transferring two adjacent Néel components (boxed) across the soliton requires at least V^{2Ms}. Transposing these two maximal components (in order to recover the Néel order to the left of the soliton) requires an additional V^{2s}. The

minimal perturbative order is thus $2s(M+1)$, where $M+1$ is odd. From Eq. (5.109), we get

$$\text{(even length)} \qquad C_s \begin{cases} > 0 & , \quad 2s \text{ odd;} \\ < 0 & , \quad 2s \text{ even.} \end{cases} \tag{5.111}$$

From Eq. (5.108) we conclude that the ground space is fourfold degenerate in each superselection sector if $2s$ is odd, and non-degenerate in each superselection sector if $2s$ is even. In the thermodynamic limit, each sector is gapless with a doubly degenerate ground state for all values of s.

Solitons of odd intermediate length Solitons of odd length have two antisymmetric halves. As an illustration, consider the soliton of length five :

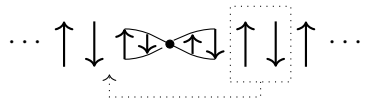

The central dot represents spin component zero if $2s$ is even, and spin component $\pm 1/2$ if $2s$ is odd. Notice that once the boxed spins have tunneled across the soliton they already fit in the Néel background, and need not be swapped, in contradistinction to the previous section. The minimal perturbative order for this transition is thus $2Ms$, where M is odd. From Eq. (5.109), we get

$$\text{(odd length)} \qquad C_s \begin{cases} > 0 & , \quad 2s \text{ odd;} \\ < 0 & , \quad 2s \text{ even,} \end{cases} \tag{5.112}$$

which is identical to the even length case, (5.111). Again, the ground space is fourfold degenerate in each superselection sector if $2s$ is odd, and non-degenerate in each superselection sector if $2s$ is even. In the thermodynamic limit, each sector is gapless with a doubly degenerate ground state for all values of s.

Disordered ground state of the open chain When applied to the open chain, the above analysis indicates that the Néel order will be destroyed as a approaches b, and the soliton becomes massless. Restricting our considerations to dominant, single-soliton excitations, we conclude that each superselection sector should present a doubly degenerate, translation-invariant ground state in the BCHI limit $||J|| \ll \min(|a|, |b|)$, with gapless excitations. This conclusion is independent of s. In each sector, the degenerate ground states have the form $\frac{1}{\sqrt{N}} \sum_\mu |\mu\rangle$ and $\frac{1}{\sqrt{N}} \sum_\mu (-1)^\mu |\mu\rangle$ when $2s$ is even, while they are $\frac{1}{\sqrt{N}} \sum_\mu (i)^\mu |\mu\rangle$ and $\frac{1}{\sqrt{N}} \sum_\mu (-i)^\mu |\mu\rangle$ when $2s$ is odd. These combinations do not depend on the perturbative coupling $|J|$. In the opposite, Haldane limit $||J|| \gg \max(|a|, |b|)$, Haldane has found convincing evidence for a nondegenerate ground state with gapped excitations when s is integer [131]. We conclude that when s is integer, and for $a = b$, there is a quantum phase transition at a critical value $|J|_c(b)$, and this transition is nonanalytic in perturbation theory over $|J|$. Haldane has recognized the essential contribution of solitons of *arbitrary* size in the destruction of Néel order as $a \to b$. It is clear from the above analysis that

the perturbative cost of translating solitons becomes progressively more prohibitive as the soliton size increases. The transition at $|J| = |J|_c$ likely involves instanton-tunneling of very large solitons, not accounted for in perturbative theory.

5.6.4.3 Large solitons

As explained in Sec. 5.6.4.2, translating a soliton of length $M > 1$ by one lattice constant requires translating the Néel background along. (In some cases, one can flip all soliton components instead. This is a costly operation even for solitons of modest size.) For solitons of length much smaller than the Néel background we argued that it was less expensive to perform translations by two lattice constants in a fixed Néel background. We now consider solitons of length M comparable to the size N of the lattice. For odd values of N, these solitons constitute the unperturbed ground states in the region $a \lesssim b$ of parameter space. Since the Néel background is comparatively short, it eventually becomes less expensive to translate it by one lattice constant than translate the soliton a second time. To illustrate our point, let us consider a soliton of large odd length M a fixed fraction of N :

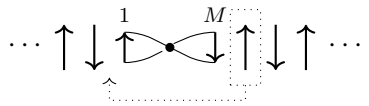

The one site translation $T_1 : |\mu\rangle \to |\mu + 1\rangle$ necessitates the concomitant inversion of the Néel background, and can be performed by transiting a Néel component (any one) along the entire chain. From Eq. (5.110), transferring it across the soliton costs $Ms + |\sum_{i=1}^{M} s_i|$, which is equal to Ms for $2s$ even, and $Ms + 1/2$ for $2s$ odd. Néel inversion costs an additional $\left(\frac{N-M}{2}\right) 2s = (N - M)s$. Thus, T_1 occurs at minimal perturbative order $\sim Ns$, while $T_2 : |\mu\rangle \to |\mu + 2\rangle$ was found to occur at order $2Ms$ in Sec. 5.6.4.2. We see that T_1 occurs earlier in perturbative theory if $M > N/2$. A similar argument can be made when M is even. We conclude that when a is close enough to b, one-site translations occur earlier in perturbation theory than two-site translations. We now briefly summarize the calculation of the perturbative ground state for *large solitons*, i.e. solitons with length $M > N/2$. In all cases, we will find that the ground state is nondegenerate in each superselection sector in the thermodynamic limit. Of course when $2s$ is odd, and since N is odd, there will be *two* superselection sectors mapped onto one another by time reversal, and the ground space will be degenerate in accordance with the Kramers degeneracy theorem.

Large even length solitons For each Néel background, the $N \times N$ Brillouin-Wigner matrix has the form $w = C\,\mathrm{circ}(0, 1, 0, \ldots, 0, 1)$, corresponding to translations $|\mu\rangle \to |\mu \pm 1\rangle$. As before (see Eq. (5.86)) the eigenvalues of w are

$$\epsilon_j = C(\omega_j + \omega_j^{N-1}) = 2C \cos \frac{2\pi j}{N}, \qquad j = 0, \ldots, N-1, \tag{5.113}$$

with corresponding eigenvectors $\frac{1}{\sqrt{N}}(1, \omega_j, \omega_j^2, \ldots, \omega_j^{N-1})^{\mathrm{T}}$, where $\omega_j = \exp(i2\pi j/N)$. The ground state corresponds to $j = 0$ when $C < 0$, and to $j = \lfloor N/2 \rfloor, \lfloor N/2 \rfloor + 1$

when $C > 0$. The sign of C is determined by the parity of the minimal perturbative order γ :

$$\begin{aligned} C = w_{2,1} &= \left(\frac{|J|}{2}\right)^{\gamma} \langle 2|S_1^- S_2^+ \left(\tfrac{Q}{E_1 - H_0}\, S_1^- S_2^+\right)^{\gamma-1} |1\rangle \\ &= (-1)^{\gamma-1} \left(\frac{|J|}{2}\right)^{\gamma} \frac{\langle 2|(S_1^- S_2^+)^{\gamma}|1\rangle}{\prod_{m=1}^{\gamma-1} |E_1 - e_m|}, \end{aligned} \tag{5.114}$$

where E_1 and e_m are defined as before, and $E_1 - e_m < 0$. The minimal perturbative order γ is obtained as above. The one-site translation T_1 occurs at the same order as the following transition : the transit of a Néel component across the soliton, plus the complete inversion of the Néel background. The first part occurs at order $Ms + |\sum_{i=1}^{M} s_i|$. The latter part occurs at order $\left(\frac{N-M-1}{2}\right) 2s = (N - M - 1)s$. Thus, T_1 is of minimal perturbative order $\gamma = (N-1)s + |\sum_{i=1}^{M} s_i|$. Since M is even, the soliton's total spin $\sum_{i=1}^{M} s_i$ is integer, and so is γ. In the limit $M \to \infty$, our semiclassical expression for the soliton yields $|\sum_{i=1}^{M} s_i| \to s$. Numerical results for small to moderate spin values (see Tables 5.1 to 5.6, and Figs. 5.4 and 5.3) also seem to suggest that for any even M, $|\sum_{i=1}^{M} s_i| = s$ or $|\sum_{i=1}^{M} s_i| = s - 1$ for integer s, and $|\sum_{i=1}^{M} s_i| = s - \frac{1}{2}$ for half-odd s. This is the case exactly for the Blume-Capel solitons of the critical line $a = b$, which are of the form $s_i = (-1)^i(s - i)$ with $i = 1, \ldots, 2s - 1$. Assuming this to hold as well for the exact quantum soliton of the region $a \lesssim b$, we find

$$\gamma = \begin{cases} Ns - \frac{1}{2} & , \quad 2s \text{ odd} \\ Ns, Ns - 1 & , \quad 2s \text{ even.} \end{cases} \tag{5.115}$$

When $2s$ is odd, $\gamma = Ns - \frac{1}{2} = N\left(s - \frac{1}{2}\right) + \frac{N-1}{2}$. Thus, the perturbative ground state is nondegenerate ($C < 0$) in each superselection sector if $s - \frac{1}{2}$ and $\frac{N-1}{2}$ are both even or both odd. The perturbative ground state is doubly degenerate in each superselection sector ($C > 0$) if exactly one among $s - \frac{1}{2}$ and $\frac{N-1}{2}$ is odd. A new feature of large solitons is that the degeneracy of the perturbative ground state when $2s$ is odd depends on the length N of the entire chain, a global property. When $2s$ is even, our analysis does not allow us to reach a conclusion, unless $a = b$, for then $|\sum_{i=1}^{M} s_i| = s - 1$ if s is odd, and $|\sum_{i=1}^{M} s_i| = s$ if s is even, implying nondegeneracy ($C < 0$) for all integer values of s on the critical line.

Large odd length solitons For each superselection sector, the $N \times N$ Brillouin-Wigner matrix has the form $w = C\,\mathrm{circ}(0, 1, 0, \ldots, 0, 1)$, corresponding to translations $|\mu\rangle \to |\mu \pm 1\rangle$. There are two sectors if $2s$ is even (the two Néel backgrounds), and there are four if $2s$ is odd (two Néel backgrounds, soliton's total spin $\sum_{i=1}^{M} s_i = \pm\frac{1}{2}$). In each sector, the eigenvalues of w are given by Eq. (5.113), and the value of C is given by Eq. (5.114). The minimal perturbative order γ to reach both one-site translations T_1, T_1^{-1} was found above to be $Ns + |\sum_{i=1}^{M} s_i|$. Our semiclassical expression for the soliton of odd length is antisymmetric with respect to the central component.

Assuming the exact quantum soliton to possess that symmetry as well, we find

$$\gamma = \begin{cases} Ns + \frac{1}{2} & , \quad 2s \text{ odd;} \\ Ns & , \quad 2s \text{ even.} \end{cases} \tag{5.116}$$

When $2s$ is odd, $\gamma = Ns + \frac{1}{2} = N\left(s - \frac{1}{2}\right) + \frac{N+1}{2}$. Thus, the perturbative ground state is nondegenerate ($C < 0$) in each superselection sector if $s - \frac{1}{2}$ and $\frac{N+1}{2}$ are both even or both odd. The perturbative ground state is doubly degenerate in each superselection sector ($C > 0$) if exactly one among $s - \frac{1}{2}$ and $\frac{N+1}{2}$ is odd. Again, we find that for large solitons, the degeneracy of the perturbative ground state when $2s$ is odd depends on the length N of the entire chain. When $2s$ is even, $\gamma = Ns$. Thus, the perturbative ground state is nondegenerate ($C < 0$) in each superselection sector if s is even, and doubly degenerate in each superselection sector ($C > 0$) if s is odd.

Chapitre 6

Troisième article.

Entanglement and correlations in $z = 2$ Lifshitz theories under wavefunction renormalization group flow

par

Christian Boudreault[1,2], Clément Berthière[2,3], William Witczak-Krempa[2,3]

[(1)]Département des sciences de la nature, Collège militaire royal de Saint-Jean, Saint-Jean-sur-Richelieu, QC, Canada, J3B 8R8

[(2)]Département de physique, Université de Montréal, C.P. 6128, succursale Centre-ville, Montréal, QC, Canada, H3C 3J7

[(3)]Centre de Recherches Mathématiques, Université de Montréal, Montréal, QC, Canada, H3C 3J7

Cet article sera soumis pour publication dans PRX Quantum

Contribution du candidat et des coauteurs :
Christian Boudreault a contribué à la conceptualisation, a effectué la majorité des calculs et rédigé l'essentiel de l'article, à l'exception de la sous-section 6.3.2.3 et de la section 6.4. Clément Berthière a contribué à la mise en forme définitive de l'article, notamment en intégrant les sections sus-mentionnées. William Witczak-Krempa a supervisé le projet, contribué à sa conceptualisation et participé à la mise en forme définitive de l'article.

Résumé. Partant du boson critique de Lifshitz $(d+1)$-dimensionnel d'exposant dynamique $z = 2$, nous proposons deux déformations non triviales préservant la structure de Rokhsar-Kivelson, par laquelle l'état fondamental est encodé dans une QFT locale d-dimensionnelle sous-jacente. En spécialisant à la dimension spatiale $d = 1$, la première déformation applique l'état fondamental sur l'oscillateur harmonique quantique, produisant un gap pour le boson scalaire. Nous étudions les fonctions de corrélations résultantes et observons une restoration de la *Cluster Decomposition*. La forme particulière de l'état fondamental permet de calculer analytiquement la c-fonction pour l'entropie d'intrication le long d'un flot du groupe de renormalization (RG) de la fonction d'onde. Comme pour les théories de champs conformes (CFT), on observe que la c-fonction est alors strictement décroissante. À partir de cette c-fonction entropique, on obtient le terme de coin pour le boson critique de Lifshitz $z =$ en dimension $2 + 1$, dans la limite d'un angle petit. La seconde déformation est non gaussienne et produit un état fondamental décrit par la mécanique conforme $SL(2, \mathbb{R})$. Cette déformation préserve la symétrie conforme de l'état fondamental et contraint la forme des corrélateurs et de l'entropie d'intrication. Nos calculs fournissent un résultat explicite pour la capacité d'intrication des théories Lifshitz, dont nous offrons une interprétation. Nous prouvons également la séparabilité de la matrice de densité réduite de deux sous-systèmes non connexes pour des fonctions d'onde réelles de RK, ce qui entraîne la disparition de la négativité logarithmique. Enfin, nous commentons sur les relations avec certaines chaînes stoquastiques de spins quantiques, les chaînes de Motzkin et de Fredkin.
Mots-clés. Boson de Lifshitz non compact $z = 2$, structure de Rokhsar-Kivelson, groupe de renormalisation de la fonction d'onde, chaînes de Motzkin et de Fredkin

Abstract. Starting from the $(d + 1)$-dimensional Lifshitz critical boson with dynamical exponent $z = 2$, we propose two nontrivial deformations that preserve the Rokhsar-Kivelson structure where the groundstate is encoded in an underlying, local d-dimensional QFT. Specializing to $d = 1$ spatial dimension, the first deformation maps the groundstate to the quantum harmonic oscillator, leading to a gap for the scalar. We study the resulting correlation functions, and find that Cluster Decomposition is restored. The special form of the groundstate allows to analytically compute the c-function for the entanglement entropy along a renormalization group (RG) flow for the wavefunction, which is found to be strictly decreasing as in conformal field theories (CFTs). From the entropic c-function, we obtain the corner term for the $z = 2$ Lifshitz critical boson in (2+1)D in the small angle limit. The second deformation is non-Gaussian and yields a groundstate described by $SL(2, \mathbb{R})$-conformal quantum mechanics. This deformation preserves the conformal spatial symmetry of the groundstate, and constrains the form of the correlators and entanglement entropy. As a byproduct of our calculations, we obtain explicit results for the capacity of entanglement in Lifshitz theories and discuss their interpretation. We also prove the separability of the reduced density matrix of two disconnected subsystems for real-valued RK wavefunctions, implying the vanishing of logarithmic negativity. Finally, we comment on the relations to certain stoquastic quantum spin chains, the Motzkin and Fredkin chains.
Keywords. Noncompact Lifshitz boson $z = 2$, Rokhsar-Kivelson structure, wavefunction renormalization group, Motzkin and Fredkin chains

6.1 Introduction

Scale invariance plays a central role in the study of dynamical critical phenomena, far-from-equilibrium statistical dynamics, and quantum criticality [148, 60, 196, 237]. Taken isotropic, scale invariance is often enhanced to conformal symmetry, with profound consequences. However, many systems at criticality exhibit anisotropic scaling between space and time, called Lifshitz scaling,

$$t \to \lambda^z t\,, \qquad \mathbf{x} \to \lambda \mathbf{x}\,, \qquad \lambda > 0\,, \tag{6.1}$$

with characteristic dynamical critical exponent $z \neq 1$. Lifshitz scaling is encountered in a variety of contexts, from nonrelativistic mechanics [84, 130, 161, 232] and critical systems [143, 23], to nonrelativistic holographic duality [253, 25, 28, 41, 169] and quantum gravity [151, 150]. In this paper, we are interested in a certain class of nonrelativistic quantum field theories admitting Lifshitz symmetry. Originally introduced as the 'quantum Lifshitz model' in $2+1$ dimensions for $z = 2$ [23], general $(d+1)$-dimensional Lifshitz theories with (even) positive integer z possess the remarkable feature that their groundstate wavefunctional takes a local form, given in terms of the action of a d-dimensional classical model. The normalization factor of the groundstate $|\Psi_0^{(d+1)}\rangle$ is then interpreted as the partition function of the lower-dimensional classical system,

$$\langle \Psi_0^{(d+1)} | \Psi_0^{(d+1)} \rangle = \mathcal{Z}_{\rm cl}^{(d)}\,. \tag{6.2}$$

Quantum states with such a property are referred to as Rokhsar–Kivelson (RK) states [231, 144]. More generally, one can in principle construct a wavefunction for a $(d+1)$-dimensional quantum theory from an arbitrary d-dimensional classical model. This quantum-classical correspondence can actually be made more precise, e.g., for lattice systems [144, 68, 241]. Because of their simple form and relation to a lower-dimensional classical theory, RK states offer a useful and controlled framework to analytically compute, e.g., correlation functions and entanglement measures such as entanglement entropy, which is notoriously hard to achieve in quantum many-body systems in general. Systems poised at a RK point have been extensively studied, in particular their entanglement properties [105, 109, 258, 153, 257, 152, 215, 260, 294, 259, 74, 300, 73, 72, 18, 17].

In this work, we study two distinct deformations of the quantum Lifshitz theory with dynamical exponent $z = 2$ where, in each case, the lower dimensional classical theory reproduced by the groundstate wavefunction is a well-known local theory. One deformation explicitly breaks Lifshitz scaling (6.1) with a mass scale, while the other preserves it. Yet both deformations retain the RK property of Lifshitz groundstates, making these theories rare examples of nonrelativistic theories which admit analytic treatment.

This paper is organized as follows. In Section 6.2, we review key concepts for Lifshitz theories, and in particular the RK property of their groundstates. We introduce in Section 6.3 a massive deformation preserving the RK property of the Lifshitz groundstate, and then proceed to study this model in $1+1$ dimensions. We present

our results on correlations and entanglement properties of the (massive) theory. We find that Cluster Decomposition, violated in the massless case, is restored by the regulating mass. Along the way, aside from Rényi entropies and mutual information, we compute other entanglement-related quantities : the capacity of entanglement, the entropic c-function, and the sharp limit coefficient of corner entanglement. Our results on the positive-field version of the massless Lifshitz theory are presented in 6.4, where we also discuss its relation to Motzkin and Fredkin spin chains and results in the literature. Section 6.5 is devoted to a non-Gaussian deformation of Lifshitz theory for which the groundstate is described by $SL(2,\mathbb{R})$-conformal quantum mechanics. As we shall see, this deformation preserves the conformal spatial symmetry of the groundstate, and constrains the form of the correlators and Rényi entropies. We conclude in Section 6.6 with a summary of our main results, and give an outlook on future study. Derivation via the replica trick of the Rényi entropy formula for Lifshitz theories can be found in Appendix 6.7.1. We prove in Appendix 6.7.2 the separability of the reduced density matrix of two disconnected subsystems. Finally, Appendix 6.7.3 completes Section 6.5, and this paper.

6.2 Lifshitz critical point

The real, noncompact $(d+1)$-dimensional $z=2$ Lifshitz quantum critical boson is the quantum field theory with Hamiltonian

$$H = \frac{1}{2}\int d^d x \left(\Pi^2 + \kappa^2 (\nabla^2\phi)^2\right), \tag{6.3}$$

with canonical commutation relations $[\phi(x),\Pi(x')] = i\delta(x-x')$. The parameter κ is dimensionless. In the field-eigenstate Schrödinger picture, canonical quantization demands $\Pi(x) = -i\delta/\delta\phi(x)$, as usual. The theory is invariant under $z=2$ Lifshitz scaling (6.1). In addition to the Lifshitz scaling symmetry, and the obvious $\mathbb{Z}_2$ symmetry, this theory is invariant under affine shifts of the field $\phi(x) \to \phi(x) + ax + b$. This is also called polynomial shift symmetry.

6.2.1 Rokhsar–Kivelson structure

The Hamiltonian (6.3) is quadratic in the operators

$$A(x) = \frac{1}{\sqrt{2}}\left(i\Pi(x) - \kappa\nabla^2\phi\right), \tag{6.4}$$

as it is easily verified that

$$H = \frac{1}{2}\int d^d x \,\{A^\dagger(x), A(x)\}. \tag{6.5}$$

Note that because $\Pi(x)$ is Hermitian, $A^\dagger(x)$ is obtained from (6.4) by the single replacement $i \to -i$. Alternatively, it will be convenient to diagonalize the Hamiltonian to the normal-ordered form

$$H = \int d^d x \; A^\dagger(x)A(x) + E_{\text{vac}}, \tag{6.6}$$

where $E_{\text{vac}} = \frac{1}{2}\int d^dx[A(x), A^\dagger(x)] = -\frac{\kappa}{2}\int d^dx\, \nabla_x^2\delta^d(x-y)|_{x=y}$ is a positive, UV-divergent multiple of the identity. As such, it can be considered as a vacuum-energy shift relating the otherwise identical eigensystems of H and $\int d^dx\, A^\dagger(x)A(x)$ [23]. A groundstate is now found satisfying

$$A(x)|\Psi_0\rangle = 0\,, \quad \forall x\,. \tag{6.7}$$

Positive semidefiniteness of $\int d^dx\, A^\dagger(x)A(x)$ ensures that such a state is indeed a groundstate. The corresponding functional-differential equation, $(\frac{\delta}{\delta\phi} - \kappa\nabla^2\phi)\Psi_0[\phi] = 0$, has nontrivial solution

$$\Psi_0[\phi] = e^{-\frac{1}{2}\int d^dx\, \kappa(\nabla\phi)^2}\,, \tag{6.8}$$

with normalization factor

$$\mathcal{Z} = \langle\Psi_0|\Psi_0\rangle = \int \mathcal{D}\phi(x)\; e^{-\int d^dx\, \kappa(\nabla\phi)^2}. \tag{6.9}$$

One recognizes $\mathcal{Z}$ as the partition function of a d-dimensional free Euclidean scalar field with classical action $S_{\text{cl}}[\phi] = \int d^dx\, \kappa(\nabla\phi)^2$. This local action appearing in Ψ_0 is conformally invariant in d (spatial) dimensions. We thus have an emergent *spatial* conformal symmetry in the groundstate of the parent Hamiltonian H. We emphasize that S_{cl} is only inherent to Ψ_0, and does not coincide with the action of the parent Hamiltonian H. (A relationship between these actions can be established via stochastic quantization [92].) Dimensionlessness of S_{cl} requires that

$$\dim\phi = (\text{length})^{-\frac{d}{2}+1}, \tag{6.10}$$

and Lifshitz scaling in turn implies

$$\dim\Pi = (\text{length})^{-\frac{d}{2}-1}. \tag{6.11}$$

Equivalently, the dimension of H is $(\text{length})^{-2}$ as expected from the Lifshitz scaling $t \sim x^z$. For simplicity, we will mostly consider the case $d = 1$, for which S_{cl} is the Euclidean action of a free nonrelativistic particle. We will derive certain properties of the entanglement entropy of the $d = 2$ theory that follow from our $d = 1$ results in Section 6.3.3. Using the Gaussian propagators of this underlying theory,

$$\langle\phi', x'|\phi, x\rangle = \sqrt{\frac{\kappa}{\pi(x'-x)}}e^{-\frac{\kappa(\phi'-\phi)^2}{x'-x}}\,, \tag{6.12}$$

with $x' > x$, one can compute groundstate correlation functions, and Rényi entanglement entropies [72].

In this work, we perform two distinct deformations of the Lifshitz point preserving the Rokhsar–Kivelson structure, that is, where one groundstate is of the form

$$\Psi_0[\phi] = e^{-\frac{1}{2}S_{\text{cl}}[\phi]}\,, \tag{6.13}$$

for some *local* Euclidean action $S_{\rm cl}[\phi]$, because the Hamiltonian maintains a form quadratic in the operators $A(x) = \frac{1}{\sqrt{2}}\left(\frac{\delta}{\delta\phi(x)} + \frac{\delta(S_{\rm cl}[\phi]/2)}{\delta\phi(x)}\right)$. Clearly, positive semidefiniteness is preserved for any deformation of the type

$$\frac{1}{2}S_{\rm cl} \mapsto \frac{1}{2}S_{\rm cl} + \Lambda\,, \tag{6.14}$$

where the deformations Λ will be real and local to ensure reality and locality of the action. With $A(x)$ mapped to

$$A'(x) = A(x) + \tfrac{\delta}{\delta\phi(x)}\Lambda = e^{-\Lambda}A(x)e^{\Lambda}\,, \tag{6.15}$$

we see that (normalizable) states annihilated either by the $A(x)$'s or the $A'(x)$'s are related under the transformation $\Psi_0' = e^{-\Lambda}\Psi_0$:

$$A(x)\Psi_0[\phi] = 0 \Longleftrightarrow A'(x)\Psi_0'[\phi] = 0\,. \tag{6.16}$$

Such states, if any, must be groundstates of their respective Hamiltonians. In Section 6.3 we consider a deformation that breaks the emergent conformal symmetry of $S_{\rm cl}[\phi]$ with a (mass) scale, whereas in Section 6.5 we consider a nontrivial deformation which preserves this symmetry when $d = 1$. (The affine field-shift symmetry is lost in both cases, and will play no further part.)

We emphasize that the new Hamiltonian H' is generally *not* the result of a simple frame transformation, as $H' \neq e^{-\Lambda}He^{\Lambda}$. ($H'$ and $e^{-\Lambda}He^{\Lambda}$ agree if and only if Λ is imaginary-valued.)

6.3 Deformation by a mass term

We now explicitly break the Lifshitz scaling symmetry of (6.3) with a length scale $1/m$, setting $\Lambda[\phi] = \frac{1}{2}\int d^dx\, m^2\phi(x)^2$, so that the Euclidean action defining the groundstate becomes

$$S_{\rm cl}[\phi] = \int d^dx\left(\kappa(\nabla\phi)^2 + m^2\phi^2\right), \tag{6.17}$$

and

$$A(x) = \frac{1}{\sqrt{2}}\left(\frac{\delta}{\delta\phi(x)} - \kappa\nabla^2\phi + m^2\phi\right). \tag{6.18}$$

Expression (6.17) is seen to correspond to the Euclidean action of a massive relativistic scalar (Klein-Gordon). The original Lifshitz Hamiltonian (6.3) is thereby deformed to

$$H_{\rm mass} = H_{\rm Lif} + \frac{1}{2}\int d^dx\left(2\kappa m^2(\nabla\phi)^2 + m^4\phi^2\right). \tag{6.19}$$

The Hamiltonians $H_{\rm mass} = \frac{1}{2}\int d^dx\ \{A^\dagger(x), A(x)\}$ and $H^{\rm normal}_{\rm mass} = \int d^dx\ A^\dagger(x)A(x)$ differ by $\frac{1}{2}\int d^dx[A^\dagger(x), A(x)] = \frac{1}{2}{\rm tr}(\kappa\nabla^2 - m^2)$, a UV-divergent multiple of the

identity. Their eigensystems are thus identical up to an infinite zero-point energy shift, with common groundstate

$$\Psi_0[\phi] = e^{-\frac{1}{2}\int d^dx\left(\kappa(\nabla\phi)^2+m^2\phi^2\right)}\,. \tag{6.20}$$

Indeed it is clear that $A(x)|\Psi_0\rangle = 0$. Due to the scale m, the new groundstate has lost conformal symmetry. $H_{\rm mass}$ has positive-infinite groundstate energy $E_{\rm vac} = \frac{1}{2}{\rm tr}(-\kappa\nabla^2+m^2)$, whereas the normal-ordered form has groundstate energy zero. The new terms in (6.19) are both relevant under RG, and the theory flows to the massive relativistic scalar in the IR. Let us be more precise : the usual RG transformation on the theory sends $x_i \to bx_i$ $(1 \le i \le d)$ and $t \to b^z t$, with $z = 2$. The scaling dimensions of $(\nabla\phi)^2$ and ϕ^2 are distinct, meaning that the fine-tuning between the mass-dependent terms in (6.19) would be lost under RG. The key to preserve the RK structure is to consider an alternative RG transformation that acts on the groundstate wavefunction (6.20), not directly on the Hamiltonian. This wavefunction RG transformation now acts on the $(0+d)$D relativistic massive Euclidean scalar. All coordinates are dilated by the same factor, $x_i \to bx_i$. The mass is relevant, and leads to the usual infinite mass trivial IR fixed point in $(0+d)$D. The wavefunction RG transformation corresponds to the trajectory in theory space where m increases in (6.19). In other words, the trajectory in the space of Hamiltonians is obtained by constructing the parent Hamiltonian for the groundstate (6.20).

The normalization factor for Ψ_0 coincides with the Euclidean partition function of the d-dimensional massive scalar,

$$\mathcal{Z} = \langle\Psi_0|\Psi_0\rangle = \int \mathcal{D}\phi\; e^{-\int d^dx\left(\kappa(\nabla\phi)^2+m^2\phi^2\right)}. \tag{6.21}$$

The (normalized) density matrix operator corresponding to Ψ_0 is

$$\rho = \frac{1}{\mathcal{Z}}\int \mathcal{D}\phi\mathcal{D}\phi'\; e^{-(S_{\rm cl}[\phi]+S_{\rm cl}[\phi'])/2}|\phi\rangle\langle\phi'|\,. \tag{6.22}$$

We now specialize to $d = 1$ with Dirichlet boundary conditions (BC) : $\phi(0) = 0 = \phi(L)$, but many of our results will also apply to other choices of boundary conditions. Apart from simplicity, one motivation for this choice is the search for the elusive effective field theories of the Motzkin and Fredkin spin chains [49, 86] whose unique, highly entangled, frustration-free groundstates reproduce the logarithmic scaling of entanglement entropy found in critical spin chains. When ϕ is used to represent a "height field" for the spin variables, i.e. $\partial_x\phi(x) = S_z(x)$, the groundstate property $S_z^{\rm tot} = 0$ translates into Dirichlet boundary conditions (up to a constant) on ϕ. The *positive*-field version of (6.3) is a parent Hamiltonian for the *positive*-field version of (6.8), which captures many spin and entanglement features of the Motzkin and Fredkin groundstates [73, 72, 205], while having a markedly different excitation spectrum [73, 72]. We note that bulk properties are expected not to depend on the field positivity constraint [73, 72].

In one dimension, $\mathcal{Z}$ is the partition function of a single particle with Euclidean Lagrangian $\mathcal{L}_m = \kappa(\partial_x\phi)^2 + m^2\phi^2$, i.e. a quantum harmonic oscillator of "mass" $M = 2\kappa$ and "frequency"

$$\omega = m/\sqrt{\kappa}\,. \tag{6.23}$$

The standard propagator of the Euclidean oscillator,

$$\langle \phi', x' | \phi, x \rangle = \int_{\phi(x)=\phi}^{\phi(x')=\phi'} \mathcal{D}\phi \; e^{-\int_x^{x'} dx \; \mathcal{L}_m} \tag{6.24}$$

is [155]

$$\begin{aligned} \langle \phi', x' | \phi, x \rangle = & \sqrt{\frac{\kappa\omega}{\pi \sinh \omega(x'-x)}} \\ & \times \exp\left[\frac{-\kappa\omega \left((\phi^2 + \phi'^2) \cosh \omega(x'-x) - 2\phi\phi' \right)}{\sinh \omega(x'-x)} \right], \end{aligned} \tag{6.25}$$

which reduces to (6.12) in the limit $m = \omega = 0$. Vacuum expectation values of local operators $\hat{\mathcal{O}}_x|\phi\rangle$ can be expressed in terms of the propagator associated to Ψ_0 via the mapping $\langle \Psi_0 | \Psi_0 \rangle = \int_{\mathrm{BC}} \mathcal{D}\phi \; e^{-\int d^d x S_{\mathrm{cl}}[\phi]}$. In particular we obtain from (6.22)

$$\langle \phi(x) \rangle = \mathrm{Tr}[\rho \hat{\phi}(x)] = \int_{-\infty}^{\infty} d\phi \; \phi \; f_1(\phi, x) \,, \tag{6.26}$$

with single-point probability distribution $f_1(\phi, x) = \mathcal{Z}^{-1} \langle 0, L | \phi, x \rangle \langle \phi, x | 0, 0 \rangle$. Since f_1 is symmetric under $\phi \to -\phi$, field and gradient have vanishing vacuum expectation values,

$$\begin{aligned} \langle \phi(x) \rangle &= \int_{-\infty}^{\infty} d\phi \; \phi \; f_1(\phi, x) = 0 \,, \\ \langle \partial_x \phi(x) \rangle &= \partial_x \langle \phi(x) \rangle = 0 \,. \end{aligned} \tag{6.27}$$

Other boundary conditions not breaking $\mathbb{Z}_2$ symmetry, periodic conditions for instance, will have the same vanishing expectations.

We may formally define the reduced density matrix on the single-point set $\{x\}$ as

$$\rho(x) = \int_{-\infty}^{\infty} d\phi \; f_1(\phi, x) |\phi, x\rangle \langle \phi, x| \,. \tag{6.28}$$

Then for a local operator $\hat{\mathcal{O}}_x$ as above, we may write $\langle \hat{\mathcal{O}}_x \rangle = \mathrm{Tr}_{\{x\}}[\rho(x) \hat{\mathcal{O}}_x] = \int_{-\infty}^{\infty} d\phi \; f_1(\phi, x) \langle \phi, x | \hat{\mathcal{O}}_x | \phi, x \rangle$. The argument is readily generalized to any product of local operators.

6.3.1 Correlations in the groundstate

In Appendix 6.7.2, we show that the reduced density matrix $\rho_{A\cup B}$ is a separable mixed state for any disconnected subsystems A, B. Therefore, A and B are not entangled, and the correlations left in $\rho_{A\cup B}$ do not arise from entanglement [213, 117, 3, 4]. As A, B come into contact, the result does not hold anymore and quantum-driven contact terms are expected. For operators $\hat{\mathcal{O}}_1, \hat{\mathcal{O}}_2$ local at x_1, x_2, respectively, we define

$$\rho(x_1, x_2) = \int_{-\infty}^{\infty} d\phi_1 d\phi_2 \; f_2 \bigotimes_{i=1,2} |\phi_i, x_i\rangle \langle \phi_i, x_i| \,, \tag{6.29}$$

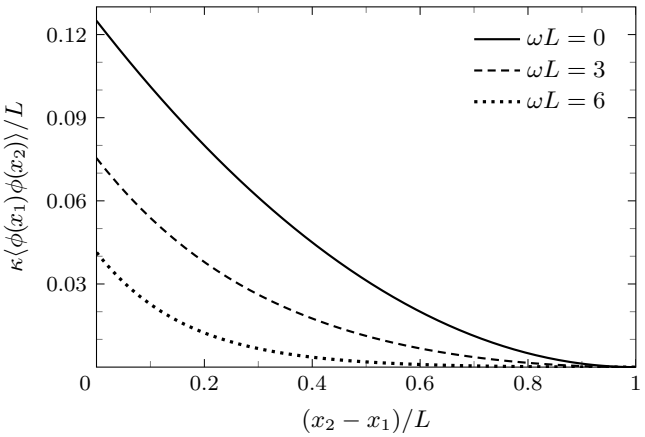

FIGURE 6.1 – Correlator $\frac{\kappa}{L}\langle\phi(x_1)\phi(x_2)\rangle$ from (6.31), for a central interval of length x_2-x_1, and for different values of ωL. Correlators vanish when $x_2-x_1\to L$ due to the boundary condition $\phi(0)=0=\phi(L)$.

with two-point probability distribution

$$\begin{aligned} &f_2(\phi_1,\phi_2,x_1,x_2)\\ &\quad=\mathcal{Z}^{-1}\langle 0,L|\phi_2,x_2\rangle\langle\phi_2,x_2|\phi_1,x_1\rangle\langle\phi_1,x_1|0,0\rangle. \end{aligned} \tag{6.30}$$

Then $\langle\hat{\mathcal{O}}_1\hat{\mathcal{O}}_2\rangle=\mathrm{Tr}_{\{x_1,x_2\}}[\rho(x_1,x_2)\hat{\mathcal{O}}_1\hat{\mathcal{O}}_2]$. The function f_2 is not symmetric under the *individual* operations $\phi_i\to-\phi_i$. The field correlator and gradient correlator at positions $x_1<x_2$ are found to be

$$\langle\phi(x_1)\phi(x_2)\rangle = \frac{\sinh\omega x_1\sinh\omega(L-x_2)}{2\kappa\omega\sinh\omega L}\,, \tag{6.31}$$

$$\langle\partial_{x_1}\phi(x_1)\partial_{x_2}\phi(x_2)\rangle = -\frac{\omega\cosh\omega x_1\cosh\omega(L-x_2)}{2\kappa\sinh\omega L}\,. \tag{6.32}$$

The correlators $\frac{\kappa}{L}\langle\phi(x_1)\phi(x_2)\rangle$ and $\kappa L\langle\partial\phi(x_1)\partial\phi(x_2)\rangle$ for a centered interval of length x_2-x_1 are displayed in Figs. 6.1 and 6.2 in terms of the dimensionless variable $(x_2-x_1)/L$. Note that these functions depend on ω and L only through the combination ωL. Because single-point field expectations vanish, we can identify two-point functions $\langle\phi_1\phi_2\rangle$ and connected correlators $C_{\phi_1,\phi_2}=\langle\phi_1\phi_2\rangle-\langle\phi_1\rangle\langle\phi_2\rangle$ for this model. By the same token, we identify $\langle\partial\phi_1\partial\phi_2\rangle$ and $C_{\partial\phi_1,\partial\phi_2}=\langle\partial\phi_1\partial\phi_2\rangle-\langle\partial\phi_1\rangle\langle\partial\phi_2\rangle$.

In the massless limit, $\omega L\to 0$, we recover the results

$$\langle\phi(x_1)\phi(x_2)\rangle = \frac{x_1(L-x_2)}{2\kappa L}\,, \tag{6.33}$$

$$\langle\partial_{x_1}\phi(x_1)\partial_{x_2}\phi(x_2)\rangle = -\frac{1}{2\kappa L}\,. \tag{6.34}$$

To obtain the thermodynamic limit, the field correlator is best written in the following form :

$$\langle\phi(x_1)\phi(x_2)\rangle = \frac{L}{8\kappa}-\frac{x_2-x_1}{4\kappa}-\frac{(x_1-\frac{L}{2})(x_2-\frac{L}{2})}{2\kappa L}\,. \tag{6.35}$$

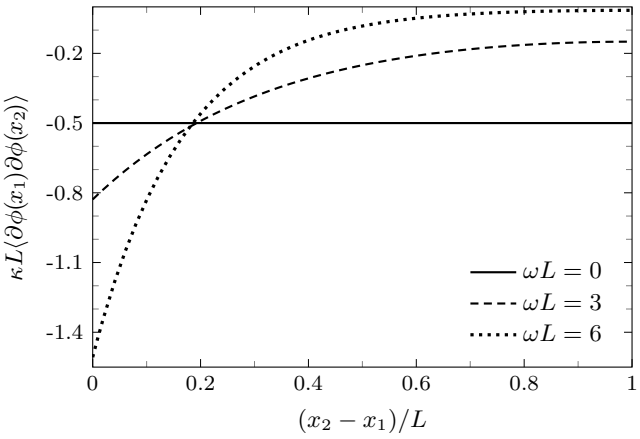

FIGURE 6.2 – Correlator $\kappa L\langle\partial\phi(x_1)\partial\phi(x_2)\rangle$ from (6.32), for a central interval of length x_2-x_1, and for different values of ωL.

The first term is a divergent contact term or bulk second moment $\langle\phi(L/2)^2\rangle$. The universal, second term is translation-invariant and linearly increasing (in absolute value) with separation, as should be since ϕ scales as $(\text{length})^{1/2}$. The final term vanishes when deep enough in the bulk. We thus conclude that the critical Lifshitz boson ($\omega=0$) violates Cluster Decomposition. Note that $\langle\partial_{x_1}\phi(x_1)\partial_{x_2}\phi(x_2)\rangle_{\text{massless}}$ is constant, and vanishes in the thermodynamic limit,

$$\lim_{L\to\infty}\langle\partial_{x_1}\phi(x_1)\partial_{x_2}\phi(x_2)\rangle_{\text{massless}}=0\,, \tag{6.36}$$

as observed in [73, 72] where it meant that bulk S_z spins are uncorrelated in the continuous limit of the groundstate of the Motzkin and Fredkin chains, a result also consistent with the discrete case [205].

Expression (6.33) confirms that Cluster Decomposition is not satisfied in the massless case. On the other hand, we see from (6.31) that Cluster Decomposition is satisfied when $\omega>0$ (or $\omega\gg 1/L$ for a finite system). Looking deep into the bulk where $\omega x_1\to\infty$ and $\omega(L-x_2)\to\infty$, we obtain for all values of $\omega(x_2-x_1)$,

$$\langle\phi(x_1)\phi(x_2)\rangle=\frac{1}{4\kappa\omega}e^{-\omega(x_2-x_1)}\,, \tag{6.37}$$

and

$$\langle\partial_{x_1}\phi(x_1)\partial_{x_2}\phi(x_2)\rangle=-\frac{\omega}{4\kappa}e^{-\omega(x_2-x_1)}\,, \tag{6.38}$$

satisfying Cluster Decomposition at large separations. Connected correlations with an exponential bound $Ce^{-m(x_2-x_1)}$ are characteristic of a gapped phase with mass m. We identify $\xi=\omega^{-1}=\sqrt{\kappa}/m$ as the correlation length, and recover the quantum critical Lifshitz boson in the massless limit. Expressions (6.37) and (6.38) do not depend on the choice of boundary conditions. We are surprised to find that when the correlation length is infinite (requiring both $\omega\to 0$ and $L\to\infty$ to be effective), the theory develops an IR divergence in bulk correlations. The corresponding limit

is singular :

$$\lim_{L\to\infty}\lim_{\omega\to 0}\langle\phi(x_1)\phi(x_2)\rangle \sim \frac{L}{8\kappa} - \frac{x_2-x_1}{4\kappa}\,, \tag{6.39}$$

and

$$\lim_{\omega\to 0}\lim_{L\to\infty}\langle\phi(x_1)\phi(x_2)\rangle \sim \frac{1}{4\kappa\omega} - \frac{x_2-x_1}{4\kappa}\,, \tag{6.40}$$

from which we may single out the nonsingular subleading behavior of the correlator, $\langle\phi(x_1)\phi(x_2)\rangle_{\rm regular} = -(x_2-x_1)/4\kappa$. A similar phenomenon is observed in the mutual information (see (6.62) and (6.63)).

We emphasize that for $x_1 < x_2$ deep within the bulk,

$$\langle\partial_{x_1}\phi(x_1)\partial_{x_2}\phi(x_2)\rangle = \begin{cases} 0\,, & m=0\,,\\ -\frac{\omega}{4\kappa}e^{-\omega(x_2-x_1)}\,, & m>0\,. \end{cases} \tag{6.41}$$

It is a remarkable fact that, contrary to intuition, this groundstate correlator becomes trivial only for the *massless* theory. Indeed, a mass for ϕ corresponds to a gap in the theory, revealed by an exponential decay of correlations in the observables. In the massless limit of large systems, the exponential decay is usually replaced by power-law on separation as the correlation length diverges, resulting in *enhanced* correlations. The vanishing of the self-correlations of an operator as the gap closes is unorthodox.

6.3.2 Entanglement in the groundstate

We consider a finite bipartition $\{A,B\}$ of a one-dimensional system. By analogy with the "entangling surface" in higher dimensions, we call "surface" the multiple-point boundary between A and B, that is $\partial A = \{x_1, x_2, \ldots, x_M\}$. The Rényi entanglement entropies are defined as

$$S_n(A) = \frac{1}{1-n}\log \mathrm{Tr}\,\rho_A^n\,, \tag{6.42}$$

where ρ_A is the reduced density matrix on subsystem A. The entanglement entropy is obtained from (6.42) by taking the replica limit $n\to 1$. In Appendix 6.7.1 we recast the replica trick in terms of the $(0+1)$-dimensional partition function $\langle\Psi_0|\Psi_0\rangle = \int_{\rm BC}\mathcal{D}\phi\; e^{-\int d^dx S_{\rm cl}[\phi]}$. We find that the bipartite Rényi entropies are given by

$$S_n(A) = \frac{1}{1-n}\log\left[\epsilon^{(n-1)M/2}\int d\boldsymbol{\phi}\;\left[f_M(\boldsymbol{\phi},\mathbf{x})\right]^n\right], \tag{6.43}$$

where $f_M(\boldsymbol{\phi},\mathbf{x}) = \mathcal{Z}^{-1}\langle 0,L|\phi_M,x_M\rangle\cdots\langle\phi_1,x_1|0,0\rangle$, and ϵ is a length scale readily identified as a UV cutoff. In a lattice regularization, for instance, ϵ is naturally present as the lattice constant. For the massive deformation with Dirichlet conditions, the Gaussian propagators (6.25) give $f_M(\boldsymbol{\phi},\mathbf{x}) = Ce^{-\boldsymbol{\phi}^T K\boldsymbol{\phi}}$ with normalization factor $C = f_M(\mathbf{0},\mathbf{x}) = \sqrt{\det K/\pi^M}$. Integrating (6.43) over $\mathbb{R}^M$, we find

$$S_n = -\log\frac{\mathcal{Z}_D^{AB}}{\mathcal{Z}} + \frac{1}{2}\log\frac{1}{\epsilon^M} - \frac{M}{2(1-n)}\log n\,, \tag{6.44}$$

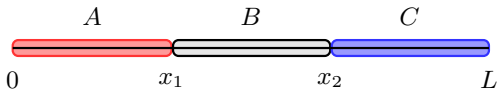

FIGURE 6.3 – Some system partitions. The single-point surface $\{x_1\}$ generates the bipartition $\{A, B \cup C\}$ with Rényi entropies $S_n(A)$ given in (6.46). The two-point surface $\{x_1, x_2\}$ generates the bipartition $\{A \cup C, B\}$ with Rényi entropies $S_n(B)$ found in (6.47).

where

$$\frac{\mathcal{Z}_D^{AB}}{\mathcal{Z}} = \frac{1}{\mathcal{Z}}\langle 0, L|0, x_M\rangle \cdots \langle 0, x_1|0, 0\rangle = f_M(\mathbf{0}, \mathbf{x}) \tag{6.45}$$

is a product of propagators with Dirichlet conditions on ∂A, normalized by the free propagator $\mathcal{Z} = \langle 0, L|0, 0\rangle$. Note that $\mathcal{Z}_D^{AB} = \mathcal{Z}_D^A \mathcal{Z}_D^B$. We see that S_n is independent of the Rényi index, up to a constant term. We have computed the bipartite Rényi entanglement entropy from first principles, and obtained (6.44). This is a generalization to our $(1+1)$-dimensional case of the celebrated Fradkin-Moore formula $S = -\log(Z_D^{AB}/Z_F)$ for the bipartite entanglement entropy of $(2+1)$-dimensional conformal quantum critical theories [105], which have the RK property and whose groundstates correspond to a lower-dimensional CFT_2. Then $Z_D^{AB} = Z_D^A Z_D^B$ is the lower-dimensional CFT_2 partition function of configurations with Dirichlet conditions on ∂A, and Z_F is the partition function of free configurations. For the massive deformation of the $(1+1)$-dimensional Lifshitz theory, however, the lower-dimensional theory is not conformal invariant, and is only $(0+1)$-dimensional, so that partition functions are simple quantum mechanical propagators. We note that expression (6.44) at finite mass generalizes naturally to other dimensions.

6.3.2.1 Rényi entanglement entropies

For a single-point surface separating the "boundary interval" A from the rest of the system as in Fig. 6.3, we find the Rényi entropies

$$S_n(A) = \frac{1}{2}\log\frac{\sinh\omega L_A \sinh\omega(L-L_A)}{\omega\epsilon\sinh\omega L} + b_1(n)\,, \tag{6.46}$$

while for a two-point surface separating the bulk interval B from the rest of the system as in Fig. 6.3, we obtain

$$S_n(B) = \frac{1}{2}\log\frac{\sinh\omega L_A \sinh\omega L_B \sinh\omega L_C}{(\omega\epsilon)^2\sinh\omega L} + b_2(n)\,, \tag{6.47}$$

where the constant $b_M(n) = \frac{M}{2}\log\frac{\pi}{\kappa} - \frac{M}{2(1-n)}\log n$, with $M = 1$ and $M = 2$ in (6.46) and (6.47), respectively. The leading universal terms are indeed independent of the Rényi index n. These expressions are in perfect agreement with the exact calculation over the discrete versions of the Hamiltonian (6.19) and groundstate (6.20). Once all interaction terms between a discrete subsystem and its complement have been

singled out, one can apply the replica trick and compute a finite number of Gaussian integrals, yielding (6.44) in the continuous limit, up to constant terms.

Let us now consider different limiting regimes of the Rényi entropies. First, in the massless case, expressions (6.46) and (6.47) reduce to

$$S_n(A) = \frac{1}{2}\log\frac{L_A(L-L_A)}{\epsilon L} + b_1(n)\,, \tag{6.48}$$

and

$$S_n(B) = \frac{1}{2}\log\frac{L_A L_B L_C}{\epsilon^2 L} + b_2(n)\,, \tag{6.49}$$

respectively. The entropy (6.49) of a bulk interval shows an IR divergence, while that of a boundary interval (6.48) does not. Formula (6.48) agrees with that obtained in [18] for the discrete massless theory, and matches (B13) of reference [73]. The massless limit of (6.47), given by (6.49), however, does not agree with the results of [73]. In fact, our entropy formula (6.43) is different from the one used in [73]. We will say more about this below (6.61).

For large systems we find

$$S_n(A) \underset{L\to\infty}{\longrightarrow} \frac{1}{2}\log\frac{\sinh\omega L_A}{\omega\epsilon} - \frac{1}{2}\omega L_A + \text{const}\,, \tag{6.50}$$

and

$$S_n(B) \underset{L_A,L_C\to\infty}{\longrightarrow} \frac{1}{2}\log\frac{\sinh\omega L_B}{(\omega\epsilon)^2} - \frac{1}{2}\omega L_B + \text{const}\,. \tag{6.51}$$

Here, the constant has the general form $b_M - \frac{Q-1}{2}\log 2$ when Q subintervals have infinite length. At low momenta, quantum fluctuations are suppressed by the effective mass and the groundstate disentangles, meaning that entanglement is localized in the smallest length scales, and only the fine-tuning of mass to zero will entangle the largest scales. A plot of $S_n(B)$ as a function of ωL_B is given in Figure 6.4. In the low mass limit, $\omega L_B \to 0$, the entropy behaves like

$$S_n(B) = \frac{1}{2}\log\omega L_B - \frac{1}{2}\omega L_B - \log\epsilon\omega + \text{const}\,, \tag{6.52}$$

departing from the area-law behavior by an unbounded logarithmic dependence on subsystem length, characteristic of a gapless system. The prefactor is independent of n. In the opposite $\omega L_B \to \infty$ limit (large mass or large subinterval),

$$S_n(B) = -\log\epsilon\omega + \text{const} = \log\frac{\xi}{\epsilon} + \text{const}\,. \tag{6.53}$$

This is an area law $S_n \sim C_{\text{upper bound}}$ for the gapped system, the general expression for the upper bound being $C_{\text{upper bound}} = \frac{M}{2}\log\frac{\xi}{\epsilon} + \text{const}$, from (6.44), where the number of surface points M is the one-dimensional analogue of a surface area. The entropy is independent of L_B in this limit, as expected for massive excitations. Recalling that the correlation length $\xi = \omega^{-1} = \sqrt{\kappa}/m$, the upper bound is seen to be a decreasing function of the mass.

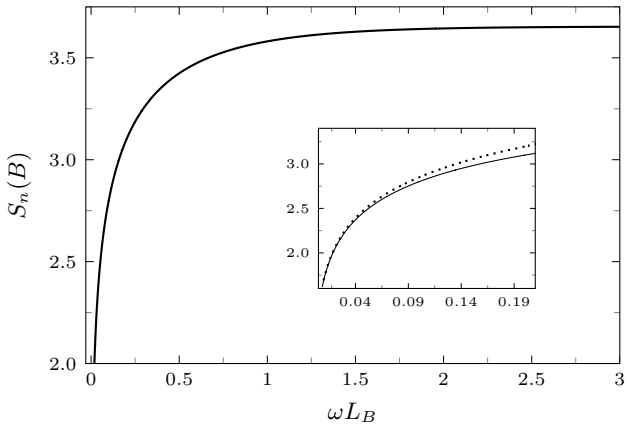

FIGURE 6.4 – Bulk interval Rényi entropy $S_n(B)$ from (6.51), as a function of dimensionless subsystem mass-length ωL_B. The order n and mass-scale ω are unspecified, contributing only an overall constant. An area-law $S_n \sim C_{\text{upper bound}}$ is observed at large values of ωL_B, suppressing dependence on L_B and maintaining only a mass-scale dependence $C_{\text{upper bound}} = \log(\xi/\epsilon) + \text{const.}$, see (6.53). **Inset :** Small ωL_B behavior of S_n compared with right-hand side of (6.52) (dashed) showing logarithmic deviation from an area-law in the massless case.

Unexpectedly, we observe a close connection between (6.51) and the entanglement entropy of a single bulk interval of length L_B (and surface area $M = 2$) in a finite temperature CFT_2 [53],

$$S_1^{\text{CFT}}(L_B, T) = \frac{c}{3} \log \frac{\sinh \pi L_B T}{\pi \epsilon T} + \text{const}\,. \tag{6.54}$$

With the identification $c = 3/2$ and $\pi T = \omega = m/\sqrt{\kappa}$, we can rewrite (6.51) as

$$S_n^{\text{Lif}}(L_B, m) = S_1^{\text{CFT}}(L_B, T) - S_1^{\text{CFT}}(L_B, \infty) + \dots\,, \tag{6.55}$$

where $S_1^{\text{CFT}}(L_B, \infty) = \frac{c}{3}\pi L_B T$ stands for the high temperature asymptotic behavior of S_1^{CFT}, that is, the thermal entropy. The ellipsis stands for nonuniversal terms independent of L_B. The moderately massive Lifshitz theory thus has the entanglement entropy of a moderately hot CFT_2, $S_n^{\text{Lif}}(L_B, m) \sim S_1^{\text{CFT}}(L_B, T)$ for small T, m. To our knowledge, only the correspondence between the massless Lifshitz theory and zero temperature CFT_2 had been observed so far.

6.3.2.2 Mutual information

Expression (6.44) enables us to give the analytic form of the mutual information $I_n(A : B) = S_n(A) + S_n(B) - S_n(A \cup B)$ between disconnected subsystems A and B,

$$I_n(A : B) = \log \frac{f_{M_A+M_B}(\mathbf{0}, \mathbf{x}_A \cup \mathbf{x}_B)}{f_{M_A}(\mathbf{0}, \mathbf{x}_A) f_{M_B}(\mathbf{0}, \mathbf{x}_B)}\,, \tag{6.56}$$

where the M_A surface points of A are positioned at $\mathbf{x}_A$, the M_B surface points of B are positioned at $\mathbf{x}_B$, and $\mathbf{x}_A \cap \mathbf{x}_B = \varnothing$. A graphical representation of formula (6.56) for two bulk intervals A, B is given in Fig. 6.5**a**. A graphical example pertaining to another partition is provided in Fig. 6.5**b**, which serves to illustrate a very peculiar property of the (massive) Lifshitz groundstate, namely that the mutual information $I(A:B)$ is insensitive to any component of A with no neighbor in B. (In Fig. 6.5**b**, one such component is A_1, with no propagators leaving or reaching its surface points.) The mutual information is universal, as expected, and independent of the Rényi index n, which will be omitted from now on. (Note that formula (6.56) holds whenever a wavefunctional can be mapped to a local action on noncompact fields with propagators that are quadratic forms of the fields, i.e. when $f_M(\boldsymbol{\phi}, \mathbf{x}) = f_M(\mathbf{0}, \mathbf{x}) e^{-\boldsymbol{\phi}^T K \boldsymbol{\phi}}$ for multiple-point surface $\partial = \{x_1, \ldots, x_M\}$, dimensionless field values $\phi_i \in \mathbb{R}$, and normalization factor $f_M(\mathbf{0}, \mathbf{x}) = \sqrt{\det K/\pi^M}$.) For two disconnected bulk intervals as in Fig. 6.5**a** we find

$$I(A:B) = \frac{1}{2} \log \frac{\sinh \omega L_{C_1 \cup A \cup C_2} \sinh \omega L_{C_2 \cup B \cup C_3}}{\sinh \omega L_{C_2} \sinh \omega L} \,, \tag{6.57}$$

which is increasing with the lengths of A, B, and decreasing with the separation L_{C_2}. In particular, $I(A:B) \to 0$ as $\omega L_{C_2} \to \infty$. In the limit $L_{C_1}, L_{C_3} \to \infty$ it becomes

$$I(A:B) = -\frac{1}{2} \log \sinh \omega L_{C_2} + \frac{1}{2} \omega L_{C_2} - \frac{1}{2} \log 2 \,, \tag{6.58}$$

showing that the dependence on L_A and L_B disappears deep in the bulk, regardless of separation. In this limit, we observe a logarithmic divergence at vanishing separations

$$I(A:B) \sim \frac{1}{2} \log \frac{1}{\omega L_{C_2}} \,, \qquad \omega L_{C_2} \to 0 \,, \tag{6.59}$$

and an exponential decay at large separations

$$I(A:B) \sim \frac{1}{2} e^{-2\omega L_{C_2}} \,, \qquad \omega L_{C_2} \to \infty \,. \tag{6.60}$$

Strangely enough, the mutual information does not vanish when the size of A and/or B vanishes. This is in stark contrast with most common theories. In a free fermion CFT_2, for instance, the mutual information between two intervals of length ℓ separated by a distance r is $I_{\text{free fermions}}(\ell, r) = \frac{1}{3} \log \frac{(r+\ell)^2}{r(2\ell+r)}$ [62, 263], which clearly vanishes as ℓ tends to zero. We note that in the massless limit of (6.57), we obtain

$$I(A:B) = \frac{1}{2} \log \frac{(L_{C_1} + L_A + L_{C_2})(L_{C_2} + L_B + L_{C_3})}{L_{C_2} L} \,, \tag{6.61}$$

which does not agree with the result found in [73] where mutual information seems to vanish. In this reference, the reduced density $\rho_{A \cup B}$ is assumed, wrongly we believe, to depend only on the difference fields $\phi_A \equiv \phi_2 - \phi_1$ and $\phi_B \equiv \phi_4 - \phi_3$, where A, B are as in Fig. 6.5**a** and $\phi_i = \phi(x_i)$. The resulting expression is of the form $\rho_{A \cup B} \sim \int \mathcal{D}\phi_A \mathcal{D}\phi_B \, h(\phi_A, \phi_B) |\phi_A \phi_B\rangle\langle\phi_A \phi_B|$, with h a Gaussian function of ϕ_A, ϕ_B.

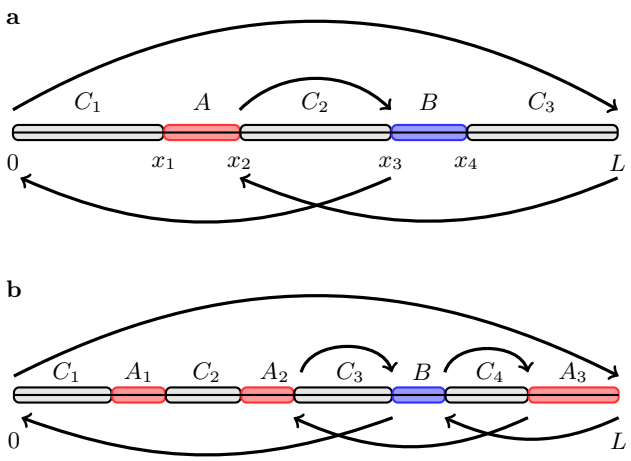

FIGURE 6.5 – Graphical representations of the mutual information between two disconnected bulk intervals A and B. In the general expression (6.56), the numerator contains all simple-interval propagators, including one propagator over the full system. Only those not present in the denominator survive, and are represented as arrows above the axis. The remaining denominator propagators are represented as arrows below the axis (with reversed orientation). The result is a cycle visiting the system's boundary, as well as surface points of one subsystem that are adjacent to a surface point of the other subsystem.

This expression, however, neglects the crucial dependence of $\rho_{A\cup B}$ on the "anchor" $\boldsymbol{\phi} = (\phi_1, \phi_2, \phi_3, \phi_4)$, as derived in (6.155). A similar comment holds for other reduced densities as well. We have already mentioned that the expression obtained in [73] for the entanglement entropy of a single bulk interval is at odds with (the massless limit of) our expression (6.47). We find that far from vanishing, the mutual information diverges like $\frac{1}{2}\log L/L_{C_2}$ deep in the bulk. This is not entirely unexpected since correlators of the massless theory do not possess the cluster decomposition property. It is another manifestation of the bulk IR divergence that develops when the correlation length goes infinite (requiring both $\omega \to 0$ and $L \to \infty$ to be effective). The corresponding limit is singular :

$$\lim_{L_{C_1}, L_{C_3}\to\infty} \lim_{\omega\to 0} I(A:B) \sim \frac{1}{2}\log L - \frac{1}{2}\log L_{C_2}\,, \tag{6.62}$$

and

$$\lim_{\omega\to 0} \lim_{L_{C_1}, L_{C_3}\to\infty} I(A:B) \sim \frac{1}{2}\log\frac{1}{\omega} - \frac{1}{2}\log L_{C_2}\,, \tag{6.63}$$

which to be compare with the divergence in field correlations in (6.39) and (6.40).

We note that the mutual information shared by two boundary intervals, i.e. taking

$L_{C_1} = L_{C_3} = 0$ in (6.61), reduces to [1]

$$I(A:B) = \frac{1}{2}\log\frac{(L-L_A)(L-L_B)}{L(L-L_A-L_B)}\,, \tag{6.64}$$

since $L = L_A+L_B+L_{C_2}$. Then, in the large L limit (or equivalently large separation), the mutual information does vanish as

$$I(A:B) \xrightarrow[L\to\infty]{} \frac{L_A L_B}{2L^2}\,. \tag{6.65}$$

The vanishing of the mutual information between two far apart boundary intervals can be understood by looking at the fields correlator (6.33). For this configuration, the two surface points separating $A\cup B$ from the rest of the system are located at $x_1 = L_A$ and $x_2 = L - L_B$, and the corresponding correlator vanishes in the regime $L \gg L_A, L_B$, i.e. $\langle\phi(x_1)\phi(x_2)\rangle = L_A L_B/(2\kappa L) \to 0$, hence recovering Cluster Decomposition.

Finally, we may also compute the mutual information between two adjacent subsystems A, B (see Fig. 6.5(a) setting L_{C_2} empty) using the entropy (6.47) for an interval in the bulk. One finds

$$I(A:B) = \frac{1}{2}\log\frac{\sinh\omega L_A \sinh\omega L_B \sinh\omega L_{C_1\cup A}\sinh\omega L_{B\cup C_3}}{(\omega\epsilon)^2\sinh\omega L\sinh\omega L_{A\cup B}}, \tag{6.66}$$

where we omitted an unimportant constant. It presents, as expected, a UV divergence. Deep in the bulk, i.e. in the limit $L_{C_1}, L_{C_3} \to \infty$, the mutual information shared by two adjacent subsystems behaves as

$$I(A:B) \sim \frac{1}{2}\log\frac{\sinh\omega L_A\sinh\omega L_B}{(\omega\epsilon)^2\sinh\omega L_{A\cup B}}\,, \tag{6.67}$$

dependent only on L_A and L_B. The massless limit of (6.66) reads

$$I(A:B) = \frac{1}{2}\log\frac{(L_{C_1}+L_A)L_A L_B(L_B+L_{C_3})}{\epsilon^2(L_A+L_B)L}\,, \tag{6.68}$$

which, deep in the bulk, yields

$$I(A:B) \sim \frac{1}{2}\log\frac{L_A L_B}{\epsilon(L_A+L_B)} + \frac{1}{2}\log\frac{L}{\epsilon}\,. \tag{6.69}$$

Taking the massless limit $\omega L_{A/B} \to 0$ from (6.67) instead, one gets

$$I(A:B) \sim \frac{1}{2}\log\frac{L_A L_B}{\epsilon(L_A+L_B)} - \frac{1}{2}\log\omega\epsilon\,. \tag{6.70}$$

1. Coincidentally, the mutual information (6.64) shared by two boundary intervals for the massless Lifshitz theory takes the exact same form (with a prefactor of 3/2) as the mutual information between two intervals separated by a distance r in an infinite system for free fermion CFT_2 [62, 263],

$$I_{\text{free fermions}}(A:B) = \frac{1}{3}\log\frac{(L_A+r)(L_B+r)}{r(L_A+L_B+r)}\,,$$

noticing that $L = L_A + L_B + r$, with $r \equiv L_{C_2}$ in (6.64).

We thus observe both UV and IR divergences in the mutual information between adjacent subsystems. The first term is of the same form as the mutual information and logarithmic negativity between two adjacent intervals in an infinite system for a CFT_2 [54].

6.3.2.3 Capacity of entanglement

We now investigate yet another information theoretic quantity, namely the capacity of entanglement (see, e.g., [85, 167, 212] for recent developments). It was introduced in [291] as the quantum information analogue of the heat capacity for thermal systems. The capacity of entanglement for the reduced density matrix ρ_A may be conveniently defined as

$$C_A = \lim_{n\to 1} n^2 \partial_n^2 \log \mathrm{Tr}\, \rho_A^n = \lim_{n\to 1} n^2 \partial_n^2 (1-n) S_n(A)\,. \tag{6.71}$$

It is seen to characterize the width of the eigenvalue spectrum of the reduced density matrix.

Using expression (6.47) for the Rényi entropy, the capacity of entanglement for the (massive) Lifshitz theory is simply given by

$$C_A = \frac{M}{2}\,. \tag{6.72}$$

We find that the capacity of entanglement is finite, independent of the mass m, follows an area law (the number of surface points M is the one-dimensional analogue of a surface area), and is thus much smaller than the entanglement entropy. The later observation is quite different from CFT results [85] where usually $C_A \sim S_A$.

An interesting take on [85] is that a capacity of entanglement much smaller than entanglement entropy could be interpreted as entanglement being effectively carried by maximally entangled EPR pairs. Conversely, quantum states for which $C_A \sim S_A$ would be better described by randomly entangled pairs of qubits. The capacity of entanglement thus provides insights into the entanglement structure of the groundstates of Lifshitz theories.

For the sake of completeness, let us anticipate the results of Section 6.4 and 6.5 where we study the positive-valued Lifshitz boson and a singular deformation of this theory. For the positive boson, using (6.93) and (6.96), we find the capacity of entanglement to be

$$C_A^{(\mathrm{pos})} = \frac{M}{2} - \Big(5 - \frac{\pi^2}{2}\Big)\,, \tag{6.73}$$

where $M = 1, 2$ corresponds to the number of surface points of A. We conjecture this expression to be valid for $M \geq 1$. For the singular deformation we obtain

$$C_A^{(\nu)} = (\nu + 1/2)^2 \psi^{(1)}(\nu+1) - \nu\,, \tag{6.74}$$

where $\psi^{(n)}(x)$ is the polygamma function of order n, and ν is related to the coupling parameter to the singular potential. This formula was derived for a boundary interval A (i.e. $M = 1$). We conjecture that for general subsystems with M surface points

$$C_A^{(\nu)} = \frac{M}{2} - (\nu + 1/2)\Big(1 - (\nu+1/2)\psi^{(1)}(\nu+1)\Big)\,, \tag{6.75}$$

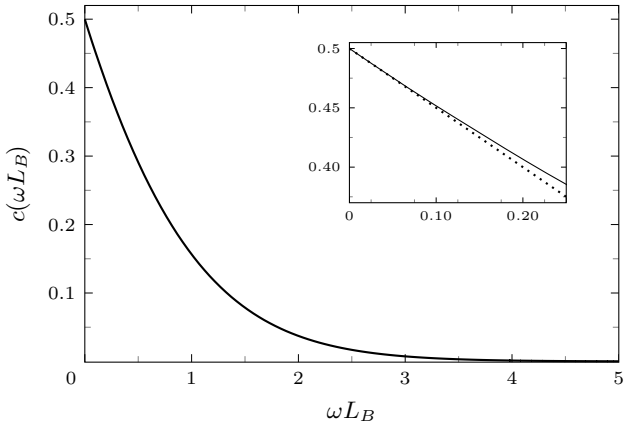

FIGURE 6.6 – Bulk interval c-function, see (6.77), as a function of dimensionless subsystem mass-length ωL_B. **Inset :** Small ωL_B behavior of c compared with right-hand side of (6.78), first line (dashed). The curve tends to the critical value $c = 1/2$.

such that we recover the positive boson result for $\nu = 1/2$ (see Section 6.5). We note that $C_A^{(\nu)} \leq C_A,\ \nu \geq 0$.

6.3.2.4 Entropic c-function

Being universal, i.e. cutoff independent, c-functions are important tools in the study of (unitary) Lorentz-invariant field theories and their RG fixed points, and are known to be monotone decreasing for such theories in two dimensions [295, 63]. The decreasing of the entanglement entropy under the RG flow is a property demonstrably true for relativistic theories [63], but known to admit nonrelativistic exceptions [181]. The entropic c_n-function is defined as

$$c_n(\ell) = \ell \frac{dS_n}{d\ell}\,, \tag{6.76}$$

where S_n is the (Rényi) entanglement entropy of an interval of length ℓ. Regrettably, c-functions are difficult to compute for general theories, and analytical answers are scarce and most explicit results are obtained numerically. Here, however, we are able to analytically compute the entropic c-function of the massive Lifshitz theory.

The entropic c_n-function corresponding to (6.51) is then

$$c(\omega L_B) = \frac{1}{2}\omega L_B(\coth \omega L_B - 1)\,, \tag{6.77}$$

with asymptotics

$$c(\omega L_B) \sim \begin{cases} \dfrac{1}{2} - \dfrac{1}{2}\omega L_B\,, & \omega L_B \ll 1\,, \\ \omega L_B\, e^{-2\omega L_B}\,, & \omega L_B \gg 1\,. \end{cases} \tag{6.78}$$

Note that we have dropped the n-dependence since it plays no role in this theory. A plot is given in Fig. 6.6. Interestingly, it is monotone decreasing under wavefunction

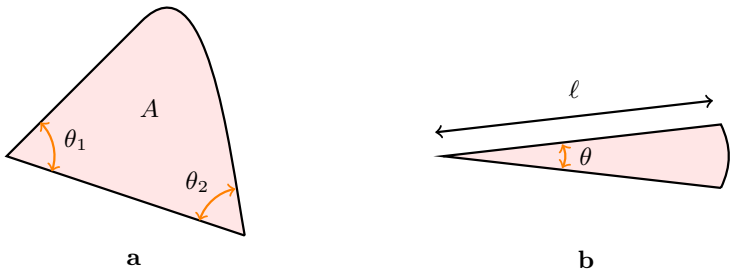

FIGURE 6.7 – **a** Subsystem A with two corners in the one-dimensional boundary, with opening angles θ_1 and θ_2. **b** Sharp corner characterized by the linear dimension ℓ.

RG flow, even though the theory is *not* Lorentz invariant. (In fact, not even Lifshitz invariant.) Lorentz invariance is thus not necessary for the monotone decreasing of the c-function. Identifying the necessary conditions is still an open question.

6.3.3 (2+1)-dimensional corner entanglement by dimensional reduction

With a few important exceptions, quantum critical states in $2+1$ spacetime dimensions have Rényi entropy that scales as

$$S(A) = \mathcal{B}\frac{\ell}{\epsilon} - \sum_i a(\theta_i) \log \frac{\ell}{\epsilon} + \text{const}\,, \tag{6.79}$$

where ℓ is a linear dimension characterizing subregion A, $\epsilon \ll \ell$ is a UV cutoff, and i ranges over corners in the one-dimensional boundary of A, each with opening angle θ_i (see Fig. 6.7 (a)). The subleading logarithmically divergent terms measure the so-called *corner entanglement*, and the corner function $a(\theta)$ is universal and expected to depend only on scale-invariant geometric features of A [64, 67, 104].

In the sharp corner limit $\theta \to 0$ of non-interacting CFTs, the corner function may be analytically computed through dimensional reduction, by first considering a rectangular strip A with length ℓ and width $r \ll \ell$. The corresponding entropy is [65]

$$S(A) = \mathcal{B}\frac{\ell}{\epsilon} - \kappa_c \frac{\ell}{r}\,, \tag{6.80}$$

where κ_c is a universal coefficient also characterizing the mutual information shared by two regions A, B of length ℓ and separation $r \ll \ell$:

$$I(A:B) = \kappa_c \frac{\ell}{r}\,. \tag{6.81}$$

Expressions (6.80) and (6.81) are examples of relations that hold when a region of interest is characterized by m large linear dimensions $\ell_1, \ldots, \ell_m$ and n small linear dimensions $r_1, \ldots, r_n$. Indeed, the entropy of such a region should be extensive in

the large dimensions ℓ_i which may then be considered periodic and Fourier analyzed, effectively reducing the dimension from $m+n$ to n. In the case of the thin rectangular strip A, the dimensional reduction leaves only one space dimension, and recasts κ_c into an integral of the entropic c-function of the lower dimensional QFT [65] :

$$\kappa_c = \frac{1}{\pi}\int_0^\infty dx\, c(x)\,. \tag{6.82}$$

A sharp corner of length ℓ and opening angle $\theta \ll 1$, as in Fig. 6.7 (b), can then be built out of thin strips of length $d\ell'$ and width $\theta\ell'$, such that from (6.80) one obtains

$$S(A) = \int_\epsilon^\ell d\ell' \left(\frac{\mathcal{B}}{\epsilon} - \frac{\kappa_c}{\theta\ell'}\right) = \mathcal{B}\frac{\ell}{\epsilon} - \frac{\kappa_c}{\theta}\log\frac{\ell}{\epsilon}\,. \tag{6.83}$$

Comparison with (6.79) gives

$$a(\theta\to 0) = \frac{\kappa_c}{\theta}\,. \tag{6.84}$$

As it characterizes the (regulator-independent) leading divergence of $a(\theta\to 0)$, κ_c is also called the *sharp limit coefficient*.

We now consider a *nonconformal* theory, namely the $(2+1)$-dimensional $z=2$ real Lifshitz theory, with Lagrangian density

$$\mathcal{L}_2 = \frac{1}{2}\left[\dot\phi^2 - \kappa^2\left(\nabla^2\phi\right)^2\right]. \tag{6.85}$$

Compactifying y to an S_1 of circumference ℓ_y, we decompose the field and the Lagrangian in Fourier modes of momenta $k = 2\pi n/\ell_y$, $n\in\mathbb{Z}$:

$$\begin{aligned}\phi(x,y) &= \sum_k e^{iky}\phi_k(x)\,,\\ \mathcal{L}_2(x,y) &= \sum_{k,k'} e^{i(k'+k)y}\mathcal{L}_{2,k,k'}(x)\,,\end{aligned} \tag{6.86}$$

with

$$\mathcal{L}_{2,k,k'} = \frac{1}{2}\left[\dot\phi_k\dot\phi_{k'} - \kappa^2\phi_k\left(\partial_x^2 - k^2\right)\left(\partial_x^2 - k'^2\right)\phi_{k'}\right]. \tag{6.87}$$

Integrating y out, we obtain $\mathcal{L}_1(x) = \int_{S_1} dy\,\mathcal{L}_2 = \ell_y\sum_k \mathcal{L}_{1,k}$ where

$$\mathcal{L}_{1,k} = \frac{1}{2}\left[|\dot\phi_k|^2 - \kappa^2|\partial_x^2\phi_k|^2 - 2\kappa m_k^2|\partial_x\phi_k|^2 - m_k^4|\phi_k|^2\right], \tag{6.88}$$

and $m_k^2 = \kappa k^2$. Since $\mathcal{L}_{1,k}(\phi_k) = \mathcal{L}_{1,k}(\mathrm{Re}\ \phi_k) + \mathcal{L}_{1,k}(\mathrm{Im}\ \phi_k)$, each decoupled mode ϕ_k is a double copy of the real $(1+1)$-dimensional massive deformation with Hamiltonian (6.19). Notice the fine-tuning of the $|\partial_x\phi_k|^2$ term, just as in (6.19), a direct consequence of the quadraticity of the Hamiltonian $\int d^dx\, A^\dagger A$. We find from the corresponding lower dimensional c-function (6.77), and identity (6.82),

$$\kappa_c = \frac{1}{\pi}\int_0^\infty dx\,\frac{x}{2}(\coth x - 1) = \frac{\pi}{24}\,. \tag{6.89}$$

This result is in agreement with previous results pertaining to the (2+1)-dimensional $z = 2$ Lifshitz theory where, owing to the *spatial* conformal invariance of the groundstate wavefunctional, the corner function may be given in closed-form [105]. It is remarkable that relationship (6.82) between κ_c and the entropic c-function still holds for the $z = 2$ Lifshitz theory, although its scale invariance is Lifshitz (anisotropic) instead of conformal. Interestingly, there is compelling evidence that the corner function can serve as a measure of the number of low-lying degrees of freedom in theories near criticality [105, 164, 51], generalizing the role played by the central charge of $(1 + 1)$-dimensional CFTs.

6.4 Positive boson and Motzkin and Fredkin chains

In this section, we consider the positive-field version of the (massless) Lifshitz groundstate (6.8). Deep inside the bulk, the constraint $\phi \geq 0$ can be ignored such that correlation and entanglement properties are identical to those of the unconstrained theory. We compute the Rényi entropies of a boundary interval and of a bulk interval as an illustration. Finally, we comment on the relation between the positive Lifshitz boson and the Motzkin and Fredkin groundstates, and discuss results in the literature.

6.4.1 Positive Lifshitz boson

The positive-field version of the groundstate (6.8) reads

$$\Psi_0[\phi] = e^{-\frac{1}{2}\int d^d x\, \kappa(\nabla\phi)^2} \prod_x \theta(\phi(x))\,, \tag{6.90}$$

where $\theta(z)$ is the Heaviside function that enforces ϕ to be non-negative. This wavefunctional was conjectured in [73, 72] to be a continuum version of the groundstate of both Motzkin and Fredkin spin chains. The $\phi \geq 0$ constraint is then applied to match that of the lattice Motzkin/Dyck paths that appear in the groundstate.

The corresponding propagator can be expressed in terms of the free one (6.12) as

$$G_{\mathbb{R}^+}(\phi', x'; \phi, x) = G_{\mathbb{R}}(\phi', x'; \phi, x) - G_{\mathbb{R}}(\phi', x'; -\phi, x)\,, \tag{6.91}$$

which explicitly reads

$$G_{\mathbb{R}^+}(\phi', x'; \phi, x) = \sqrt{\frac{\kappa}{\pi(x'-x)}}\left(e^{-\frac{\kappa(\phi'-\phi)^2}{x'-x}} - e^{-\frac{\kappa(\phi'+\phi)^2}{x'-x}}\right). \tag{6.92}$$

By construction, the propagator $G_{\mathbb{R}^+}(\phi', x'; \phi, x)$ vanishes for $\phi = 0$ or $\phi' = 0$. Upon setting Dirichlet boundary conditions at $x = 0, L$, one thus needs to introduce a regulator h, i.e. $\phi(0, t) = \phi(L, t) = h$, which will be sent to zero at the end of the calculations. Furthermore, as the $M(>1)$-point functions for the positive boson are not Gaussian (they are sums of Gaussians), one cannot apply the (generalized) Fradkin-Moore formula (6.44). Instead, we compute the Rényi entropies directly from (6.43).

For a boundary interval A, as in Fig. 6.3, it is straightforward to find

$$S_n(A) = \frac{1}{2}\log\frac{L_A(L-L_A)}{\epsilon L} + b(n)\,, \tag{6.93}$$

where $b(n) = \frac{2n+1}{2(n-1)}\log n + \frac{1}{1-n}\log\frac{\Gamma(n+1/2)}{\Gamma(3/2)^n} - \frac{1}{2}\log 4\kappa$.

For an interval B in the bulk (see Fig. 6.3), the moments of the associated reduced density matrix are given by the following complicated expression in terms of the hypergeometric function :

$$\begin{aligned}
&\operatorname{Tr}\rho_B^n \\
&= \frac{1}{\pi}\Big(\frac{n\pi}{4\kappa}\Big)^{1-n}\left(\frac{L_AL_BL_C}{\epsilon L}\right)^{(1-n)/2} w^{n/2}(w-1)^{n+1/2} \\
&\quad\times\sum_{k=0}^{n}(-1)^k\binom{n}{k}\left[\tfrac{1}{n^2}\Gamma\big(\tfrac{n+1}{2}\big)^2\,{}_2F_1\big(\tfrac{n+1}{2},\tfrac{n+1}{2},\tfrac{1}{2},\tfrac{a_k^2}{w}\big)\right. \\
&\quad+\tfrac{\sqrt{w}\Gamma(n/2)^2}{2(n+1)^2a_k}\Big((w^{-1}a_k^2-1)\,{}_2F_1\big(\tfrac{n+2}{2},\tfrac{n+2}{2},\tfrac{-1}{2},\tfrac{a_k^2}{w}\big) \\
&\quad\left.+(1-2(n+2)a_k^2w^{-1})_2F_1\big(\tfrac{n+2}{2},\tfrac{n+2}{2},\tfrac{1}{2},\tfrac{a_k^2}{w}\big)\Big)\right],
\end{aligned} \tag{6.94}$$

where $w = (L_A+L_B)(L_B+L_C)/(L_AL_C)$, and $a_k = 1-2k/n$. However, deep in the bulk, i.e. for $w\to 1$, only the $k=0,n$ terms contribute to leading order in the sum above. We find

$$\begin{aligned}
&\operatorname{Tr}\rho_B^n \\
&\simeq \frac{1}{\pi}\Big(\frac{n\pi}{4\kappa}\Big)^{1-n}\left(\frac{L_AL_BL_C}{\epsilon L}\right)^{(1-n)/2} w^{n/2}(w-1)^{n+1/2} \\
&\qquad\times\left[n^{-2}2\sqrt{\pi}\Gamma\big(n+\tfrac{1}{2}\big)\frac{1}{(w-1)^{n+1/2}}+\cdots\right] \\
&= \left(\frac{L_AL_BL_C}{\epsilon L}\right)^{(1-n)/2}\Big(\frac{n\pi}{4\kappa}\Big)^{1-n}\frac{2}{n^2\sqrt{\pi}}\Gamma\big(n+\tfrac{1}{2}\big)+\cdots\,,
\end{aligned} \tag{6.95}$$

and one can check that this expression is properly normalized for $n=1$. Finally, the Rényi entropy reads

$$\begin{aligned}
S_n(B) &= \frac{1}{2}\log\frac{L_AL_BL_C}{\epsilon^2 L} + \text{const}\,, \\
&\sim \frac{1}{2}\log\frac{L_B}{\epsilon}+\frac{1}{2}\log\frac{L}{\epsilon}
\end{aligned} \tag{6.96}$$

valid for $L_A, L_C \sim L \gg L_B$. We thus retrieve the entropy of the free massless theory in the regime where B is deep enough in the bulk. This is actually a general feature ; the constraint $\phi \geq 0$ is inconsequential deep inside the bulk due to the exponentially small probability of ϕ approaching zero. Thus, in that regime, we expect correlation functions [2] and Rényi entropies to be given by those for the unconstrained boson

2. The (connected) correlation functions for the positive Lifshitz boson may be found in Section 6.5, setting $\nu = 1/2$ in the corresponding expressions.

(see Section 6.3). In particular, the mutual information of two disconnected intervals deep in the bulk is given by (6.62), i.e.

$$I(A:B) \sim \frac{1}{2}\log\frac{L}{L_{C_2}}\,, \tag{6.97}$$

and that of two adjacent intervals by (6.69), that is

$$I(A:B) \sim \frac{1}{2}\log\frac{L_A L_B}{\epsilon(L_A+L_B)} + \frac{1}{2}\log\frac{L}{\epsilon}\,. \tag{6.98}$$

The former is only IR divergent while the later is both UV and IR divergent.

6.4.2 Relation to Motzkin and Fredkin chains

The wavefunctional (6.90) of the positive Lifshitz boson was conjectured in [73, 72] to capture the groundstates of both Motzkin and Fredkin spin chains in the continuum limit. The only difference between the two being encoded in the dimensionless parameter κ. Indeed, expression (6.93) for the Rényi entropy of a boundary interval matches exactly the results for the Motzkin model [205, 73] and for the Fredkin spin chain [86, 72], provided $\kappa = 3/4,\, 2$ in the Motzkin and Fredkin groundstates, respectively. Correlation functions can be shown to match as well. However, our field theory result (6.96) for the (Rényi) entropy of a bulk interval does not agree with the spin chains calculations [205, 87]. Our formula does reproduce the 'geometric' part (i.e. the $1/2\log L_B$ term) of the entropy of Motzkin and Fredkin groundstates, but we also observe an additional IR divergent term that does not appear for the spin chains. We are thus lead to conclude that, as it stands, the continuum limit of Motzkin and Fredkin groundstates is not adequately described by the positive Lifshitz boson groundstate. In the Discussion, we discuss one modification to the wavefunctional that could potential cure the discrepancies, namely making the field compact.

Let us close this section with a remark on the mutual information for the Motzkin and Fredkin groundstates, which was studied in [87]. There, the author finds that the mutual information of two disconnected subsystems inside the bulk does not depend on their separation, and takes the form

$$I(A:B) \sim \frac{1}{2}\log\frac{L_A L_B}{L_A+L_B} + \text{const}\,, \tag{6.99}$$

in the limit $L_A, L_B \gg 1$, where L_X is the number of spins in the subsystem X. Oddly enough, this formula coincides with the geometric term (first term) in (6.98), which gives the mutual information shared by two *adjacent* intervals for the Lifshitz groundstate. Furthermore, a length scale seems to be missing in (6.99) if one wishes to take the continuum limit. Indeed, expression (6.99) would then appear to be UV divergent, which is in contradiction with the fact that mutual information between disconnected subsystems must be UV finite.

6.5 Deformation by a singular potential

We now return to the original Lifshitz theory (6.3) and perform a nontrivial deformation (for $d \neq 2$) that preserves the Lifshitz scale invariance in all dimensions, as well as the spatial conformal symmetry of the groundstate when $d = 1$. Set $\Lambda[\phi] = \int d^dx\, \frac{g}{4}\phi(x)^{2d/(d-2)}$, so that the classical action becomes $S_{\rm cl}[\phi] = \int d^dx \left(\kappa(\nabla\phi)^2 + \frac{g}{2}\phi^{2d/(d-2)}\right)$, and

$$A(x) = \frac{1}{\sqrt{2}}\left(\frac{\delta}{\delta\phi(x)} - \kappa\nabla^2\phi + \frac{gd}{2(d-2)}\phi^{\frac{d+2}{d-2}}\right). \tag{6.100}$$

The corresponding groundstate of $H^{\rm normal}_{\rm sing} = \int d^dx\, A^\dagger(x)A(x)$ is

$$\Psi_0[\phi] = e^{-\frac{1}{2}\int d^dx\left(\kappa(\nabla\phi)^2 + \frac{g}{2}\phi^{2d/(d-2)}\right)}. \tag{6.101}$$

The parameter g is dimensionless for all d, and the operators $A(x)$ are invariant under Lifshitz rescaling $(\mathbf{x}, t) \to (\lambda\mathbf{x}, \lambda^2 t)$, as per (6.10) and (6.11). (The affine field-shift symmetry is lost however.) As a consequence, the groundstate wavefunctional $\Psi_0[\phi]$ is invariant under spatial scaling $\mathbf{x} \to \lambda\mathbf{x}$. Yet, $H^{\rm normal}_{\rm sing}$ hardly qualifes as a *bona fide* parent Hamiltonian for $|\Psi_0\rangle$, because it contains the awkward UV-divergent term

$$\frac{1}{2}{\rm tr}(\kappa\nabla^2 - g\tfrac{d(d+2)}{2(d-2)^2}\phi^{\frac{-4}{d-2}}), \tag{6.102}$$

whose physical meaning is rather opaque. Note that this term is nothing but the commutator $\frac{1}{2}\int d^dx\, [A^\dagger(x), A(x)]$. But we can no longer rely on the deformed Lifshitz theory $H^+_{\rm sing} = \frac{1}{2}\int d^dx\, \{A^\dagger(x), A(x)\}$, even though it is without divergence, since it differs from $H^{\rm normal}_{\rm sing}$ by precisely (6.102), which is *not* a multiple of the identity, so this time $H^{\rm normal}_{\rm sing}$ and $H^+_{\rm sing}$ do not share their eigenstates.

6.5.1 Supersymmetric deformation

The way around this difficulty is to deform $H^+_{\rm sing}$ (and its Hilbert space) to include fermionic degrees of freedom [92]. Define the operators

$$Q = \int d^dx\, \bar\psi(x)A(x)\,, \qquad \bar Q = \int d^dx\, \psi(x)A(x)^\dagger\,, \tag{6.103}$$

with $\{\psi(x), \bar\psi(y)\} = \delta(x-y)$. In the Schrödinger picture, where $\psi(x)$ is a multiplication operator and $\bar\psi(x) = \delta/\delta\psi(x)$, consider the normalized Grassmann-valued functional $\Psi_F[\psi] = \prod_x \psi(x)$. Then $\psi(x)|\Psi_F\rangle = 0$ for all x. The Hamiltonian

$$H^{\rm SUSY}_{\rm sing} = \frac{1}{2}\{\bar Q, Q\} \tag{6.104}$$

is part of a supersymmetric structure

$$\{Q, Q\} = 0 = \{\bar Q, \bar Q\}\,, \quad [Q, H^{\rm SUSY}_{\rm sing}] = 0 = [\bar Q, H^{\rm SUSY}_{\rm sing}] \tag{6.105}$$

with unbroken supersymmetry : for $|\Omega\rangle = |\Psi_0\rangle \otimes |\Psi_F\rangle$, where $\langle\phi|\Psi_0\rangle = \exp(-S_{\rm cl}[\phi])$ as before, we have

$$Q|\Omega\rangle = 0 = \bar{Q}|\Omega\rangle\,. \tag{6.106}$$

As in the work of Dijkgraaf *et al.* [92], the presence of the fermionic sector enables both Q and $\bar{Q}$ to annihilate $|\Omega\rangle$, making it a groundstate of the *divergenceless* anticommutator $\{\bar{Q}, Q\}$. Since the product $\Psi_F[\psi] = \prod_x \psi(x)$ has no spatial entanglement, the supersymmetric groundstate $|\Omega\rangle$ and the bosonic groundstate $|\Psi_0\rangle$ possess the same structure of spatial entanglement. Moreover, $H^{\rm SUSY}_{\rm sing}$ is an unambiguous parent Hamiltonian for $|\Omega\rangle$. Interestingly, this type of supersymmetric structure naturally emerges when stochastically quantizing a classical action $S_{\rm cl}$ [219]. The parent Hamiltonian $H^{\rm SUSY}$ is then physically realized as the stochastic field theory whose $t \to \infty$ equilibrium correlations yield the correlations of the quantized action. Expanding (6.104), we get

$$\begin{aligned} H^{\rm SUSY}_{\rm sing} &= \frac{1}{2}\int d^dx \left[\Pi^2 + \tfrac{1}{2}(S'_{\rm cl})^2 + \tfrac{1}{2}\big(\bar{\psi}S''_{\rm cl}\psi - \psi S''_{\rm cl}\bar{\psi}\big)\right] \\ &= H^+_{\rm sing} + \frac{1}{4}\int d^dx \left[\bar{\psi}S''_{\rm cl}\psi - \psi S''_{\rm cl}\bar{\psi}\right]. \end{aligned} \tag{6.107}$$

In the first line, we have written $S^{(n)}_{\rm cl} = (\delta^n/\delta\phi^n)S_{\rm cl}$, for short. We emphasize that $|\Psi_0\rangle \otimes |\Psi_F\rangle$ is a groundstate of the above Hamiltonian, despite the fact that $|\Psi_0\rangle$ is not a groundstate of $H^+_{\rm sing}$. The corresponding Euclidean theory has partition function

$$\mathcal{Z}_E = \int \mathcal{D}\phi\mathcal{D}\psi\mathcal{D}\bar{\psi}\; e^{-\int d\tau d^dx\, \mathcal{L}_E}\,, \tag{6.108}$$

where, up to boundary terms,

$$\mathcal{L}_E = \frac{1}{2}\big(\partial_\tau\phi + \tfrac{1}{2}S'_{\rm cl}\big)^2 - \bar{\psi}\big(\partial_\tau + \tfrac{1}{2}S''_{\rm cl}\big)\psi\,. \tag{6.109}$$

Specializing again to $d = 1$, we find

$$H^+_{\rm sing} = H_{\rm Lif} + \frac{1}{2}\int dx \left(\frac{g\kappa}{\phi^3}\nabla^2\phi + \frac{g^2}{4\phi^6}\right), \tag{6.110}$$

and

$$\begin{aligned} \mathcal{L}_E = {} & \tfrac{1}{2}(\partial_\tau\phi)^2 + \tfrac{\kappa^2}{2}(\nabla^2\phi)^2 + \tfrac{g\kappa}{2}\phi^{-3}\nabla^2\phi + \tfrac{g^2}{8}\phi^{-6} \\ & - \bar{\psi}(\partial_\tau - \kappa\nabla^2 + \tfrac{3g}{2}\phi^{-4})\psi\,. \end{aligned} \tag{6.111}$$

We will mostly consider the stable case $g > 0$, for which the singular potential in (6.110) prevents the field from vanishing anywhere. Without loss of generality, we can restrict ϕ to strictly positive real values $\phi(x) \in \mathbb{R}^{>0}$. The boundary conditions are chosen to be $\phi(0,t) = \phi(L,t) = h$, for an arbitrary but strictly positive regulator $h = 0^+$, preventing the divergence of the potential energy term. (Our analysis also holds for negative values of g as long as the regulating condition $\phi \geq h > 0$ is maintained.) The normalization factor of $|\Omega\rangle = |\Psi_0\rangle \otimes |\Psi_F\rangle$ is

$$\mathcal{Z} = \langle\Psi_0|\Psi_0\rangle = \int_{\phi(0)=h=\phi(L)} \mathcal{D}\phi\; e^{-\int dx\left(\kappa(\partial_x\phi)^2 + \frac{g}{2\phi^2}\right)}. \tag{6.112}$$

One can recognize $\mathcal{Z}$ as the partition function of a single quantum mechanical particle with Euclidean Lagrangian $\mathcal{L}_g = \kappa(\partial_x\phi)^2 + \frac{g}{2\phi^2}$. The theory in spatial dimension $d = 1$ stands out as having full conformal spatial symmetry. The group of dilations $x \to \lambda x$, $\lambda > 0$, may be extended to the $SL(2,\mathbb{R})$ group of transformations

$$x \to x' = \frac{\alpha x + \beta}{\gamma x + \delta}\,, \qquad \alpha\delta - \beta\gamma = 1\,, \tag{6.113}$$

with Jacobian determinant

$$\frac{\partial x'}{\partial x} = \frac{1}{(\gamma x + \delta)^2} > 0\,. \tag{6.114}$$

Fields transform as tensor densities of weight 1/2 corresponding to their length dimension

$$\phi'(x') = \sqrt{\frac{\partial x'}{\partial x}}\phi(x) = \frac{\phi(x)}{\gamma x + \delta}\,. \tag{6.115}$$

(The sign of $\gamma x + \delta$ is immaterial, the action being quadratic in the field, so we drop the absolute value bars.) The action $\int dx\ \mathcal{L}_g(\phi, \partial_x\phi)$ is called $SL(2,\mathbb{R})$-conformal because it is invariant, up to a boundary term, under the joint transformations (6.113) and (6.115). The quantized theory, conformal quantum mechanics (CQM), has been known for a long time [84, 161]. Stochastic quantization of $\mathcal{L}_g$ generates the $(1+1)$-dimensional field theory $H^{\rm SUSY}_{\rm sing}$, whose supersymmetric groundstate $|\Psi_0\rangle \otimes |\Psi_F\rangle$ contains the propagators of CQM. Conversely, knowledge of the propagators of CQM is analytic knowledge about $|\Psi_0\rangle \otimes |\Psi_F\rangle$ and its parent theory. Because $|\Psi_F\rangle$ is a spatial product, the bosonic groundstate $|\Psi_0\rangle$ and the supersymmetric groundstate $|\Psi_0\rangle \otimes |\Psi_F\rangle$ have the same spatial entanglements. The (normalized) eigenstates of the CQM Hamiltonian, $H_g = -\frac{1}{4\kappa}\partial_\phi^2 + \frac{g}{2\phi^2}$, were identified in [161, 84] :

$$(H_g - E)\psi_E = 0 \iff \psi_E(\phi) = \sqrt{2\kappa\phi}J_\nu(\phi\sqrt{4\kappa E})\,, \tag{6.116}$$

where $\nu = \sqrt{2g\kappa + \frac{1}{4}}$ and J_ν is a Bessel function of the first kind of order ν. We will only consider nonnegative values of ν (i.e. $g \geq -1/8\kappa$). The propagators are readily computed :

$$\langle\phi', x'|\phi, x\rangle = \tfrac{2\kappa\sqrt{\phi'\phi}}{x'-x}\exp\left[-\kappa\left(\tfrac{\phi'^2+\phi^2}{x'-x}\right)\right] I_\nu\left(\tfrac{2\kappa\phi'\phi}{x'-x}\right), \tag{6.117}$$

with I_ν the modified Bessel function of the first kind of order ν. Deep in the bulk, where $\langle\phi'\phi\rangle$ is large compared to $x' - x$ (see below), the singular potential is ineffective and we recover the free massless boson propagator $G_{\mathbb{R}}(\phi', x'; \phi, x) = \sqrt{\frac{\kappa}{\pi(x'-x)}}\exp\left[-\frac{\kappa(\phi'-\phi)^2}{x'-x}\right]$. On the other hand, in the limit $g \to 0$ (i.e. $\nu \to 1/2$), and using the fact that $I_{\frac{1}{2}}(z) = \sqrt{\frac{2}{\pi z}}\sinh z$, we find the propagator of the positive-valued free field

$$\begin{aligned} &G_{\mathbb{R}^{>0}}(\phi', x'; \phi, x) \\ &\quad = \sqrt{\frac{\kappa}{\pi(x'-x)}}\left(e^{-\frac{\kappa(\phi'-\phi)^2}{x'-x}} - e^{-\frac{\kappa(\phi'+\phi)^2}{x'-x}}\right), \end{aligned} \tag{6.118}$$

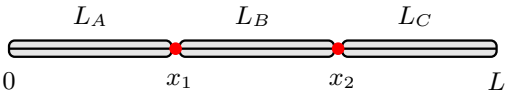

FIGURE 6.8 – The field correlator $\langle\phi(x_1)\phi(x_2)\rangle_\nu$ over the bulk interval B, in the presence of the singular potential, is given in (6.124).

because nothing is left of the singular potential but the constraint $\phi > 0$. We emphasize that the singular deformation in not a perturbation of the original Lifshitz point, but of the positive-valued free field. However, the propagators $G_{\mathbb{R}}$ and $G_{\mathbb{R}^{>0}}$ are indistinguishable deep in the interior.

6.5.2 Correlations in the groundstate

Obviously, the field has nonvanishing vacuum expectation values

$$\langle\phi(x)\rangle_\nu = \int_h^\infty d\phi\ \phi f_1^{(\nu)}(\phi, x) = \frac{\Gamma(\nu+\frac{3}{2})}{\Gamma(\nu+1)}\sqrt{\frac{x(L-x)}{\kappa L}}\,, \tag{6.119}$$

where $f_1^{(\nu)}(\phi, x) = \langle h, L|h, 0\rangle^{-1}\langle h, L|\phi, x\rangle\langle\phi, x|h, 0\rangle$ and $h = 0^+$ is the field regulator introduced below (6.111) to prevent the divergence of the potential energy term. The regulator h is also necessary to prevent the individual vanishing of the propagators, given by (6.117). However, the integral in (6.119), and similar integrals, have a well-defined limit as h is sent to zero. We will work in that limit from now on. Interestingly, the only difference between first moments with different values of ν (or g) is a real-number prefactor. An even stronger relationship holds between all higher moments (see Appendix 6.7.3) :

$$\langle\phi^\alpha(x)\rangle_\mu = R(x, x, \mu, \nu)\langle\phi^{\alpha+2(\mu-\nu)}(x)\rangle_\nu\,, \tag{6.120}$$

with

$$R(x_1, x_2, \mu, \nu) = \frac{\Gamma(1+\nu)}{\Gamma(1+\mu)}\left(\frac{\kappa L}{x_1(L-x_2)}\right)^{\mu-\nu}. \tag{6.121}$$

In particular, higher moments can be obtained from the *first* moment of the (positive-valued) free boson via the relations $\langle\phi^{1+2\mu}(x)\rangle_\nu \propto \langle\phi(x)\rangle_{\nu+\mu} \propto \langle\phi(x)\rangle_{1/2}$. The general expression is

$$\langle\phi^{1+2\mu}(x)\rangle_\nu = \frac{\Gamma(\mu+\nu+\frac{3}{2})}{\Gamma(\nu+1)}\left(\frac{x(L-x)}{\kappa L}\right)^{\frac{1}{2}+\mu}. \tag{6.122}$$

Deep in the bulk, $\langle\phi^{1+2\mu}(x)\rangle_\nu \sim (\sqrt{L})^{1+2\mu}$ for any ν.

Once again, the reduced density $\rho_{A\cup B}$ is a separable mixed state for any disconnected subsystems A, B (see Appendix 6.7.2). Therefore, A and B are not entangled, and their correlations are non-entangling [213, 117, 3, 4], coming from the statistical mixture left in $\rho_{A\cup B}$, if any. As A, B come into contact, the result does not hold

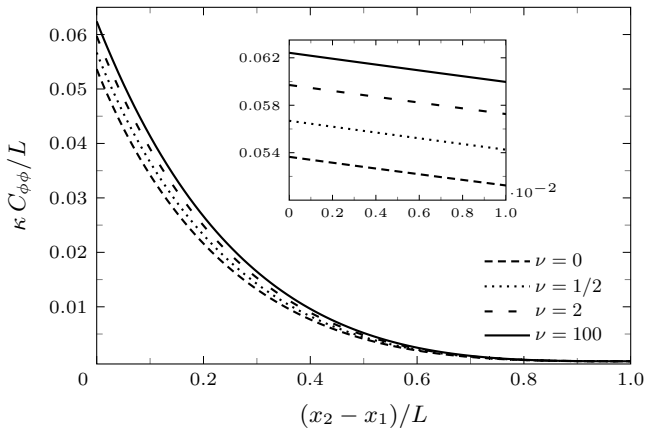

FIGURE 6.9 – Connected correlator $\frac{\kappa}{L} C_{\phi_1,\phi_2}(x_1, x_2)$ for a central interval of length $x_2 - x_1$, and for $\nu = 0, 1/2, 2, 20$, obtained analytically from (6.119) and (6.124). **Inset :** $\frac{\kappa}{L} C_{\phi_1,\phi_2}(x_1, x_2)$ for small central intervals. The linear behavior is in perfect agreement with (6.128).

anymore and quantum-driven contact terms are expected. To compute the two-point function $\langle \phi(x_1)\phi(x_2)\rangle_\nu$, we find it best to express it in terms of the variable

$$w = \frac{(L_A + L_B)(L_B + L_C)}{L_A L_C}\,, \tag{6.123}$$

with subinterval lengths L_A, L_B, L_C as in Fig. 6.8. We find

$$\begin{aligned}\langle \phi(x_1)\phi(x_2)\rangle_\nu = \frac{L_B}{\kappa}\left[\frac{\Gamma(\frac{3}{2}+\nu)}{\Gamma(1+\nu)}\right]^2 \frac{(w-1)^{1+\nu}}{w^{\frac{3}{2}+\nu}} \\ \times\ {}_2F_1\left[\tfrac{3}{2}+\nu, \tfrac{3}{2}+\nu; 1+\nu; \tfrac{1}{w}\right],\end{aligned} \tag{6.124}$$

where ${}_2F_1(a, b; c; x)$ is the Gaussian hypergeometric function. From (6.119) and (6.124), we can obtain analytic expressions for the connected correlator $C_{\phi_1,\phi_2} = \langle \phi_1\phi_2\rangle_\nu - \langle \phi_1\rangle_\nu\langle \phi_2\rangle_\nu$ and, by repeated differentiation, for the connected correlator $C_{\partial\phi_1,\partial\phi_2} = \langle \partial\phi_1\partial\phi_2\rangle_\nu - \langle \partial\phi_1\rangle_\nu\langle \partial\phi_2\rangle_\nu$. Here we omit the full expressions, but in Fig. 6.9 we plot $C_{\phi_1,\phi_2}(x_1, x_2)$ (in units of κ/L) for a central interval of length $x_2 - x_1$, and different values of ν. In Fig. (6.10) we plot $C_{\partial\phi_1,\partial\phi_2}(x_1, x_2)$ (in units of κL) for the same interval and values. Deep in the bulk, where $w \to 1$, we may expand (6.124) in powers of

$$w - 1 = \frac{L L_B}{L_A L_C} = \frac{L(x_2 - x_1)}{x_1(L - x_2)} \sim \frac{1}{L}\,, \tag{6.125}$$

leading to

$$\langle \phi(x_1)\phi(x_2)\rangle_\nu = \frac{(1+\nu)L}{4\kappa} - \frac{x_2 - x_1}{4\kappa} + O(1/L)\,. \tag{6.126}$$

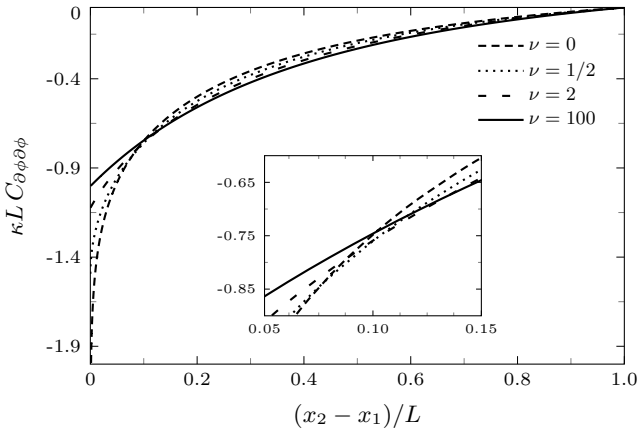

FIGURE 6.10 – Connected correlator $\kappa L C_{\partial\phi_1,\partial\phi_2}(x_1, x_2)$ for a central interval of length $x_2 - x_1$, and for $\nu = 0, 1/2, 2, 20$, obtained analytically from (6.119) and (6.124). **Inset :** Correlations are almost independent of ν when $x_2 - x_1 \sim 0.1L$.

This expression is not restricted to central intervals. For the special case $\nu = 1/2$, we recover

$$\langle\phi(x_1)\phi(x_2)\rangle_{1/2} = \frac{3L}{8\kappa} - \frac{x_2 - x_1}{4\kappa} + O(1/L)\,, \tag{6.127}$$

in agreement with the positive-valued boson. The field connected correlator deep in the bulk is found to be

$$\begin{aligned} C_{\phi,\phi}(x_1, x_2) &= \langle\phi(x_1)\phi(x_2)\rangle_\nu - \langle\phi(x_1)\rangle_\nu\langle\phi(x_2)\rangle_\nu \\ &= \frac{\alpha_\nu L}{\kappa} - \frac{x_2 - x_1}{4\kappa} + O(1/L)\,, \end{aligned} \tag{6.128}$$

with α_ν a finite, positive constant independent of L :

$$\alpha_\nu = \frac{1}{4}\left[1 + \nu - \left(\frac{\Gamma(\nu + \frac{3}{2})}{\Gamma(\nu + 1)}\right)^2\right]. \tag{6.129}$$

The bulk two-point function (6.126), and the bulk connected correlator (6.128) consist in a constant leading term which diverges like L in the thermodynamic limit, followed by a universal, translation-invariant bulk term linear in $x_2 - x_1$, and independent of ν. The universal behavior $\langle\phi(x_1)\phi(x_2)\rangle_\nu \sim (x_2 - x_1)^\Delta$, with exponent $\Delta = 1$, is a joint consequence of the dimension of the fields, $\dim\phi = \sqrt{\text{length}}$, and of the absence of a length scale other than L. Non-dependence of this term on ν is yet another indication that the singular potential is ineffective in the bulk.

From (6.128) and dimensionality, we expect $\partial\phi\partial\phi$ correlations to vanish in the limit $L \to \infty$. To obtain an analytic bulk expansion for $C_{\partial\phi_1,\partial\phi_2}$ beyond the leading order we find it necessary to restrict ν to chosen intervals or values. We provide four cases, beginning with $\nu = 0$, and the interval $\nu \in (0, 1)$.

Case $\nu = 0$:

$$C_{\partial\phi,\partial\phi} = \frac{\beta_0}{\kappa L} + \frac{1}{4\kappa L}\log\frac{x_2-x_1}{L} - \frac{3(x_2-x_1)}{4\kappa L^2}\log\frac{x_2-x_1}{L} + \frac{\delta_0}{\kappa L^2}(x_2-x_1) + O(1/L^3)\,, \tag{6.130}$$

with $\beta_0 = -\frac{1}{2}\log 2$, and $\delta_0 = \frac{3}{2}\log 2 - 1$.

Case $0 < \nu < 1$:

$$C_{\partial\phi,\partial\phi} = \frac{\beta_\nu}{\kappa L} + \frac{\gamma_\nu}{\kappa L^{1+\nu}}(x_2-x_1)^\nu + O(1/L^2) \tag{6.131}$$

with

$$\beta_\nu = -1 - \frac{1}{4\nu}\,, \quad \gamma_\nu = 4^\nu\left[\frac{\Gamma(\nu+3/2)}{\Gamma(\nu+1)}\right]^2 \csc\pi\nu\,. \tag{6.132}$$

The leading term $\beta_\nu/\kappa L$, with coefficient given in (6.132), is actually valid for all nonzero values of ν. The coefficient of fractional order γ_ν diverges near $\nu = 0$ and $\nu = 1$. As $\nu \to 1$, term $O(1/L^2)$ in (6.131) can no longer be neglected. We also provide the expansions for the integer values $\nu = 1$ and $\nu = 2$.

Case $\nu = 1$:

$$C_{\partial\phi,\partial\phi} = \frac{\beta_1}{\kappa L} - \frac{9}{4\kappa L^2}(x_2-x_1)\log(x_2-x_1) + \frac{\delta_1}{\kappa L^2}(x_2-x_1) + O(1/L^3)\,. \tag{6.133}$$

Case $\nu = 2$:

$$C_{\partial\phi,\partial\phi} = \frac{\beta_2}{\kappa L} + \frac{\delta_2}{\kappa L^2}(x_2-x_1) + O(1/L^3)\,, \tag{6.134}$$

where $\delta_1 = \frac{9}{2}\log 2 - \frac{15}{4}$, and $\delta_2 = \frac{45}{8}$. In contrast to the $\phi\phi$ correlator, the nonconstant leading term of the $\partial\phi\partial\phi$ correlator is strongly sensitive to the value of ν, not only in its coefficient but even in its functional dependence to the subinterval length $x_2 - x_1$. Case $\nu = 0$ presents a quasiconstant term $O(\log(x_2-x_1))$, while case $\nu = 1$ has a quasilinear term $O((x_2-x_1)\log(x_2-x_1))$. For general integer ν, it is tempting to expect a quasipolynomial term $O((x_2-x_1)^\nu\log(x_2-x_1))$, subleading for $\nu \geq 2$.

Finally, the correspondence (6.120) between higher moments can be generalized to multipoint functions deep in the bulk. For the points $0 < x_1 < x_2 < \cdots < x_N < L$ with $x_1 \sim L/2 \sim L - x_N$, and writing $\phi(x_i) = \phi_i$, we find

$$\langle\phi_1^{\alpha_1}\cdots\phi_N^{\alpha_N}\rangle_\mu = R(x_1,x_N,\mu,\nu)\langle\phi_1^{\alpha_1+\mu-\nu}\phi_2^{\alpha_2}\cdots\phi_{N-1}^{\alpha_{N-1}}\phi_N^{\alpha_N+\mu-\nu}\rangle_\nu\,. \tag{6.135}$$

These relationships are a manifestation of the fact that bulk propagators are free, see Appendix 6.7.3. The effect of the singular potential on (6.135) arises solely from the surface propagators $\langle\phi_1, x_1|h, 0\rangle$ and $\langle h, L|\phi_N, x_N\rangle$ between the system's boundaries and ϕ_1, ϕ_N. All other propagators are free. More generally, when some points are close to the boundary, more bulk propagators become boundary propagators. If, say, x_1 is close to the boundary, both $\langle\phi_1, x_1|h, 0\rangle$ and $\langle\phi_2, x_2|\phi_1, x_1\rangle$ will be boundary propagators, and α_2 will be modified accordingly in (6.135).

6.5.3 Entanglement in the groundstate

We now compute the Rényi entanglement entropies of a boundary interval A as in Fig. 6.3, which are given by

$$S_n(A) = \frac{1}{1-n} \log \int_h^\infty d\phi \ \left[f_1^{(\nu)}(\phi, L_A) \right]^n + \frac{1}{2} \log \frac{1}{\epsilon}, \tag{6.136}$$

where $f_1^{(\nu)} = \mathcal{Z}^{-1} \langle h, L | \phi, L_A \rangle \langle \phi, L_A | h, 0 \rangle$ is the single-point probability distribution obtained from the propagator (6.117), $h = 0^+$ is the field regulator introduced below (6.111), and $\mathcal{Z}$ is a normalization factor given in (6.112). Note that the (generalized) Fradkin-Moore formula (6.44) is not applicable here because its derivation requires that M-point functions be Gaussian. In the limit of vanishing regulator, we obtain

$$S_n(A) = \frac{1}{2} \log \frac{L_A(L - L_A)}{\epsilon L} + b(n, \nu) \,, \tag{6.137}$$

with

$$b(n,\nu) = \tfrac{n(1+2\nu)+1}{2(n-1)} \log n + \tfrac{1}{1-n} \log \tfrac{\Gamma((1+n+2n\nu)/2)}{\Gamma(1+\nu)^n} - \tfrac{1}{2} \log 4\kappa. \tag{6.138}$$

Comparing (6.137) with the entropy (6.48) in the (undeformed) massless case then reveals the same entanglement behavior for all values of ν. In particular, all c_n-functions are identically equal to $1/2$, consistent with the unbroken spatial conformal symmetry of the groundstate wavefunctional deep in the bulk.

6.6 Discussion and outlook

In this work, we considered two nontrivial deformations of the noncompact (1+1)-dimensional $z = 2$ Lifshitz theory that preserve the RK structure of the original theory. Accordingly, the correlators of the groundstate wavefunctional are encoded in the partition function of a lower-dimensional, local action. For the massive deformation studied in Section 6.3, which explicitly breaks Lifshitz scaling, groundstate correlations are given by the Euclidean harmonic oscillator. As expected, we found an exponential decay of correlations with correlation length $\xi \sim m^{-1}$, and observed that Cluster Decomposition, violated in the massless case, is restored by the regulating mass.

We further computed, from first principles (Appendix 6.7.1), the Rényi entanglement entropy over a general bipartition $\{A, B\}$ with finitely many surface points, $\partial A = \{x_1, \ldots, x_M\}$, and the corresponding c-function (independent of the Rényi index n). Expression (6.44) for $S_n(A)$ generalizes to our $(1+1)$-dimensional non-Lifshitz-invariant case the celebrated Fradkin-Moore formula [105] pertaining to the $(2+1)$-dimensional $z = 2$ Lifshitz theory. Application of this formula yields a general expression for the UV-finite mutual information between disjoint subsystems A_1 and A_2. When A_1, A_2 are two intervals, the mutual information decays exponentially with separation, unless the mass is zero. In the massless case, the mutual information is IR divergent and persists at all separations, which can be seen as a consequence of the Cluster Decomposition being violated.

One motivation for starting this work was in relation to the Motzkin and Fredkin spin chains [49, 86]. The positive-field version of the Lifshitz groundstate (6.8) was believed to be the continuum limit of the Motzkin and Fredkin groundstates, and, indeed, captures many of their spin and entanglement features [73, 72, 205].

In comparing our field theory predictions to the spin chains results in the literature, the entanglement entropy of a bulk interval (6.49) obtained here does not agree with that computed in [205]. An extra IR piece, absent for the spin chains, is at the origin of the discrepancy. This also implies that the form of the mutual information (6.97) cannot be that for Motzkin and Fredkin groundstates. Indeed, the mutual information (6.97) for disconnected intervals obtained here does not agree with that of [87] computed on the lattice. However, as argued in Section 6.4, the expression found in [87] (see (6.99)) does not possess a sensible continuum limit. Still, as it stands, the positive Lifshitz boson cannot be taken as the continuum limit of Motzkin and Fredkin groundstates. It thus raises the question of which field theory does ? A possible direction would be to look at the *compact* Lifshitz boson groundstate. As may be observed in [300] in $(2+1)$ dimensions, potential IR divergent terms in the mutual information get canceled against an additional contribution coming from the winding modes present in the compact case. It would thus be interesting to generalize our work for the one-dimensional theory to compact fields.

As a byproduct of our results on Rényi entropies, we computed the capacity of entanglement C_A. This quantity, analogue of the heat capacity for thermal states, characterizes the width of the entanglement spectrum. We found that for the groundstate of Lifshitz theories, the capacity of entanglement is finite and follows an area law. Comparison of capacity of entanglement with entanglement entropy tells us something about the entanglement structure of the quantum state under study. We found $C_A \ll S_A$ for Lifshitz groundstates, which could be interpreted as entanglement being effectively carried by maximally entangled EPR pairs in such systems.

We also observed a relationship between corner entanglement in the $(2+1)$-dimensional $z=2$ Lifshitz theory and the c-function of the $(1+1)$-dimensional massive deformation. Specifically, the sharp-limit coefficient κ_c of the corner entanglement is found to be

$$\kappa_c = \frac{1}{\pi}\int_0^\infty dx\, c(x)\,, \tag{6.139}$$

for our non-Lorentz-invariant theory. This is a generalization of the corresponding relation between the sharp-limit coefficient of a CFT_3 and the entropic c-function of a lower-dimensional QFT [65]. Interestingly, the entropic c-function is found to decrease under wavefunction RG flow even though the theory is not Lorentz-invariant. (In fact, not even Lifshitz-invariant.) Whether a similar result may hold for higher dimensional versions of the massive deformation presented in this work is worth investigating, especially in dimension $2+1$, where the F-theorem for CFTs guaranties the monotone decreasing of the entanglement entropy of a disk under RG flow [66]. We leave this for future study.

A deformation by a singular potential which preserves Lifshitz scaling was next studied in Section 6.5. The singular deformation is actually supersymmetric in order to avoid technical issues but the fermionic sector of the groundstate is without

entanglement, and all correlations are ultimately given by the CQM bosonic sector. We found that the universal part of bulk connected correlators is independent of the coupling g to the singular potential, an indication that the potential is ineffective in the bulk. The leading IR-divergent term is however strongly dependent on the coupling ($\sim \sqrt{g}$) as it is essentially a boundary effect. For a single interval in contact with the boundary, the Rényi entanglement entropy reveals the same entanglement behavior for all values of g, up to a constant. In particular, all entropic c_n-functions are equal to $1/2$, consistent with the unbroken spatial conformal symmetry of the groundstate wavefunctional deep in the bulk. We thus find an entire line of critical theories in parameter space, corresponding to the values $g \in [0, \infty)$.

Finally, we proved in Appendix 6.7.2 that for real-valued RK wavefunctionals (i.e. of the form (6.13)) of $(d+1)$-dimensional quantum field theories, the reduced density matrix $\rho_{A\cup B}$ of two disconnected subsystems A and B is (mixed) separable, meaning that the partial trace over C (the complement of $A\cup B$) disentangles A from B. Accordingly, the mutual information results entirely from classical and quantum non-entangling correlations [213, 117, 3, 4]. Furthermore, the separability of $\rho_{A\cup B}$ for two disjoint subsystems implies the vanishing of the logarithmic negativity. This is in agreement with previous results where the logarithmic negativity was shown to vanish ; in [72] for the groundstate of the noncompact free massless $z = 2$ Lifshitz boson, and in [18] for local groundstates of free massless Lifshitz theories with even positive integer z, both for compact and noncompact fields.

6.7 Appendices

6.7.1 Replica trick in the dynamics associated to the groundstate wavefunctional

In this appendix, we derive formula (6.43) for the Rényi entanglement entropies for the deformed $(1+1)$-dimensional Lifshitz theories. We begin with normalized states formally written $|\Psi\rangle = \int \mathcal{D}\phi \ \Psi[\phi]\,|\phi\rangle$, in one-to-one correspondence with Schrödinger wavefunctionals Ψ, and we make two assumptions :

Assumption 1. The ϕ are dimensionless, real classical fields almost everywhere C^1 on $[0, L]$, and $\mathcal{D}\phi$ is a measure for such fields.

Field eigenstates

$$\chi_\phi[\phi'] = \begin{cases} 1\,, & \phi' = \phi, \\ 0\,, & \text{otherwise}, \end{cases} \tag{6.140}$$

have no spatial entanglement : for almost any open partition $\{A, B\}$ of the physical space, $\chi_\phi = \chi_{\phi|_A} \otimes \chi_{\phi|_B}$. Equivalently,

$$|\phi\rangle = |\alpha\rangle_{\boldsymbol{\phi}} \otimes |\beta\rangle_{\boldsymbol{\phi}}\,, \tag{6.141}$$

where $\alpha = \phi|_A$ and $\beta = \phi|_B$ are C^1 almost everywhere on their respective domain, and $\boldsymbol{\phi} = \{\phi_1, \ldots, \phi_M\}$ is an *anchor* for these fields : $\alpha(x_i) = \phi_i = \beta(x_i)$ for each x_i at the common boundary of A and B. We now make an assumption specific to a distinguished state $|\Psi\rangle$:

Assumption 2. Ψ is real-valued, and for α, β as above, $\Psi[\phi] = a[\alpha] \otimes b[\beta]$ for some real functionals a, b.

Then

$$\begin{aligned} |\Psi\rangle &= \int d\boldsymbol{\phi} \int (\mathcal{D}\alpha)_{\boldsymbol{\phi}}\; a[\alpha] |\alpha\rangle_{\boldsymbol{\phi}} \otimes \int (\mathcal{D}\beta)_{\boldsymbol{\phi}}\; b[\beta] |\beta\rangle_{\boldsymbol{\phi}} \\ &= \int d\boldsymbol{\phi}\; |\Psi_A\rangle_{\boldsymbol{\phi}} \otimes |\Psi_B\rangle_{\boldsymbol{\phi}}\,, \end{aligned} \tag{6.142}$$

which formally resembles a Schmidt decomposition for $|\Psi\rangle$ with anchors as Schmidt index, and can be cast in actual Schmidt form $|\Psi\rangle = \sum_{i=1}^{\infty} \sigma_i |u_i\rangle \otimes |v_i\rangle$, if necessary, by expressing the $\boldsymbol{\phi}$-integral as a convergent sum over increasingly fine mesh elements such that the ith mesh element contains point $\boldsymbol{\phi}_i$, and where $\{|u_i\rangle\}$ and $\{|v_i\rangle\}$ are respectively obtained by Gram-Schmidt orthonormalization of the sets $\{|\Psi_A\rangle_{\boldsymbol{\phi}_i} - \sum_{j \prec i} |\Psi_A\rangle_{\boldsymbol{\phi}_j}\}$, and $\{|\Psi_B\rangle_{\boldsymbol{\phi}_i} - \sum_{j \prec i} |\Psi_B\rangle_{\boldsymbol{\phi}_j}\}$. (Here, $j \prec i$ means that j is a coarser mesh element containing i.) We will not require the Schmidt decomposition, and will be content with (6.142). Actually, we will use Assumption 2 only at the end of the argument, so for now we simply write the state in terms of anchored fields, $|\Psi\rangle = \int d\boldsymbol{\phi} \int (\mathcal{D}\alpha\beta)_{\boldsymbol{\phi}}\; \Psi[\alpha\beta] |\alpha\rangle_{\boldsymbol{\phi}} \otimes |\beta\rangle_{\boldsymbol{\phi}} = \int d\boldsymbol{\phi}\; |\Psi\rangle_{\boldsymbol{\phi}}$. The corresponding density is

$$\begin{aligned} \rho &= |\Psi\rangle\langle\Psi| \\ &= \int (d\boldsymbol{\phi}\boldsymbol{\phi'})(\mathcal{D}\alpha\beta)_{\boldsymbol{\phi}} (\mathcal{D}\alpha'\beta')_{\boldsymbol{\phi'}}\; |\alpha\rangle_{\boldsymbol{\phi}} |\beta\rangle_{\boldsymbol{\phi}}\; \Psi[\alpha\beta] \\ &\qquad\qquad \otimes \Psi^*[\alpha'\beta']\, {}_{\boldsymbol{\phi'}}\langle\alpha'|_{\boldsymbol{\phi'}} \langle\beta'|\,, \end{aligned} \tag{6.143}$$

and the reduced density is

$$\begin{aligned} \rho_A &= \mathrm{Tr}_B\, \rho \\ &= \int d\boldsymbol{\phi} (\mathcal{D}\alpha\alpha'\beta)_{\boldsymbol{\phi}}\; |\alpha\rangle_{\boldsymbol{\phi}} \left(\Psi[\alpha\beta]\Psi^*[\alpha'\beta]\right)\, {}_{\boldsymbol{\phi}}\langle\alpha'|\,. \end{aligned} \tag{6.144}$$

Note that all fields now have the same anchor due to the partial trace $\mathrm{Tr}_B(\cdot) = \int d\boldsymbol{\phi} (\mathcal{D}\beta)_{\boldsymbol{\phi}}\; {}_{\boldsymbol{\phi}}\langle\beta| \cdot |\beta\rangle_{\boldsymbol{\phi}}$. When $\mathrm{Tr}_A\, \rho_A^n$ is explicitly written out, we find a cyclic product of projectors of the form

$$\begin{aligned} &\mathrm{Tr}_A \left(\cdots |\alpha_i\rangle_{\boldsymbol{\phi}_i \boldsymbol{\phi}_i} \langle\alpha_i'|\alpha_{i+1}\rangle_{\boldsymbol{\phi}_{i+1} \boldsymbol{\phi}_{i+1}} \langle\alpha_{i+1}'| \cdots \right) \\ &\qquad = \prod_i \delta_{\alpha_i' \alpha_{i+1}} \delta_{\boldsymbol{\phi}_i \boldsymbol{\phi}_{i+1}}\,, \end{aligned} \tag{6.145}$$

forcing all anchors to agree : $\boldsymbol{\phi}_1 = \cdots = \boldsymbol{\phi}_n = \boldsymbol{\phi}$. Thus

$$\begin{aligned} \mathrm{Tr}_A\, \rho_A^n &= \int d\boldsymbol{\phi} \prod_i \int (\mathcal{D}\alpha_i\beta_i)_{\boldsymbol{\phi}}\; |\Psi[\alpha_i\beta_i]|^2 \\ &= \int d\boldsymbol{\phi} \left[\int (\mathcal{D}\alpha\beta)_{\boldsymbol{\phi}}\; |\Psi[\alpha\beta]|^2 \right]^n \\ &= \int d\boldsymbol{\phi} \left[{}_{\boldsymbol{\phi}}\langle\Psi|\Psi\rangle_{\boldsymbol{\phi}} \right]^n. \end{aligned} \tag{6.146}$$

Manifestly, $\mathrm{Tr}_A\,\rho_A^n = \mathrm{Tr}_B\,\rho_B^n$. Up to this point we have only used Assumption 1. If we now use the second assumption, we obtain

$$\mathrm{Tr}_A\,\rho_A^n = \int d\boldsymbol{\phi}\left[\int (\mathcal{D}\alpha)_{\boldsymbol{\phi}}\; a^2[\alpha]\int (\mathcal{D}\beta)_{\boldsymbol{\phi}}\; b^2[\beta]\right]^n. \tag{6.147}$$

Furthermore, on any interval $U = (x_{i_1}, x_{i_2})$ for x_i at the common boundary of A and B, the functional Ψ factors as $\Psi|_U \times \cdots$, and we may consistently define a local "action" by adjoining pieces of the form

$$\frac{1}{2}S_U = -\log \Psi|_U\,. \tag{6.148}$$

Then (6.147) splits into factors of the form $\langle \phi_{i_2}, x_{i_2}|\phi_{i_1}, x_{i_1}\rangle \stackrel{\mathrm{def}}{=} \int (\mathcal{D}\alpha)_{\boldsymbol{\phi}}\; (\Psi|_U)^2[\alpha] = \int (\mathcal{D}\alpha)_{\boldsymbol{\phi}}\; e^{-S_U[\alpha]}$, which we identify as the propagators of the dynamics associated to Ψ. It follows that

$$\mathrm{Tr}_A\,\rho_A^n = \int d\boldsymbol{\phi}\,[f_M(\boldsymbol{\phi}, \mathbf{x})]^n\,, \tag{6.149}$$

with $f_M(\boldsymbol{\phi}, \mathbf{x}) = \langle h_2, L|\phi_M, x_M\rangle \cdots \langle \phi_1, x_1|h_1, 0\rangle$ for boundary conditions $\phi(0) = h_1$, $\phi(L) = h_2$. If the system is periodic, the (variable) boundary value $\phi_0 = \phi(0) = \phi(L)$ is an additional anchor to be integrated on in (6.149).

For the dimensionful fields of the main text, as in (6.10), we have dim $f_M =$ (length)$^{-M/2}$. Under the rescaling $\phi \to \sqrt{\epsilon}\phi$, $f_M \to \epsilon^{-M/2} f_M$, where ϵ is a local length scale (e.g. a lattice constant or UV cutoff), we have

$$\int d\boldsymbol{\phi}\,[f_M]^n \to \epsilon^{(n-1)M/2}\int d\boldsymbol{\phi}\,[f_M]^n, \tag{6.150}$$

which, using (6.149) in (6.42), yields the Rényi entropies

$$S_n(A) = \frac{1}{1-n}\log\left[\epsilon^{(n-1)M/2}\int d\boldsymbol{\phi}\;\,[f_M(\boldsymbol{\phi}, \mathbf{x})]^n\right], \tag{6.151}$$

as advertised in the main text in (6.43).

6.7.2 Separability of $\rho_{A\cup B}$ for disjoint subsystems

We show that for both models considered in the present work, and in fact general states satisfying the RK property, the reduced density $\rho_{A\cup B}$ is (mixed) separable,

$$\rho_{A\cup B} = \sum_{j\in J} p_j(\rho_{A,j}\otimes\rho_{B,j})\,, \tag{6.152}$$

for any disconnected subsystems A and B. In the above expression, J is some index set, and p is a probability distribution on J. Thus, tracing out the complement of $A\cup B$ completely disentangles $|\Psi_0\rangle$. However, as long as p is not the trivial distribution, A and B will share mutual information.

Consider a general tripartition $\{A, B, C\}$, where C is to be traced out. From (6.144), a state satisfying both assumptions of Appendix 6.7.1 has reduced density

$$\langle \alpha\beta|\rho_{A\cup B}|\alpha'\beta'\rangle = \int (\mathcal{D}\gamma)_{\boldsymbol{\phi}} \Psi[\alpha\beta\gamma]\Psi[\alpha'\beta'\gamma]\,, \tag{6.153}$$

where α, β are as in (6.141), $\boldsymbol{\phi}$ is the anchor for these fields, and γ is restricted to the complement of $A \cup B$. By the second assumption, $\Psi[\alpha\beta\gamma] = a[\alpha]b[\beta]\Gamma[\gamma]$, where Γ is the restriction of Ψ to the complement of $A \cup B$, so

$$\langle \alpha\beta|\rho_{A\cup B}|\alpha'\beta'\rangle = \int (\mathcal{D}\gamma)_{\boldsymbol{\phi}} a[\alpha]b[\beta]\Gamma^2[\gamma]a[\alpha']b[\beta']\,. \tag{6.154}$$

Therefore, the reduced density is a separable mixed state

$$\rho_{A\cup B} = \int d\boldsymbol{\phi}\; p(\boldsymbol{\phi})\; \rho_A(\boldsymbol{\phi}) \otimes \rho_B(\boldsymbol{\phi})\,, \tag{6.155}$$

with probability distribution

$$p(\boldsymbol{\phi}) = \int (\mathcal{D}\gamma)_{\boldsymbol{\phi}}\; \Gamma^2[\gamma]\,, \tag{6.156}$$

and subsystem densities

$$\begin{aligned} \rho_A(\boldsymbol{\phi}) &= \int (\mathcal{D}\alpha\alpha')_{\boldsymbol{\phi}}\; |\alpha\rangle_{\boldsymbol{\phi}} a[\alpha]a[\alpha']_{\boldsymbol{\phi}}\langle\alpha'| = |\Psi_A\rangle_{\boldsymbol{\phi}\boldsymbol{\phi}}\langle\Psi_A|\,, \\ \rho_B(\boldsymbol{\phi}) &= \int (\mathcal{D}\beta\beta')_{\boldsymbol{\phi}}\; |\beta\rangle_{\boldsymbol{\phi}} b[\beta]b[\beta']_{\boldsymbol{\phi}}\langle\beta'| = |\Psi_B\rangle_{\boldsymbol{\phi}\boldsymbol{\phi}}\langle\Psi_B|\,. \end{aligned} \tag{6.157}$$

If necessary, the integral in (6.155) can be converted to a convergent countable sum over increasingly fine mesh elements, in the same way the (discrete) Schmidt form was obtained in Appendix 6.7.1. As obvious from the subsystem densities (6.157), $\rho_{A\cup B}$ is invariant under partial transpositions

$$\rho_{A\cup B}^{T_A} = \rho_{A\cup B} = \rho_{A\cup B}^{T_B}\,. \tag{6.158}$$

This is consistent with the known fact that, for Gaussian states like the massive deformation groundstate considered in the main text, invariance under partial transposition implies separability [182]. That observation was used in [18] to prove mixed separability in the massless Lifshitz theory. Our treatment is quite general, valid for real-valued RK wavefunctionals, independently of the dimension of the underlying classical theory. It thus provides the explicit separability of $\rho_{A\cup B}$ for quantum states satisfying the aforementioned properties, which includes both the massive deformation (Gaussian) and the singular deformation (non-Gaussian) of the Lifshitz theory considered in this work.

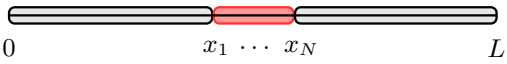

FIGURE 6.11 – N ordered points $x_1 < \cdots < x_N$ deep in the bulk.

6.7.3 Detailed relationships between moments for the singular deformation

Consider N ordered points $x_1 < x_2 < \cdots < x_N$ deep in the bulk, as shown in Fig. 6.11, and let us write $\phi(x_i) = \phi_i$. Based on the fact that propagators become free in the bulk, we expect a relationship between the functions

$$f_N^{(\nu)}(\boldsymbol{\phi}, \mathbf{x}) = \frac{\langle h, L|\phi_N, x_N\rangle}{\langle h, L|h, 0\rangle} \prod_{i=1}^{N-1} \langle \phi_{i+1}, x_{i+1}|\phi_i, x_i\rangle \langle \phi_1, x_1|h, 0\rangle \tag{6.159}$$

with different values of ν. As in the main text, $h = 0^+$ is a field regulator preventing the potential energy term from diverging. The propagators are given in (6.117), which is repeated here for convenience :

$$\langle \phi', x'|\phi, x\rangle = \tfrac{2\kappa\sqrt{\phi'\phi}}{x'-x} \exp\left[-\kappa\left(\tfrac{\phi'^2+\phi^2}{x'-x}\right)\right] I_\nu\left(\tfrac{2\kappa\phi'\phi}{x'-x}\right). \tag{6.160}$$

The only dependence in ν is in the Bessel function. Assume that $x_1 \sim L/2 \sim x_N$. From (6.126), we know that $\langle \phi_{i+1}\phi_i\rangle \sim L$, and therefore $\langle \phi_{i+1}\phi_i\rangle/(x_{i+1} - x_i) \gg 1$ for each $1 \leq i \leq N-2$. Neglecting fluctuations, and with $I_\nu(z) \sim e^z/\sqrt{2\pi z}$ for $z \gg 1$, we find that bulk propagators are asymptotic to those of the positive-valued free boson

$$\langle \phi_{i+1}, x_{i+1}|\phi_i, x_i\rangle_\nu \sim G_{\mathbb{R}^{>0}}(\phi_{i+1}, x_{i+1}; \phi_i, x_i), \tag{6.161}$$

as shown in the text in (6.118). Thus, $f_N^{(\nu)}(\boldsymbol{\phi}, \mathbf{x})$ will depend on ν only through the boundary propagators

$$\frac{\langle h, L|\phi_N, x_N\rangle\langle \phi_1, x_1|h, 0\rangle}{\langle h, L|h, 0\rangle}, \tag{6.162}$$

and ratios $f_N^{(\mu)}(\boldsymbol{\phi}, \mathbf{x})/f_N^{(\nu)}(\boldsymbol{\phi}, \mathbf{x})$ will be independent of bulk propagators. From (6.119) we know that $\langle \phi_1\rangle/x_1 \sim L^{-1/2} \sim \langle \phi_N\rangle/(L - x_N)$. Therefore, both $\langle h\phi_1\rangle/x_1$ and $\langle h\phi_N\rangle/(L - x_N)$ will be much smaller than 1 for small values of h. With $I_\nu(z) \sim \frac{(z/2)^\nu}{\Gamma(1+\nu)}$ for $z \ll 1$, we find

$$\frac{f_N^{(\mu)}(\boldsymbol{\phi}, \mathbf{x})}{f_N^{(\nu)}(\boldsymbol{\phi}, \mathbf{x})} = R(x_1, x_N, \mu, \nu)(\phi_1\phi_N)^{\mu-\nu}, \tag{6.163}$$

with

$$R(x_1, x_N, \mu, \nu) = \frac{\Gamma(1+\nu)}{\Gamma(1+\mu)} \left(\frac{\kappa L}{x_1(L - x_N)}\right)^{\mu-\nu}. \tag{6.164}$$

Thus,

$$\begin{aligned}
&\langle \phi_1^{\alpha_1} \cdots \phi_N^{\alpha_N} \rangle_\mu \\
&= \int d\boldsymbol{\phi}\ \phi_1^{\alpha_1} \cdots \phi_N^{\alpha_N} f_N^{(\mu)}(\boldsymbol{\phi}, \mathbf{x}) \\
&= R(x_1, x_N, \mu, \nu) \int d\boldsymbol{\phi}\ \phi_1^{\alpha_1} \cdots \phi_N^{\alpha_N} (\phi_1 \phi_N)^{\mu-\nu} f_N^{(\nu)}(\boldsymbol{\phi}, \mathbf{x}) \\
&= R(x_1, x_N, \mu, \nu) \langle \phi_1^{\alpha_1+\mu-\nu} \phi_2^{\alpha_2} \cdots \phi_{N-1}^{\alpha_{N-1}} \phi_N^{\alpha_N+\mu-\nu} \rangle_\nu \,,
\end{aligned} \tag{6.165}$$

which is identical to (6.135). The single-point relation (6.120) is a special case, but its validity is actually slightly more general because it contains no bulk propagator. Thus the above result carries through even if x is close to the boundary, as long as the regulator h is 0^+. Relationship (6.165) is easily generalized if some points are close to the boundary. Then (6.162) has to be modified to account for the additional boundary propagators.

Conclusion

Dans cette thèse, nous avons étudié des systèmes quantiques locaux en dimension réduite, du point de vue de la théorie de l'information quantique. La première partie (Chapitres 1 et 2) était consacrée aux applications d'hamiltoniens locaux pour les fins du calcul quantique universel automatisé. Réciproquement, la seconde partie (Chapitres 3 à 6) mettait à l'œuvre les outils de la théorie quantique de l'information pour étudier les états fondamentaux d'hamiltoniens locaux à corps multiples (*many-body*). Les systèmes considérés étaient principalement de dimension 0 ou 1, avec quelques exceptions en dimension supérieure.

Dans le cadre du premier article (Chapitre 2), nous avons exploré la possibilité de regrouper les qubits physiques par paires, dans des systèmes à quatre niveaux nommés *quansistors* et munis d'une symétrie (invariance sous les ω-rotations) protégeant partiellement les opérations logiques effectuées sur ces paires. Nous avons proposé un ensemble strictement universel à deux qubits, $\{\mathsf{V}, \mathsf{W}\}$, qui s'avère particulièrement robuste face à un certain type d'erreurs, soit les rotations intempestives de qubits par rapport aux axes x et z. Une réduction par un seul ordre de grandeur du couplage aux rotations en y procure déjà un avantage significatif à l'ensemble $\{\mathsf{V}, \mathsf{W}\}$, comparativement à d'autres ensembles universels, dont l'ensemble de Kitaev [172]. L'effet d'électrodes semi-infinies identiques, couplées par effet tunnel aux quansistors, a été explicitement considéré pour réaliser l'initialisation et la lecture (*readout*) des qubits, mais également parce que ce type de couplage est la source dominante de décohérence dans de nombreuses réalisations de qubits en état solide, notamment les qubits supraconducteurs et les points quantiques semiconducteurs [197]. Nous avons montré que la symétrie des quansistors permettait de réaliser les opérations logiques, V et W entre autres, à l'abri de l'influence des électrodes. En établissant une relation entre l'invariance sous les ω-rotations et une structure de jauge $\mathbf{U}(1)$, il nous a été possible d'identifier de potentielles implémentations physiques pour les quansistors, faisant intervenir des systèmes chargés sous l'influence d'un champ électromagnétique, ou encore des systèmes neutres sous l'influence d'un champ de jauge synthétique [14]. Enfin, nous avons proposé un mécanisme par lequel des quansistors distants pourraient entrer en interaction intriquante, produisant une plateforme évolutive pour le calcul quantique universel, où le nombre de quansistors requis est proportionnel au nombre de qubits de calcul.

Dans la suite de nos travaux, il sera nécessaire d'estimer la robustesse de notre proposition face à un ensemble plus large de types d'erreurs, notamment par l'analyse comparative randomisée (*randomized benchmarking*) [177]. Il sera aussi intéressant de déterminer dans quelle mesure l'anisotropie observée pour l'ensemble $\{\mathsf{V}, \mathsf{W}\}$ est propre à cet ensemble ou, au contraire, est une caractéristique de la symétrie elle-même. De nombreux aspects de notre proposition se généralisent à d'autres symétries, ainsi qu'à des systèmes à plus de quatre niveaux. D'autres symétries protègent-elles mieux les opérations internes au quansistor ? Des systèmes de plus haut niveau

offriraient-ils des avantages pour la communication quantique ? Et quelle est la relation exacte entre la symétrie du quansistor et sa résilience face aux erreurs ? Ces questions seront l'objet d'investigations futures.

Le second article (Chapitre 5) portait sur les chaînes de spins géométriquement frustrées et leurs propriétés d'intrication. Le théorème de Toulouse et Vannimenus implique qu'un système classique (de dimension quelconque) est frustré si et seulement s'il contient des sous-systèmes équivalents à des chaînes antiferromagnétiques sur des parcours fermés de longueur impaire [265, 270]. L'ordre de Néel est alors frustré par le nombre impair de sites. Le théorème peut être généralisé aux frustrations géométriques des systèmes quantiques (qui peuvent en outre présenter des frustrations dues aux intrications locales) [114, 198]. Il apparaît donc que les chaînes antiferromagnétiques de longueur impaire constituent l'élément universellement présent dans les frustrations géométriques des systèmes classiques ou quantiques, ce qui suggère le rôle essentiel qu'elles sont appelées à jouer dans la compréhension des propriétés microscopiques et macroscopiques propres aux systèmes frustrés. L'omniprésence des frustrations dans les systèmes naturels, leur caractère non perturbatif et leurs éventuelles applications aux technologies de l'information justifient l'intérêt croissant dont elles bénéficient.

Nous avons considéré un secteur particulier de la chaîne antiferromagnétique XXZ de spins élevés, pourvue d'une anisotropie à ion unique (*single-ion*), telle qu'introduite par Haldane [131]. Dans la limite considérée, le terme d'anisotropie (classique) était dominant, favorisant localement un ordre de Néel, tandis que l'interaction de Heisenberg était traitée perturbativement. Nous avons étudié les solitons de la chaîne périodique frustrée par un nombre impair N de sites imposant un défaut — le soliton — dans l'ordre Néel naturel de ce secteur. Les états du spectre perturbatif forment alors une bande sans gap, constituée des superpositions à poids égaux des différentes positions du soliton. Bien que la présence du soliton soit due à une propriété topologique ou globale, la parité de N, son profil semi-classique n'est déterminé que par les interactions locales de l'hamiltonien. Nous avons montré qu'en variant les couplages, la frustration des termes locaux d'interaction pouvait prendre toutes les valeurs possibles, de frustration faible $f \approx 0$ pour un soliton de longueur $M = O(1)$, à frustration forte $f \approx 1$ lorsque $M \approx N$. L'identification explicite du spectre d'intrication bipartite de l'état fondamental nous a permis de calculer l'entropie d'intrication et la capacité d'intrication. Pour une frustration faible, nous trouvons pour l'entropie d'intrication une violation algébrique de la loi d'aire, ainsi qu'une saturation pour les grands sous-systèmes, en accord parfait avec les résultats rapportés dans la littérature pour d'autre chaînes faiblement frustrées [115]. Notre analyse nous a permis, de plus, d'explorer le régime de forte frustration, ce qui constitue notre résultat principal. Nous y trouvons une entropie d'intrication *extensive* dans la taille du sous-système, ainsi qu'une divergence infrarouge logarithmique, i.e. $S \sim \log N$ pour un système de taille N.

Pour toutes les tailles du soliton (i.e. toutes les valeurs de la frustration), la forte violation de la loi d'aire élimine la possibilité d'une description effective de basse énergie à l'aide d'une CFT_2 [149] ou du boson non compact de Lifshitz $z = 2$ [72]. En particulier, un soliton de taille $M = O(N)$ confère au système une échelle macro-

scopique de longueur, incompatible avec une théorie invariante d'échelle. L'entropie d'intrication correspondante rappelle alors, par certains aspects, celle observée dans les théories non locales de champs [227] (avec d'importantes différences, soulevées au Chapitre 5). Ce constat peut-il nous guider dans la recherche d'une théorie effective pour la chaîne fortement frustrée ? Les propriétés d'intrications que nous identifions en frustration forte se retrouvent-elles sur d'autres chaînes fortement frustrées ? Ces propriétés peuvent-elles contribuer à élucider la phénoménologie des frustrations géométriques en dimensions supérieures ? Telles seront les prochaines orientations de notre étude.

Le troisième et dernier article (Chapitre 6) explorait les corrélations et l'intrication dans les états fondamentaux de deux déformations du boson non compact de Lifshitz $z = 2$ [23]. Bien que présentant des symétries et des espaces cibles distincts, les deux déformations ont en commun de préserver la structure de Rokhsar-Kivelson (RK) de la théorie originale, de telle sorte que les corrélateurs de la fonctionnelle d'onde fondamentale en dimension $D + 1$ sont encodés dans la fonction de partition d'une action locale $(D + 0)$-dimensionnelle [68]. Nous nous sommes concentrés principalement sur le cas $D = 1$. La première déformation brise l'invariance de Lifshitz par une échelle de masse. Ses corrélateurs, pour $D = 1$, correspondent aux propagateurs de l'action euclidienne de l'oscillateur harmonique, et nous sommes en mesure de les exploiter pour calculer analytiquement plusieurs indicateurs d'intrication et de corrélations, tels que les entropies bipartites de Rényi d'ordre n et la c-fonction entropique correspondante (indépendante de n), l'information mutuelle entre deux intervalles et la capacité d'intrication bipartite. Tel que prévu, nous observons un rétablissement de la propriété de *Cluster Decomposition* dû à la régularisation massive. L'entropie d'intrication d'un intervalle satisfait la loi d'aire et permet d'observer la transition à une violation logarithmique lors du passage à la criticalité $m \to 0$. L'expression que nous obtenons pour l'entropie de Rényi d'une bipartition quelconque généralise à la théorie massive en dimension $1+1$, non invariante de Lifshitz, la formule de Fradkin-Moore [105] valide pour la théorie Lifshitz non compacte en dimension $2 + 1$. Elle permet d'obtenir une expression universelle et indépendante de n pour l'information mutuelle entre deux sous-systèmes. Pour deux intervalles profondément dans le volume, en particulier, le résultat confirme que l'information mutuelle décroît exponentiellement avec la séparation, à l'exception du cas sans masse, pour lequel on découvre une divergence infrarouge persistant à toutes les séparations et négligée dans la littérature [73]. De plus, nous formulons un argument général de séparabilité de la matrice densité réduite $\rho_{A\cup B}$ pour des sous-systèmes A et B non connexes, applicable à la fonctionnelle fondamentale réelle d'une QFT $(D+1)$-dimensionnelle de type RK. La séparabilité (mixte) indique que l'information mutuelle résulte entièrement de corrélations classiques et de corrélations quantiques non intriquantes [213, 117, 3, 4].

Nous avons déterminé le comportement de la c-fonction entropique sous le flot de RG de la *fonction d'onde* de l'état fondamental. (Ce flot de RG *spatial* appliqué à l'action euclidienne $(1 + 0)$-dimensionnelle équivaut à imposer un réglage fin à l'hamiltonien et préserve sa structure RK.) Bien que la théorie massive ne soit pas invariante conforme (ni même invariante de Lifshitz), sa c-fonction s'avère monotone

décroissante sous le flot de RG. Nous sommes également surpris de découvrir une relation entre l'intrication de coin de la théorie Lifshitz ($z = 2$) en dimension $2 + 1$ et la c-fonction de la théorie massive en dimension $1 + 1$, qui généralise la relation correspondante entre l'intrication de coin d'une CFT_3 et la c-fonction d'une QFT de dimension inférieure [65]. Enfin, la capacité d'intrication obtenue satisfait une loi d'aire, résultat indépendant de la masse et qui demeure valide pour le cas critique $m = 0$. L'existence d'une borne supérieure (modeste, de surcroît) pour la capacité d'intrication atteste d'une faible variance des valeurs propres de la matrice densité réduite, et suggère que l'intrication dans l'état fondamental est effectivement portée par des paires EPR maximalement intriquées [85]. Par contraste, les CFT présentent habituellement une capacité d'intrication asymptotiquement comparable à l'entropie d'intrication, indiquant le rôle dominant de paires effectives de qubits arbitrairement intriqués.

La seconde déformation considérée fait intervenir le couplage à un potentiel singulier qui préserve la symétrie Lifshitz, mais sépare la théorie en deux secteurs équivalents de telle sorte que l'espace cible naturel pour ϕ est $\mathbb{R}^{>0}$. Les corrélateurs de la fonction d'onde sont ici donnés par les propagateurs de la mécanique quantique conforme [84]. (Pour des raisons techniques, la déformation est supersymétrique, mais le fondamental fermionique est sans intrication.) La partie universelle des corrélateurs connectées du volume est indépendante du couplage g au potentiel singulier, confirmant que le potentiel singulier est ineffectif dans le volume. La divergence infrarouge, en revanche, dépend fortement de g puisque s'agissant d'un phénomène de frontière. Nous montrons que l'effet du potentiel singulier sur les entropies d'intrication de Rényi d'un intervalle collé au bord se résume à une constante et que, par conséquent, les c-fonctions sont toutes égales à $1/2$, en accord avec l'invariance conforme spatiale de la fonctionnelle d'onde fondamentale. L'ensemble des valeurs de $g \in [0, \infty)$ correspond à une ligne de théories critiques dans l'espace des paramètres.

L'une des raisons à l'origine de ce travail était l'hypothèse que l'état fondamental du boson Lifshitz positif (ou du boson singulier pour $g = 0$) correspondait à la limite continue des états fondamentaux des chaînes de Motzkin et de Fredkin [49, 86]. Or, bien que plusieurs propriétés de corrélations et d'intrication soit correctement rendues par le boson positif, il apparaît que l'entropie d'intrication d'un intervalle du volume diverge dans l'infrarouge pour le boson, tandis qu'une telle divergence est absente des chaînes de Motzkin et de Fredkin. En conséquence, l'information mutuelle du boson positif présente également une divergence IR qui n'est pas observée sur le réseau [87]. Quelle est donc la véritable limite continue des états fondamentaux Motzkin et Fredkin ? La question demeure en suspend et sera l'objet de nos prochains travaux. La régularisation des divergences IR passera vraisemblablement par la brisure de la symétrie affine de la théorie sans masse. Une approche prometteuse est la compactification du boson Lifshitz. En effet, dans le cas du boson Lifshitz compact en dimension $2 + 1$, la contributions de modes zéros (*winding modes*) permet d'annuler exactement les termes potentiellement divergents infrarouges de l'information mutuelle [300]. D'autre part, il sera intéressant de passer aux dimensions supérieures, où la structure RK pourra également être mise à profit pour analyser les corrélations et les intrications. En particulier, nous tenterons de déterminer si l'on retrouve en di-

mension 2+1 un phénomène analogue à la monotonicité de la c-fonction sous le flot de RG de la fonctionnelle d'onde. Un résultat positif généraliserait le F-théorème [66], applicable aux CFT_3.

Au moment d'écrire ces lignes, le rythme des activités de recherche et de publication scientifique se rapportant à la fois à la matière condensée, à la physique des hautes énergies et à l'information quantique, témoigne de la rencontre extrêmement fertile de ces disciplines. Nous nous sommes penchés sur deux aspects de cette rencontre, complémentaires à bien des égards, soit d'une part la conception de systèmes quantiques à corps multiples qui réaliseront des calculateurs quantiques plus robustes, et d'autre part les opportunités offertes par la théorie de l'information quantique pour la résolution des difficiles problèmes soulevés par les systèmes quantiques à corps multiples, sur réseau ou dans le continuum. Nous avons omis de nombreux aspects de ce vaste champ de recherche, notamment la communication quantique [229, 186, 112], la simulation quantique [108, 15], la métrologie [118], les techniques holographiques [234], ainsi que la classification des ordres topologiques à l'aide de la théorie des catégories monoïdales [162], qui sont autant de gages de la vitalité de ce programme.

Bibliographie

[1] Aaronson, S., "Np-complete problems and physical reality," *Electron. Colloquium Comput. Complex.*, 2005.

[2] Abrahamsen, N., "A polynomial-time algorithm for ground states of spin trees," *arXiv : Quantum Physics*, 2019.

[3] Adesso, G., Bromley, T. R., and Cianciaruso, M., "Measures and applications of quantum correlations," *J. Phys. A*, vol. 49, no. 47, p. 473001, 2016.

[4] Adesso, G., Cianciaruso, M., and Bromley, T. R., "An introduction to quantum discord and non-classical correlations beyond entanglement," Nov. 2016.

[5] Aharon, E., Pozner, R., Lifshitz, E., and Peskin, U., "Multi-bit dark state memory : Double quantum dot as an electronic quantum memory," *Journal of Applied Physics*, vol. 120, p. 244301, 12 2016.

[6] Aharonov, D., van Dam, W., Kempe, J., Landau, Z., Lloyd, S., and Regev, O., "Adiabatic quantum computation is equivalent to standard quantum computation," in *45th Annual IEEE Symposium on Foundations of Computer Science*, pp. 42–51, 2004.

[7] Aharonov, D., "A simple proof that toffoli and hadamard are quantum universal," 2003.

[8] Aharonov, D., Arad, I., and Irani, S., "Efficient algorithm for approximating one-dimensional ground states," *Phys. Rev. A*, vol. 82, p. 012315, Jul 2010.

[9] Aharonov, D., Arad, I., Landau, Z., and Vazirani, U., "The detectability lemma and quantum gap amplification," *Proceedings of the Annual ACM Symposium on Theory of Computing*, 12 2008.

[10] Aharonov, D., Arad, I., Vazirani, U., and Landau, Z., "The detectability lemma and its applications to quantum hamiltonian complexity," *New Journal of Physics*, vol. 13, p. 113043, 11 2011.

[11] Aharonov, D., Harrow, A., Landau, Z., Nagaj, D., Szegedy, M., and Vazirani, U., "Local tests of global entanglement and a counterexample to the generalized area law," *Proceedings - Annual IEEE Symposium on Foundations of Computer Science, FOCS*, 10 2014.

[12] Aharony, A., Gurvitz, S., Tokura, Y., Entin-Wohlman, O., and Dattagupta, S., "Partial decoherence in mesoscopic systems," *Physica Scripta*, vol. T151, p. 014018, nov 2012.

[13] Aidelsburger, M., Atala, M., Lohse, M., Barreiro, J. T., Paredes, B., and Bloch, I., "Realization of the hofstadter hamiltonian with ultracold atoms in optical lattices," *Phys. Rev. Lett.*, vol. 111, p. 185301, Oct 2013.

[14] Aidelsburger, M., Nascimbene, S., and Goldman, N., "Artificial gauge fields in materials and engineered systems," *Comptes Rendus Physique*, vol. 19, no. 6, pp. 394–432, 2018. Quantum simulation / Simulation quantique.

[15] Altman, E., Brown, K. R., Carleo, G., Carr, L. D., Demler, E., Chin, C., DeMarco, B., Economou, S. E., Eriksson, M. A., Fu, K.-M. C., and et al., "Quantum simulators : Architectures and opportunities," *PRX Quantum*, vol. 2, Feb 2021.

[16] Anderson, B., Juzeliūnas, G., Spielman, I., and Galitski, V., "Synthetic 3d spin-orbit coupling," *Physical Review Letters*, vol. 108, 12 2011.

[17] Angel-Ramelli, J., "Entanglement Entropy of Excited States in the Quantum Lifshitz Model," *J. Stat. Mech.*, vol. 2101, p. 013102, 2021.

[18] Angel-Ramelli, J., Berthiere, C., Puletti, V. G. M., and Thorlacius, L., "Logarithmic Negativity in Quantum Lifshitz Theories," *JHEP*, vol. 09, p. 011, 2020.

[19] Anshu, A., Arad, I., and Gosset, D., "An area law for 2d frustration-free spin systems," 2021.

[20] Anshu, A., Harrow, A. W., and Soleimanifar, M., "From communication complexity to an entanglement spread area law in the ground state of gapped local hamiltonians," 2020.

[21] Arad, I., Kitaev, A., Landau, Z., and Vazirani, U., "An area law and sub-exponential algorithm for 1d systems," 2013.

[22] Arad, I., Landau, Z., and Vazirani, U., "Improved one-dimensional area law for frustration-free systems," *Phys. Rev. B*, vol. 85, p. 195145, May 2012.

[23] Ardonne, E., Fendley, P., and Fradkin, E., "Topological order and conformal quantum critical points," *Annals of Physics*, vol. 310, p. 493–551, Apr 2004.

[24] Bacon, D., Kempe, J., DiVincenzo, D. P., Lidar, D. A., and Whaley, K. B., "Encoded universality in physical implementations of a quantum computer," 2001.

[25] Balasubramanian, K. and McGreevy, J., "Gravity duals for nonrelativistic CFTs," *Phys. Rev. Lett.*, vol. 101, p. 061601, 2008.

[26] Bandyopadhyay, S., Boykin, P., Roychowdhury, V., and Vatan, F., "A new proof for the existence of mutually unbiased bases," *Algorithmica (New York)*, vol. 34, 04 2001.

[27] Barahona, F., "On the computational complexity of ising spin glass models," *Journal of Physics A*, vol. 15, pp. 3241–3253, oct 1982.

[28] Barbón, J. L. F. and Fuertes, C. A., "On the spectrum of nonrelativistic AdS/CFT," *JHEP*, vol. 09, p. 030, 2008.

[29] Barbón, J. L. and Fuertes, C. A., "Holographic entanglement entropy probes (non)locality," *Journal of High Energy Physics*, vol. 2008, p. 096–096, Apr 2008.

[30] Barenco, A., "A universal two-bit gate for quantum computation," *Proceedings of the Royal Society of London. Series A : Mathematical and Physical Sciences*, vol. 449, pp. 679 – 683, 1995.

[31] Barenco, A., Bennett, C., Cleve, R., DiVincenzo, D., Margolus, N., Shor, P., Sleator, T., Smolin, J., and Weinfurter, H., "Elementary gates for quantum computation," *Physical Review A*, vol. 52, 03 1995.

[32] Bartlett, S. D. and Sanders, B. C., "Universal continuous-variable quantum computation : Requirement of optical nonlinearity for photon counting," *Physical Review A*, vol. 65, Mar 2002.

[33] Bechmann-Pasquinucci, H. and Tittel, W., "Quantum cryptography using larger alphabets," *Phys. Rev. A*, vol. 61, p. 062308, May 2000.

[34] Bekenstein, J., "Black holes and the second law," *Lettere al Nuovo Cimento (1971-1985)*, vol. 4, pp. 737–740, 1972.

[35] Bekenstein, J. D., "Do we understand black hole entropy ?," in *7th Marcel Grossmann Meeting on General Relativity (MG 7)*, 7 1994.

[36] Benioff, P., "The computer as a physical system : A microscopic quantum mechanical hamiltonian model of computers as represented by turing machines," *Journal of Statistical Physics*, vol. 22, pp. 563–591, 05 1980.

[37] Bennett, C. H., Bernstein, E., Brassard, G., and Vazirani, U., "Strengths and weaknesses of quantum computing," *SIAM J. Comput.*, vol. 26, pp. 1510–1523, 1997.

[38] Bermudez, A., Schaetz, T., and Porras, D., "Synthetic gauge fields for vibrational excitations of trapped ions," *Phys. Rev. Lett.*, vol. 107, p. 150501, Oct 2011.

[39] Bermudez, A., Schaetz, T., and Porras, D., "Photon-assisted-tunneling toolbox for quantum simulations in ion traps," *New Journal of Physics*, vol. 14, p. 053049, may 2012.

[40] Berry, M. V., "Quantal phase factors accompanying adiabatic changes," *Proceedings of the Royal Society of London. Series A, Mathematical and Physical Sciences*, vol. 392, no. 1802, pp. 45–57, 1984.

[41] Bertoldi, G., Burrington, B. A., and Peet, A. W., "Thermodynamics of black branes in asymptotically Lifshitz spacetimes," *Phys. Rev. D*, vol. 80, p. 126004, 2009.

[42] Binder, K. and Young, A. P., "Spin glasses : Experimental facts, theoretical concepts, and open questions," *Rev. Mod. Phys.*, vol. 58, pp. 801–976, Oct 1986.

[43] Blais, A., Grimsmo, A. L., Girvin, S. M., and Wallraff, A., "Circuit quantum electrodynamics," 2020.

[44] Blatt, R. and Wineland, D., "Entangled states of trapped atomic ions," *Nature*, vol. 453, no. 7198, pp. 1008–1015, 2008.

[45] Blume, M., "Theory of the first-order magnetic phase change in uo_2," *Phys. Rev.*, vol. 141, pp. 517–524, Jan 1966.

[46] Bramwell, T. and Gingras, M., "Spin ice state in frustrated magnetic pyrochlore materials," *Science (New York, N.Y.)*, vol. 294, pp. 1495–501, 12 2001.

[47] Brandão, F. and Horodecki, M., "An area law for entanglement from exponential decay of correlations," *Nature Physics*, vol. 9, pp. 721–726, 2013.

[48] Brandao, F. and Horodecki, M., "Exponential decay of correlations implies area law," *Communications in Mathematical Physics*, vol. 333, 06 2012.

[49] Bravyi, S., Caha, L., Movassagh, R., Nagaj, D., and Shor, P. W., "Criticality without frustration for quantum spin-1 chains," *Phys. Rev. Lett.*, vol. 109, p. 207202, Nov 2012.

[50] Bravyi, S. and Kitaev, A., "Fermionic quantum computation," *Annals of Physics*, vol. 298, 03 2000.

[51] Bueno, P. and Witczak-Krempa, W., "Bounds on corner entanglement in quantum critical states," *Phys. Rev. B*, vol. 93, p. 045131, Jan 2016.

[52] Calabrese, P., Mintchev, M., and Vicari, E., "Entanglement entropies in free-fermion gases for arbitrary dimension," *EPL (Europhysics Letters)*, vol. 97, p. 20009, Jan 2012.

[53] Calabrese, P. and Cardy, J., "Entanglement entropy and quantum field theory," *Journal of Statistical Mechanics : Theory and Experiment*, vol. 2004, p. P06002, Jun 2004.

[54] Calabrese, P., Cardy, J., and Tonni, E., "Entanglement negativity in quantum field theory," *Phys. Rev. Lett.*, vol. 109, p. 130502, 2012.

[55] Callan, C. and Wilczek, F., "On geometric entropy," *Physics Letters B*, vol. 333, p. 55–61, Jul 1994.

[56] Capel, H., "On the possibility of first-order phase transitions in ising systems of triplet ions with zero-field splitting," *Physica*, vol. 32, no. 5, pp. 966–988, 1966.

[57] Capel, H., "Phase transitions in spin-one ising systems," *Physics Letters*, vol. 23, no. 5, pp. 327–328, 1966.

[58] Capel, H., "On the possibility of first-order transitions in ising systems of triplet ions with zero-field splitting ii," *Physica*, vol. 33, no. 2, pp. 295–331, 1967.

[59] Cardy, J. L., Castro-Alvaredo, O. A., and Doyon, B., "Form factors of branch-point twist fields in quantum integrable models and entanglement entropy," *Journal of Statistical Physics*, vol. 130, p. 129–168, Oct 2007.

[60] Cardy, J., *Scaling and Renormalization in Statistical Physics*. Cambridge Lecture Notes in Physics, Cambridge University Press, 1996.

[61] Cardy, J. L. and Peschel, I., "Finite-size dependence of the free energy in two-dimensional critical systems," *Nuclear Physics B*, vol. 300, pp. 377–392, 1988.

[62] Casini, H., Fosco, C. D., and Huerta, M., "Entanglement and alpha entropies for a massive Dirac field in two dimensions," *J. Stat. Mech.*, vol. 0507, p. P07007, 2005.

[63] Casini, H. and Huerta, M., "A finite entanglement entropy and the c-theorem," *Physics Letters B*, vol. 600, p. 142–150, Oct 2004.

[64] Casini, H. and Huerta, M., "Universal terms for the entanglement entropy in 2+1 dimensions," *Nuclear Physics B*, vol. 764, p. 183–201, Mar 2007.

[65] Casini, H. and Huerta, M., "Entanglement entropy in free quantum field theory," *Journal of Physics A : Mathematical and Theoretical*, vol. 42, p. 504007, Dec 2009.

[66] Casini, H. and Huerta, M., "Renormalization group running of the entanglement entropy of a circle," *Physical Review D*, vol. 85, Jun 2012.

[67] Casini, H., Huerta, M., and Leitao, L., "Entanglement entropy for a Dirac fermion in three dimensions : Vertex contribution," *Nucl. Phys. B*, vol. 814, pp. 594–609, 2009.

[68] Castelnovo, C., Chamon, C., Mudry, C., and Pujol, P., "From quantum mechanics to classical statistical physics : Generalized rokhsar–kivelson hamiltonians and the "stochastic matrix form" decomposition," *Annals of Physics*, vol. 318, p. 316–344, Aug 2005.

[69] Castro-Alvaredo, O. A., De Fazio, C., Doyon, B., and Szécsényi, I. M., "Entanglement content of quantum particle excitations. part i. free field theory," *Journal of High Energy Physics*, vol. 2018, Oct 2018.

[70] Castro-Alvaredo, O. A., De Fazio, C., Doyon, B., and Szécsényi, I. M., "Entanglement content of quasiparticle excitations," *Physical Review Letters*, vol. 121, Oct 2018.

[71] Castro Neto, A., Guinea, F., Peres, N., Novoselov, K., and Geim, A., "The electronic properties of graphene," *Review of Modern Physics*, vol. 81, 10 2007.

[72] Chen, X., Fradkin, E., and Witczak-Krempa, W., "Gapless quantum spin chains : multiple dynamics and conformal wavefunctions," *Journal of Physics A : Mathematical and Theoretical*, vol. 50, p. 464002, Oct 2017.

[73] Chen, X., Fradkin, E., and Witczak-Krempa, W., "Quantum spin chains with multiple dynamics," *Physical Review B*, vol. 96, Nov 2017.

[74] Chen, X., Witczak-Krempa, W., Faulkner, T., and Fradkin, E., "Two-cylinder entanglement entropy under a twist," *J. Stat. Mech.*, vol. 1704, no. 4, p. 043104, 2017.

[75] Chi-Chih Yao, A., "Quantum circuit complexity," in *Proceedings of 1993 IEEE 34th Annual Foundations of Computer Science*, pp. 352–361, 1993.

[76] Cho, J., "Sufficient condition for entanglement area laws in thermodynamically gapped spin systems.," *Physical review letters*, vol. 113 19, p. 197204, 2014.

[77] Cho, J., "Realistic area-law bound on entanglement from exponentially decaying correlations," *Physical Review X*, vol. 8, 07 2018.

[78] Chowdhury, F. T., "Undecidability in mathematics and physics," 02 2019.

[79] Chubb, C. T. and Flammia, S., "Computing the degenerate ground space of gapped spin chains in polynomial time," *ArXiv*, vol. abs/1502.06967, 2016.

[80] Cramer, M., Eisert, J., Plenio, M. B., and Dreissig, J., "Entanglement-area law for general bosonic harmonic lattice systems," *Phys. Rev. A*, vol. 73, p. 012309, Jan 2006.

[81] Cubitt, T. S., Perez-Garcia, D., and Wolf, M. M., "Undecidability of the spectral gap," *Nature*, vol. 528, p. 207–211, Dec 2015.

[82] Cucchietti, F. M., Paz, J. P., and Zurek, W. H., "Decoherence from spin environments," *Physical Review A*, vol. 72, Nov 2005.

[83] da Fonseca, C. and Petronilho, J. *Lin. Alg. and Apps.*, vol. 325, pp. 7–21, 2001.

[84] de Alfaro, V., Fubini, S., and Furlan, G., "Conformal invariance in quantum mechanics," *Il Nuovo Cimento A (1965-1970)*, vol. 34, no. 4, pp. 569–612, 1976.

[85] de Boer, J., Järvelä, J., and Keski-Vakkuri, E., "Aspects of capacity of entanglement," *Physical Review D*, vol. 99, Mar 2019.

[86] Dell'Anna, L., Salberger, O., Barbiero, L., Trombettoni, A., and Korepin, V. E., "Violation of cluster decomposition and absence of light cones in local integer and half-integer spin chains," *Physical Review B*, vol. 94, Oct 2016.

[87] Dell'Anna, L., "Long-distance entanglement in motzkin and fredkin spin chains," *SciPost Physics*, vol. 7, Oct 2019.

[88] Deutsch, D., Barenco, A., and Ekert, A., "Universality in quantum computation," *Proc. Roy. Soc. of London*, vol. 449, 05 1995.

[89] Devadutta Kulkarni, D. S. and Tsui, S.-K. *Lin. Alg. and Appl.*, pp. 63–80, 1999.

[90] Devoret, M. H. and Schoelkopf, R. J., "Superconducting circuits for quantum information : an outlook," *Science*, vol. 339, no. 6124, pp. 1169–1174, 2013.

[91] Dhar, D., "Lattices of effectively nonintegral dimensionality," *Journal of Mathematical Physics*, vol. 18, pp. 577–585, 04 1977.

[92] Dijkgraaf, R., Orlando, D., and Reffert, S., "Relating Field Theories via Stochastic Quantization," *Nucl. Phys. B*, vol. 824, pp. 365–386, 2010.

[93] DiVincenzo, D. P., "Two-bit gates are universal for quantum computation," *Phys. Rev. A*, vol. 51, pp. 1015–1022, Feb 1995.

[94] Dunlap, D. H. and Kenkre, V. M., "Dynamic localization of a charged particle moving under the influence of an electric field," *Phys. Rev. B*, vol. 34, pp. 3625–3633, Sep 1986.

[95] Durt, T., Englert, B.-G., Bengtsson, I., and Życzkowski, K., "On mutually unbiased bases," *International Journal of Quantum Information*, vol. 08, no. 04, pp. 535–640, 2010.

[96] Dutta, A. and Bhattacharjee, J. K., "Phase transitions in the quantum ising and rotor models with a long-range interaction," *Phys. Rev. B*, vol. 64, p. 184106, Oct 2001.

[97] Eisert, J., Cramer, M., and Plenio, M. B., "Colloquium : Area laws for the entanglement entropy," *Reviews of Modern Physics*, vol. 82, p. 277–306, Feb 2010.

[98] Eisert, J. and Osborne, T., "General entanglement scaling laws from time evolution," *Physical review letters*, vol. 97, p. 150404, 11 2006.

[99] Elliott, R. J., "Phenomenological discussion of magnetic ordering in the heavy rare-earth metals," *Phys. Rev.*, vol. 124, pp. 346–353, Oct 1961.

[100] Evenbly, G. and Vidal, G., "Algorithms for entanglement renormalization," *Physical Review B*, vol. 79, Apr 2009.

[101] Feynman, R. P., "Simulating Physics with Computers," *International Journal of Theoretical Physics*, vol. 21, pp. 467–488, June 1982.

[102] Fisher, M. E., Ma, S.-k., and Nickel, B. G., "Critical exponents for long-range interactions," *Phys. Rev. Lett.*, vol. 29, pp. 917–920, Oct 1972.

[103] Fisher, M. E. and Selke, W., "Infinitely many commensurate phases in a simple ising model," *Phys. Rev. Lett.*, vol. 44, pp. 1502–1505, Jun 1980.

[104] Fradkin, E., *Field Theories of Condensed Matter Physics*. Cambridge University Press, 2 ed., 2013.

[105] Fradkin, E. and Moore, J. E., "Entanglement entropy of 2d conformal quantum critical points : Hearing the shape of a quantum drum," *Physical Review Letters*, vol. 97, Aug 2006.

[106] Frahm, K. M., Fleckinger, R., and Shepelyansky, D. L., "Quantum chaos and random matrix theory for fidelity decay in quantum computations with static imperfections," *The European Physical Journal D - Atomic, Molecular and Optical Physics*, vol. 29, p. 139–155, Apr 2004.

[107] Fredenhagen, K., "A remark on the cluster theorem," *Communications in Mathematical Physics*, vol. 97, 09 1985.

[108] Freedman, M. H., Kitaev, A., and Wang, Z., "Simulation of topological field theories by quantum computers," *Communications in Mathematical Physics*, vol. 227, p. 587–603, Jun 2002.

[109] Furukawa, S. and Misguich, G., "Topological entanglement entropy in the quantum dimer model on the triangular lattice," *Phys. Rev. B*, vol. 75, p. 214407, 2007.

[110] Galitski, V., Juzeliūnas, G., and Spielman, I. B., "Artificial gauge fields with ultracold atoms," *Physics Today*, vol. 72, pp. 38–44, Jan. 2019.

[111] Galitski, V. and Spielman, I., "Spin-orbit coupling in quantum gases," *Nature*, vol. 494, pp. 49–54, 02 2013.

[112] Gavinsky, D., Kempe, J., Kerenidis, I., Raz, R., and de Wolf, R., "Exponential separations for one-way quantum communication complexity, with applications to cryptography," in *Proceedings of the Thirty-Ninth Annual ACM Symposium on Theory of Computing*, STOC '07, (New York, NY, USA), p. 516–525, Association for Computing Machinery, 2007.

[113] Giampaolo, S., Simonov, K., Capolupo, A., and Hiesmayr, B., "The interplay between frustration and entanglement in many-body systems," *Journal of Statistical Mechanics Theory and Experiment*, vol. 2018, p. 023101, 07 2016.

[114] Giampaolo, S. M., Gualdi, G., Monras, A., and Illuminati, F., "Characterizing and quantifying frustration in quantum many-body systems.," *Physical review letters*, vol. 107 26, p. 260602, 2011.

[115] Giampaolo, S. M., Ramos, F. B., and Franchini, F., "The frustration of being odd : universal area law violation in local systems," *Journal of Physics Communications*, vol. 3, p. 081001, aug 2019.

[116] Gioev, D. and Klich, I., "Entanglement entropy of fermions in any dimension and the widom conjecture," *Phys. Rev. Lett.*, vol. 96, p. 100503, Mar 2006.

[117] Giorda, P. and Paris, M. G. A., "Gaussian quantum discord," *Phys. Rev. Lett.*, vol. 105, p. 020503, Jul 2010.

[118] Giovannetti, V., Lloyd, S., and Maccone, L., "Quantum-enhanced measurements : Beating the standard quantum limit," *Science (New York, N.Y.)*, vol. 306, pp. 1330–6, 12 2004.

[119] Gori, G., Paganelli, S., Sharma, A., Sodano, P., and Trombettoni, A., "Explicit hamiltonians inducing volume law for entanglement entropy in fermionic lattices," *Phys. Rev. B*, vol. 91, p. 245138, Jun 2015.

[120] Gottesman, D., "Stabilizer codes and quantum error correction," 1997. Caltech Ph.D. thesis.

[121] Gottesman, D., "Theory of fault-tolerant quantum computation," *Physical Review A*, vol. 57, no. 1, p. 127, 1998.

[122] Gottesman, D., "Fault tolerant quantum computation with higher dimensional systems," *Chaos Solitons Fractals*, vol. 10, pp. 1749–1758, 1999.

[123] Gottesman, D. and Hastings, M., "Entanglement vs. gap for one-dimensional spin systems," *New Journal of Physics - NEW J PHYS*, vol. 12, 02 2010.

[124] Gottesman, D., Kitaev, A., and Preskill, J., "Encoding a qubit in an oscillator," *Phys. Rev. A*, vol. 64, p. 012310, Jun 2001.

[125] Goussev, A., Jalabert, R. A., Pastawski, H. M., and Wisniacki, A., "Loschmidt echo," *Scholarpedia*, vol. 7, no. 8, p. 11687, 2012.

[126] Grifoni, M. and Hänggi, P., "Driven quantum tunneling," *Physics Reports*, vol. 304, no. 5, pp. 229 – 354, 1998.

[127] Gu, M., Chrzanowski, H., Assad, S., Symul, T., Modi, K., Ralph, T., Vedral, V., and Lam, P., "Observing the operational significance of discord consumption," *Nature Physics*, vol. 8, pp. 671–675, 2012.

[128] Haegeman, J., Osborne, T. J., Verschelde, H., and Verstraete, F., "Entanglement renormalization for quantum fields in real space," *Physical Review Letters*, vol. 110, Mar 2013.

[129] Hafezi, M., "Synthetic gauge fields with photons," *International Journal of Modern Physics B*, vol. 28, 12 2013.

[130] Hagen, C. R., "Scale and conformal transformations in galilean-covariant field theory," *Phys. Rev. D*, vol. 5, pp. 377–388, Jan 1972.

[131] Haldane, F. D. M., "Nonlinear field theory of large-spin heisenberg antiferromagnets : Semiclassically quantized solitons of the one-dimensional easy-axis néel state," *Phys. Rev. Lett.*, vol. 50, pp. 1153–1156, Apr 1983.

[132] Hallgren, S., "Polynomial-time quantum algorithms for pell's equation and the principal ideal problem," *Journal of the ACM*, vol. 54, 01 2002.

[133] Hamza, E., Sims, R., and Stolz, G., "Dynamical localization in disordered quantum spin systems," *Communications in Mathematical Physics*, vol. 315, 08 2011.

[134] Hastings, M., "An area law for one dimensional quantum systems," *Journal of Statistical Mechanics Theory and Experiment*, vol. 2007, 05 2007.

[135] Hastings, M., "Quasi-adiabatic continuation for disordered systems : Applications to correlations, lieb-schultz-mattis, and hall conductance," *arXiv : Mathematical Physics*, 2010.

[136] Hastings, M., "Random mera states and the tightness of the brandao-horodecki entropy bound," *Quantum Information and Computation*, vol. 16, 05 2015.

[137] Hastings, M. and Koma, T., "Spectral gap and exponential decay of correlations," *Communications in Mathematical Physics*, vol. 265, pp. 781–804, 2005.

[138] Hastings, M. B., "Lieb-schultz-mattis in higher dimensions," *Phys. Rev. B*, vol. 69, p. 104431, Mar 2004.

[139] Hastings, M. B., "Entropy and entanglement in quantum ground states," *Phys. Rev. B*, vol. 76, p. 035114, Jul 2007.

[140] Hauke, P., Tieleman, O., Celi, A., Ölschläger, C., Simonet, J., Struck, J., Weinberg, M., Windpassinger, P., Sengstock, K., Lewenstein, M., and Eckardt, A., "Non-abelian gauge fields and topological insulators in shaken optical lattices," *Phys. Rev. Lett.*, vol. 109, p. 145301, Oct 2012.

[141] Hawking, S. W., "Black hole explosions," *Nature*, vol. 248, pp. 30–31, 1974.

[142] Hayden, P., Leung, D., Shor, P., and Winter, A., "Randomizing quantum states : Constructions and applications," *Communications in Mathematical Physics*, vol. 250, pp. 371–391, 2004.

[143] Henkel, M., "Phenomenology of local scale invariance : From conformal invariance to dynamical scaling," *Nucl. Phys. B*, vol. 641, pp. 405–486, 2002.

[144] Henley, C. L., "From classical to quantum dynamics at Rokhsar Kivelson points," *Journal of Physics Condensed Matter*, vol. 16, pp. S891–S898, Mar. 2004.

[145] Henley, C. L., "Power-law spin correlations in pyrochlore antiferromagnets," *Physical Review B*, vol. 71, Jan 2005.

[146] Hertz, J. A., "Quantum critical phenomena," *Phys. Rev. B*, vol. 14, pp. 1165–1184, Aug 1976.

[147] Heshami, K., England, D., Humphreys, P., Bustard, P., Acosta, V., Nunn, J., and Sussman, B., "Quantum memories : emerging applications and recent advances," *Journal of Modern Optics*, vol. 63, 11 2015.

[148] Hohenberg, P. C. and Halperin, B. I., "Theory of dynamic critical phenomena," *Rev. Mod. Phys.*, vol. 49, pp. 435–479, Jul 1977.

[149] Holzhey, C. F. E., Larsen, F., and Wilczek, F., "Geometric and renormalized entropy in conformal field theory," *Nuclear Physics*, vol. 424, pp. 443–467, 1994.

[150] Hořava, P., "Membranes at Quantum Criticality," *JHEP*, vol. 03, p. 020, 2009.

[151] Horava, P., "Quantum Gravity at a Lifshitz Point," *Phys. Rev. D*, vol. 79, p. 084008, 2009.

[152] Hsu, B. and Fradkin, E., "Universal Behavior of Entanglement in 2D Quantum Critical Dimer Models," *J. Stat. Mech.*, vol. 1009, p. P09004, 2010.

[153] Hsu, B., Mulligan, M., Fradkin, E., and Kim, E.-A., "Universal entanglement entropy in 2D conformal quantum critical points," *Phys. Rev.*, vol. B79, p. 115421, 2009.

[154] Huang, Y., "A polynomial-time algorithm for the ground state of one-dimensional gapped hamiltonians," 2015.

[155] Ingold, G.-L., "Path integrals and their application to dissipative quantum systems," *Lecture Notes in Physics*, vol. 611, p. 1–53, 2002.

[156] Irani, S., "Ground state entanglement in one dimensional translationally invariant quantum systems," *Journal of Mathematical Physics*, vol. 51, 01 2009.

[157] Ischi, B., Hilke, M., and Dubé, M., "Decoherence in a n-qubit solid-state quantum register," *Physical Review B*, vol. 71, no. 19, p. 195325, 2005.

[158] Ising, E., "Beitrag zur theorie des ferromagnetismus," *Zeitschrift für Physik*, vol. 31, no. 1, pp. 253–258, 1925.

[159] Itzykson, C. and Drouffe, J.-M., *Statistical Field Theory*, vol. 1 of *Cambridge Monographs on Mathematical Physics*. Cambridge University Press, 1989.

[160] Ivanov, P. A. and Vitanov, N., "Two-qubit quantum fourier transform and entanglement protected by circulant symmetry," *arXiv : Quantum Physics*, 2020.

[161] Jackiw, R., "Introducing scale symmetry," *Phys. Today*, vol. 25N1, pp. 23–27, 1972.

[162] Johnson-Freyd, T., "On the classification of topological orders," 2020.

[163] Kachru, S., Liu, X., and Mulligan, M., "Gravity duals of lifshitz-like fixed points," *Physical Review D*, vol. 78, Nov 2008.

[164] Kallin, A. B., Stoudenmire, E. M., Fendley, P., Singh, R. R. P., and Melko, R. G., "Corner contribution to the entanglement entropy of an o(3) quantum critical point in 2 + 1 dimensions," *Journal of Statistical Mechanics : Theory and Experiment*, vol. 2014, p. P06009, Jun 2014.

[165] Karchmer, M. and Wigderson, A., "Monotone circuits for connectivity require super-logarithmic depth.," *SIAM J. Discrete Math.*, vol. 3, pp. 255–265, 01 1990.

[166] Karczmarek, J. and Rabideau, C., "Holographic entanglement entropy in nonlocal theories," *Journal of High Energy Physics*, vol. 2013, pp. 1–24, 2013.

[167] Kawabata, K., Nishioka, T., Okuyama, Y., and Watanabe, K., "Probing Hawking radiation through capacity of entanglement," *JHEP*, vol. 05, p. 062, 2021.

[168] Kempe, J., Bacon, D., DiVincenzo, D. P., and Whaley, K. B., "Encoded universality from a single physical interaction," 2001.

[169] Keränen, V., Sybesma, W., Szepietowski, P., and Thorlacius, L., "Correlation functions in theories with lifshitz scaling," *Journal of High Energy Physics*, vol. 2017, May 2017.

[170] Kiktenko, E. O., Fedorov, A. K., Man'ko, O. V., and Man'ko, V. I., "Multilevel superconducting circuits as two-qubit systems : Operations, state preparation, and entropic inequalities," *Phys. Rev. A*, vol. 91, p. 042312, Apr 2015.

[171] Kiktenko, E., Fedorov, A., Strakhov, A., and Man'ko, V., "Single qudit realization of the deutsch algorithm using superconducting many-level quantum circuits," *Physics Letters A*, vol. 379, no. 22, pp. 1409 – 1413, 2015.

[172] Kitaev, A. Y., "Quantum computations : algorithms and error correction," *Russian Mathematical Surveys*, vol. 52, pp. 1191–1249, dec 1997.

[173] Kitaev, A., "Fault-tolerant quantum computation by anyons," *Annals of Physics*, vol. 303, p. 2–30, Jan 2003.

[174] Kliuchnikov, V., Maslov, D., and Mosca, M., "Asymptotically optimal approximation of single qubit unitaries by clifford and t circuits using a constant number of ancillary qubits," *Physical Review Letters*, vol. 110, pp. 1–5, December 2012.

[175] Knill, E., "Fermionic linear optics and matchgates," 2001.

[176] Knill, E., Laflamme, R., and Milburn, G. J., "A scheme for efficient quantum computation with linear optics," *Nature*, vol. 409, no. 6816, pp. 46–52, 2001.

[177] Knill, E., Leibfried, D., Reichle, R., Britton, J., Blakestad, R. B., Jost, J. D., Langer, C., Ozeri, R., Seidelin, S., and Wineland, D. J., "Randomized benchmarking of quantum gates," *Physical Review A*, vol. 77, Jan 2008.

[178] Koong, Z.-X., Ballesteros-Garcia, G., Proux, R., Dalacu, D., Poole, P. J., and Gerardot, B. D., "Multiplexed single photons from deterministically positioned nanowire quantum dots," *Phys. Rev. Applied*, vol. 14, p. 034011, Sep 2020.

[179] Kreinovich, V., "Why some physicists are excited about the undecidability of the spectral gap problem and why should we," *Bull. EATCS*, vol. 122, 2017.

[180] Kuwahara, T. and Saito, K., "Area law of noncritical ground states in 1d long-range interacting systems," *Nature Communications*, vol. 11, 2020.

[181] Laflorencie, N., "Quantum entanglement in condensed matter systems," *Phys. Rept.*, vol. 646, pp. 1–59, 2016.

[182] Lami, L., Serafini, A., and Adesso, G., "Gaussian entanglement revisited," Dec. 2016.

[183] Landau, Z., Vazirani, U., and Vidick, T., "A polynomial-time algorithm for the ground state of 1d gapped local hamiltonians," 2013.

[184] Latorre, J., Rico, E., and Vidal, G., "Ground state entanglement in quantum spin chains," *Quantum Inf. Comput.*, vol. 4, pp. 48–92, 2004.

[185] Lawrence, J., Brukner, C., and Zeilinger, A., "Mutually unbiased binary observable sets on n qubits," *Physical Review A*, vol. 65, 04 2001.

[186] Le Gall, F., "Exponential separation of quantum and classical online space complexity," *Theory of Computing Systems*, vol. 45, 06 2006.

[187] Leinaas, J., Myrheim, J., and Ovrum, E., "Geometrical aspects of entanglement," *Physical Review A*, vol. 74, p. 012313, 2006.

[188] Li, H.-O., Cao, G., Yu, G.-D., Xiao, M., Guo, G.-C., Jiang, H.-W., and Guo, G.-P., "Controlled quantum operations of a semiconductor three-qubit system," *Physical Review Applied*, vol. 9, no. 2, p. 024015, 2018.

[189] Lieb, E. and Robinson, D., "The finite group velocity of quantum spin systems," *Communications in Mathematical Physics*, vol. 28, 09 1972.

[190] Lloyd, S., "Almost any quantum logic gate is universal," *Phys. Rev. Lett.*, vol. 75, pp. 346–349, Jul 1995.

[191] Lloyd, S., "Universal quantum simulators," *Science*, vol. 273, no. 5278, pp. 1073–1078, 1996.

[192] Lloyd, S. and Braunstein, S. L., "Quantum computation over continuous variables," *Phys. Rev. Lett.*, vol. 82, pp. 1784–1787, Feb 1999.

[193] Loss, D. and DiVincenzo, D. P., "Quantum computation with quantum dots," *Phys. Rev. A*, vol. 57, pp. 120–126, Jan 1998.

[194] Marić, V., Franchini, F., Kuić, D., and Giampaolo, S. M., "Resilience of the topological phases to frustration," *Scientific Reports*, vol. 11, Mar 2021.

[195] Marić, V., Giampaolo, S., and Franchini, F., "Quantum phase transition induced by topological frustration," *Communications Physics*, vol. 3, 12 2020.

[196] Marro, J. and Dickman, R., *Nonequilibrium Phase Transitions in Lattice Models*. Collection Alea-Saclay : Monographs and Texts in Statistical Physics, Cambridge University Press, 1999.

[197] Martinis, J. M., Nam, S., Aumentado, J., Lang, K., and Urbina, C., "Decoherence of a superconducting qubit due to bias noise," *Physical Review B*, vol. 67, no. 9, p. 094510, 2003.

[198] Marzolino, U., Giampaolo, S., and Illuminati, F., "Frustration, entanglement, and correlations in quantum many body systems," *Physical Review A*, vol. 88, 02 2013.

[199] Masanes, L., "Area law for the entropy of low-energy states," *Physical Review A*, vol. 80, 07 2009.

[200] Mead, C. A., "The geometric phase in molecular systems," *Rev. Mod. Phys.*, vol. 64, pp. 51–85, Jan 1992.

[201] Michalakis, S. and Zwolak, J. P., "Stability of frustration-free hamiltonians," *Communications in Mathematical Physics*, vol. 322, pp. 277–302, 2013.

[202] Mikeska, H.-J. and Kolezhuk, A. K., *One-dimensional magnetism*, pp. 1–83. Berlin, Heidelberg : Springer Berlin Heidelberg, 2004.

[203] Moessner, R., Sondhi, S. L., and Fradkin, E., "Short-ranged resonating valence bond physics, quantum dimer models, and ising gauge theories," *Phys. Rev. B*, vol. 65, p. 024504, Dec 2001.

[204] Movassagh, R. and Shor, P., "Power law violation of the area law in quantum spin chains," *Bulletin of the American Physical Society*, 2015.

[205] Movassagh, R., "Entanglement and correlation functions of the quantum Motzkin spin-chain," *Journal of Mathematical Physics*, vol. 58, p. 031901, Mar. 2017.

[206] Mozaffar, M. and Mollabashi, A., "Entanglement in lifshitz-type quantum field theories," *Journal of High Energy Physics*, vol. 2017, 05 2017.

[207] Nakamura, Y., Pashkin, Y. A., and Tsai, J. S., "Coherent control of macroscopic quantum states in a single-cooper-pair box," *nature*, vol. 398, no. 6730, pp. 786–788, 1999.

[208] Nayak, C., Simon, S. H., Stern, A., Freedman, M., and Sarma, S. D., "Non-abelian anyons and topological quantum computation," *Reviews of Modern Physics*, vol. 80, no. 3, p. 1083, 2008.

[209] Nielsen, M. and Chuang, I., *Quantum Computation and Quantum Information*. Cambridge : Cambridge University Press, 2010. 10th Anniversary Edition.

[210] Nilsson, H., Thelander, C., Fröberg, L., Wagner, J., and Samuelson, L., "Nanowire-based multiple quantum dot memory," *Applied Physics Letters*, vol. 89, pp. 163101–163101, 10 2006.

[211] O'Brien, J. L., Pryde, G. J., White, A. G., Ralph, T. C., and Branning, D., "Demonstration of an all-optical quantum controlled-not gate," *Nature*, vol. 426, no. 6964, pp. 264–267, 2003.

[212] Okuyama, K., "Capacity of entanglement in random pure state," *Phys. Lett. B*, vol. 820, p. 136600, 2021.

[213] Ollivier, H. and Żurek, W., "Quantum discord : A measure of the quantumness of correlations," *Physical review letters*, vol. 88, p. 017901, 02 2002.

[214] Osborne, T. J., "Hamiltonian complexity," *Reports on Progress in Physics*, vol. 75, p. 022001, Jan 2012.

[215] Oshikawa, M., "Boundary Conformal Field Theory and Entanglement Entropy in Two-Dimensional Quantum Lifshitz Critical Point," 2010.

[216] Owerre, S. A. and Paranjape, M. B., "Macroscopic quantum spin tunneling with two interacting spins," *Phys. Rev. B*, vol. 88, p. 220403, Dec 2013.

[217] Ozawa, T., Price, H. M., Amo, A., Goldman, N., Hafezi, M., Lu, L., Rechtsman, M. C., Schuster, D., Simon, J., Zilberberg, O., and Carusotto, I., "Topological photonics," *Rev. Mod. Phys.*, vol. 91, p. 015006, Mar 2019.

[218] Palma, G. M., Suominen, K.-A., and Ekert, A., "Quantum computers and dissipation," *Proceedings of the Royal Society of London. Series A : Mathematical, Physical and Engineering Sciences*, vol. 452, no. 1946, pp. 567–584, 1996.

[219] Parisi, G. and Wu, Y.-s., "Perturbation Theory Without Gauge Fixing," *Sci. Sin.*, vol. 24, p. 483, 1981.

[220] Peres, A., "Stability of quantum motion in chaotic and regular systems," *Phys. Rev. A*, vol. 30, pp. 1610–1615, Oct 1984.

[221] Pirandola, S., "Quantum discord as a resource for quantum cryptography," *Scientific reports*, vol. 4, 09 2013.

[222] Plenio, M. B., "Logarithmic negativity : A full entanglement monotone that is not convex," *Physical Review Letters*, vol. 95, Aug 2005.

[223] Plenio, M. B., Eisert, J., Dreissig, J., and Cramer, M., "Entropy, entanglement, and area : Analytical results for harmonic lattice systems," *Phys. Rev. Lett.*, vol. 94, p. 060503, Feb 2005.

[224] Poplavskiĭ, R. P., "Thermodynamic models of information processes," *Soviet Physics Uspekhi*, vol. 18, pp. 222–241, mar 1975.

[225] Qualls, J. D., "Lectures on conformal field theory," 2016.

[226] Quantiki, "Bipartite states and schmidt decomposition," Mar 2019.

[227] Rabideau, C., "Perturbative entanglement entropy in nonlocal theories," *Journal of High Energy Physics*, vol. 2015, Sep 2015.

[228] Raussendorf, R., Browne, D. E., and Briegel, H. J., "Measurement-based quantum computation on cluster states," *Phys. Rev. A*, vol. 68, p. 022312, Aug 2003.

[229] Raz, R., "Exponential separation of quantum and classical communication complexity," in *Proceedings of the Thirty-First Annual ACM Symposium on Theory of Computing*, STOC '99, (New York, NY, USA), p. 358–367, Association for Computing Machinery, 1999.

[230] Reck, M., Zeilinger, A., Bernstein, H. J., and Bertani, P., "Experimental realization of any discrete unitary operator," *Phys. Rev. Lett.*, vol. 73, pp. 58–61, July 1994.

[231] Rokhsar, D. S. and Kivelson, S. A., "Superconductivity and the quantum hard-core dimer gas," *Phys. Rev. Lett.*, vol. 61, pp. 2376–2379, Nov 1988.

[232] Romero, J. M., Cuesta Sánchez, V., García, J., and Vergara, J., "Conformal anisotropic mechanics and hořava gravity," *AIP Conference Proceedings*, vol. 1361, pp. 344–348, 09 2011.

[233] Rosen, K. H., *Discrete Mathematics and Its Applications*. McGraw-Hill Higher Education, 5th ed., 2002.

[234] Ryu, S. and Takayanagi, T., "Aspects of holographic entanglement entropy," *Journal of High Energy Physics*, vol. 2006, p. 045–045, Aug 2006.

[235] Sachdev, S., *Quantum Phase Transitions*. Cambridge University Press, 2 ed., 2011.

[236] Sachdev, S., *Quantum Phase Transitions*. Cambridge University Press, 2 ed., 2011.

[237] Sachdev, S. and Keimer, B., "Quantum criticality," *Physics Today*, vol. 64, p. 29–35, Feb 2011.

[238] Sachdev, S. and Senthil, T., "Zero temperature phase transitions in quantum heisenberg ferromagnets," *Annals of Physics*, vol. 251, p. 76–122, Oct 1996.

[239] Saglamyurek, E., Hrushevskyi, T., Rastogi, A., Heshami, K., and LeBlanc, L., "Coherent storage and manipulation of broadband photons via dynamically controlled autler-townes splitting," *Nature Photonics*, vol. 12, 12 2018.

[240] Sanders, Y. R., Wallman, J. J., and Sanders, B. C., "Bounding quantum gate error rate based on reported average fidelity," *New Journal of Physics*, vol. 18, no. 1, p. 012002, 2015.

[241] Santos, L. H., "Rokhsar-kivelson models of bosonic symmetry-protected topological states," *Physical Review B*, vol. 91, p. 155150, 2015.

[242] Schaefer, H., *Topological Vector Spaces*. New York : Springer-Verlag, 1999.

[243] Schuch, N. and Cirac, J. I., "Matrix product state and mean-field solutions for one-dimensional systems can be found efficiently," *Phys. Rev. A*, vol. 82, p. 012314, Jul 2010.

[244] Schuch, N., Wolf, M. M., Verstraete, F., and Cirac, J. I., "Entropy scaling and simulability by matrix product states," *Physical Review Letters*, vol. 100, Jan 2008.

[245] Segal, I. E., "Irreducible representations of operator algebras," *Bulletin of the American Mathematical Society*, vol. 53, no. 2, pp. 73 – 88, 1947.

[246] Selinger, P., "Efficient clifford+t approximation of single-qubit operators," *Quantum Information and Computation*, vol. 15, 12 2012.

[247] Shi, Y., "Both toffoli and controlled-not need little help to do universal quantum computation," *Quantum Information and Computation*, vol. 3, 06 2002.

[248] Shiba, N. and Takayanagi, T., "Volume law for the entanglement entropy in non-local qfts," *Journal of High Energy Physics*, vol. 2014, pp. 1–16, 2014.

[249] Shor, P. W., "Scheme for reducing decoherence in quantum computer memory," *Physical review A*, vol. 52, no. 4, p. R2493, 1995.

[250] Shor, P. W., "Polynomial-time algorithms for prime factorization and discrete logarithms on a quantum computer," *SIAM Journal on Computing*, vol. 26, p. 1484–1509, Oct 1997.

[251] Simon, B., "Holonomy, the quantum adiabatic theorem, and berry's phase," *Phys. Rev. Lett.*, vol. 51, pp. 2167–2170, Dec 1983.

[252] Sleator, T. and Weinfurter, H., "Realizable universal quantum logic gates," *Phys. Rev. Lett.*, vol. 74, pp. 4087–4090, May 1995.

[253] Son, D. T., "Toward an AdS/cold atoms correspondence : A Geometric realization of the Schrodinger symmetry," *Phys. Rev. D*, vol. 78, p. 046003, 2008.

[254] Sørensen, A. S., Demler, E., and Lukin, M. D., "Fractional quantum hall states of atoms in optical lattices," *Phys. Rev. Lett.*, vol. 94, p. 086803, Mar 2005.

[255] Srednicki, M., "Entropy and area," *Physical Review Letters*, vol. 71, p. 666–669, Aug 1993.

[256] Steane, A., "Multiple particle interference and quantum error correction," *Proceedings of the Royal Society A : Mathematical, Physical and Engineering Sciences*, vol. 452, 01 1996.

[257] Stéphan, J.-M., Misguich, G., and Pasquier, V., "Rényi entropy of a line in two-dimensional ising models," *Phys. Rev. B*, vol. 82, p. 125455, 2010.

[258] Stéphan, J.-M., Furukawa, S., Misguich, G., and Pasquier, V., "Shannon and entanglement entropies of one- and two-dimensional critical wave functions," *Phys. Rev. B*, vol. 80, p. 184421, Nov. 2009.

[259] Stéphan, J.-M., Ju, H., Fendley, P., and Melko, R. G., "Entanglement in gapless resonating-valence-bond states," *New Journal of Physics*, vol. 15, no. 1, p. 015004, 2013.

[260] Stéphan, J.-M., Misguich, G., and Pasquier, V., "Phase transition in the rényi-shannon entropy of luttinger liquids," *Phys. Rev. B*, vol. 84, p. 195128, 2011.

[261] Stoudenmire, E. M., Gustainis, P., Johal, R., Wessel, S., and Melko, R. G., "Corner contribution to the entanglement entropy of strongly interacting o(2) quantum critical systems in 2+1 dimensions," *Physical Review B*, vol. 90, Dec 2014.

[262] Struck, J., Ölschläger, C., Weinberg, M., Hauke, P., Simonet, J., Eckardt, A., Lewenstein, M., Sengstock, K., and Windpassinger, P., "Tunable gauge potential for neutral and spinless particles in driven optical lattices," *Phys. Rev. Lett.*, vol. 108, p. 225304, May 2012.

[263] Swingle, B., "Mutual information and the structure of entanglement in quantum field theory," 10 2010.

[264] Terhal, B. and DiVincenzo, D., "Classical simulation of noninteracting-fermion quantum circuits," *Physical Review A*, vol. 65, 08 2001.

[265] Toulouse, G., Vannimenus, J., and Maillard, J.-M., "Spin glasses and roughening transition," *Journal De Physique Lettres*, vol. 38, pp. 459–461, 1977.

[266] Valiant, L. G., "Quantum computers that can be simulated classically in polynomial time," in *Proceedings of the Thirty-Third Annual ACM Symposium on Theory of Computing*, STOC '01, (New York, NY, USA), p. 114–123, Association for Computing Machinery, 2001.

[267] Valiant, L., "The complexity of computing the permanent," *Theoretical Computer Science*, vol. 8, no. 2, pp. 189–201, 1979.

[268] van Dam, W., Hallgren, S., and Ip, L., "Quantum algorithms for some hidden shift problems," *SIAM Journal on Computing*, vol. 36, 11 2002.

[269] van Zuylen, A., Bieron, J., Schalekamp, F., and Yu, G., "An upper bound on the number of circular transpositions to sort a permutation," 2014.

[270] Vannimenus, J. and Toulouse, G., "Theory of the frustration effect. II. ising spins on a square lattice," *Journal of Physics C : Solid State Physics*, vol. 10, pp. L537–L542, sep 1977.

[271] Verstraete, F. and Cirac, J. I., "Continuous matrix product states for quantum fields," *Physical Review Letters*, vol. 104, May 2010.

[272] Verstraete, F., Wolf, M., Perez-Garcia, D., and Cirac, J., "Criticality, the area law, and the computational power of projected entangled pair states," *Physical review letters*, vol. 96, p. 220601, 07 2006.

[273] Vidal, G., "Efficient classical simulation of slightly entangled quantum computations.," *Physical review letters*, vol. 91 14, p. 147902, 2003.

[274] Vidal, G., Latorre, J. I., Rico, E., and Kitaev, A., "Entanglement in quantum critical phenomena," *Physical Review Letters*, vol. 90, Jun 2003.

[275] Vidal, G. and Werner, R. F., "Computable measure of entanglement," *Physical Review A*, vol. 65, Feb 2002.

[276] Vitagliano, G., Riera, A., and Latorre, J., "Volume-law scaling for the entanglement entropy in spin-1/2 chains," *New Journal of Physics*, vol. 12, p. 113049, 11 2010.

[277] Watson, T., Philips, S., Kawakami, E., Ward, D., Scarlino, P., Veldhorst, M., Savage, D., Lagally, M., Friesen, M., Coppersmith, S., and others, "A programmable two-qubit quantum processor in silicon," *nature*, vol. 555, no. 7698, pp. 633–637, 2018.

[278] Wen, X. G., "Topological orders in rigid states," *Int. J. Mod. Phys. B*, p. 239, 1990.

[279] Werlang, T. and Rigolin, G., "Thermal and magnetic quantum discord in heisenberg models," *Phys. Rev. A*, vol. 81, p. 044101, Apr 2010.

[280] White, S. R., "Density matrix formulation for quantum renormalization groups," *Phys. Rev. Lett.*, vol. 69, pp. 2863–2866, Nov 1992.

[281] Wilczek, F. and Zee, A., "Appearance of gauge structure in simple dynamical systems," *Phys. Rev. Lett.*, vol. 52, pp. 2111–2114, Jun 1984.

[282] Wilson, K. G., "Renormalization group and critical phenomena. i. renormalization group and the kadanoff scaling picture," *Phys. Rev. B*, vol. 4, pp. 3174–3183, Nov 1971.

[283] Wilson, K. G., "Renormalization group and critical phenomena. ii. phase-space cell analysis of critical behavior," *Phys. Rev. B*, vol. 4, pp. 3184–3205, Nov 1971.

[284] Wilson, K. G. and Fisher, M. E., "Critical exponents in 3.99 dimensions," *Phys. Rev. Lett.*, vol. 28, pp. 240–243, Jan 1972.

[285] Wolf, M., "Violation of the entropic area law for fermions," *Physical review letters*, vol. 96, p. 010404, 02 2006.

[286] Wolf, M. M., Verstraete, F., and Cirac, J. I., "Entanglement and frustration in ordered systems," *International Journal of Quantum Information*, vol. 01, pp. 465–477, 2003.

[287] Wolf, M. M., Verstraete, F., Hastings, M. B., and Cirac, J. I., "Area laws in quantum systems : Mutual information and correlations," *Physical Review Letters*, vol. 100, Feb 2008.

[288] Xiao, D., Chang, M.-C., and Niu, Q., "Berry phase effects on electronic properties," *Rev. Mod. Phys.*, vol. 82, pp. 1959–2007, Jul 2010.

[289] Yang, K., "Ferromagnetic transition in one-dimensional itinerant electron systems," *Phys. Rev. Lett.*, vol. 93, p. 066401, Aug 2004.

[290] Yao, A., "Some complexity questions related to distributive computing(preliminary report)," in *STOC '79*, 1979.

[291] Yao, H. and Qi, X.-L., "Entanglement entropy and entanglement spectrum of the kitaev model," *Physical Review Letters*, vol. 105, Aug 2010.

[292] Yao, N. Y., Jiang, L., Gorshkov, A. V., Maurer, P. C., Giedke, G., Cirac, J. I., and Lukin, M. D., "Scalable architecture for a room temperature solid-state quantum information processor," *Nature communications*, vol. 3, no. 1, pp. 1–8, 2012.

[293] Young, S. M., Zaheer, S., Teo, J. C. Y., Kane, C. L., Mele, E. J., and Rappe, A. M., "Dirac semimetal in three dimensions," *Phys. Rev. Lett.*, vol. 108, p. 140405, Apr 2012.

[294] Zaletel, M. P., Bardarson, J. H., and Moore, J. E., "Logarithmic terms in entanglement entropies of 2d quantum critical points and shannon entropies of spin chains," *Phys. Rev. Lett.*, vol. 107, p. 020402, 2011.

[295] Zamolodchikov, A. B., "Irreversibility of the Flux of the Renormalization Group in a 2D Field Theory," *JETP Lett.*, vol. 43, pp. 730–732, 1986.

[296] Zeng, B., Chen, X., Zhou, D., and Wen, X.-G., *Quantum Information Meets Quantum Matter – From Quantum Entanglement to Topological Phase in Many-Body Systems*. New York : Springer, 08 2015.

[297] Zhang, Z., Ahmadain, A., and Klich, I., "Quantum phase transition from bounded to extensive entanglement entropy in a frustration-free spin chain," 2016.

[298] Zhang, Z., Ahmadain, A., and Klich, I., "Novel quantum phase transition from bounded to extensive entanglement," *Proceedings of the National Academy of Sciences*, vol. 114, no. 20, pp. 5142–5146, 2017.

[299] Zhang, Z. and Klich, I., "Entropy, gap and a multi-parameter deformation of the fredkin spin chain," *Journal of Physics A : Mathematical and Theoretical*, vol. 50, p. 425201, Sep 2017.

[300] Zhou, T., Chen, X., Faulkner, T., and Fradkin, E., "Entanglement entropy and mutual information of circular entangling surfaces in the $2 + 1$-dimensional quantum lifshitz model," *Journal of Statistical Mechanics : Theory and Experiment*, vol. 2016, p. 093101, Sep 2016.

[301] Zwanenburg, F. A., Dzurak, A. S., Morello, A., Simmons, M. Y., Hollenberg, L. C., Klimeck, G., Rogge, S., Coppersmith, S. N., and Eriksson, M. A., "Silicon quantum electronics," *Reviews of modern physics*, vol. 85, no. 3, p. 961, 2013.